

Thesis  
2125

**THE USE OF CONTEXTUAL TECHNIQUES  
AND TEXTURAL ANALYSIS OF SATELLITE IMAGERY IN  
GEOLOGICAL STUDIES OF ARID REGIONS**

---

**KAMEL MOHAMMED AHMED SHEIKHO**

**THE UNIVERSITY OF STIRLING  
DEPARTMENT OF ENVIRONMENTAL SCIENCE**

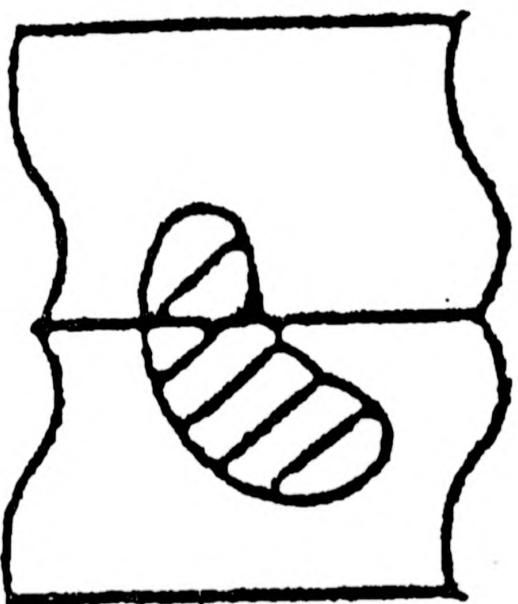
**THESIS SUBMITTED IN FULFILMENT OF THE  
REQUIREMENT OF THE DEGREE OF  
DOCTOR OF PHILOSOPHY**



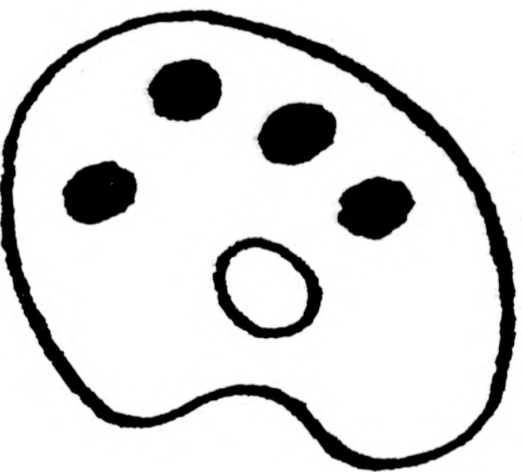
7/93

VARIABLE PRINT

QUALITY



# NUMEROUS ORIGINALS IN COLOUR



**DECLARATION**

I hereby declare that the work presented in this thesis has been composed by myself and is the result of my own research. It has neither been accepted or submitted for any other degrees. All the sources of information have been duly acknowledged.

**KAMEL MOHAMMED AHMED SHEIKHO**



January 1993

## ACKNOWLEDGEMENTS

The author wishes to express his gratitude to all those who contributed towards the completion of this research, in particular to the following persons and institutions:-

**Dr Alistair I Watson**, Lecturer, Department of Environmental Science, University of Stirling, for his dedicated supervision and support during the practical period and for his advice and criticism of the text.

**Prof Michael F Thomas**, Environmental Science Department, University of Stirling, for his comment and criticism, particularly in geological discussion, interpretation and for reading my Thesis.

**King Abdulaziz City for Science and Technology (KACST)**, for providing me with all the satellite data and for their financial support.

**Deputy Ministry for Mineral Resources; Ministry of Petroleum and Mineral Resources, Kingdom of Saudi Arabia**, for providing me with all the necessary geological maps.

**John McArthur**, Chief Technician, remote Sensing Unit of Environmental Science Department, for his help and advice in solving computing problems.

**Mr Mohammed M Abdulaziz** for his driving during part of the field trip.

Finally, a thank you to all members of my family who have supported me throughout with patience to finish my thesis. A special thank you, goes to my parents and my wife for her understanding, patience and support.

**DEDICATION**

*TO MY FATHER AND MOTHER*

*TO MY WIFE AND SISTER,*

*TO MY BROTHERS, AHMED AND TARIQ,*

*TO MY SONS AYMAN AND ABDULRHMAN AND*

*TO MY DAUGHTER AFNAN*

**ABSTRACT**

This Thesis examines the problem of extracting spatial information (context and texture) of use to the geologist, from satellite imagery. Part of the Arabian Shield was chosen to be the study area. Two new contextual techniques; (a) Ripping Membrane and (b) Rolling Ball were developed and examined in this study. Both new contextual based techniques proved to be excellent tools for visual detection and analysis of lineaments, and were clearly better than the 'traditional' spatial filtration technique. This study revealed structural lineaments, mostly mapped for the first time, which are clearly related to regional tectonic history of the area.

Contextual techniques were used to perform image segmentation. Two different image segmentation methods were developed and examined in this study. These methods were the automatic watershed segmentation and ripping membrane/Laserscan system method (as this method was being used for the first time). The second method produced high accuracy results for four selected test sites.

A new automatic lineament extraction method using the above contextual techniques was developed. The aim of the method was to produce an automatic lineament map and the azimuth direction of these lineaments in each rock type, as defined by the segmented regions. 75-85% of the visually traced lineaments were extracted by the automatic method. The automatic method appears to give a dominant trend slightly different ( $10^{\circ}$  -  $15^{\circ}$ ) from the

visually determined trend.

It was demonstrated that not all the different types of rock could be discriminated using the spectral image enhancement techniques (band ratio, principal components and decorrelation stretch). Therefore, the spatial grey level dependency matrix (SGLDM) was used to produce a texture feature image, which would enable distinctions to be made and overcome the limitations of spectral enhancement techniques. The SGLDM did not produce any useful texture features which can discriminate between every rock type in the selected test sites. It did, however, show some acceptable texture discrimination between some rock types. The remote sensing data examined in this thesis were the Landsat (multispectral scanner, Thematic Mapper), SPOT, and Shuttle Imaging Radar (SIR-B).

## CONTENTS

	<u>Page</u>
<b>ACKNOWLEDGEMENTS</b> . . . . .	<b>i</b>
<b>DEDICATION</b> . . . . .	<b>ii</b>
<b>ABSTRACT</b> . . . . .	<b>iii</b>
<b>CONTENTS</b> . . . . .	<b>v</b>
<b>LIST OF FIGURES</b> . . . . .	<b>ix</b>
<b>LIST OF TABLES</b> . . . . .	<b>xiii</b>
<b>LIST OF PLATES</b> . . . . .	<b>xiv</b>
<b>CHAPTER 1: INTRODUCTION</b>	
1.1 Introduction . . . . .	1
1.2 Purpose of Present Study . . . . .	2
1.3 Structure of the Thesis . . . . .	4
1.4 Spectral Reflectance of rocks and Minerals - Basic Concept . . . . .	5
1.5 Definition of Contextual Information . . . . .	18
1.6 Location and Description of Study Area . . . . .	22
1.7 Geology . . . . .	24
1.7.1 Geology of Arabian Shield . . . . .	24
1.7.2 Najd Fault System . . . . .	29
1.7.3 Geology of the Study Area . . . . .	33
<b>CHAPTER 2: PREPROCESSING OF REMOTELY SENSED DATA</b>	
2.1 Introduction . . . . .	44
2.2 Landsat Satellite . . . . .	46
2.3 SPOT Satellite . . . . .	50
2.4 Imaging Radar . . . . .	56
2.5 Image Processing System . . . . .	64

2.6	General Methods for Preprocessing of Remotely Sensed Data . . . . .	66
2.6.1	De-Stripping Method . . . . .	67
2.6.2	Atmospheric Effects and Corrections Method . . . . .	67
2.6.3	Image-to-Image Registration Method . . . . .	71
2.7	Summary . . . . .	75
 <b>CHAPTER 3: THE USE OF NEW CONTEXTUAL TECHNIQUES IN LINEAMENT MAPPING AND ANALYSIS: AN OVERVIEW</b>		
3.1	Introduction . . . . .	78
3.2	Definition of Lineament . . . . .	78
3.3	Spatial Filtration Technique . . . . .	83
3.4	The New Contextual Techniques . . . . .	89
3.4.1	'Ripping' Membrane Technique . . . . .	89
3.4.2	Rolling Ball Technique . . . . .	96
3.5	Arithmetic Operations . . . . .	98
3.6	Summary . . . . .	100
 <b>CHAPTER 4: THE USE OF NEW CONTEXTUAL TECHNIQUES IN LINEAMENTS MAPPING AND ANALYSIS: AN APPLICATION</b>		
4.1	Introduction . . . . .	103
4.2	Data Selection and Methodology . . . . .	104
4.3	Geology of the Test Site (Jibal Rummàn Area) . . . . .	109
4.4	Comparison Between the Techniques and their Results . . . . .	115
4.5	General Lineaments Interpretation and Mapping . . . . .	145
4.6	Lineaments Analysis (Rose Diagram) . . . . .	148
4.7	Discussion . . . . .	154
4.8	Summary . . . . .	157

<b>CHAPTER 5: THE USE OF CONTEXTUAL TECHNIQUES IN IMAGE SEGMENTATION FOR GEOLOGICAL APPLICATIONS</b>	
5.1	Introduction . . . . . 160
5.2	Computer Vision . . . . . 160
5.3	Density Slicing . . . . . 162
5.4	Definition of Image Segmentation . . . . . 163
5.5	Review of Image Segmentation Methods . . . . . 165
5.6	Watershed Image Segmentation Method . . . . . 170
5.7	Image Segmentation by Laserscan System Method . . . . . 176
5.8	Discussion . . . . . 188
5.9	Summary . . . . . 190
<b>CHAPTER 6: THE USE OF CONTEXTUAL TECHNIQUES IN AUTOMATIC LINE AND LINEAMENT FEATURE EXTRACTIONS ANALYSIS</b>	
6.1	Introduction . . . . . 192
6.2	Automatic Line and Lineament Feature Extraction and Analysis: A Review . . . . . 193
6.3	Automatic Line and Lineament Feature Extraction and Analysis: Methodology . . . . . 198
6.4	Automatic Line and Lineament Feature Extraction and Analysis: Application . . . . . 204
6.5	Discussion . . . . . 229
6.6	Summary . . . . . 232
<b>CHAPTER 7: THE USE OF SPECTRAL ENHANCEMENT TECHNIQUES IN ROCK DISCRIMINATION</b>	
7.1	Introduction . . . . . 234
7.2	Band Combination and Contrast Manipulation . . . . . 235
7.3	Colour Ratio Composite . . . . . 236
7.4	Principal Component Analysis . . . . . 241

7.5	Band Selection of Landsat TM Data for Rock Discrimination . . . . .	243
7.6	Image Interpretation . . . . .	247
7.7	Discussion . . . . .	268
7.8	Summary . . . . .	270
<b>CHAPTER 8: THE USE OF TEXTURE ANALYSIS IN ROCK DISCRIMINATION AND IMAGE CLASSIFICATION</b>		
8.1	Introduction . . . . .	272
8.2	Texture Analysis . . . . .	274
	8.2.1 Fourier Transform . . . . .	275
	8.2.2 First Order Texture Measures . . . . .	275
	8.2.3 Second Order Texture Measures . . . . .	276
8.3	Spatial Grey Level Dependency Matrix . . . . .	277
8.4	The Use of Texture Analysis in Geological Studies . . . . .	282
8.5	Result and Discussion . . . . .	284
8.6	Summary . . . . .	294
<b>CHAPTER 9: CONCLUSION</b>		
9.1	Conclusion . . . . .	297
9.2	Future Work . . . . .	305
<b>REFERENCES</b> . . . . .		309
<b>APPENDICES</b> . . . . .		338

## LIST OF FIGURES

	<u>Page</u>
1.1 The electromagnetic spectrum . . . . .	6
1.2 The number and position of features due to electronic transitions in minerals . . . . .	9
1.3 Iron oxides and hydroxides display absorption features due to crystal field effects . . . . .	9
1.4 Features due to vibrational process in the spectra of four hydroxyl-bearing minerals commonly present in hydrothermally altered rocks . . . . .	11
1.5 Bidirectional reflectance spectra of igneous rocks, separated vertically for clarity. Reflectance divisions are 10% . . . . .	11
1.6 Laboratory reflectance of selected rocks of (a) metamorphic rock, and (b) sedimentary rock. Reflectance divisions are 10% . . . . .	13
1.7 Emissivity spectra of silicate rocks . . . . .	17
1.8 Types of spatial relationship . . . . .	20
1.9 Index map of the Arabian Peninsula showing the location of the study area . . . . .	23
1.10 Generalised geological map of the Arabian Peninsula . . . . .	25
1.11 Tectonic sketch map of the Arabian Shield, showing terrane and suture zones . . . . .	27
1.12 Schematic tectonic diagrams showing evolutionary stages of Arabian Shield development . . . . .	28
1.13 Outcrop traces of major faults of the Najd Fault System in the Arabian Shield . . . . .	32
1.14 Aeromagnetic lineaments attributable to structures in the Najd Fault System . . . . .	34
2.1 Landsat-5 orbit . . . . .	47
2.2 Landsat TM scanning arrangement . . . . .	49
2.3 Path-row co-ordinates in the Landsat-4 and 5 worldwide reference system (WRS), sheet 12 for area in and around Saudi Arabia . . . . .	52

	x
2.4 Design of SPOT Satellite . . . . .	54
2.5 Geometric characteristic terminology of side looking radar (SLAR) . . . . .	58
2.6 The geometric effects of SLAR images . . . . .	60
2.7 Fundamental concept of a synthetic-aperture radar system . . . . .	62
2.8 Flow Chart showing the methodology used for image -to- image registration in this study . . . . .	76
3.1 The moving spatial window concept . . . . .	86
3.2 The convolution matrix for a low-pass filter . . . . .	87
3.3 Convolution matrices for edge detection or high- pass filtering . . . . .	88
3.4 Four directional filters enhancing only lines trending near the specified azimuth . . . . .	90
3.5 Derive directional components from the low-pass image . .	91
3.6 Flow chart of the stages used during this study to produce a final result from the ripping membrane technique for lineament detection only . . . . .	95
3.7 Schematic representation of the rolling ball algorithm used for background normalisation . . . . .	97
3.8 Digital ball . . . . .	97
4.1 Flow chart showing the different steps followed to complete lineament identification and analysis. . . . .	110
4.2 Geologic map of the Jibal Rumman (test site) area . . .	111
4.3 Structural sketch map for the study area . . . . .	116
4.4 Lineament map for the test site area, derived from the TM images . . . . .	128
4.5 Lineament map drawn from the ripping membrane technique resultant image for the test site . . . . .	129
4.6 Lineament map drawn from the rolling ball technique resultant image for the test site . . . . .	130
4.7 Lineament map drawn from the northeast-southwest directional high-pass filtered TM band 5 image . . . . .	131

4.8	Lineament map drawn from the northwest-southeast directional high-pass filtered TM band 5 image . . . . .	132
4.9	Lineament map drawn from the east-west directional high-pass filtered TM band 5 image . . . . .	133
4.10	Lineament map drawn from the north-south directional high-pass filtered TM band 5 image . . . . .	134
4.11	Lineament map drawn from non-directional high-pass filtered TM band 5 image . . . . .	135
4.12	Lineament map drawn from the TM band 5 image . . . . .	136
4.13	The rolling ball edge enhancement . . . . .	139
4.14	The spatial filtration enhancement . . . . .	140
4.15	Lineament map drawn from the MSS band 4 enhanced image . . . . .	143
4.16	The lineaments which were observed in the field . . . . .	146
4.17	Rose diagram of the azimuthal frequency distribution of lineaments in the first rock unit (granite rock) . . . . .	149
4.18	Rose diagram of azimuthal frequency distribution of the lineaments in the first rock unit (alkali granite rock) area . . . . .	151
4.19	Rose diagram of the azimuthal frequency distribution of all the lineaments in the second rock unit . . . . .	152
4.20	Rose diagram of the azimuthal frequency distribution of all the lineaments in the test site area . . . . .	154
4.21	Rose diagram for distribution of total length for each interval of azimuthal angle for all the lineaments in the test site . . . . .	154
4.22	Rose diagram summarising the azimuthal frequency distribution of the test site drawn from the MSS data . . . . .	155
5.1	Flow chart showing the different steps followed for automatic watershed segmentation . . . . .	175
5.2	Hand traced segmentation map based on TM data for the first extract are . . . . .	180
5.3	Hand traced segmented map based on TM data for the second extract area . . . . .	185
6.1	Flow chart of processing used in automatic	

	line and lineament feature extraction method . . . . .	199
6.2	Hand traced map segmentation based on the TM data, for the first extract . . . . .	206
6.3	Lineament map identified from Plate 6.1(a) visually tracing method for first (TM) extract . . . . .	210
6.4	Rose diagram of the azimuthal frequency distribution of the lineaments in the first (TM) extract . . . . .	213
6.5	Possible of two pixel lineament in length connected to one pixel (undirected short lines) . . . . .	214
6.6	Hand traced segmentation map based on TM data for the second (TM) extract . . . . .	215
6.7	Lineament map drawn from Plate 6.5(a) by visually tracing method for the second (TM) extract . . . . .	221
6.8	Rose diagram of the azimuthal frequency distribution of the lineaments in the Hadn Formation region . . . . .	222
6.9	Rose diagram of the azimuthal frequency distribution of the lineaments in the second (TM) extract . . . . .	224
6.10	Visually traced lineament map identified from Plate 6.9(a) . . . . .	228
7.1	Suppression of illumination difference as a ratio image . . . . .	237
7.2	Spectral curves of the two objects A and B; $\tau_1$ and $\tau_2$ being the two sensor spectral bands . . . . .	239
7.3	Reflectance spectra of rock and mineral samples related to Landsat MSS TM spectral bands . . . . .	244
7.4	Geologic map for the first test site (Wadi ad Duwadimi area) . . . . .	254
7.5	Geologic map for the second test site area (Wadi Al Qahad area) . . . . .	260
7.6	Geologic map for the third test site (Jabal Muwaysil area) . . . . .	265
8.1	Resolution cells 1 and 5 are $0^\circ$ (horizontal) nearest neighbours to resolution cell; resolution cells 2 and 6 are $135^\circ$ nearest neighbours; resolution cells 3 and 7 are $90^\circ$ nearest neighbours; and resolution cells 4 and 8 are $45^\circ$ nearest neighbours to * . . . . .	280

## LIST OF TABLES

	<u>Page</u>
1.1 Idealised mineral assemblages associated with alteration zones . . . . .	17
1.2 Summary of precambrian rock units in the Arabian Shield . . . . .	31
1.3 Summary of the rock units in the study area in respect to their age . . . . .	36
2.1 Thematic Mapper spectral bands . . . . .	50
2.2 SPOT satellite details and HRV sensor . . . . .	55
2.3 The details of all the satellite images used in this study . . . . .	56
2.4 Shuttle Imaging Radar-B (SIR-B) system characteristics . . . . .	65
3.1 Scale of some linear traces without obvious displacements . . . . .	83
4.1 The comparison between the different individual enhanced image results regarding the lineament type and number . . . . .	118
4.2 Comparisons between the spatial filtration technique and the new contextual techniques . . . . .	138
4.3 The total number and the lineaments detected in each rock unit . . . . .	150
7.1 Common ratios used in discrimination of surface types . . . . .	240
7.2 All the false colour composites (FCC's) that have been tested in this study . . . . .	248
7.3 The common single ratios used in rock discrimination and their purpose . . . . .	249
7.4 All the colour ratio composites (CRC) have been examined in this study . . . . .	250
7.5 Showing different TM bands (bands 1-5 and 7) combinations from the optimum index factor (OIF) for all the selected test site images . . . . .	251
7.6 Selected rock types from the three test sites and their brightness in specific single ratio . . . . .	252
8.1 Example data and derived grey-tone spatial dependency matrices . . . . .	278

## LIST OF PLATES

	<u>Page</u>
4.1 The Hadn Formation in the field . . . . .	112
4.2 The Alkali granite in the field . . . . .	114
4.3 Contrast-stretched TM band 5 for the test site (Jibal Rummàn) area . . . . .	119
4.4 Edge enhanced images using the contextual techniques for the test sites; (a) ripping membrane, (b) rolling ball . . . . .	120-121
4.5 Edge enhanced images using spatial filtration for the test site . . . . .	122-127
4.6 Contrast stretched MSS band 4 for the test site (Jibal Rummàn) area . . . . .	141
4.7 Edge enhanced images for MSS band 4 using the new contextual techniques for the test site (Jibal Rummàn) area; (a) rolling ball technique, (b) ripping membrane technique . . . . .	142
5.1 Lineally contrast stretched TM band 5 for the first extract area . . . . .	181
5.2 Three false colour composite image of TM band 7,5 and 4 in red, green and blue respectively. These images were smoothed by the ripping membrane technique . . . . .	182
5.3 The resultant image of ripping membrane/Laserscan image segmentation method for the first extract . . . . .	184
5.4 Linearly contrast stretched TM band 5 for the first extract area . . . . .	186
5.5 Three false colour composite of TM band 7, 5 and 4 in red, green and blue respectively for the second extract area. These images were smoothed by the ripping membrane techniques . . . . .	187
5.6 The resultant image of the ripping membrane and Laserscan image segmentation methods for the second extract area . . . . .	189
6.1 Preprocessed image using the rolling ball technique for the first TM extract . . . . .	207
6.2 Binary image for the first (TM) extract. This image	

	is resultant from a single threshold process for Plate 6.1a . . . . .	208
6.3	The resultant image of ripping membrane/Laserscan image segmentation method for the first (TM) extract . .	208
6.4	Lineament map produced by the automatic method from the first (TM) extract . . . . .	211
6.5	Preprocessed image using the rolling ball technique for the second (TM) extract . . . . .	217
6.6	Binary image for the second (TM) extract. This image is resultant from a single threshold process for image in Plate 6.5(a) . . . . .	218
6.7	The resultant image of ripping membrane/Laserscan image segmentation method for the second (TM) extract. All the small labelled regions were eliminated . . . . .	218
6.8	Lineament map produced by the automatic method for the second (TM) extract image . . . . .	220
6.9	Preprocessed image using the rolling ball technique for the SPOT extract . . . . .	226
6.10	Binary image for the SPOT extract. This image results from a single threshold process for image in Plate 6.9(a) . . . . .	227
6.11	Lineament map produced by the automatic method from the SPOT image . . . . .	228
6.12	One of the Hadn Formation (hu) spots within the alkali granite area (ag) . . . . .	231
7.1	False colour composite of TM bands 7, 5 and 3 in red, green and blue respectively, covering the first test site (Wadi ad Duwadimi) area . . . . .	256
7.2	The two Cenozoic basalt lavas in ground base view; (a) Lava (A), (b) Lava (B) . . . . .	257
7.3	False colour composite of TM bands 5, 3 and 1 in red, green and blue respectively, covering the second test site (Wadi Al Qahad) area . . . . .	263
7.4	Digitally enhanced TM images for third test site (Jabal Muwayhsil) area; (a) False colour composite (FCC) of TM band 7, 4 and 1 in red, green and blue respectively; (b) Colour composite (CRC) of 7/5, 5/4 and 4/2 in red, green and blue respectively . . . . .	267

8.1 Linearly contrast stretched TM band 5 image for the first test site (Wadi ad Duwadimi) area . . . . . 289

8.2 The resultant image of applying the SGLDM measure for the first test site (Wadi ad Duwadimi) area, (a) Entropy measure, (b) Inverse difference moment (IDM) . . . . . 290

8.3 Linearly contrast stretched TM band 5 for the second test site (Wadi al Qahad) area. (b) Resultant image from applying the sum entropy of the SGLDM measures for the second test site area . . . . . 292

**CHAPTER ONE**  
**INTRODUCTION**

- 1.1 INTRODUCTION
- 1.2 PURPOSE OF PRESENT STUDY
- 1.3 STRUCTURE OF THE THESIS
- 1.4 SPECTRAL REFLECTANCE OF ROCKS AND  
MINERALS-BASIC CONCEPT
- 1.5 DEFINITION OF CONTEXTUAL INFORMATION
- 1.6 LOCATION AND DESCRIPTION OF STUDY AREA
- 1.7 GEOLOGY
  - 1.7.1 GEOLOGY OF THE ARABIAN SHIELD
  - 1.7.2 NAJD FAULT SYSTEM
  - 1.7.3 GEOLOGY OF THE STUDY AREA

### 1.1 INTRODUCTION:

Remote Sensing can be defined as the acquisition of information without direct contact. In addition, there is frequently an implication that the systems used will provide the information in a geometrically coherent fashion. Thus, images acquired using electromagnetic radiation as the intermediary between the observer and observed are obviously the essence of remote sensing.

The process of acquiring the information about the earth's surface may be divided into two parts:

1. The platforms and systems used to generate the images.
2. The techniques used to extract from the images the information needed.

The first part involves the use of aircraft and satellites (e.g. Landsat) which may carry a variety of sensor systems. These systems frequently generate digital images. The second part in the process involves the use of computers and software to analyse the digital data.

Remote Sensing techniques are multivariate, multispectral, multiplatform, multiscale, multienhancement, multiregional and multidisciplinary. The images obtained permit scientists in many different fields (e.g. geography, geology, forestry, engineering, etc.) to observe previously unobserved objects.

Image processing was first applied to geological studies in

the 1970's, primarily with Landsat MSS data, although earlier Skylab data was also digitally processed. Many of the standard techniques were first described in the classic paper of Rowan (1975). Comprehensive coverage of both optical and digital image processing techniques as they are applied to geological studies, can be found in Seigal and Gillespie, 1980; Williams, 1983; and more recent texts with useful information include Drury, 1987; Sabins, 1987; and Gupta, 1991.

Multispectral data has shown tremendous potential for applications in various branches of geology - structure, mineral and oil exploration, geomorphology, lithological mapping, stratigraphical delineation, geo-environmental studies, etc.

However, the contextual and textural information contained in images has not been fully exploited, and this thesis is intended to remedy this deficiency. This chapter starts with a brief discussion of the purpose and the structure of this thesis. Next follows a discussion of the concept of spectral and contextual information in remote sensing. This is followed by general geological description of the Arabian Shield, Najd Fault System and the study area.

## **1.2 PURPOSE OF PRESENT STUDY**

The aim of this study is to investigate the use of satellite imagery (Landsat TM, MSS and SPOT) and radar (Shuttle Imaging Radar SIR-B) using the digital image processing techniques for

geological studies.

The primary aim is an evaluation of the relative merits of spatial information for geological studies for part of the Arabian Shield. In this thesis spatial information will be interpreted as a context and texture, following the suggestion made by Gurney and Townshend (1983).

Spatial information has been neglected compared to the spectral information in geological studies and in an attempt to redress the balance, several new contextual techniques were developed and tested:

1. Rolling ball transformation (technique).
2. Ripping membrane (relaxation) technique.
3. Automatic Watershed image segmentation method.
4. New method for image segmentation.
5. Automatic lineament extraction and analysis method.

Several traditional image processing techniques, using spatial data (spatial filtration and texture analysis techniques), and using spectral data (e.g. contrast manipulation, arithmetic operations, box classification, maximum likelihood classification, principal components and decorrelation stretch) are also evaluated. A careful comparison was made between the results obtained by all the techniques (for lineament detection and analysis and for lithological discrimination) to evaluate their relative merits.

A further objective was the production of lineament maps, and lineament rose diagrams, and lithological discrimination for a few selected test sites. The results were compared with existing geological maps and field data.

The Arabian Shield forms a large part of the Arabian Peninsula and is composed of different lithologies and structure. Therefore, it provides a unique area for testing and evaluating remote sensing techniques. There have been a few geological investigations of the Arabian Shield using Landsat Multispectral Scanner (MSS) (e.g. Boldget et al 1978; Boldget and Brown, 1982; Davis and Grolier, 1984) and Thematic Mapper (TM) (e.g. Loughlin and Tawfiq, 1985; Bird et al., 1985; Davis and Berlin, 1989; Al-sari, 1989 and Qari, 1990). TM imagery has been used for lineament mapping, (e.g Qari, 1990). The shuttle imaging radar (SIR-B) has been used for lineament detection and for ground water studies by Berlin et al., (1987). However there is still a need to investigate the Arabian Shield using remote sensing in order to study or to discover ore deposits, ground water, and to further the study of the geological structure. In this study the study area is part of the Arabian Shield.

### **1.3 STRUCTURE OF THE THESIS**

This thesis contains nine Chapters. Chapter 1 contains an introduction and general geology of the Arabian Shield and the study area. Chapter 2 explains the general preprocessing techniques for remotely sensed data. Chapter 3 introduces the

general definition of lineament and reviews the known image processing techniques and the new contextual techniques in lineament detection and analysis.

Chapter 4 contains a comparison between the new contextual techniques with the traditional, mainly filter based techniques for lineament detection and analysis. Chapter 5 contains the examination of the automatic watershed image segmentation and new method for image segmentation in rocky area. Chapter 6 discusses the contextual information and techniques in automatic lineament and linear feature extraction. Chapter 7 examines the application of spectral information in rock discrimination in an arid area. Chapter 8 consists of the use of texture analysis in rock discrimination and image classification. Chapter 9 is the conclusion and future work.

#### **1.4 SPECTRAL REFLECTANCE OF ROCKS AND MINERALS: BASIC CONCEPT**

The source of electromagnetic radiation (EMR) is either the sun or the earth's emitted heat, or an artificial source such as microwave radar. The EMR is measured and recorded by sensors that may be in the form of a camera, radiometer, or electronic sensor on board a platform such as an aircraft/satellite. The EMR occurs as a continuum of wavelengths and frequencies called the electromagnetic spectrum (Figure 1.1). It extends from short wavelengths with high frequency (eg. ultraviolet) to long wavelengths with low frequency (eg. radio waves). Remote sensing commonly uses EMR from about  $0.4\mu\text{m}$  to about 30 cm (Gupta, 1991).

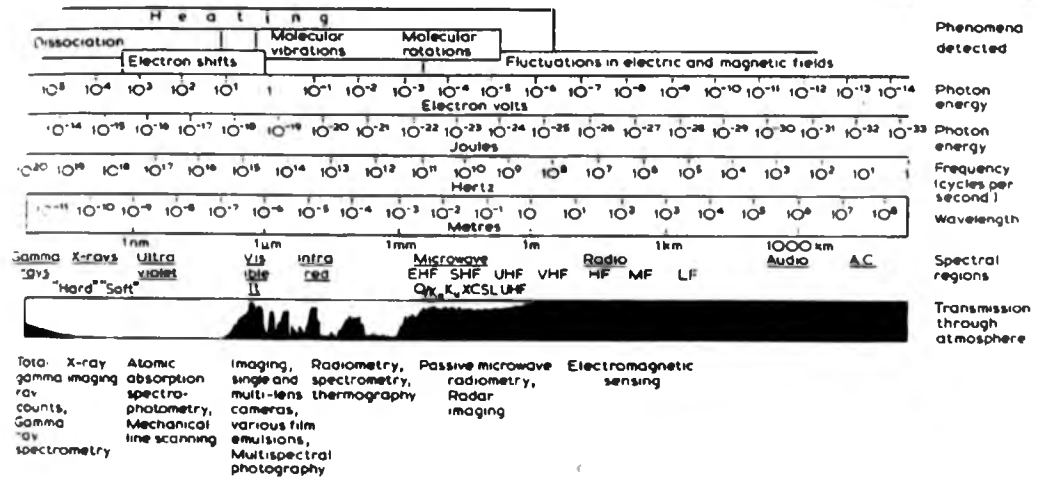


FIGURE 1.1

The electromagnetic spectrum, The scales give the energy of the photons corresponding to radiation of different frequencies and wavelengths. The product of any wavelength and frequency is the speed of light. Phenomena detected at different wavelengths are shown and the principal techniques for environmental remote sensing. (From: Barrets and Curtis, 1982).

In order to understand how information can be gathered that is useful for rock discrimination or mapping, it is necessary to understand the interaction between electromagnetic radiation and the rocks or minerals being observed.

Spectral reflectance is defined as the ratio of light reflected from light incident on an object, and is a function of wavelength. The spectral reflectance and spectral emittance characteristics of rocks and minerals at different wavelength regions are the result of different physical and chemical properties (Goetz et al., 1983). The minerals making up the rock may be chemically simple or complex. Most of the minerals have a unique spectral reflectance curves, and the presence of absorption features in these curves is diagnostic of the presence of certain mineral types (Hunt, 1977, 1979; Hunt and Ashley, 1979; Hunt and Salisbury, 1970, 1971; Hunt et al., 1971). These features which appear in the visible and near infrared spectra of particulate mineral and rock may result from either electronic transition or vibrational transition (Hunt and Salisbury, 1970). The electronic processes, which occur predominantly in the visible near infrared, that produce absorption features, are:-

1. Transitions between energy levels which are the result of the interaction between a central atom and the crystal field. For example, (Figure 1.2) shows reflectance spectra of several iron bearing minerals, which show absorption features, due to electronic

transitions in ferrous ( $\text{Fe}^{+2}$ ) ions. The different wavelengths of the absorption features can be related to the co-ordination of the ferrous ions in the different minerals, the symmetry and degree of lattice distortion.

2. Electronic transitions between energy levels of the metal ion. A typical example is, again, iron. Ferric iron exhibits pronounced absorption features at around  $0.87\mu\text{m}$  and  $0.35\mu\text{m}$  (Gupta, 1991).
3. Charge transfer transitions are a special case of semiconductor behaviour, in which electrons do not enter into a conduction band but rather transfer from one atom to another and remain localised in the lattice or, in other words, the charge transfer is the absorption of energy which results in the migration of electrons between neighbouring ions. It can occur in a mineral and it is most commonly involved in the migration of electron from iron (Fe) to oxygen ( $\text{O}_2$ ) and results in the Fe-O transfer band at wavelengths shorter than about  $0.55\mu\text{m}$ . (Figure 1.3). This charge transfer is common in many iron containing minerals and is responsible for a steep decline in reflectance towards the blue end of the spectrum.

Vibrational processes, which yield features in the infrared regions of the spectrum, are the result of the excitation of overtones and combination tones of the fundamental vibrational mode of anion groups (such as silicates, carbonate and

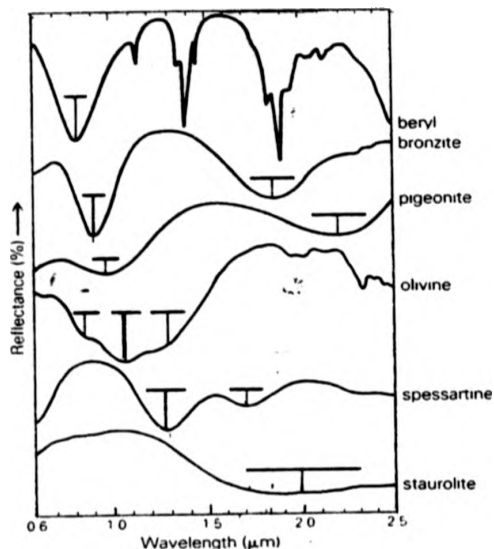


FIGURE 1.2

The number and position of features due to electronic transitions in iron minerals (T-shaped symbols) depend on the co-ordination of  $Fe^{2+}$  ions in the molecular structures of the minerals concerned. The spectra are offset vertically for clarity. (From: Drury, 1987).

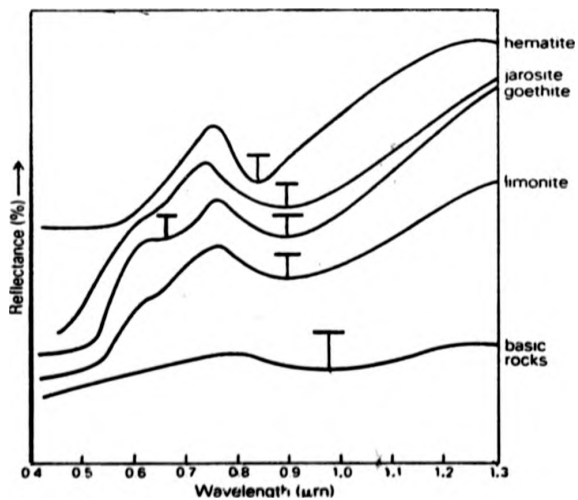


FIGURE 1.3

Iron oxides and hydroxides display absorption features due to crystal field effects. (T-shaped symbols) and Fe-O charge minerals superimposes similar features on clay spectra. The spectra are offset for clarity. (From: Drury 1987).

hydroxyls). These vibrational modes also include the vibrations which are associated with the lattice structure of the crystal (Hunt and Salisbury, 1970).

The most important vibrational transition processes are those associated with presence of hydroxyl ( $\text{OH}^-$ ) ions or water molecules, either bound in structure or present in fluid inclusions. This fundamental  $\text{OH}^-$  stretching mode may form combination tones with other components of the lattice, such as  $\text{Al} - \text{OH}$  or  $\text{Mg} - \text{OH}$  bending modes, which produces an absorption features at  $2.2 \mu\text{m}$  or  $2.3 \mu\text{m}$  respectively (Figure 1.4). Such features are prominent in mica and clay minerals and provide a signature for hydroxylated minerals.

The carbonate minerals (eg. calcite, magnesite, siderite and dolomite) display a series of features between  $1.6 \mu\text{m}$  to  $2.5 \mu\text{m}$  which are due to combinations and overtones of  $\text{CO}_3$  ion (Hunt and Salisbury, 1971).

Rocks are assemblages of minerals and therefore their spectra are composites of their constituents. Laboratory spectra of different minerals and rocks (igneous metamorphic and sedimentary) have been studied by Hunt and Salisbury, (1976a, 1976b); Hunt et al., (1970, 1974) and Salisbury and Hunt, (1974), in the visible and near infrared (Figures 1.5 and 1.6 a,b). Figure 1.5 shows how the abundance of opaque minerals in igneous rocks can be used as an indicator for rock classification (Hunt et al.,

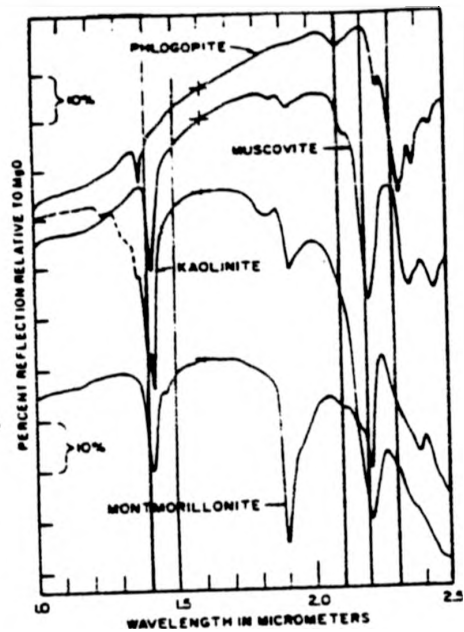


FIGURE 1.4

Features due to vibrational process in the spectra of four hydroxyl-bearing minerals commonly present in hydrothermally altered rocks. Spectra are displaced vertically. (From: Hunt and Ashley, 1979).

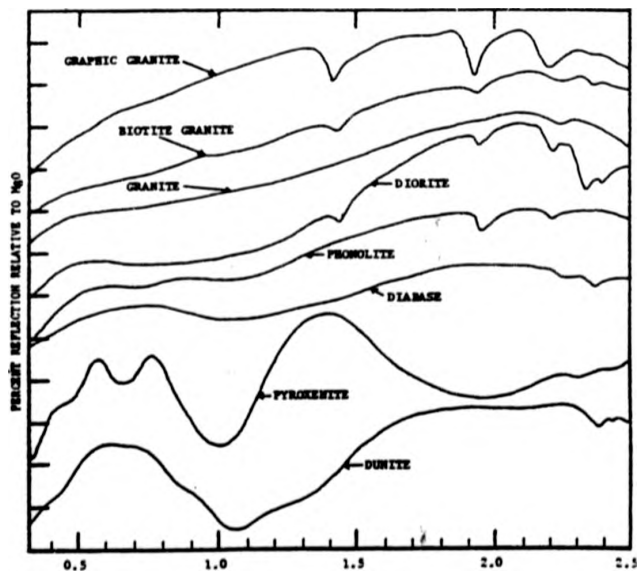


Figure 1.5 Bidirectional reflectance spectra of igneous rocks, separated vertically for clarity. Reflectance divisions are 10%. (From: Salisbury and Hunt, 1974).

1974; Salisbury and Hunt, 1974). From this figure it is clear that the degree of acidity, which varies from granite at the top to mafic rocks, at the bottom, affects the spectral behaviour.

Graphic granite displays absorption features at  $1.4\mu\text{m}$ ,  $1.9\mu\text{m}$  and about  $2.2\mu\text{m}$ , which are due to vibrational overtones and combination of  $\text{H}_2\text{O}$  and  $\text{OH}^-$  (hydroxyl). In biotite granite and granite the absorption features are less obvious, because they contain less water. Intermediate and basic (mafic) rocks contain more opaque minerals (magnetite) and less water than the above. This affects the spectral absorption and causes a strong absorption at  $1.0\mu\text{m}$  and near  $2.0\mu\text{m}$ .

Figure 1.6a shows the typical laboratory spectra (in visible and near infrared) of common metamorphic rock types. The broad absorption, due to ferrous ion, is prominent in rocks like hornblende-schists, tremolite-schists, marble, and quartzite. Marble contains carbonate which gives distinctive features in the visible and near infrared. Figure 1.6b shows laboratory spectral responses of important sedimentary rock types in the visible and near infrared.

Whilst it would be an advantage to use all wavelengths, unfortunately, the atmosphere absorbs many wavebands, including the  $1.4 - 1.9\mu\text{m}$  region, and therefore it is difficult to utilise this waveband in rock discrimination. (See Figure 1.1 for other significant atmospheric absorption regions).

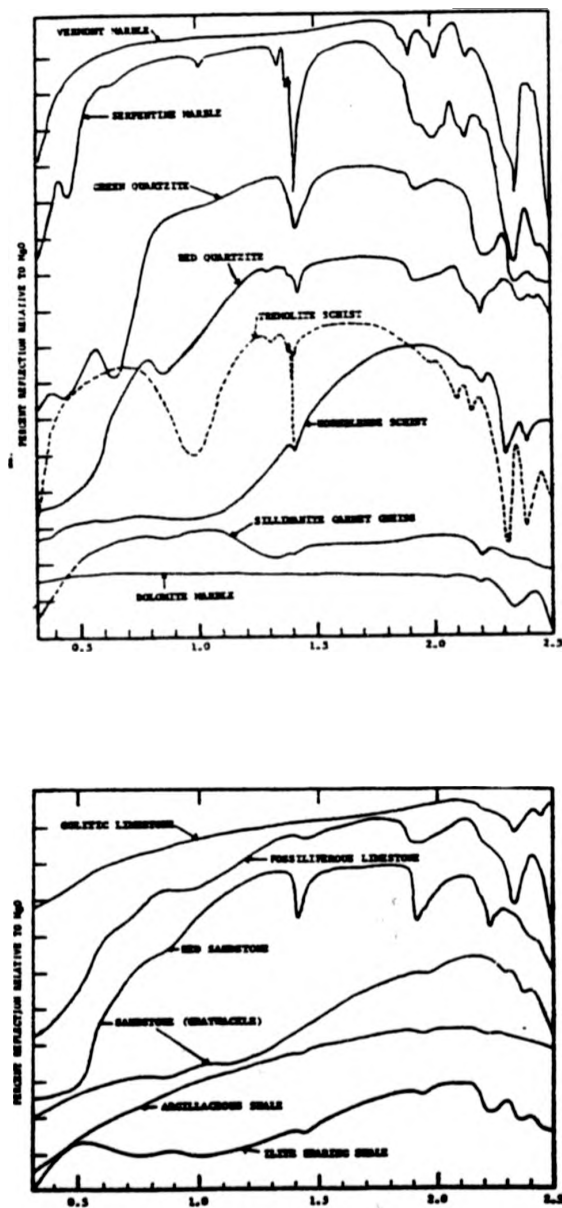


FIGURE 1.6  
 Laboratory reflectance of selected rocks of (a) metamorphic rock  
 and (b) sedimentary rock. (Reflectance divisions are 10%).  
 (From Salisbury and Hunt, 1974).

In rock discrimination, weathered minerals play a very important role in controlling the spectral reflectance of the real rock surface. Buckingham and Sommer (1983) showed that, in visible and near infrared, it is only the top  $0.50\mu\text{m}$  of surface materials which interact with the radiation, therefore it is important to understand the contribution of the weathered surface (such as clays and oxides), and its relationship with underlying rock. In arid areas desert varnish is prevalent. Amorphous silica, alumina, iron and manganese rich compounds are predominate constituents of this varnish (Spetz et al., 1989).

Alteration zones are important guides for mineral exploration. During Late Stage vulcanism, sulphide rich fluids are injected into the host rock. The injection process and the subsequent weathering alters the mineralogy of the host rock in zones surrounding the sulphide. The most intensely altered rock occurs adjacent to the sulphide injection. The degree of alteration grades away from the sulphide into unaltered host rock. When viewed at the surface, hydrothermally altered rock presents a bleached appearance and the rock is often coated with an iron oxide layer from the weathered pyrite (Buckingham and Sommer, 1983). Table 1.1 indicates that the minerals may occur in idealised alteration zones. In this table, most of these minerals with an asterisk produce recognisable spectral features in the visible and near infrared region. Both absorption features, electronic and vibrational, are used as indicators for alteration (or unaltered) zones. The mineralogic differences

**TABLE 1.1**  
**Idealized Mineral Assemblages Associated**  
**with Alteration Zones**  
**(From Buckingham and Sommer, 1983).**

ZONE	MINERALOGY
Propylitic	Albitized plagioclase Chlorite* Epidote* Carbonate* Montmorillonite*
Argillic	Quartz Kaolinite* Chlorite* Montmorillonite*
Phyllic	Quartz Sericite Pyrite
Advanced argillic	Quartz Alunite* Pyrophyllite* Kaolinite-dickite opal* K-mica*
Silicified	Quartz Alunite* Pyrophyllite* Kaolinite-dickite* K-mica*

\* Minerals with asterisks produce recognisable spectral features in the visible and near infrared region.

give rise to spectral features, useful in the delineation of hydrothermal alteration (Buckingham and Sommer, 1983). But in arid lands the production of clays by weathering, will be slow, so the clay concentration can be very low in altered rock unless the clay has been inherited from a former humid geological period (Thomas pers.comm. 1992).

The thermal infrared between  $8\mu\text{m}$  and  $12\mu\text{m}$  is important for remote sensing (Kahle and Rowan, 1980). In this region of the spectrum, various vibrational transitions in non-silicates (mafic and ultramafic) produce spectral features that are different from those of silicates (felsic). From Figure 1.7 one sees that the position of the silicate emittance minimum shifts to longer wavelengths as the content of  $\text{Si-O}_2$  decreases. The position of the absorption feature is dependent on the extent of interconnection of the  $\text{Si-O}_2$  tetrahedra comprising the crystal lattice. The temperature of a surface can be estimated from the radiation emitted between  $8\text{-}14\mu\text{m}$ . The temperature of a rock surface is dependent on the rocks' thermal capacity and thermal conductivity and its emissivity which is also dependent on the nature of the rock. Thus, at any one instant in time, the surfaces of a variety of different rocks will be at different apparent temperatures. Whilst the precise temperature is not indicative of any one rock, nevertheless the rock differences can be easily identified. Thus temperature does provide some information of use in rock discrimination.

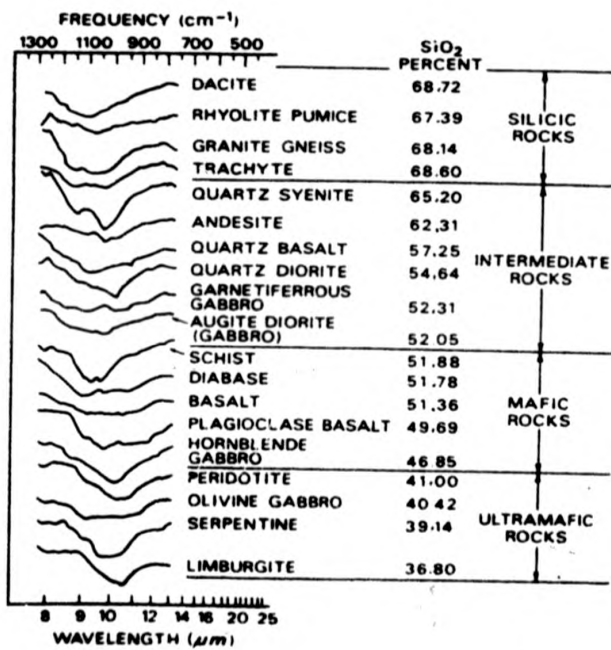


FIGURE 1.7 Emissivity spectra of silicate rocks.  
(From: Lo, 1987).

Microwave measurements in the region of 3 and 25 cm wavelength have been used in resource exploration (mineral exploration). Side Looking Airborne Radar (SLAR) and shuttle imaging radar (SIR-A-B), have been investigated but they cannot, as yet, help to identify rocks or minerals directly. (Section 2.4) Chapter 7 will be concerned with the use of spectral reflectance of rock in lithological discrimination.

### 1.5 DEFINITION OF CONTEXTUAL INFORMATION

Digital remote sensing images can be considered to contain three types of information:-

1. Spectral information from the interaction between the earth's surface and the electromagnetic radiations (Section 1.4, Chapter 7).
2. Spatial information, that represents the spatial organisation (arrangement) of pixels in the image. This has been divided into two types of information - textural and contextual (Gurney and Townshend, 1983).
3. The temporal information derived from different images for the same area at different times. This information can be used to monitor the temporal changes (i.e. sand dune movement, agriculture, urban, etc.).

The contextual information is spatial information and it is concerned with the relation between pixels and objects. It conveys information about the size, shape and position of objects in a scene (Oldfield and Elgy, 1987), and in addition, the rela-

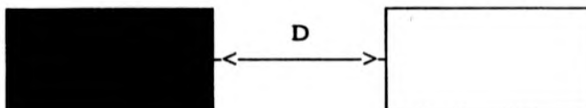
tionship of an object to other nearby objects (Mather, 1987). Also the context of a pixel (or group of pixels) in a remote sensing image can refer to its spatial relationships with other pixels in the image or sub-image (Gurney and Townshend, 1983). Thus, the contextual methods of analysis for any pixel may involve any other pixel or group of pixels in the same image (Haralick et al., 1973; Gurney and Townshend, 1983).

According to Gurney and Townshend, (1983) contextual (spatial) relationships have been categorised into four different types. These are:- distance, direction, connectivity and containment, and therefore the contextual information is not only a pixel based property, but, also it is region based property. (Figure 1.8).

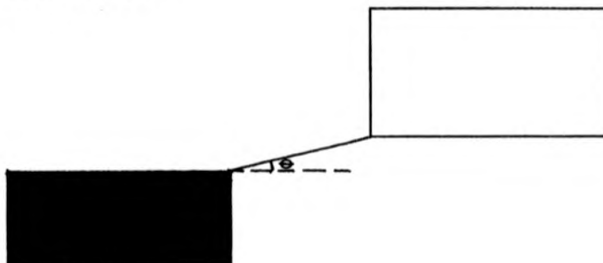
**Distance and Direction** - The distance and direction from any pixel to another set of pixels or objects of the same class, can be measured. These two relationships will be applied in Chapter 6 (Automatic Line and Lineament feature extraction method).

**Connectivity** - This relationship may be relevant, if there are pixels and other contiguous pixels of the same class, in an image.

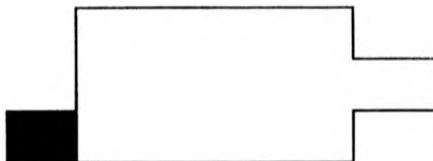
## 1. Distance



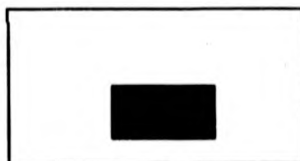
## 2. Direction



## 3. Connectivity



## 4. Containment



P The set of pixels of interest



S The set of pixels related to p

Figure 1.8 shows types of spatial relationship (From Gurney and Townshend, 1983).

**Containment** - This relationship may be relevant if there is an object surrounded by or contained within another object. Connectivity and containment can only apply where some preliminary segmentation of the data has been made (Chapter 5).

Alonso and Soria (1991), defined the contextual classifier as those image classification techniques that consider simultaneously the spectral and spatial characteristics (or information) of the image. The results of classification obtained from classification of satellite images, by the traditional methods, can be improved, if the spatial information is considered jointly with the spectral information (Swain et al., 1979).

The contextual methods are mainly used in human interpretation, and are not widely available in automated systems (Townshend, 1981 and Mather, 1987). These methods usually result in lower error rates, and seem to work particularly well in homogenous areas (Hjort et al., 1986).

Contextual methods have been used in remote sensing by many authors - (e.g. Swain et al., 1979, 1981; Siegal et al., 1980; Hjort and Mohn, 1984; Kittler and Föglein, 1984; Besag, 1986; Harris, 1985; Hjort et al., 1986; Oldfield, 1988; Alonso and Soria, 1991). Only one study concerned with geologic investigation has so far (Oldfield, 1988) used contextual classification, to classify different rock types in Argentina.

### 1.6 LOCATION AND DESCRIPTION OF THE STUDY AREA

The study area was located within the North Central part of the Arabian Shield, in Hail Province, Saudi Arabia (Figure 1.9). The area lies within latitudes between 26°00' and 27°00'N and longitudes 40°42' and 41°45'E and is part of the Wadi Ash Shu'bah quadrangle, Sheet 26E, (Geologic map scale 1:250000, compiled by Quick and Doebrich, 1987). The study area is very large. It occupies an area approximately 11,542 Km<sup>2</sup>.

The study area was crossed by a small road that connects Hail (city) and Al Madinah (city). There are very few graded service roads, and desert tracks provided the only access to most points in the study area.

In a physiographic sense, a considerable portion of the region has a relatively flat pediment surface with scattered hills. Altitude ranges from about 800 meters to nearly 1500 meters above sea level (Quick and Doebrich, 1987). Drainage is primarily to the south east, by way of tributaries of Wadi Ash Shu'bah, all the streams are intermittent and belong to the Wadi Ar-Rimah drainage system.

Most of the permanent settlements in the study area are located near Jibal Al Rumman, where ground water is available for agricultural activity. The natural vegetation is sparse, but there are unattended palm trees within the valleys.

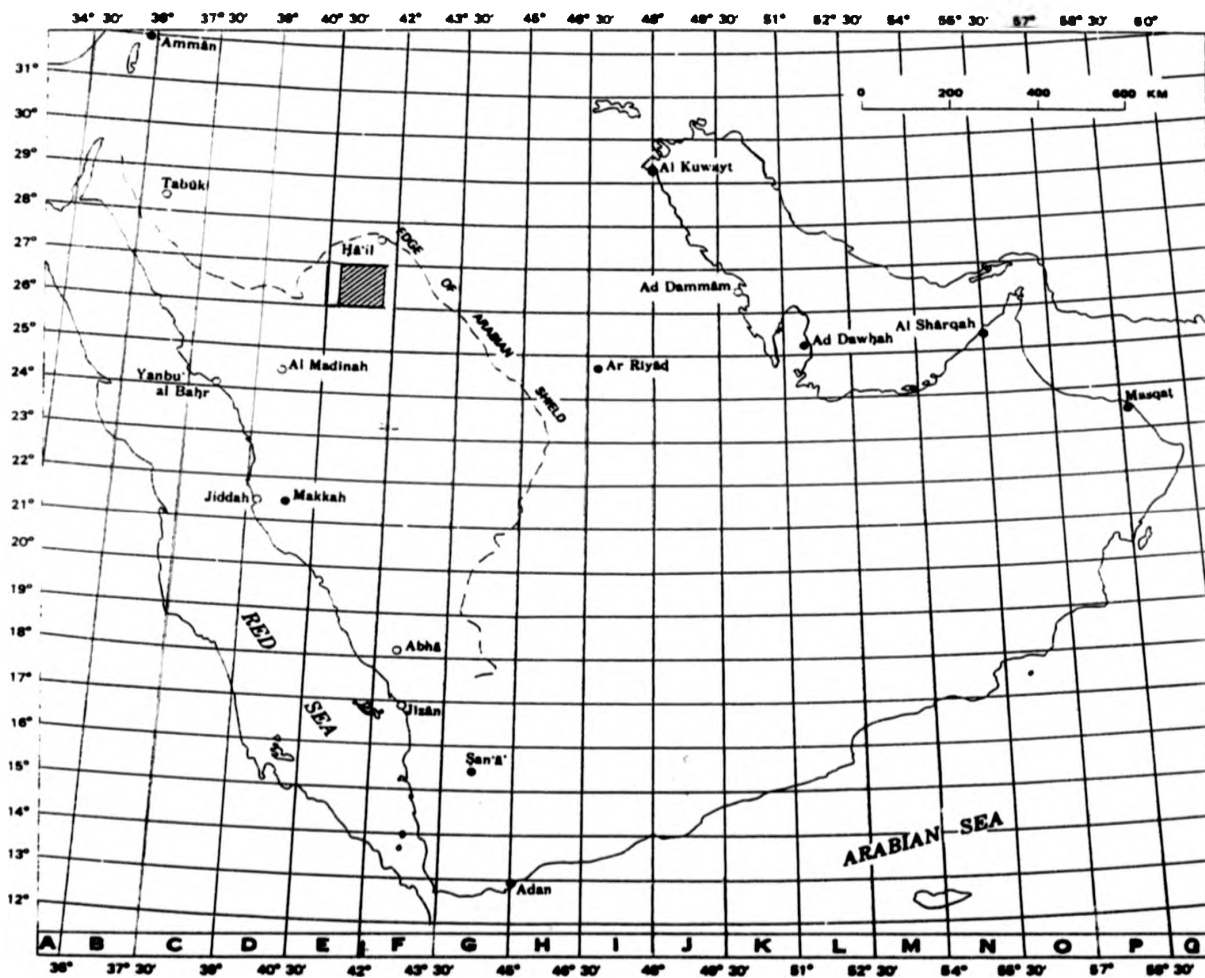


FIGURE 1.9

Index map of the Arabian Peninsula showing the location of the study area. (From: Quick and Doebrich, 1987).

## 1.7 GEOLOGY

This section contains a geologic description of the Arabian Shield, Najd Fault System, and the study area.

### 1.7.1 Geology of the Arabian Shield

The Arabian Peninsula, lying between Africa and Western Asia, has been of interest to geologists since the end of the last century. Its importance comes from its relationship to the rifting in the Red Sea, the separation of Arabia and Africa, continental drift, and plate tectonics.

The Arabian Peninsula can be divided into two parts; the Arabian Shelf and Arabian Shield. The Arabian Shelf is composed of sedimentary rocks, and has been divided into different formations and different ages (Figure 1.10). The Arabian Shield is the oldest massive rock body and occupies an area of about 770,000 Km<sup>2</sup>. It is located in the western part of the Arabian Peninsula and consists of basement rock, plutonic rock, sedimentary rocks and Tertiary Volcanics.

There are many theories about the accretion of the Arabian Shield. Gass (1977, 1981) and Camp (1984) have a tectonic model, which supposes that the main shield was formed from an oceanic island arc between about 700 and 670 Ma. The second model is "tectonic modification by arc magmatism" was proposed by Engel *et al.*, (1980).

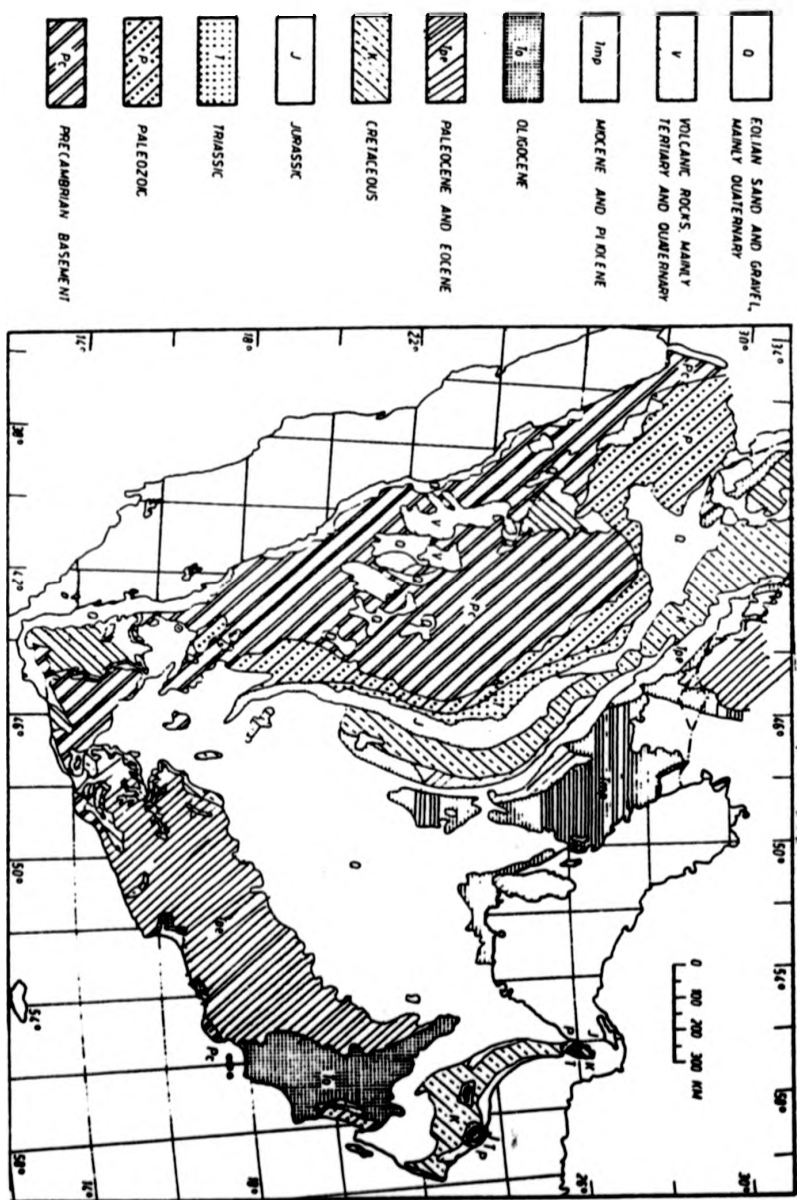


FIGURE 1.10

Generalised geologic map of the Arabina Peninsula. (From: Al-Siyari and Zötel, 1978).

Others have argued for purely tectonic models of the Arabian Shield. A discussion of these interpretations or argument is beyond the scope of the present study (for more detail see Gass 1977, 1981; Engel et al., 1980; Camp 1984; and Stoesser and Camp 1985).

The most recent theoretical model by Stoesser and Camp, (1985) proposes a microplate accretion model for the pan-African evolution of the Arabian Shield. They believe their model resolves many differences between earlier models. In this model, during the late Proterozoic, the Arabian Shield was divided into five distinct terranes (microplates), separated by four suture zones (Figures 1.11-1.12). Three intraoceanic islands (terranes) in the west of the shield (Hijaz, Asir, Midyan), are separated by two suture zones; the Yanbu suture zone and the Bir Umq suture zone. There are two continental affinity terranes in the eastern shield (Ar-Rayan and Afif). These two terranes are separated by one suture zone (Al-Amar suture zone).

The Hijaz terrane contains three superimposed magmatic assemblages. First, oceanic island arc sequence, this assemblage is the oldest, and the rocks here are well exposed along the terrane's southern margin, where they are associated with tectonically emplaced and dismembered ophiolite in the Bir Umq suture zone (Stoesser and Camp, 1985). The second, the Hijaz arc assemblage, was the result of southeast subduction at the Yanbu

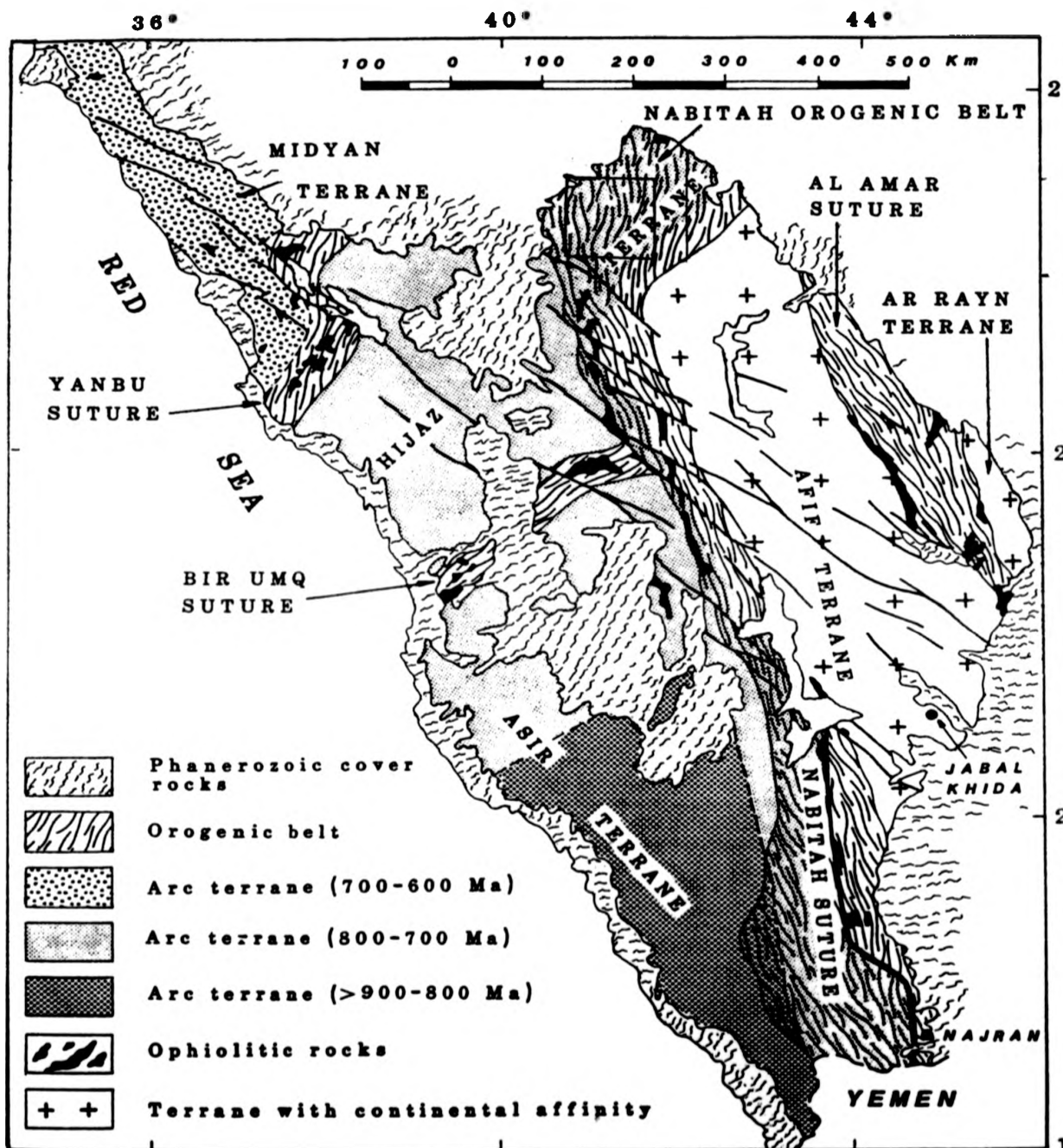


FIGURE 1.11

Tectonic sketch map of the Arabian Shield showing terranes and suture zones. Northwest-trending solid lines indicate fractures of the Najd Fault System. (From: Stoesser and Camp, 1985). Study area is shown by the superimposed rectangle

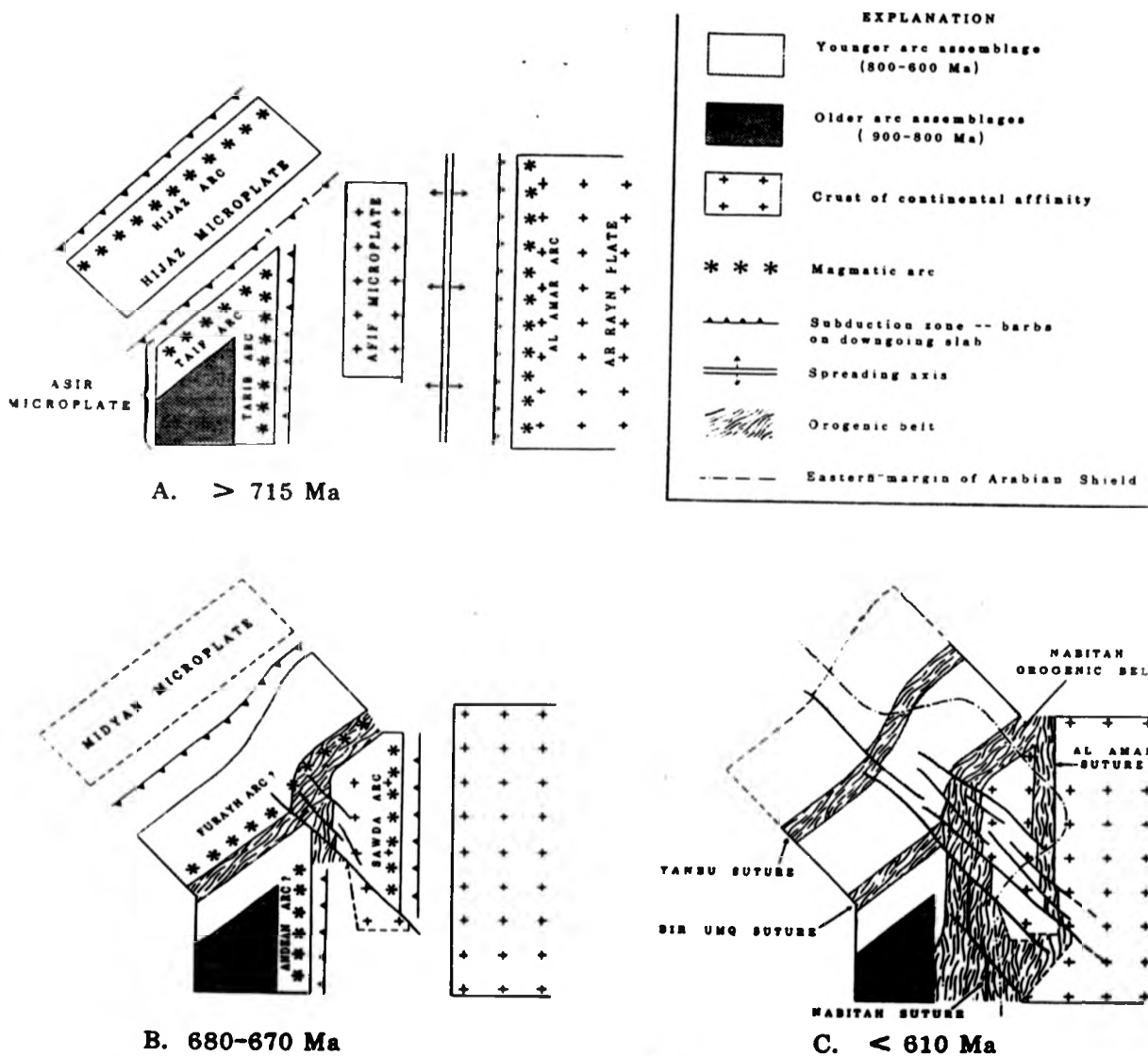


FIGURE 1.12 Schematic tectonic diagrams showing evolutionary stages of Arabian Shield development: A. formation of younger magmatic arcs, B. terrane accretion, and C. intracratonic deformation. Northwest-trending solid lines are fractures of the Najd fault system. (From: Stoesser and Camp, 1985).

suture. The Hijaz arc magmatism was followed by the Samran orogeny (major orogenesis), during which the northwest-trending Samran fold belt was formed by arc collision along the Bir Umq suture zone (Stoeser and Camp, 1985). The third magmatic assemblage occurs as a northeast-trending belt of volcanics, deposited over the older subaqueous rocks of the sutured Hijaz terrane. The northeastern part of the belt is characterised by rhyolitic volcanic rocks (Shammar Group) that were deposited over the remobilised crust of the Nabitah orogenic belt (Stoeser and Camp, 1985).

One of the explanations of the vulcanism within the Arabian shield is that it formed during oblique crustal extension, related to a period of intracratonic shear (final tectonism), and final cratonization events of the Arabian Shield. The Hijaz cycle presents a complex strike slip faulting in late Proterozoic and early Phanerozoic time called Najd fault (faulting) system (Section 1.7.2).

Most of the workers in the Arabian Shield have divided the rocks into ten rock units (Table 1.2). These are Baish-Baha Group, Jeddah Group, Ablah Group, Fatimah Group, Al Ays Group, Silasia formation, Hulaban Group, Murdama Group, Shummer Group and Jubalah Group (for more detail see Brown et al., 1989).

#### **1.7.2 The Najd Fault System (NFS):**

The Najd Fault System (NFS) is a strike-slip fault system

which extends over the Arabian Shield. The NFS events or Najd orogeny was the final cratonisation events of the Arabian Shield. This can be seen in the long northwesterly trending left lateral faults that have displaced some rock units as much as 240 Km. The total possible length of the NFS is more than 2000 Km with an annual movement of 0.5 cm (Moore, 1979; Agar, 1987). The igneous intrusion associated with NFS tectonic event, has produced dike swarms and small plutons. There has been widespread hydrothermal activity in some areas giving rise to small ore deposits (Moore, 1979).

Secondary structures recognised in association with NFS include, strike and oblique slip faults, normal and reverse fault structures, thrusts and folds (Moore, 1979; Agar, 1987). The major fractures have weathered and formed valleys in most cases. Moore (1979) has divided the associated minor structures within the NFS into two types: the first pre-date, or are independent of major faults, and the second, are those minor structures related to the master structure. The most important example of the first type is the Riedel Shear Fault, which is a set of subordinate wrench faults, which form in a zone of simple shear, not marked by a continuous fault. The second type consists of minor structures occurring around the termination of major fault strands. These structures can be found in massive country rock (Moore, 1979). Figure 1.13 shows the outcrop traces of major faults of the NF System in the Arabian Shield and

**TABLE 1.2**  
**Summary of Precambrian Rock Units**  
**in The Arabian Shield**  
 (Summarised from Brown et al 1989)

ROCK UNITS	MAJOR ROCK TYPE
JUBALAH GROUP	Sedimentary beds Volcanic clastic
SHAMMAR GROUP	Undivided
MURDAMA GROUP	Undivided
HALABAN GROUP	Undivided
SILASIA FORMATION	Slate, Shale, Schist, Marble, arkose and conglomerate
AL AYS GROUP	Clastic volcanic sequence
FATIMAH GROUP	Clastic volcanic sequence
ABLAH GROUP	Metasedimentary and metavolcanic rock
JEDDAH GROUP	Undivided
BAISH-BAHAH GROUP	Undivided metasedimentary and metavolcanic sequence largely tholeiitic.

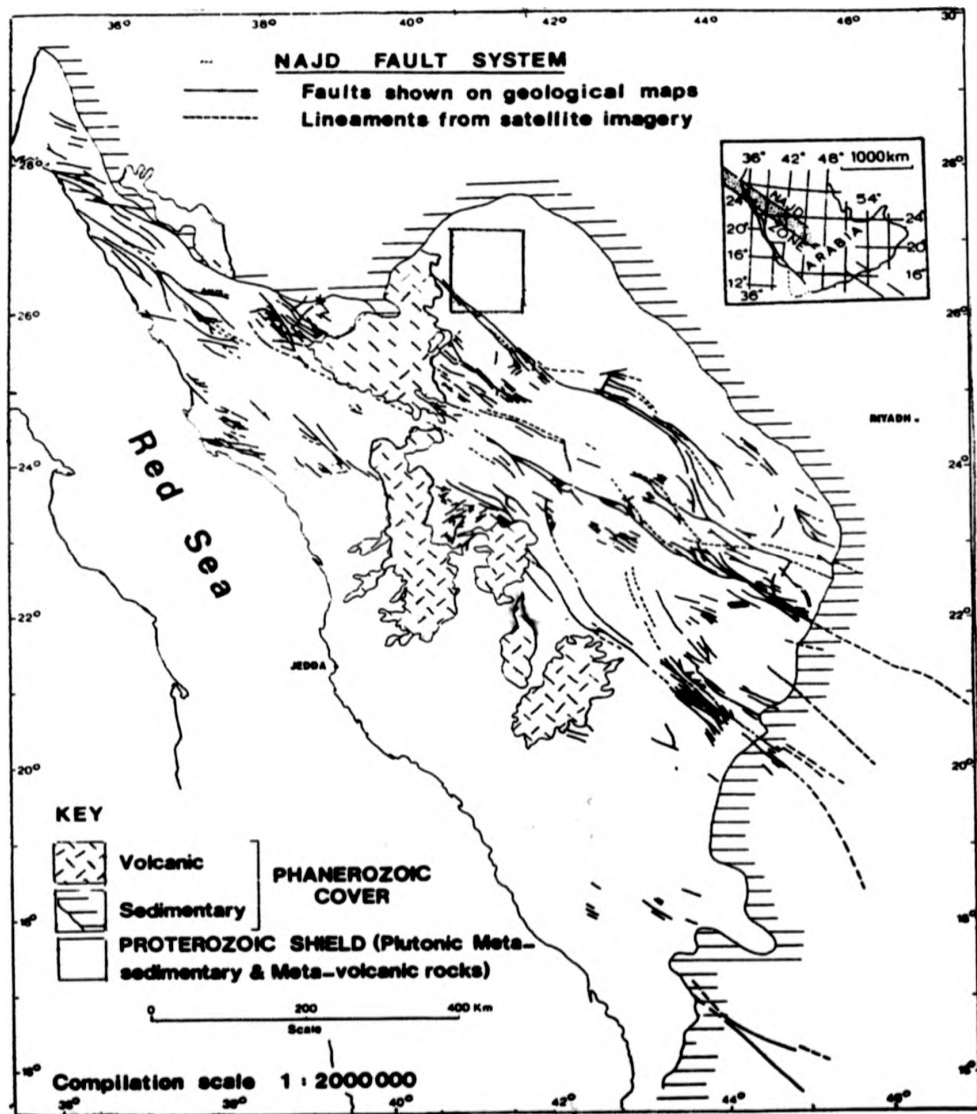


FIGURE 1.13

Outcrop traces of major faults of the Najd Fault System in the Arabian Shield. Insert. Location map showing the Najd Belt prior to Tertiary rifting in the Red Sea region. (From Moore, 1979). The study area is shown by superimposed rectangle.

(Figure 1.14) shows the Aeromagnetic lineaments are attributable to structures in the NF System. The study area is shown by the rectangle. For more details about NFS see Moore 1979; Agar 1987; Sultan *et al.*, 1988; and Duncan *et al.*, 1990).

### 1.7.3 General Geology of the Study Area

The study area is located in the North central part of the Arabian Shield of Saudi Arabia. It is underlain by rocks that are late Proterozoic to Cenozoic age and composed of different plutonic rocks and six distinct groups of volcanic and sedimentary rocks (see geologic map for the study area in Appendix 1).

The study area is located in the Hijaz terrane and within the Nabitah orogenic belt (Figure 1.11). The study area has been named as the Wadi ash Shu'bah area. This area has been covered by geologic maps of two different scales: six 1:100,000-scale geologic map quadrangles (reconnaissance studies) cover the study area, (Quick, 1983; 1984; 1985; Leo, 1984; O'Neill and Ferris, 1985; and Williams and Simons, 1985 and one 1:250,000-scale geologic Quick and Doebrich, 1987). All the names of the rock units and symbols used in this thesis are derived from the recent geologic map and report, (ie, Quick and Doebrich, 1987).

Quick and Doebrich, (1987) have divided all the rock units in the study area as follows: (1) Precambrian volcanic and sedimentary Formations, (2) Precambrian Intrusive rocks, (3) Late

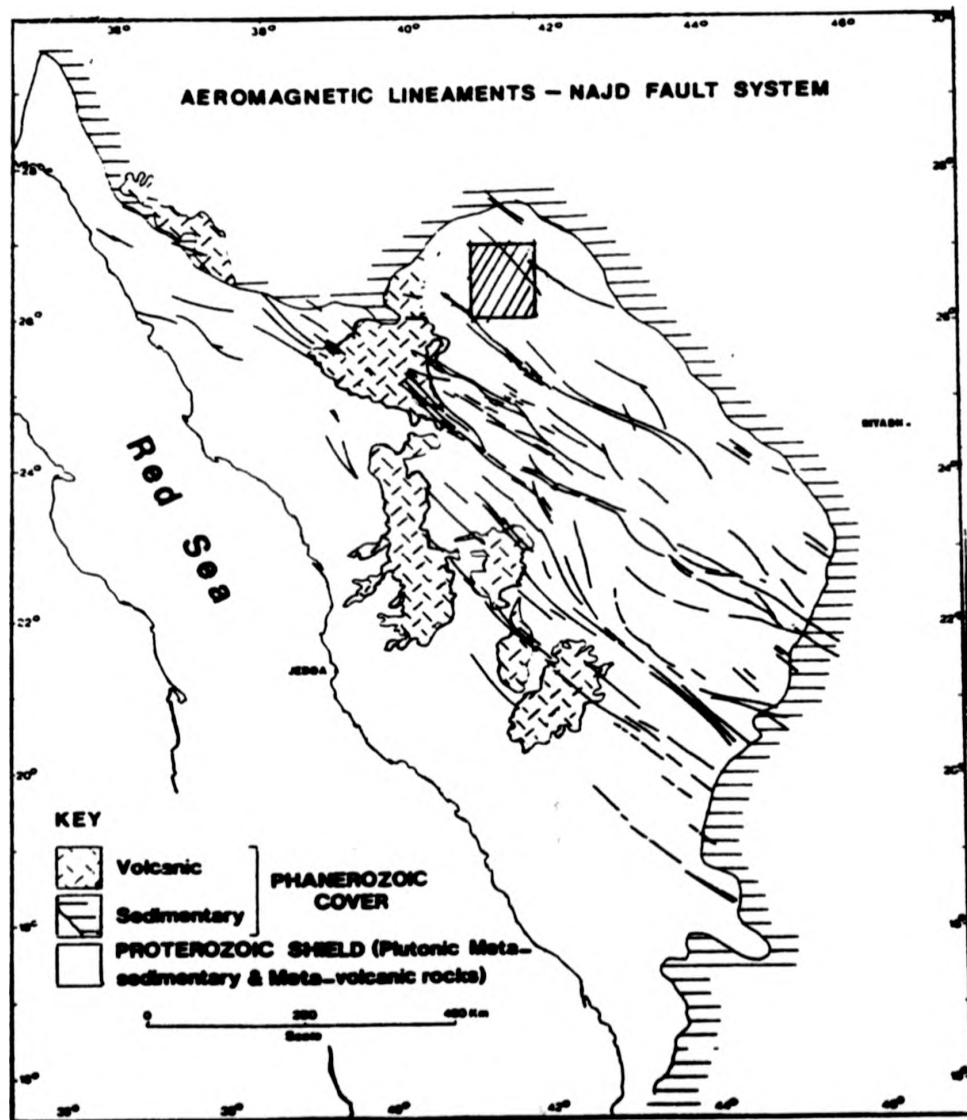


FIGURE 1.14

Aeromagnetic lineaments attributable to structures in the Najd Fault System. (From: Moore, 1979). The study area is shown by superimposed rectangle.

Proterozoic to early Paleozoic volcanic and sedimentary rocks,  
(4) Late Proterozoic to early Paleozoic Intrusive rocks (See  
Table 1.3 for the subdivisions).

1. **The Precambrian Volcanic and sedimentary rocks** in the  
study area were divided into (Table 1.3):-

- Zarghat Formation which is the youngest
- Jurdawiyah Group
- Hadn Formation
- Marghan Formation
- Hulayfah Group which is the oldest

The plutonic rocks in the study area have been divided by  
Quick and Doebrich, (1987) into four principal magmatic epi-  
sodes, based on their ages relative to the Hulayfah Group and  
Hadn Formation (Table 1.3). The Hulayfah Group, in general,  
is composed of moderately metamorphosed basalt, andesite,  
sedimentary and silicic volcanic rocks. These have been  
divided into Banana Formation, Sufrun Formation, and Afna  
Formation.

The Banana Formation (bg) consists of metamorphosed basaltic  
to andesitic volcanic rocks. Its topography is gentle with  
some hills as high as 100m with no cliffs. These rocks have  
recrystallised at lower to middle greenschist facies in most  
places. The Sufran Formation (sv) crops out in close associ-  
ation with the Banana Formation in the study area, but it is

**TABLE 1.3**  
**Summary of the Rock Units in the Study Area**  
**in respect of their age.**  
**(Summarised From: Quick and Doebrich, 1987)**

<b>CENOZOIC SEDIMENTS AND VOLCANIC ROCKS</b> Undivided Quaternary Deposits	<b>LATE PROTEROZOIC TO EARLY PALAEZOIC INTRUSIVE AND VOLCANIC AND SEDIMENTARY ROCKS</b>
Basalt  <b>Precambrian Volcanic and Sedimentary Rocks</b>  Zarghat Formation Basalt Conglomerates Member Basalt Member Mixed Volcanic and Sedimentary Rocks  Jurdhawiyah Group Hadn Formation Sandstone and Conglomerates Member  Maraghan Formation Hulayfah Group Afna Formation Limestone and Marble Member Sedimentary and Volcanic Member Sufran Formation Banana Formation	Jibalah Group Gabbro  <b>Precambrian Intrusive Rocks</b> Intrusive Rhyolite Dikes Granophyre Post-Zarghat Intrusive Rocks Salma granite Complex Alkali granite Arfredsonite Alakali Feldspar Granite Alkali Feldspar Granite Tulqah Complex As Safra Syenogranite Jufayfah Syenogranite  Post Hadn Intrusive Rocks Ash sh'bah Complex Bagham Granite  Post Hulayfah Intrusive Rocks Shuwayman Suite Quartz Rich Pegmatite Kilab Monzogranite Murran Suite Baayith Complex Maa Complex Juwayy Rashid Complex

distinguished by a greater abundance of sedimentary and silicic volcanic rocks.

The Sufran Formation contains, mostly, silicic volcanic lava flows and ash flow tuffs, that are interbedded with lesser amounts of graywacke, conglomerate, breccia, basalt and andesite. The silicic volcanic rocks are recrystallised, although the effects of metamorphism are more subtle, than in the Banana Formation.

The Afna Formation (ha) is composed of basaltic to andesite volcanic rock and breccia. These rocks underlie extensive areas in the study area. The Afna Formation is interbedded with sedimentary and volcanic members (asv).

The Maraghan Formation (mu) consists of light olive green, locally calcareous, fine-grained sandstone, siltstone and shale. Marble occurs as boudin-like masses as much as 100m thick and thin limestone lenses occur throughout the section.

The Hadn Formation consists of two parts; the major part is a massive rhyolitic and rhyodacitic lava flow with minor amounts of arkosic sandstone and conglomerate (hu). Dacitic, andesitic and basaltic lava flows are scarce. This part is more resistant to erosion than the Hulayfah Group of rocks. The second part is a sandstone and conglomerate member (hc). The thickness of Hadn Formation is around 3

to 5 Km and the internal stratigraphy of the Hadn Formation is poorly understood (Quick and Doebrich, 1987). All the rocks mapped as the Hadn Formation unconformably overlie the Hulayfah Group.

The Jurdhawiyah Group (jd) is composed of interbedded andesite flows and volcanic breccia. These rocks are approximately the same age as the Hadn Formation. The Zarghat Formation is divided into three members; first, a basal conglomerate member (zc), second, a basalt member (zb), third, a mixed volcanic and sedimentary rock member (zu). The thickness of the Zarghat Formation is estimated to be about 3Km.

**2. The Precambrian intrusive rocks** In the study area these rocks have been divided into five groups of rocks. These are:-

**a. Juwayy Rashib Complex: (qdd)**

This is composed of quartz diorite and diorite that crop out in close association with greenstone of the Hulayfah Group. The rock forms outcrops of low-lying hills. These rocks are interpreted to be the plutonic equivalent of the mafic and intermediate volcanic rocks of the Hulayfah Group.

**b. Post-Hulayfah intrusive rocks:**

These rocks have been divided into the Murran Suite and the Shuwayman Suite. The Murran Suite has been subdivided into two rock complexes; these are the Maa

Complex and the Baayith Complex. The Maa Complex (gd) is composed of medium to coarse grained hornblende-bearing rocks that grade in composition from granodiorite to tonalite. These rocks out crop as low, grey to dark hills. The exposures of tonalite are rare in comparison to granodiorite exposures. The Maa Complex is younger than the Hulayfah Group and Juwayy Rashib Complex but older than the Hadn and Zarghat Formations. The Baayith Complex: (gns) This is composed of gneissic and schistose granodioritic rock. This complex is poorly exposed and its outcrop style and appearance, where exposed, are similar to those of the Maa Complex except the rocks have a poorly developed gneissic to schistose fabric. The Shuwayman Suite is mapped first as mostly Kilab monzogranite, and second, as small exposures of quartz-rich pegmatite. Kilab monzogranite (mg) underlies extensive areas of the study area and forms low lying out-crops that are covered with a distinctive white grus. It is unconformably overlain by the Hadn Formation, while it intrudes the Hulayfah Group wherever they are in contact.

**c. Post-Hadn intrusive rocks:**

The post-Hadn intrusive rocks have been divided into three groups of rocks. These are: Ash Shu bah Complex, As Safra synogranite, Tulqah Complex. The first group, the Ash Shu bah Complex forms a large pluton, and has been divided into two different granite rocks; the

Bagham granite, and the Jufayfah Syenogranite. These are Bagham granite (peralkaline granite) which outcrop as rugged high hills with steep walls and cliffs, and undivided granite (sga), which is composed of alkali-feldspar granite to alkali feldspar-rich monzogranite. Poor exposure makes subdivision of these units difficult (Quick and Doebrich, 1987). The Jufayfah syenogranite (sgj) forms numerous white to tan granites. Its contacts with the Hadn Formation, the Maa Complex, the Juwayy Rashib Complex and the Banana Formation are clearly exposed. The second group is As Safra synogranite (sg), which crops out as buff coloured hills, and is poorly exposed except as small inselbergs. The third group is the Tulqah Complex (sm) which is composed of quartz syenite and quartz monzonite.

**d. Post-Zarghat intrusive rocks:**

These rocks have been divided into four groups: Salma granite Complex, granophyre, dikes and intrusive rhyolite. The Salma granite Complex is subdivided into biotite alkali-feldspar granite (afg), arfvedsonite alkali-feldspar granite (afga) and alkali granite (ag). The alkali granite (ag) is the most abundant and is readily distinguishable from the surrounding granites.

The granophyric intrusions are of two types, the feldspar granophyre (gph1) and alkali-feldspar granophyre (gph2). Bodies that have uncertain mineralogy are

mapped as undivided granophyre (gph). All these intrusions form small, isolated, irregular outcrops in the study area. Dikes are abundant in the study area, and are generally less than two meters wide. They are readily discernable where they cut granite, granodiorite or dioritic rocks, because they are more resistant and weather to dark hues. Most of the dikes are felsic in composition and are composed mainly of quartz and feldspar. Intrusive rhyolite (ry) crops out as a red aphanatic rock that occurs as structureless, weathered dark red to black masses.

### **3. Late Proterozoic to early Paleozoic rocks.**

These rocks have been divided into sedimentary rocks and intrusive rocks. The sedimentary rocks in the study area are represented by the Jibalah Group. This group is composed of conglomerate, well bedded marble, and calcereous sandstone. This rock was deposited in a narrow Graben formed by north-west-trending Najd fault system (NFS) (Section 1.7.2). The late Proterozoic to early Paleozoic intrusive rock in the study area is represented by gabbro (gb) only. It crops out as small plutons, dikes and plugs.

### **4. Cenozoic volcanic and sedimentary rocks.**

These rocks are basalt (Qtb), terrace gravel (Qt), pediment gravel Quaternary deposits (undivided) (qu), alluvium (Qal) and playa lake deposits (qp). The most important rock, is the Cenozoic basalt, which forms long flows extending from Harrat Kaybar into the study area (Quick and Doebrich, 1987).

The flows are composed of black, vesicular basalt.

All the Precambrian rocks in the study area are cut by an extensive network of faults.

Most displacement has been along northwest-striking faults that belong to the Najd Fault system. The Najd fault system appears to have had a complex history that has involved components of both strike-slip and dip-slip movement. A subordinate system of northeast-striking faults is developed in the northwestern part of the study area and is referred to as the Saqf Faulting System which is named for the main northeasterly-striking fault in the study area.

The study area is very large, therefore it is necessary to select test sites areas within the study area. Appendix 1 shows the location of the selected test sites and extract used in this study. The test sites have been chosen to test and evaluate the image processing techniques.

## **CHAPTER TWO**

### **PREPROCESSING OF REMOTELY SENSED DATA**

- 2.1 INTRODUCTION
- 2.2 LANDSAT SATELLITE
- 2.3 SPOT SATELLITE
- 2.4 IMAGING RADAR
- 2.5 IMAGE PROCESSING SYSTEM
- 2.6 GENERAL METHODS FOR PREPROCESSING OF REMOTELY SENSED DATA
  - 2.6.1 DE-STRIPING METHOD
  - 2.6.2 ATMOSPHERIC EFFECTS AND CORRECTION METHOD
  - 2.6.3 IMAGE-TO-IMAGE REGISTRATION METHOD
- 2.7 SUMMARY

## 2.1 INTRODUCTION

In general, the majority of remotely sensed satellite data, including Landsat (MSS and TM) and SPOT are not acquired as hard prints (pictures), but are acquired in a digital format, on computer compatible tapes (CCT's). Each CCT from any remote sensing satellite contains a very large quantity of digital data, for example, a single Landsat TM scene covering 170 Km x 185 Km on the ground, contains 273 megabytes of data and occupies seven magnetic tapes (CCT's) when written at a tape density of 1600 bits per inch (Harris, 1987). Therefore, the remote sensing interpreters have to use digital image processing techniques in order to view the images. The human eye can be used for interpretation of black and white or colour images, which restricts the human interpreter to the use of a combination of, at most, three bands of data (Harris, 1987).

Because of this restriction, and to overcome many other human limitations, many processing techniques have been developed. Digital image processing falls into three major areas of computer operation (processing); these are image restoration and rectification (preprocessing), image enhancement and image classification.

Remotely sensed data from a satellite may contain different image defects (errors). These defects may be caused by the satellite system, or they could be caused by the atmosphere (Short, 1982) divided the 'errors' into four groups; platform,

sensor, scene, and atmosphere effect. The preprocessing is concerned with correcting a degraded (i.e. distorted, noisy) digital image to its intended form. Image correction is one of the most important stages of digital processing, because many image enhancement and classification operations will emphasise image imperfections to such an extent, that useful information can be obscured (Condit and Chavez, 1979).

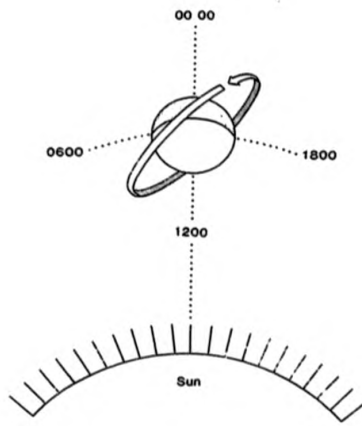
Image enhancement is used to improve the detectability of objects or patterns in digital images for visual interpretation (e.g. contrast manipulation, spatial filtration, arithmetic operation, principal component, decorrelation stretch, etc.). Image classification provides quantitative decision rules, that classify or identify objects or patterns, on the basis of their multispectral radiance values. Image classification has been divided into two categories; supervised and unsupervised classification.

In this Chapter, a Landsat satellite system (with a multispectral scanner (MSS) and Thematic Mapper (TM) sensors), SPOT, and imaging radar will be outlined. Only the preprocessing methods that have been applied during the course of this study will be discussed in detail. All the image enhancement and classification techniques used in this study will be discussed in the next six Chapters.

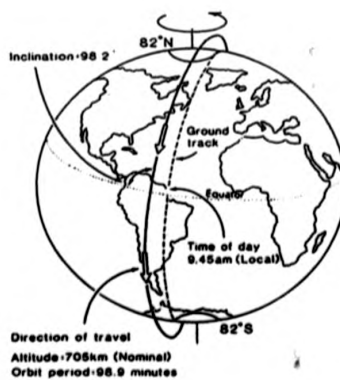
## 2.2 LANDSAT SATELLITE

The Landsat series of satellites have provided an exciting and useful view of the earth since the launch of Landsat-1 in 1972. The Landsat satellites have two generations; the first generation was named as Landsat-1, 2 and 3 and the second generation named as Landsat-4 and 5. Although several instruments have been carried by these satellites (RBV, TM), data acquired by the multispectral scanner (MSS) have been the most widely utilised.

The Landsat-5 carries two different scanners, the Thematic Mapper (TM) and Multispectral Scanner (MSS) with different spectral and spatial resolution. Landsat-5 was redesigned for higher stability and placed in a relatively lower orbit to permit higher spatial resolution of the TM Sensor. It has circular, sun-synchronous, near-polar orbits (Figure 2.1a) with a height 705 Km above the surface of the earth and the orbits have an inclination angle of  $98.2^\circ$  ( $8.2^\circ$  from normal) with respect to the equator. The satellite crosses the equator on the north to south portion of each orbit at 9:45 a.m. local suntime. Each orbit takes approximately 99 minutes (Figure 2.1b). The lowered altitude of Landsats-4 and -5 compared to the first Landsat generation (918 Km) means that 233 orbits and 16 days are needed to cover the earth. Paths are numbered 1 to 233, east to west respectively crossing the equator at longitude  $64^\circ 36' W$ . The MSS on board Landsat-5 captures a scene approximately  $185 \times 185$  Km. A typical scene contains approximately 2340 scan lines with



(a)



(b)

FIGURE 2.1 (a) General sun-synchronous orbit  
(b) The orbit specification

(From Mather, 1987).

about 3210 pixels per line. The MSS has four wavelength bands (1 - 4), two in the visible spectrum at 0.5 to 0.6  $\mu\text{m}$  (green) and 0.6 to 0.7  $\mu\text{m}$  (red) and two in the near infrared at 0.7 to 0.8  $\mu\text{m}$  and 0.8 to 1.1  $\mu\text{m}$ . The total field of view scanned is approximately 14.92°.

The instantaneous field of view (IFOV) is 82 x 82 meters (Lillesand and Kiefer, 1987). The scanner system is a line scanning device which uses an oscillating mirror to continuously scan the ground. During each mirror oscillation, six contiguous lines are scanned simultaneously, and therefore 24 detectors are used, 6 in each of the 4 wavelength bands.

Thematic Mapper (TM) scan mirror or cross tracks mirror sweeps the TM line of sight back and forth seven times each second in a direction normal to the orbital ground track to form a raster of 16 lines in bands 1-5 and 7, and four times in band 6. Data are collected during both the forward [west to east] and reverse [east to west] mirror scan. The scan velocity is essentially constant during both directions of the mirror scan (Figure 2.2). The TM has a better spectral and spatial resolution compared with the MSS. The TM scanner records six bands of reflected visible and infrared radiation and has a 30 meter instantaneous field of view (IFOV) for bands 1-5 and 7, (band 6 has an IFOV of 120 Meters). Each TM band uses an array of 24 detectors except band 6 which uses only 4 detectors (Sabins, 1987). Table (2.1) shows the TM spectral bands and their

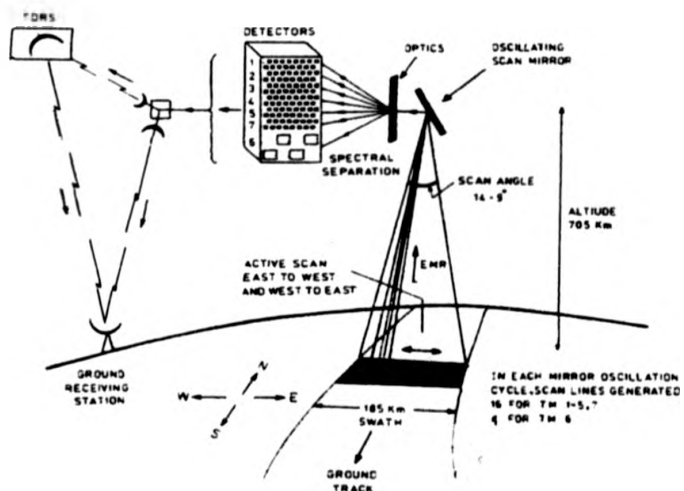


FIGURE 2.2

Landsat TM scanning arrangement. The sensor records data in 7 bands (1-7). The detectors in the VNIR region are placed at the primary focal plane and those in the SWIR-TIR region at the cooled focal plane. A total of 16 scan lines are concurrently generated for bands 1 to 5 and 7 and four lines for band 6. (From: Gupta, 1991).

**TABLE 2.1**  
**Thematic Mapper Spectral Bands**  
 (From Lillesand and Keifer, 1987).

Band	Wavelength ( $\mu\text{m}$ )	Nominal Spectral Location	Principal Applications
1	0.45 - 0.52	Blue	Designed for water body penetration, making it useful for coastal water mapping. Also useful for soil/vegetation discrimination, forest type mapping, and cultural feature identification.
2	0.52 - 0.60	Green	Designed to measure green reflectance peak of vegetation for vegetation discrimination and vigor assessment. Also useful for cultural feature identification.
3	0.63 - 0.69	Red	Designed to sense in a chlorophyll absorption region aiding in plant species differentiation. Also useful for cultural feature identification.
4	0.76 - 0.90	Near-infrared	Useful for determining vegetation types, vigor, and biomass content, for delineating water bodies, and for soil moisture discrimination.
5	1.55 - 1.75	Mid-infrared	Indicative of vegetation moisture content and soil moisture. Also useful for differentiation of snow from clouds.
6*	10.4 - 12.5	Thermal infrared	Useful in vegetation stress analysis, soil moisture discrimination and thermal mapping applications.
7*	2.08 - 2.35	Mid-infrared	Useful for discrimination of mineral and rock types. Also sensitive to vegetation moisture content.

\* Bands 6 and 7 are out of wavelength sequence because band 7 was added to the TM late in the original system design process.

principal applications.

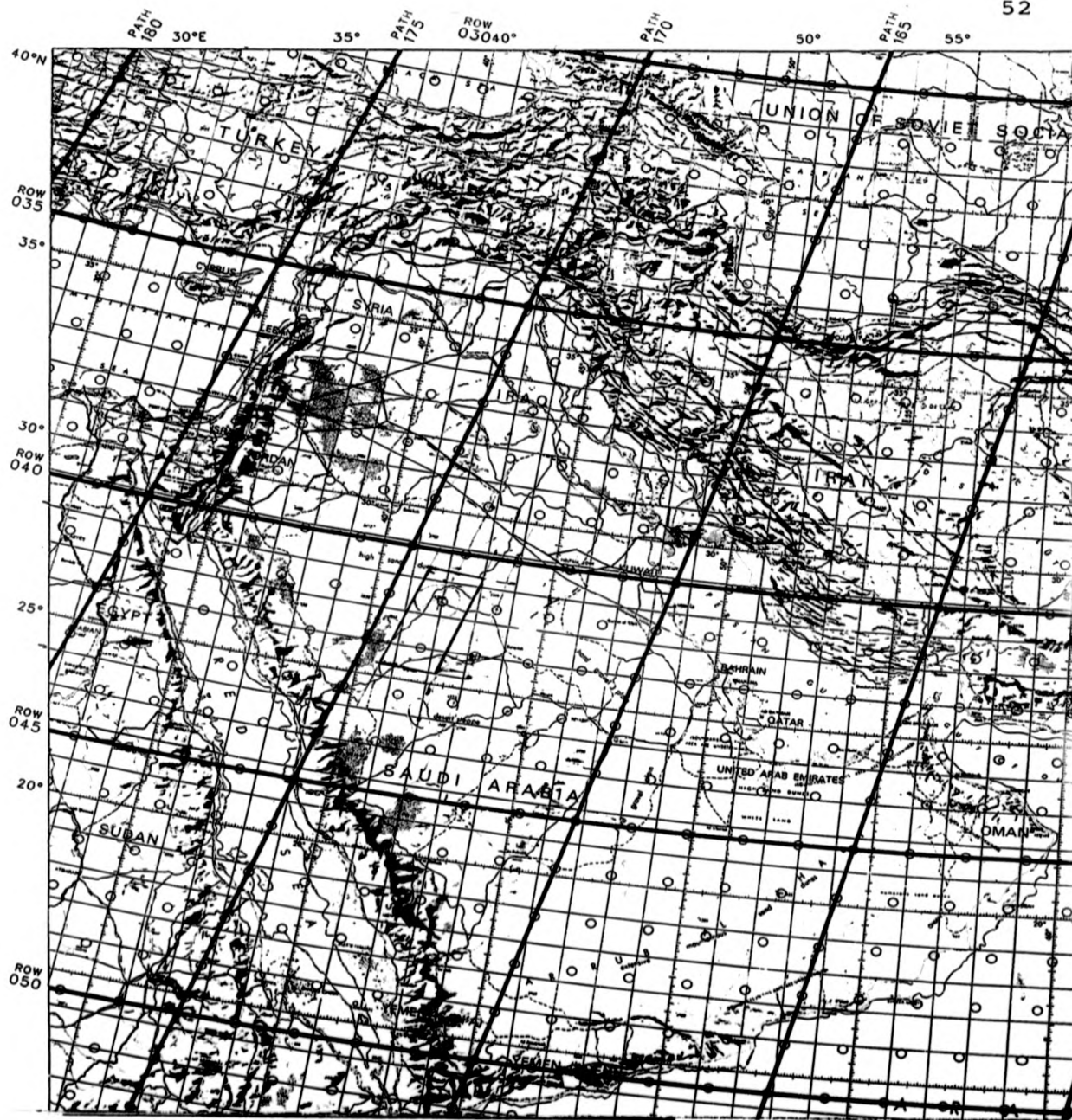
In this study only MSS bands 3 and 4 were examined. Bands 1 and 2 were nearly always badly affected by atmospheric dust haze. The six TM bands (1-5 and 7) were used during the course of this study because they are spectrally and spatially significant for geological applications. Band 6 (thermal band) was not used, because of its very poor quality.

The Location of each Landsat-5 scene can be specified by its path and row co-ordinates in the Landsat worldwide reference system (WRS). (The study area is in WRS Sheet 12. Figure 2.3).

The Landsat MSS and TM data used in this study were obtained from the Saudi Arabian Remote Sensing Centre and receiving station on 9-track (CCT's), with a data density of 6250 bpi and stored in band sequential (BSQ) format. The data density had to be changed to 1600 bpi in order to read the data on the available tape-drive at Stirling University. In order to do that, the data in each CCT was divided into two CCT's using the University of Stirling mainframe computer (Unix). The TM data were used for all the image processing and interpretation, while the MSS was mainly for image-to-image registration or for lineament detection and analysis.'

### **2.3 SPOT SATELLITE**

The SPOT (Satellite pour l'observation de la terre) was

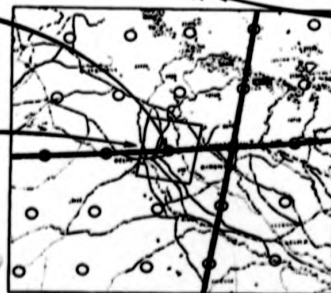


**NOMINAL SCENE CENTER**

Actual image center can vary as much as 20 kilometers

**NOMINAL SCENE AREA**

Actual area of nominal scene varies according to latitude



**PATH**

Orbit paths are numbered westward, with path number 001 passing through eastern Greenland and South America

**040 ROW**

Image rows are numbered southward, beginning from 80°N latitude

**FIGURE 2.3**

Path-row co-ordinates in the Landsat-4 and 5 worldwide reference system (WRS) Sheet 12 for the area in and around Saudi Arabia. The two scenes used in this study are 169/41-42.

launched into space in February 1986. SPOT-1 and SPOT-2 are identical and have a circular, near polar, sun-synchronous orbit, 832 Km high and with an inclination of 78.7°. This satellite covers the earth every 26 days, and in addition has a pointable optics system that enables off-nadir viewing up to 27° during satellite passes (Lillesand and Kiefer, 1987). This off-nadir viewing capability enables stereoscopic coverage of a scene to be obtained by imaging the same area on a different orbit (Harris, 1987; Figure 2.4).

The sensor on board SPOT consists of two high resolution-visible (HRV) imaging systems and an auxiliary magnetic tape recorder. Each HRV is operating in two different modes as follows:-

1. In the Multispectral mode (MLA), the ground resolution is 20 Meters and three wavebands in the visible and near infrared over ranges (Band 1, 0.05 to 0.59 $\mu\text{m}$ ; Band 2, 0.61 to 0.68 $\mu\text{m}$  and Band 3, 0.79 to 0.89 $\mu\text{m}$ ; See Table 2.2).
2. In the Panchromatic mode (PLA) (black and white), 10 meter resolution over the range 0.51 to 0.73  $\mu\text{m}$ ; (See Table 2.2).

The scanning system is a push-broom system with no mirror and consists of a linear array of CCD's arranged side-by-side along a line perpendicular to the satellite orbit track.

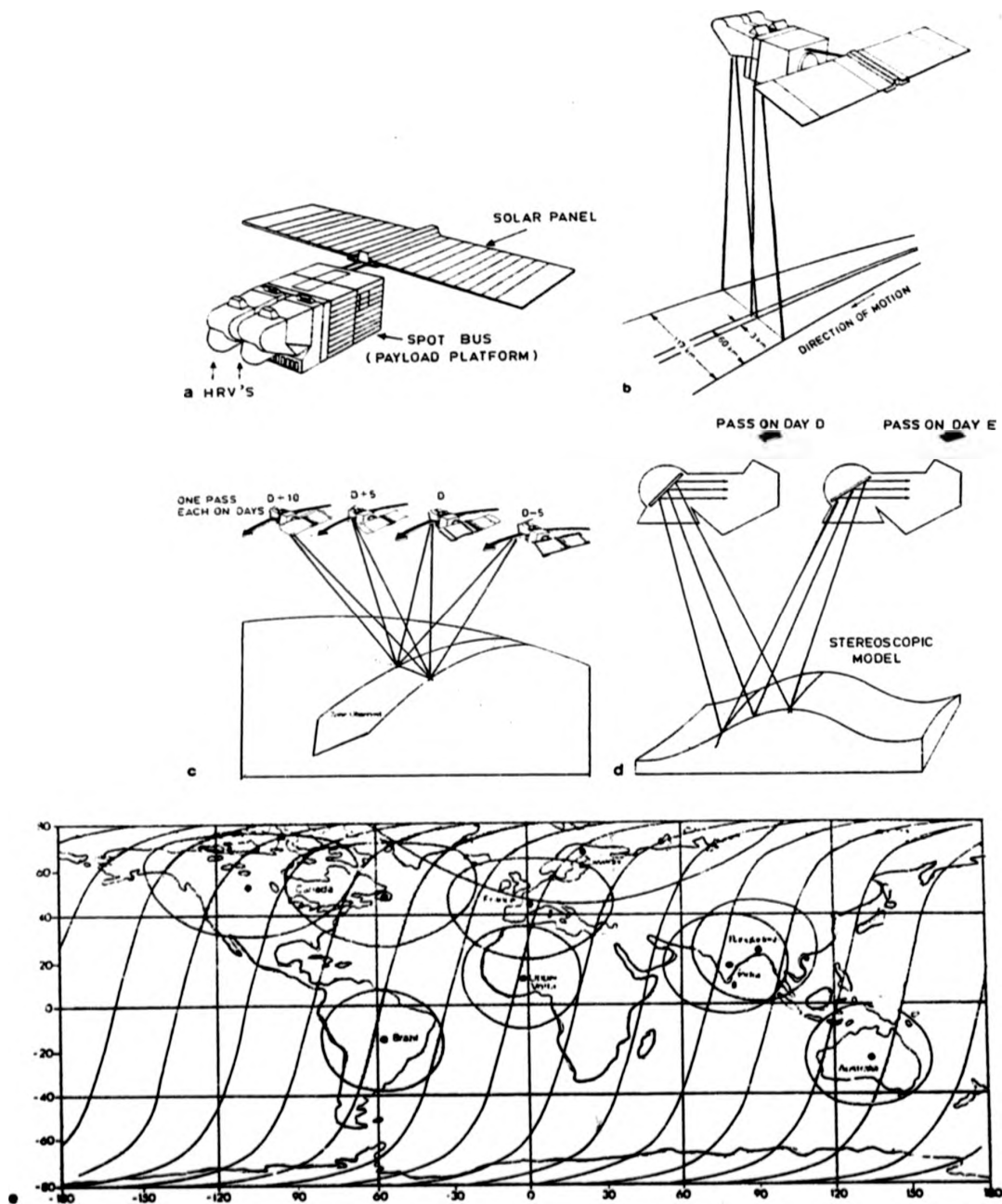


FIGURE 2.4 DESIGN OF SPOT

- (a) The three main components of SPOT are: a solar panel, a payload platform and the sensor instrument.
- (b) Nadir-viewing HRV configuration.
- (c) Revisit by off-nadir viewing.
- (d) Stereo capability.
- (e) Location and area coverage of SPOT data receiving stations. (From: Gupta, 1991).

**TABLE 2.2**  
**SPOT Satellite Details and HRV Sensor**  
 (From Mather, 1987)

HRV Sensor		SPOT Satellite
Channel	Waveband ( $\mu\text{m}$ )	
1 2 3	Multispectral 0.50-0.59 0.61-0.68 0.79-0.89	Orbit: near-polar. Sun-synchronous Altitude: 832 km Inclination: 98.7° Equatorial crossing time: 1030 Repeat cycle: 26 days
1	Panchromatic 0.51-0.73	
Spatial resolution: 20 m (multispectral) (at nadir) 10 m (panchromatic)		
Radiometric resolution: 8 bits (multispectral) 6 bits (panchromatic)		
Swath width: 117 km (60 km per HRV, 3 km overlap)		
Angular field of view 4.13		
Off-nadir viewing $\pm 27$ in 45 steps of 0.6 (= $\pm 475$ km from nadir)		

In this study, only SPOT-2 panchromatic mode was used because the Saudi Arabian Remote Sensing Centre and Receiving Station, which provided the SPOT data, receives only this mode at the time of this study.

The SPOT data covering part of the study area were provided on 9-track (CCT's) with a data density of 6250 bpi. The data density had to be changed to 1600 bpi in order to read the data on the available tapedrive. This process was carried out on the University of Stirling mainframe computer. (UNIX). Table (2.3) shows all the satellite images used in this study, and their path and row, sun azimuth sun elevation and date of receiving.

**TABLE 2.3**  
**Showing all the Satellite Images**  
**used in this Study**

DATA	SATELLITE	SUN AZIMUTH	SUN ELEVATION	DATE	PATH/ ROW
TM	Landsat-5	125.52°	49.5°	23 Mar'90	169/41
TM	Landsat-5	125.52°	49.5°	23 Mar'90	169/42
MSS	Landsat-5	125.52°	49.5°	23 Mar'90	169/41
MSS	Landsat-5	125.52°	49.5°	23 Mar'90	169/42
SPOT	SPOT-2	096°	072°	26 Jun'90	135/297

#### 2.4 IMAGING RADAR

Radar is an acronym for Radio Detection and Ranging. The radar system is an active device, i.e. provides its own illumination energy which can produce images in darkness, haze, rain or snow. In general, radar systems produce images or non-imaging results, and they may be ground or mounted on platforms. The non-imaging radar includes: a) Doppler radar systems which can be used in determining an object's velocity and, b) the plan position indicator (PPI) radar which is used for forecasting navigation of air traffic control.

The side looking radar (SLAR) is an imaging system usually used for remote sensing imaging. The basic mode of operation of a radar system consists of:-

1. The system sends out short powerful pulses of microwave

frequency energy at regular intervals in a certain direction.

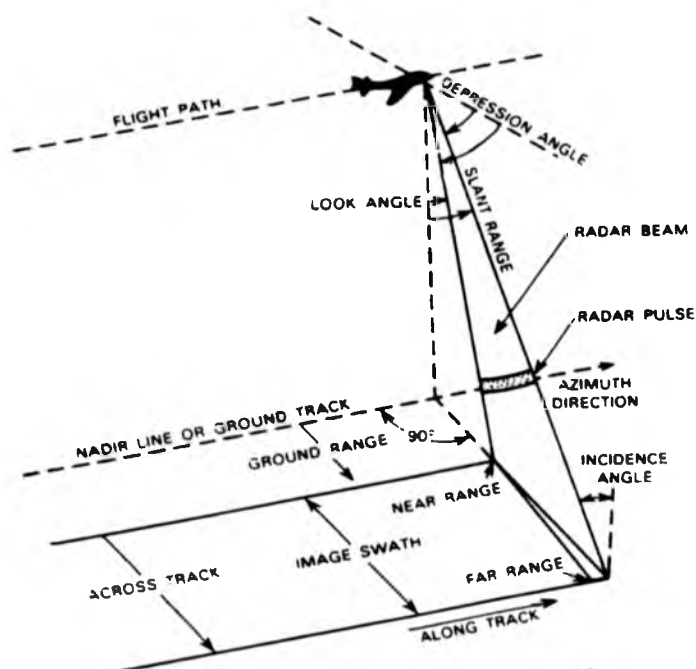
2. The pulses strike an object (target) and they are reflected back to receiver.

3. The distance, time (to the object) and the strength of reflection can be measured and displayed.

Figure 2.5 shows the geometry characteristics and terminology of the SLAR system.

SLAR has two different resolutions which are range resolution and azimuth resolution. The range resolution (perpendicular to ground track) is determined by length of the radar pulse. For example, to image two ground objects that have equal reflectivity and are close together, all parts of their reflected signals must be received at the antenna at different times or they will be blurred.

The azimuth (long-track) resolution is determined by the width of the terrain strip illuminated by a radar pulse which is a function of the beam width (Avery and Berlin, 1985). Therefore to separate two targets in the long-track direction it is necessary that their separation on the ground be greater than the width of the radar beam. There are different types of geometric distortions which affect the interpretation and SLAR image application (For detail see Macdonald 1976; Avery and Berlin 1985; Lillesand and Kiefer 1987). These are polarisation, foreshortening, layover, shadows, (Figure 2.6) but the most



- \* Slant range: the line of sight distance measured from the antenna to the object.
- \* Ground range: the horizontal distance measured along the surface from the ground track or nadir line to the object.
- \* Near range: the area closest to ground track where a radar pulse intercepts the terrain.
- \* Far range: the area of pulse termination farthest from ground track.
- \* Depression angle: the angle measured between a horizontal plane relative to the earth's surface and the radar beam. The far range and near range represent the minimum and maximum depression angles, respectively over the entire image swath.
- \* Look angle: the angle measured from a vertical plane to the radar beam.
- \* Incident Angle: the angle measured between the normal to the local surface.

FIGURE 2.5 Geometric Characteristic terminology of side looking radar (SLAR).  
(From: Avery and Berlin, 1985).

important are:-

1. **Layover:**

This occurs when the look angle is smaller than the foreslope angle, for example, when the slant angle distance to top of the feature (e.g. mountain or hill) is less than that to the base. Thus, the radar pulse will intercept and image the top of the hill before it strikes the base.

2. **Foreshortening:**

In imaging a variable topographic area, if there is an elevated point it will be displayed as if it were nearer the sensorcraft (owing to decreased slant range distance Gupta, 1991). This will cause a shortening of all the facets slope (foreslopes) toward the antenna.

3. **Radar Shadow:**

The topographic features can prevent the radar beam from striking the slope facing away from the radar beam. This area will appear black in a positive image because no backscatter is returned to the antenna from their surfaces, thus, different topographic features show different shadows in a radar image and topographic feature parallel or oblique to the beam front are enhanced in the images.

According to Avery and Berlin (1985), the parameters that determine the size of radar shadows are the relative topography of the terrain depression angle, antenna and the slant angle (Figure 2.5):



- shadow lengths of terrain features (topography features) of equal height and slope become proportionally longer as range increases because radar striking becomes more oblique in the far range.
- the smaller the depression angle, the longer the shadow.
- at a given depression and at a common range, the highest obstruction will produce the longest shadow. Since radar shadows may be controlled, they may be used to deliberately highlight certain terrain features.

There are two types of radar designed for use with the SLAR system: the real aperture radar (RAR) and synthetic aperture radar (SAR). The primary difference between the two systems depends on how the azimuth resolution is obtained. The real aperture radar makes use of the physical antenna to transmit and receive the pulse and needs a long antenna.

The synthetic aperture radar is most important for use in studying the earth's surface. The synthetic aperture radar (SAR) uses sophisticated signal storage and processing techniques to produce an effective narrow beam width without the use of long physical antenna or a short operating wavelength (Figure 2.7).

The antenna transmits phase-coherent passes at regular intervals along the flight line's pass. The echoes from each terrain feature are recorded as phase histories on high density tape (HDT) for digital processing (or signal, on optical processing) (Avery and Berlin, 1985).

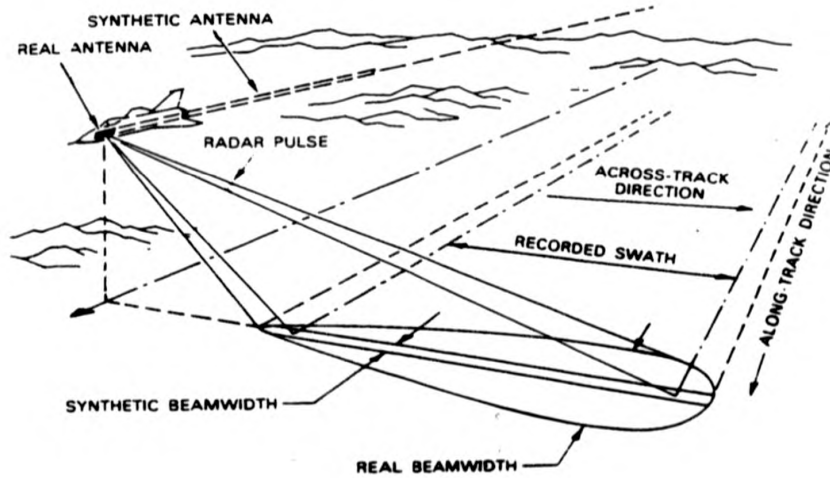


FIGURE 2.7 Fundamental concept of a synthetic-aperture radar system.  
(From: Avery and Berlin, 1985).

SAR system produces a high resolution and constant resolution image which is ideally for high level range application (i.e. it is capable of producing images of 3-M resolution).

A SAR system was flown on the Seasat Satellite (only operated from 26 June 1978 until 9 October 1978). This satellite provided much useful data for scientific examination and as input to the future design of radar systems. The first shuttle imaging radar experiment (SIR-A and SIR-B) were launched in 1981 and 1984 respectively and both are SAR systems. The two main differences between the two systems are:

1. The incident angle, which is  $40^\circ$  in SIR-A and  $30^\circ$  to  $75^\circ$  for SIR-B.
2. Most of SIR-B images were recorded digitally.

The radar images have been used in geological applications such as:-

1. Lithological Mapping using the texture analysis. (Chapter 8).
2. Structure studies using the radar shadows, (e.g. Lineament detection).
3. Soil moisture mapping.
4. Depth penetration of the radar pulse to discover the sub-surface water streams.
5. Sand dune movements using radar data with different date.
6. Roughness of the terrain (Since the radar pulse intensity can be used as an indication for the inter-rela-

tionship between the roughness of an object's surface and radar's wavelength and incident angle). Therefore surface with micro-relief less than a wavelength wide will appear smooth (little or no return). Surfaces with roughness equal to or greater than wavelength will appear brighter.

In this study the radar data (SIR-B) will be examined to see if it can be used for lithological discrimination and mapping, using the texture analysis. (Chapter 8). Table 2.4 shows the characteristics of SIR-B.

## **2.5 IMAGE PROCESSING SYSTEM**

R-CHIPS, which has been designed for image processing purposes on a PC, was used interactively to investigate imagery. The system has a menu with a list of program options, which are displayed on the VDU. This menu is divided into seven submenus:-

1. Display submenu
2. Enhancement submenu
3. Statistics submenu
4. Mathematic submenu
5. Classification submenu
6. Image inspection submenu,
7. Overlays submenu

The user can select items from either the main menu or a submenu. The R-CHIPS hardware was composed of graphic display card, hosted by a 386 IBM compatible PC. This card is capable

**TABLE 2.4**  
**SHUTTLE IMAGING RADAR-B**  
**(SIR-B) SYSTEM CHARACTERISTICS**  
**H: Horizontal**

PARAMETER	MEASURE
L-Band Wavelength	23.5 cm
Polarisation	HH
Aperture Type	Synthetic
Correlation Type	Digital
Centre Incidence Angle	50°
Centre Depression Angle	40°
Centre Resolution: Ground Range Azimuth	18.4 m 32.1 m
Shuttle Altitude	354.7 km
Data	10.4
Scene	011-013

\* For the parameter definition see Figure (2.6-2.7), Avery and Berlin, 1985; Lillesand and Kiefer, 1987, and Sabins, 1987.

of displaying a 512 pixels by 512 line image. The graphics card is split into four boards, red, green, blue and overlay. These boards are used by R-CHIPS individually and concurrently. (For more detail see R-CHIPS Image Processing Software User Guide. (User Guide, Version 1988).

Most of the image processing techniques used in this study (e.g. de-stripping, principal component, atmospheric correction, new contextual techniques, decorrelation stretching, median filter, image segmentation and texture analysis), were performed on a Micro-Vax computer. The images, once processed, were transferred to the R-CHIPS PC for visual analysis.

A standard 35 mm camera was used, with a normal lens, to take pictures of the images from the colour monitor, to record the results.

## **2.6 GENERAL METHODS FOR PREPROCESSING OF REMOTELY SENSED DATA**

It is difficult to decide what should be included in the preprocessing techniques or methods, because the definition of what is or is not an error in the data will, to a large extent, depend on the use to which this data is to be put (Mather 1987). By observing the image data (MSS, TM) for the study area, it was found that several preprocessing methods were necessary in order to correct the data for further processing. These methods included de-stripping, atmospheric correction and image-to-image registration.

### **2.6.1 De-stripping Method**

The radiometric stripping is a common problem with Landsat MSS data, but not with TM. The Landsat MSS has a six detector array for each of the four spectral bands, enabling six ground strips to be imaged simultaneously, during each sweep of the mirror. However, because the detectors have slightly different output responses, the resulting raw images often exhibit a six-line striping effect, that can reduce the visual appearance of an image, and reduce the accuracy of automatic image processing.

All the raw MSS images of the study area were reviewed and it was found that they were all striped. Therefore, it was decided to clean up the MSS data by removing these strips. The MSS data has to be de-striped before any image enhancement is attempted, otherwise the strips may become enhanced and lead to errors in the final results.

A de-strip program called DEST on the Micro-Vax system was used to remove the strips in the MSS data (bands 3 and 4). This program calculates the average for each scan line across the whole subscene (512 x 512 pixels), then the average for each scan line is compared with this global scan average. The differences are used to correct each pixel of the strip line to produce a less striped image.

### **2.6.2 Atmospheric Effect and Correction Method**

The sunlight is the main source for remote sensing radiation. The radiation passes through the atmosphere twice from the

sun to sensor. In this process, the radiation interacts with atmospheric constituents such as gases, suspended materials, dust particles, etc. As the altitude of the sensor platform above the earth increases, so the amount of the atmosphere through which the energy must pass, increases. A major consideration in the interpretation of data acquired by means of remote sensing, is the effect of the earth's atmosphere on electromagnetic radiation.

The atmospheric effect can be divided into two processes -

- a. Atmospheric absorption, which converts energy present in electromagnetic radiation into the internal energy of the absorbing molecule.
- b. Atmospheric scattering which is the result of interaction between the electromagnetic radiation and the suspended particles or gas molecules, which are present in the atmosphere.

There are three common types of scattering -

1. Rayleigh scattering is the result of the presence in the atmosphere of molecules, and other very small particles with diameters much less than the wavelength of the radiation under consideration. Rayleigh scattering is most obvious on clear days. Its intensity is inversely proportional to the fourth power of the wavelength and hence gives the sky its 'blue' colour.
2. Mie Scattering occurs when there are, for example, water

vapour, smoke and dust, which are essentially spherical particles, present in the atmosphere, with diameters approximately the same as the wavelength of visible radiation.

3. Non selective scattering occurs when the particles in the atmosphere are several times larger in diameter than the wavelength of the radiation being transmitted.

Both scattering and absorption may vary in their effects from one part of the spectrum to another, (e.g. scattering has more effect on the shorter wavelengths).

Remote sensing is impossible, in those parts of the spectrum, that are seriously affected by scattering and/or absorption. The atmospheric scattering gives rise to an additional radiance from the atmosphere itself, that increases the overall digital value (brightness level) at shorter wavelengths, and causes low image contrast (Robinson and Carroll, 1977). There exist sophisticated techniques, which rely on direct meteorological measurements, for calculating the expected atmospheric spectro-radiances under specific weather conditions (Dozier and Frew, 1981). Unfortunately, this is an ideal, and most users must work with remotely sensed data without the benefit of weather information.

A correction for atmospheric scattering is necessary if:-

1. the scattering level varies from one part of the image to another;

2. a set of multi-images is to be analysed and scattering level varies with time (e.g. multitemporal analysis);
3. certain types of processing are to be performed on the data, such as spectral band ratios (Section 7.3).

The problem with many of the atmospheric correction techniques, is that the haze value for each spectral band is often selected independently, which can create problems, because atmospheric scattering is highly wavelength dependent in the visible part of the electromagnetic spectrum, and the scattering values are correlated with each other (Chavez, 1988). In this study two different atmospheric correction methods were applied to the image data. In the first method, the image was run through a program called HIST (on the Micro-Vax System), the function of which is to count the number of pixels in every DN interval, and find the minimum value for the band. This minimum was subtracted from all the pixel values for each band (TM bands 1-4). At the end, the original histograms were shifted to the left.

The second method used in this study, was the 'improved dark-object' subtraction method for atmospheric scattering correction. This method was proposed by Chavez (1988); and is an improvement on the existing dark-object methods, that derive the correction DN values solely from the digital data with no outside information. The user selects a starting band dark-object subtraction haze value, using the histogram of one of the spectral bands. The

user then selects a relative scattering model that he feels best represents the atmospheric conditions at the time of data collection. The amplitude of the starting haze can be used as a guide to identify the type of atmospheric conditions that may have existed during data collection (i.e. very clear, moderate, hazy or very hazy; See Tables 4 and 5 in Chaviz 1988). It is recommended that a spectral band in the visible part of the spectrum should be used as the starting haze value. The starting haze DN value must not over predict the values for other bands (Chavez, 1988).

These two methods have been applied to correct different extracts, and it was found that the 'dark-object' method showed the best result. Large extracts (1024 x 1024 pixels) were used from each quad of TM data to find out the starting haze values.

For some image extracts it was found that the atmospheric correction does improve the imaging, especially in areas where mountains are present. However, the atmospheric correction was carried out only when ratioing techniques (Section 7.3) were to be used (Davis et al., 1987; Drury 1987; Davis and Berlin 1989, and Johari, 1990).

### **2.6.3 Image-to-Image Registration**

'Image-to-image registration' is necessary to form image mosaics, compare images from different sensors (with different resolution), and spectral wavelength (i.e. MSS, TM, SPOT and radar) or to map temporal changes accurately, from different

images for the same area.

The accuracy of the registration depends on many factors. Among these factors, which are relevant to Saudi Arabian desert areas was the availability or rather, the lack of ground control points (GCP's). Very few 'cultural' features were available to be used and many 'natural' boundaries/intersections were not well defined.

There are two main methods for digital image registration; these are; automatic image registration and manual image registration.

**1. Automatic Registration:**

This method can be applied using some measure of dissimilarity or similarity between two images that calculates the function of relative shift between the two images (Schowengerdt, 1983). This method can be used without generating ground control points. A more detailed account can be found in Schowengerdt (1983). In this study, the automatic registration was not used.

**2. Manual Registration:**

This method involves the visual examination of the images and the location of the selected ground control (points) features (GCP's) in the two images to be registered (e.g. TM and MSS images). This method is particularly efficient with the aid of an image displaying system with a movable cursor that can provide pixel co-

ordinates in the displayed image (Showendgerdt, 1983).

In this study, the second method was used and the registration was carried out in three stages:-

**1. Selection of clear ground control points (GCP'S)**

The GCP's were selected from Landsat MSS band 4 (0.8-1.1 $\mu$ m) and either TM band 5 (1.55-1.75 $\mu$ m) or band 7 (2.08-2.35 $\mu$ m) images. These bands were found to be the best in terms of contrast, definition of features and less atmospheric interference in the infrared bands. An interactive linear contrast stretch was applied to all the bands, to enhance the features in the images. Attempts were made to obtain as many GCP's as possible. According to the literature, 30 or more should be used for each TM quad of the full scene, but in this study a much smaller number had to be settled for. For each TM quad, the GCP's were selected from: road intersection, playa, rock boundaries, service roads in agricultural fields and the green field edges. Identification of GCP's proved to be difficult due to the lack of distinctive features in the alluvial sediments and sand dunes. For this reason, the GCP's selected were not distributed evenly throughout the images but were more along the roads (mainly small roads) or around the agricultural areas. One of the main problems encountered in using these intersections was their lack of definition.

## 2. Image-to-image registration

A regression method was used to define the relationship between the co-ordinates of any of two images. For this purpose a MINITAB program was used which was available on the University of Stirling mainframe UNIX system. Once the best regression equation had been found, the images were resampled.

The images were resampled using one of the following operations:-

a) **Nearest neighbour resampling;** the DN value of the output image is equal to that of the nearest input pixel.

b) **Bilinear interpolation;** This takes a distance-weighted average of digital pixel values of the four nearest pixels.

c) **Cubic convolution;** by using this method the output DN's are assigned on the basis of a weighted average of input DN's from sixteen surrounding pixels (Avery and Berlin, 1985).

## 3. Measurement of Offsite between images

In this study, the TM imagery was taken as a reference frame. All the resampling (operations) methods were tested in order to select the best method which introduced the minimum errors! By displaying the registered image over the TM image it was found that the cubic convolution method introduced the minimum of geometric error of 2 to 3.5 pixels at best. This error went up in

areas for which there were no selected GCP's. For this reason the author decided not to use the registered images in any rock discrimination study (Chapter 7). Figure (2.8) shows a diagram illustrating the methodology used for image-to-image registration.

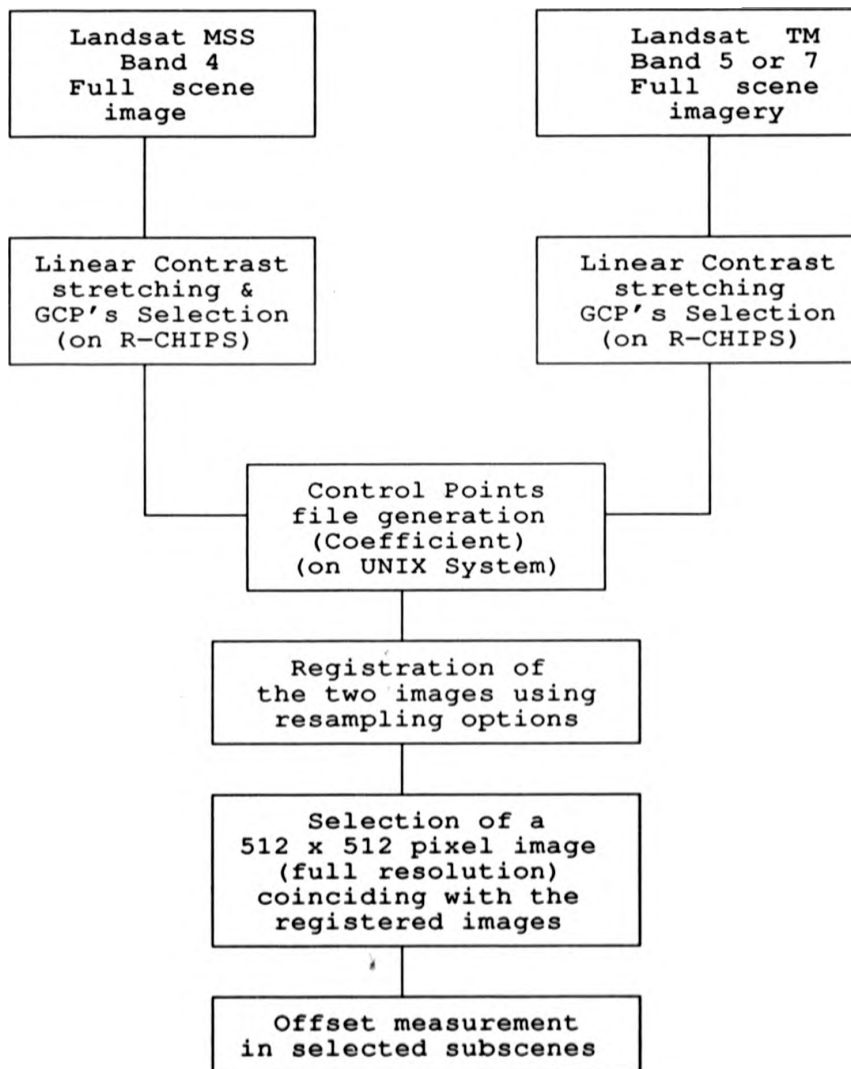
## 2.7 SUMMARY

There are different remote sensing sensors available at the present time which, can be used in different applications. In this Chapter, only the remote sensing sensors and their data which have been examined in this study, were outlined. These were Landsat, SPOT and imaging radar.

Digital image processing is extremely broad, and it often involves procedures, which can be mathematically complex. However, in this Chapter, only a brief and general introduction is given to the preprocessing techniques, which would help in reducing the expected error during any further image processing. The de-stripping method, atmospheric correction and image-to-image registration have been discussed and applied in this study. Only the first two were of benefit and improved the distorted images. Image registration was not sufficiently accurate enough, because of a lack of ground control points.

FIGURE 2.8

A Flow Chart showing the methodology used for image-to-image registration in this study



## **CHAPTER THREE**

### **THE USE OF NEW CONTEXTUAL TECHNIQUES IN LINEAMENT MAPPING AND ANALYSIS: AN OVERVIEW**

3.1 INTRODUCTION

3.2 DEFINITION OF LINEAMENT

3.3 SPATIAL FILTRATION TECHNIQUE

3.4 THE NEW CONTEXTUAL TECHNIQUES

3.4.1 RIPPING MEMBRANE TECHNIQUE

3.4.2 ROLLING BALL TECHNIQUE

3.5 ARITHMETIC OPERATIONS

3.6 SUMMARY

### 3.1 INTRODUCTION

There are two general objectives in the use of satellite remote sensing data (images) for geological studies. These are the detection of geological linear features (lineaments) and rock type discrimination.

A considerable effort has been directed towards the detection of lineaments from remote sensing images, using digital image processing techniques (mainly spatial filtration). The definition of lineament will be discussed in this Chapter.

New contextual techniques have been developed and examined during the course of this study. The theoretical ideas of these techniques, spatial filtration, and the arithmetic operation will be discussed in this Chapter.

### 3.2 DEFINITION OF LINEAMENTS

The word lineament was introduced into the geological literature by Hobbs (1904). They were defined as "significant lines of landscape that reveal the hidden architecture of rock basement". O'Leary et al., (1976) refined the concept and defined the term lineament as "a mappable simple or composite linear feature of a surface, whose parts are aligned in rectilinear or slightly curvilinear relationship, and which differs distinctly from the patterns of adjacent features, and presumably reflects some sub-surface phenomenon". Stefouli and Osmaston

(1984) have individually defined the term linear features "any linear image formed by points or groups of points which possess certain similarities of relief, tone, texture or pattern, different from those of the surrounding area; or a boundary which divides two areas that differ in one or more of these properties".

From these definitions, it is clear that the study of lineaments in aerial photographs or satellite images is of great interest to the structural geologist. In addition, geologists have been interested in tracing lineaments from satellite images for practical purposes, (e.g. fault and joints in rock provide a key to the occurrence of minerals, ground water and petroleum).

The most important lineaments (or geological linear features) in remote sensing are fault and joints. The fault is a "planar discontinuity between blocks of rock that have been displaced past one another in a direction parallel to the discontinuity" (Hobbs et al., 1976). The interpretation of faulting systems and faulted rocks is complex and it is beyond the scope of this study. In remote sensing images, faults provide straight linear features and are easily detected, because they usually form a zone of weathering and weakness.

Most rocks are broken by relatively smooth features known as joints. Their length is measured in feet, tens of feet, or hundreds of feet, and the distance between these features is usually of the same order of magnitude (Billings, 1972).

Usually there is no visible movement parallel to the surface at a joint. Joints may have any attitude; some joints are vertical, or horizontal and many are inclined at an angle. Differences in jointing can help in distinguishing between rocks. For example, granite and sandstone both show light colour in black and white images but granite shows irregular joint patterns compared with sandstone (Drury, 1987).

The lineaments studied in remote sensing range from small scale (i.e. hundred meters) to enormous sizes (i.e. continental). Satellite studies of lineaments have found applications in numerous fields of earth sciences, for example, lineament detection has been used to map previously unknown faults (e.g. Johnston et al., 1975; Johnson and Frost, 1977; Gold, 1980; Williams, Jr., 1983; Berhe and Rothery, 1985 and Sabins, 1987), to delineate fractures or fracture systems in different parts of the world (e.g. Viljoen et al., 1975; Sesöern, 1976; Johnson and Frost, 1977; Offield, 1977; Ramberg et al., 1977; Kim, 1979; Iranpanah and Esfandiari, 1980; Csillag, 1982; Cochrane and Tianfeng, 1983; Moore and Waltz, 1983; Stefouli and Osmaston, 1984; Belliss et al., 1985; Isiorho 1984, Parson and Yearley, 1986; Maude, 1987 and Reddy, 1991), to carry out structural analysis of global or regional tectonics (e.g. Molnar and Tapponier, 1975; Cardamone et al., 1976; Dikkers, 1977; Forst, 1977; Braun, 1982; Marrs and Raines, 1984; Zilioli and Antonietti, 1987; Johari, 1990; Qari, 1990; Alonso and Tahon, 1991 and Duncan et al., 1990). In more practical areas, lineaments have

been studied in general geological exploration, for example, to find likely areas of base metal deposits (e.g. Tiwari and Jhingran, 1991), to find ground water (e.g. Moore and Hinkle, 1977; Vincent and Scott, 1978; and Berlin *et al.*, 1987) and petroleum (e.g. Halbouty, 1976).

Stefouli and Osmaston, (1984) indicated that an image consists of basic units, that are points (pixels) and if a point is to be assigned to a linear feature or lineament, then the point has to satisfy some criteria; first, the point must be adjacent to at least another similar point, and they must form a linear feature. Secondly, the geometric characteristics of the length, shape and orientation are also discerned, and contribute to the recognition of the lineament. Thirdly, the points must share a property common to all members of the feature and which is not shared with points outside the line, and these properties are based on the texture and tone of the image, or the reflections pattern.

Also there are lineaments which, strictly speaking, are not themselves composed of identifiable points, but are the boundary between two areas which differ in tone, texture, etc., for example, linear topographic features, relief change lines, textural lines and linear drainage channels (Stefouli and Osmaston, 1984).

According to Short and Lowman, (1973), and Johari, (1990),

lineaments may be distinguished on Landsat satellite images by one or more of the following indicators:-

- a) Alignment of topographic forms often emphasised by shadowing.
- b) Alignment of drainage patterns.
- c) Bands of variable widths which contrast in tone to the immediately adjacent areas.
- d) Lines of variable length, straightness and continuity as set apart by tonal contrasts in the image.
- e) Co-alignment of cultural features, (e.g. farms, road patterns, etc.) with underlying structural and/or surrounding topographic control.
- f) Association of vegetation along linear trends.

Lineaments may be continuous or discontinuous. Continuous lineaments are the continuous straight lines. In discontinuous lineaments the separate features are aligned in a consistent direction and are relatively closely spaced. Lineaments may be simple or composite. Composite lineaments are defined by more than one type of feature; simple lineaments are formed by a single type of feature. Table 3.1 shows the scale of some linear features on the earth's surface, without obvious displacements.

Lineaments in an image can usually be identified by visual interpretation using tone, colour, texture, pattern, association etc. However, many lineaments are subtle and require image

**TABLE 3.1**  
**Scale of some linear traces without obvious**  
**displacements (From: Gold, 1980)**

<b>SURFACE FEATURES</b>	<b>SIZE</b>	<b>MAPPING BASE</b>	<b>POSSIBLE STRUCTURES</b>
Joint Traces	Centimetres to tens of meters	Outcrop maps, orientation diagrams, large scale aerial photographs	Bedding
Fracture traces	Approx. 100 m to 1.6 km	Aerial photographs, largescale topographic maps	Narrow, steeply dipping zones of joint connections up to 33m wide
Lineaments	(a) Short: 1.6 to 10 km	Topographic maps, small scale aerial photographs	Broad zones of up to a few km wide of disrupted rock, including concentrations of narrow fracture zones
	(b) Intermed: 10 to 100 km	Topographic maps and relief models (1:250,000), high altitude imagery	
	(c) Long: 100 to 500 km	Satellite imagery, small scale relief models	Petrographic provinces and aligned volcanic centres, rift valleys, aulacogens and continental sutures as much as 100 km wide
	(d) Megalineaments: 500 km	Satellite imagery, and mosaics of Landsat imagery	

processing enhancement. Spatial filtration techniques have been the most common method of enhancing lineaments. These techniques and the new contextual techniques will be discussed in the next sections.

### **3.3 SPATIAL FILTRATION TECHNIQUES**

Spatial information, (and lineaments are one type of spatial information), in digital remote sensing images can be thought of

as the spatial distribution of the grey levels or texture (Schowengerdt, 1983), (Chapter 8). Texture, in general, can be divided into two different types, coarse texture and fine texture. The first one contains low spatial frequencies, while the second one contains high spatial frequencies (Stefouli, 1983).

Filtering techniques when applied to a digital image, are designed to enhance different scales of tonal or DN value "roughness" (i.e. different spatial frequencies). Spatial filtering depends, not only upon the value of the pixel being processed, but also on the pixel values surrounding it. In this regard, spatial filtering is an area operation. Spatial filters can be used, either to emphasise, or to de-emphasise the abrupt changes in pixel DN's, thereby altering an image's textural appearance (Lillesand and Kiefer, 1987).

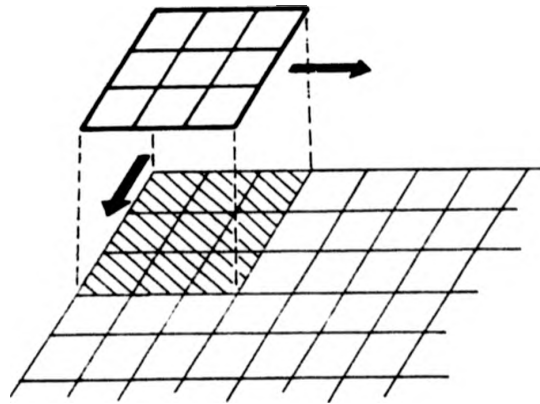
Any digital image contains both low and high frequency spatial information, and their sum constitutes the original image. The low-frequency component represents gradual DN changes, over a relatively large number of pixels (i.e. low tonal variance). Therefore, it is defined as the "smooth" component of the image. The high frequency component on the other hand, consists of DN's changes over a short spatial dimension representing abrupt boundaries, edges, or lineaments.

The high frequency component is often a good indicator of geological features; it may be shadowing as a consequence of topography, which could possibly reflect rock types with different resistance to erosion or it may be linear features, such as faults or joints, or it may be boundaries between rocks with different reflective properties, soils, derived from different rock types, or vegetation boundaries that have an underlying geological correlation.

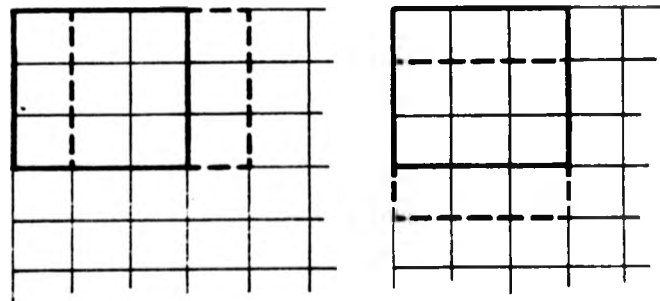
Convolution filters are frequently used to detect and enhance the various spatial frequencies in an image. These involve two procedures:-

1. A moving window is established which has an array of coefficients or weighting factors (the arrays are referred to as the filters or kernels).
2. The kernel starts from the top left corner of the image. Each coefficient factor is multiplied by the corresponding pixel value (DN), and the result stored in an output image (Lilliesand and Kiefer, 1987). Figure 3.1 shows the moving spatial window concept.

The low-pass spatial filters are performed by calculating a local DN average of the digital array, or window, centred around the pixel being processed (Figure 3.2).



(a) PROJECTION OF WINDOW ONTO IMAGE BEING PROCESSED



pixel-to-pixel within  
a line

line-to-line

(b) CONSECUTIVE WINDOW CALCULATIONS

FIGURE 3.1 The moving spatial window concept.  
(From: Schowengardt, 1983).

**Figure 3.2**  
**The convolution matrix for a low-pass filter;**  
**a 3 x 3 matrix of equally weighted cells.**  
 (From: Drury, 1987)

$$\begin{array}{|c|c|c|} \hline 1/9 & 1/9 & 1/9 \\ \hline 1/9 & 1/9 & 1/9 \\ \hline 1/9 & 1/9 & 1/9 \\ \hline \end{array} \quad 1/9 \times \quad \begin{array}{|c|c|c|} \hline 1 & 1 & 1 \\ \hline 1 & 1 & 1 \\ \hline 1 & 1 & 1 \\ \hline \end{array}$$

The DN average of the filter box is considered to be the low frequency component. The low pass algorithm reduces the deviations within the image and this produces an image smoothing or blurring, which increases as the filter size increases. Because of the blurring effect, low pass filtering is useful for reducing certain noise patterns and for smoothing blocky image data, before visual interpretation or digital analysis.

The simplest means of high-pass filtering can be done by subtracting a low pass filtered image from the original image (Figure 3.3), (Drury, 1987). In general, a high pass filter enhances features that are less than half the size of the window being used, at the same time de-emphasising features that are more than half the window size. For this reason, these filters, with different sized windows, are used to highlight small, intermediate and large scale structures (Avery and Berlin, 1985), depending on the size of the filter. In the case of geological features of regional dimensions such as major lineaments, very large matrices must be used.

**Figure 3.3**  
 Convolution matrices for edge detection or high-pass filtering can be achieved by subtracting the results of a low-pass convolution from the original image (a) or devising matrices based on more complex algorithms (b) and (c). Edge enhancement matrices result from adding the edge detector to the original image (d)-(f).  
 (From: Drury, 1987).

$$\frac{1}{9} \times \begin{array}{|c|c|c|} \hline 1 & -1 & -1 \\ \hline -1 & 8 & -1 \\ \hline -1 & -1 & -1 \\ \hline \end{array}$$

(a)

$$\frac{1}{2} \times \begin{array}{|c|c|c|} \hline 0 & -1 & 0 \\ \hline -1 & 4 & -1 \\ \hline 0 & -1 & 0 \\ \hline \end{array}$$

(b)

$$\begin{array}{|c|c|c|} \hline 1 & -2 & 1 \\ \hline -2 & 4 & -2 \\ \hline 1 & -2 & 1 \\ \hline \end{array}$$

(c)

$$\frac{1}{9} \times \begin{array}{|c|c|c|} \hline -1 & -1 & -1 \\ \hline -1 & 9 & -1 \\ \hline -1 & -1 & -1 \\ \hline \end{array}$$

(d)

$$\frac{1}{2} \times \begin{array}{|c|c|c|} \hline 0 & -1 & 0 \\ \hline -1 & 5 & -1 \\ \hline 0 & -1 & 0 \\ \hline \end{array}$$

(e)

$$\frac{1}{2} \times \begin{array}{|c|c|c|} \hline 1 & -2 & 1 \\ \hline -2 & 5 & -2 \\ \hline 1 & -2 & 1 \\ \hline \end{array}$$

(f)

Special high-pass filters are used to detect edges and lineaments with specific directions (Figure 3.4). The linear features that tend obliquely to the filter direction can be enhanced. However, in order to exhaust the different possible orientations of a lineament, several filters, with different directional sensitivity, should be used. Moore and Waltz (1983) used a method to extract lineaments from MSS imagery, using different directional filters (Figure 3.5). This method has five stages:-

- (a) generating a low spatial frequency image with an averaging function,
- (b) extracting directional data with a convolution filter,
- (c) smoothing the directional data with an averaging, or tangent function,
- (d) further smoothing the data by extracting directional trends in the tail of the image histograms,
- (e) adding the enhanced directional trends to the original image.

### **3.4 THE NEW CONTEXTUAL TECHNIQUES**

Two different contextual techniques are discussed in this section; these are the ripping membrane technique and the rolling ball technique.

#### **3.4.1 Ripping Membrane Technique**

The ripping membrane (RM) technique was proposed by Blake and Zisserman, (1983) as an algorithm, and constitutes a powerful filter. This algorithm has the ability to detect discontinuities

**Figure 3.4**  
**Four directional filters enhancing only**  
**lines trending near the specified azimuth**  
**(e.g. northeast, southwest).**  
**(a) East-west enhancement, (b) North-south enhancement,**  
**(c) Northeast-southwest enhancement,**  
**(d) Northwest-southeast enhancement.**  
**(From: Maude, 1987).**

1	-1	-1
0	0	0
1	1	1

(a)

-1	0	1
-1	0	1
-1	0	1

(b)

-1	-1	0
-1	0	1
0	1	1

(c)

0	-1	-1
1	0	-1
1	1	0

(d)

**Figure 3.5**  
 Derive directional components from the low-pass image.  
 The digital value of each pixel in the low-pass image is replaced with a value produced by the windows. Each pixel in the window is multiplied by the indicated number; the final value for the central pixel is a sum of these products.  
 (From: Moore and Waltz, 1983).

**East-West**

-1	-2	-1
2	4	2
-1	-2	-1

**North-South**

-1	2	-1
-2	4	-2
-1	2	-1

**NW-SE**

2	-1	-2
-1	4	-1
-2	-1	2

**NE-SW**

-2	-1	2
-1	4	-1
2	-1	-2

**WNW-ESE**

1	-2	-2
1	4	1
-2	-2	1

**NNW-SSE**

1	1	-2
-2	4	-2
-2	1	1

**ENE-WSW**

-2	-2	1
1	4	1
1	-2	-2

**NNE-SSW**

-2	1	1
-2	4	-2
1	1	-2

and localise them accurately and with stability, unlike the kernel filters. Many methods have been proposed for detecting edges or discontinuities in intensity data. The abrupt changes in the visible surfaces are indicated by the step discontinuities in the intensity or DN's in the digital image. For example, where one surface or object ends and another begins (e.g. the contact between two different rock types or lineament lines), there is an abrupt change in the DN values.

The ripping membrane technique is based on the analogy with an elastic membrane which is capable, when stretched sufficiently, of ripping. Imagine an image (grey level) as a topography, with the height being proportional to the DN values. At each point in the image, a spring is anchored to the height of the image at that point, the other end is attached to an elastic sheet. Depending on the relative strength of the springs and the elasticity of the membrane, the shape of the membrane will come to an equilibrium. Using the principle that any system will, at equilibrium, have a minimum of energy, then it is possible to find mathematically, the equilibrium position of the membrane. However, it is possible that, if the membrane is stretched too much, as across a large sharp boundary in the image, it will rip. The mathematical solution of such a problem is complex, and Black and Zisserman (1983) have prepared one possible solution. The solution, they propose, describes the surface of the membrane, depending on the three factors, (a) the topography of the DN values and how closely the membrane follows

this surface (this depends on the strength of the spring), b) the elasticity of the membrane (this determines how well the membrane follows the local average, and ignores individual departures), c) the 'ripping point' of the membrane (this determines where the contextual average is discounted in favour of a discontinuous break (cliff) or rip).

By varying these factors, various solutions can be found. These solutions can be continuously varied from one which closely follows the topography of the DN values, to one which closely follows the large scale average of the topography of the DN values.

In this study, the interest lay in the detection of lineaments, and the detection of gross lithological boundaries (large changes in DN values) was of secondary importance. Therefore, the 'ripping point' was kept fixed, and the relative strength of the strings and the elasticity of the membrane was systematically varied. Thus, only one parameter, called the 'range' was varied. The larger the 'range', the more the elasticity of the membrane dominated over the strength of the strings, and hence, the more the solution reflected the contextual average. The smaller the range, the more the solution followed the topography of the DN values. Where the 'range' is large, then a 'smooth' topography will result, with 'rips' only where the discontinuities in the DN values, are large and continuous. The difference between the original image and the 'membrane' solution, was

expected to reveal the 'local variations'. The size of the 'local variation' would, of course, be dependent on the 'range' parameter. In effect, the membrane defines a contextually dependent density slice, and enables the local variations to be examined, independent of the context (i.e. absolute DN value). This is an important feature in the detection of large scale lineaments, where they are expected to go through several 'regions' with highly different brightnesses.

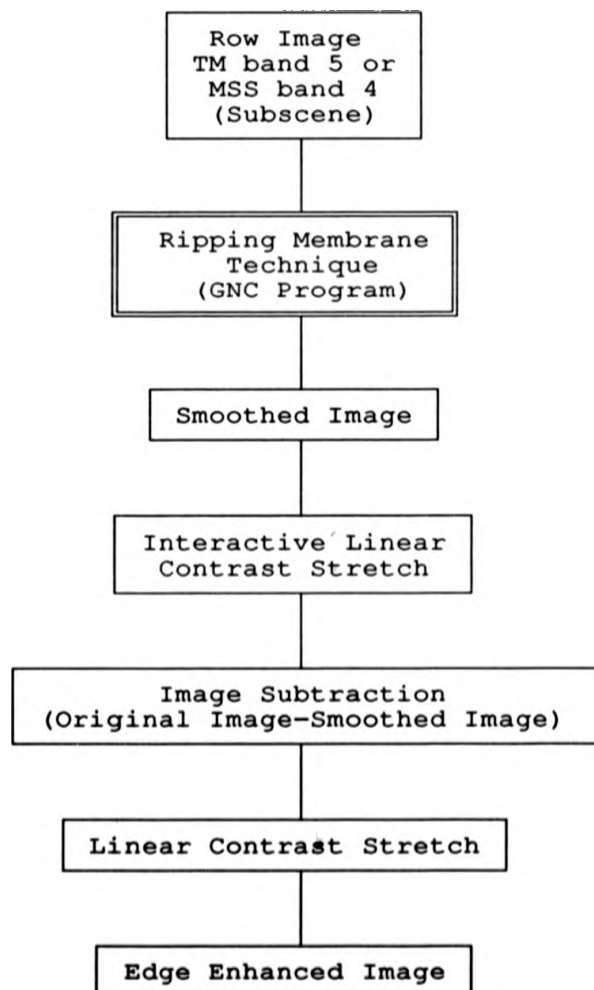
A program called GNC has been written, (Watson, per.comm, 1990), which implemented the proposed ripping membrane model, and this was examined and developed during the course of this study.

The author examined this program over different 512 x 512 pixels or 1024 x 1024 pixels extracts from the study area in order to choose the best 'range' to use. For more information about the application of this technique, see Chapters 4 and 5.

Three stages were used during this study, to produce a final image from the ripping membrane (RM) technique for lineament detection (Figure 3.6).

1. applying the GNC (RM technique) program for 512 x 512 pixels or 1024 x 1024 pixels with a variety of ranges to produce a variety of smoothing.
2. Once the smooth image has been produced, it is subtracted from the original image band.
3. The resultant image is stretched linearly.

**Figure 3.6**  
Flow chart of the stages used during this study to produce a final result from the ripping membrane technique for lineament detection only. Double line box for image processing carried out on Micro-Vax computer using GNC algorithm before the processed data was transferred to R-CHIPS system.



### 3.4.2 Rolling Ball Technique

Sternberg (1983), developed a variety of algorithms for use on parallel computers, to analyse medical images. The algorithms enabled the detection of particles (local variations) despite gross variations in the background intensities. In this respect, they had obvious similarities to the 'ripping membrane' technique.

In order to develop the algorithms Sternberg, (1983) needed to view the image as a set of "boxels" or cubic pixels in a 3-D volume. This representation, Sternberg, (1983), called the umbra of a grey level image. The rolling ball transformation can be visualised as a solid sphere, that moves freely within the image umbra, but is constrained by the upper surface of the umbra, as shown in Figures 3.7 - 3.8. The process of finding the minima and then maxima of these minima is the algorithm's way of finding the position of the centre of the ball. The sphere diameter can be selected so that it is considerably wider than any of the 'objects' in the image. However, the diameter of the spherical structuring element is small enough to follow the smooth contours of the changing background intensity. The background is smooth with respect to the sphere, but the upward peaks or spikes are not. The trajectory of the centre of the ball can be followed and this is in fact the 'smoothed' image. Once the smoothed image has been generated from below, the same process is applied from above. In this case the 'dimples' are not followed by the ball. By combining the two smooth components and the original,

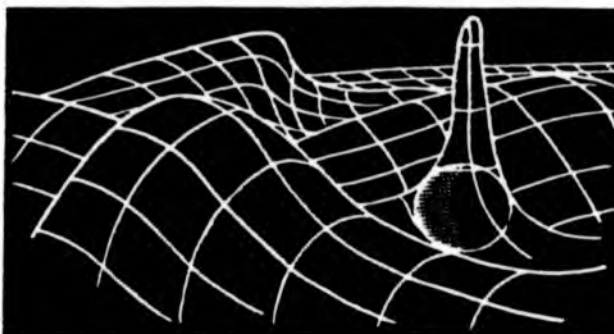


FIGURE 3.7 Schematic representation of the rolling ball algorithm used for background normalisation. The ball follows the smooth background contours but does not penetrate the spot peaks. Rolling a ball is equivalent to eroding and dilating by a spherical structuring element.



FIGURE 3.8 Digital ball. This shaded structuring element is obtained by dilating a single point by a sequence of 26 gray-scale neighborhood operations.

two possible resultant images can be generated. One a completely smooth image with both 'spikes' and 'dimples' removed. The other is a combination of the 'spikes' and 'dimples'. As the size of the ball increases, wider 'spikes' and 'dimples' are separated from an increasing smooth component. Thus the rolling ball transformation can systematically separate the spatial variability from the smooth component of an image. A program called ROLL was written for this study (Watson, per. comm, 1990).

This program implemented the Sternberg (1983) algorithm for a 'rolling ball' transformation, which enabled an estimate of the background level, across a single grey level image, to be made. For more detail about the application of this technique, see Chapters 4 and 6.

### **3.5 ARITHMETIC OPERATIONS**

Arithmetic or mathematical operations are operations which can be used in image contrast or enhancement or to find difference between images. These operations are:-

1. Image addition
2. Image subtraction
3. Image multiplication
4. Image division (ratioing)

These operations are usually used on two images for the same area. For more detail see Mather (1987). In this study, only three operations have been used in lineament detection methods and these are image addition, multiplication and subtraction.

### 1. Image Addition:

In image addition, all the DN values (reflectance) in two spectral bands are added to form a single new image, so that contrast becomes stronger. This process of addition is carried out on a pixel by pixel basis. Mather (1987) has expressed this process as follows:-

$$G_{sum}(x,y) = (G_1(x,y) + G_2(x,y)) / 2$$

$G_1(x,y)$  and  $G_2(x,y)$  are the images to be added.

The result number of the addition has been divided by two in order to ensure that image  $G_{sum}(x,y)$  has a dynamic range of 0-255.

In addition to increasing the contrast, this process can be used to reduce overall noise in the image (Mather, 1987). The single image might be expressed in terms of the following model:-

$$\text{Result image} = \text{true image} + \text{the random noise component}$$

Image addition has been used during this study in lineament detection techniques (Chapter 4), image segmentation (Chapter 5), and texture analysis applications (Chapter 8).

### 2. Image Subtraction:

This process can be applied to two images and these images have to have at least some differences. This process is often used in the detection of temporal changes between two images, acquired at different times. This process is performed on point-by-point (pixel-by-pixel) basis (Mather, 1987). Mather (1987) explained this process as the following equation:-

Difference image = (maximum DN value + first image - second image)

### 3. Image Multiplication:

Image multiplication is very rarely used in image processing of remote sensing data. It is useful only if an image of interest is composed of two or more distinctive regions and if the photo interpreter is interested only in one of these regions (Mather, 1987).

### 4. Image Division:

Image division is universally known as ratioing or band ratioing, and it is one of the most commonly used transformations applied to remote sensing images and interpretation. A band ratio is, the ratio of one band to another, and is prepared simply by dividing the DN of a pixel in one band, by the corresponding pixel in another band. This technique is usually used in surface discrimination (i.e. rock discrimination). More discussion of using band ratio and ratio colour composite are in (Section 7.3).

### 3.6 SUMMARY

Satellite images have provided an excellent tool for lineament detection in geological investigation. This Chapter is an overview of the definition of lineament and a review of their application in geological studies in general. Spatial filtration is an important technique of image processing in enhancing the edges and the lineaments. This technique, and the

two new contextual techniques (ripping membrane and rolling ball), were discussed in detail in this Chapter. This was followed by a very brief definition of the arithmetic operations of image processing, which will be used in the following Chapters.

## **CHAPTER FOUR**

### **THE USE OF NEW CONTEXTUAL TECHNIQUES IN LINEAMENTS MAPPING AND ANALYSIS: AN APPLICATION**

- 4.1 INTRODUCTION
- 4.2 DATA SELECTION AND METHODOLOGY
- 4.3 GEOLOGY OF THE TEST SITE (JIBAL RUMMAN AREA)
- 4.4 COMPARISON BETWEEN THE TECHNIQUES AND  
THEIR RESULTS
- 4.5 GENERAL LINEAMENTS INTERPRETATION AND MAPPING
- 4.6 LINEAMENTS ANALYSIS (ROSE DIAGRAM)
- 4.7 DISCUSSION
- 4.8 SUMMARY

#### 4.1 INTRODUCTION

The study of lineaments has found applications in numerous fields of structural geology e.g. delineation of major structural units and contacts, global tectonic studies and analysis of structural deformation patterns (Gupta, 1991).

The investigation in this Chapter mainly deals with the detection of lineaments from Landsat-5 data (MSS and TM). Thus, two different spatial resolutions have been examined. Several digital enhancement techniques have been tried to identify the maximum number of lineaments in the chosen test site.

The analysis of lineaments in general is a two stage process:- identification followed by analysis. The first stage involves the recognition of lineaments from a source image (original or enhanced image). The second stage involves the actual analysis of the derived Lineament map.

The main purpose of this Chapter is as follows:-

1. To test and develop new digital image processing techniques (contextual techniques) that can be used for lineament detection,
2. To interpret and compare the results obtained by different lineament detection techniques,
3. To prepare one lineament map based on all the different technique results and compare it with geologic map and field observation,

4. This study does not attempt to analyse individual lineaments, but the main interest of this study will depend on the statistical significance of the lineament pattern as a whole, rather than an interpretation of the individual lineament within that pattern. The Azimuthal distribution diagram will be produced to show the major trend and density of the lineaments in the test site in general, and for each individual rock type.
5. To relate the structural features to the tectonic history of the study area.
6. To choose the best images to be used in the automatic line and lineament feature extraction method. (Chapter 6)

Two main categories of techniques were applied during the image processing stage; the first category is spatial image filtration (i.e. directional and non-directional spatial high-pass filtration), (Section 3.3); the second category is the new contextual techniques which include ripping membrane and rolling ball techniques, (Section 3.4).

#### **4.2 DATA SELECTION AND METHODOLOGY**

The Landsat-5, MSS and TM data was acquired in the winter period where low sun elevation angles enhance the visibility of topographic variation, and help in lineament detection and interpretation. The best sun-evaluation angle depends on the terrain itself. The angle of 35° to 45°, for example, is near

optimum for slightly rolling terrain (Moore and Waltz, 1983). However lineaments running parallel to the sun azimuth on the acquired data, will be hard to detect. (Table 2.3). The MSS band 4 and TM bands 5 and 7 were found to be the best in terms of contrast, definition of geological features and topographic shadows - a key feature in the lineament identification. These features are more uniformly apparent, across a wide range of surface types at infrared wavelengths. Further, there is less atmospheric interference in the infrared bands.

The author has used various edge enhancement and new contextual techniques in order to identify lineaments. The lineaments were identified in the images by visual interpretation. Although this method has been criticised as subjective by Moore and Waltz, (1983), who argued in favour of machine processing, due to inter and intra operator variance. This argument will be discussed in more detail in Chapter (6). The author followed four steps to complete the lineament identification, mapping, interpretation and analysis:-

#### **1. Image processing techniques:**

A variety of edge enhancement techniques have been tested on the test site image data. These include high pass filters both directional, and non-directional, to enhance linear features, oriented in north-south, northeast-southwest, northwest-southeast, and east-west directions. (Section 3.3), (Figure 3.4).

Only 3 x 3 Kernel filter operator sizes are available on R-CHIPS image processing system (Section 2.5). The two new contextual techniques were examined and developed for the same purpose (ripping membrane technique and rolling ball techniques, Section 3.4). The ripping membrane program called GNC was applied to Landsat TM, band 5 and MSS band 4 subscenes image data (512 x 512 and 1024 x 1024 pixels in size) with different ranges (Section 3.4.1) (2, 5, 10, 15, 20, 25, 30, 35, 40 and 60). Ten different ranges for the TM bands and five ranges for the MSS band 4 have been interpreted separately, to find out the best range which produce maximum number of lineaments. The range (40) was found to be the best for TM, and range (25) for MSS. The rolling ball method is the second contextual technique examined and developed. The rolling ball program called ROLL was applied to TM band 5 and MSS band 4 subscenes image data (512 x 512 and 1024 x 1024 pixels in size). Six different ball diameters were applied (Section 3.4.2), (2, 3, 6, 8 and 10).

The results for each range were carefully compared and interpreted separately, in order to find the best range or ball size to be used in visual lineament detection. A range (ball size) of 8 or 10 for TM image and range 3 for MSS were found to be the best ranges to enhance the images. Any range less than these kept some smooth frequencies, and hence did not produce a clear definition of the lineaments within the mountains, while the higher range took a very long time to process (12 Hours). Both resultant images of the contextual

techniques were combined with the original image using the arithmetic operations (addition and multiplication) (Section 3.5). But this did not show any acceptable result for interpretation or for further processing.

## **2. Lineament identification stage:**

The lineaments were identified and traced from eight different images (four directional high-pass filtered, one non-directional high-pass filter, two new contextual techniques for the same image data and the original image band 5), by visual inspection, with or without a magnifying lens (power 2 x, 4x).

The lineaments were then recorded on transparent overlays as ruled straight lines. Some of the edges are boundaries between rocks with different properties, and there were excluded from this interpretation.

Each of the seven images was interpreted separately to produce preliminary lineament maps. Any linear features present in more than one of the preliminary lineament maps were then traced onto a final interpretation map. The result is an interpretation that includes only the most definite lineaments. This procedure is considered to be more objective (Maude, 1987). Lineament tracing has been prepared without prior knowledge of the available sketch structure map and the geological map. Two lineament types were identified; first, clear lineaments which were defined as those clearly expressed in the image by straight distinct tonal contrast and, second, the weak lineaments which were

defined as narrow straight lines. This study was carried out on lineaments of more than 1.5 kilometres in length.

**3. Comparison of the different preliminary lineament map:**

All the interpreted lineaments were compared with the available geological maps and reports (Section 1.7.3). The comparison was first made between the lineament map and the 1:100,000 scale map (reconnaissance map), there then followed a comparison with 1:250,000 respectively.

**4. Field visit and inspection:**

The final lineament interpretation map was produced before the ground inspection. Around 50 mapped lineaments were observed during the field survey and these were plotted on a map and on full resolution SPOT panchromatic image and geological map (scale 1:100,000). No aerial photographs for the study area were available. Field work included checking the features that were accessible. Inaccessibility of certain areas in the field imposed limitations on the field checking of the Landsat lineaments.

**5. Lineaments analysis (Rose Diagram):**

Lineament mapped on any remote sensing images might show a spatial variation in trend (orientation), frequency and length. The final step in the analysis was to construct a diagram, which would show the azimuth frequency of lineaments, in the expectation that this would reveal the significant trend of lineaments. The counting of lineaments for number and length was carried out manually.

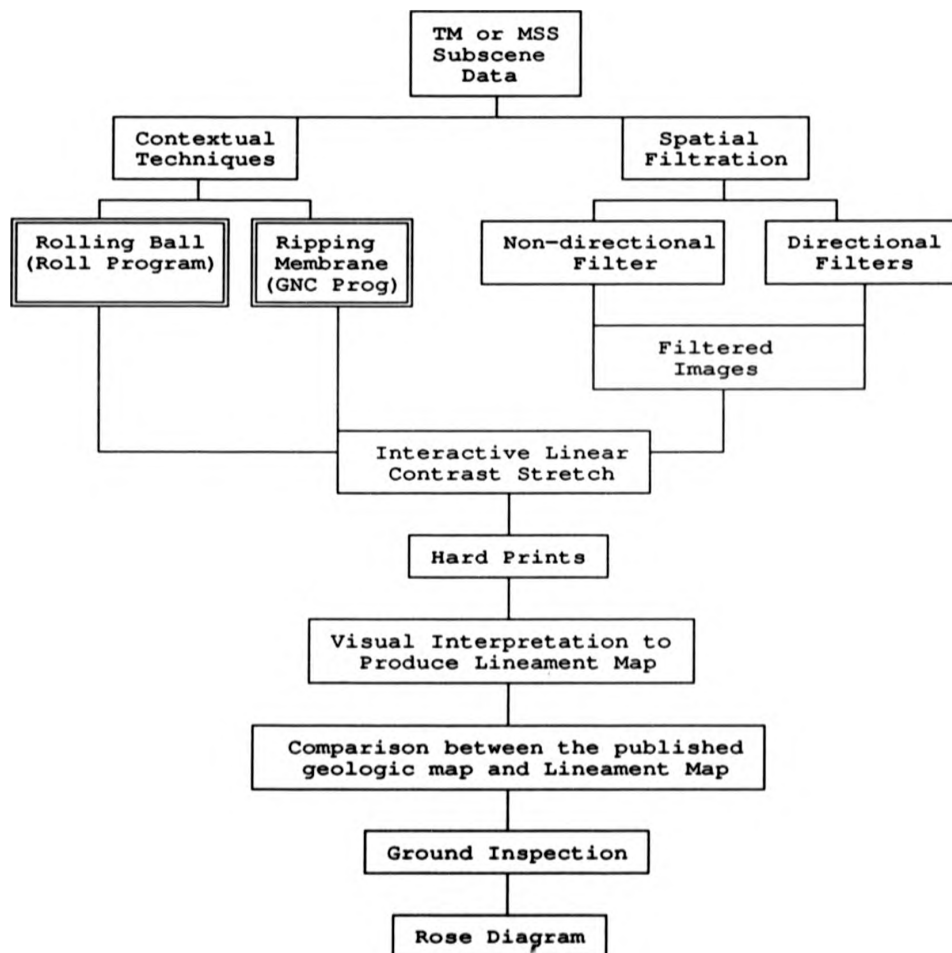
In the analysis of lineaments, it should be realised, that

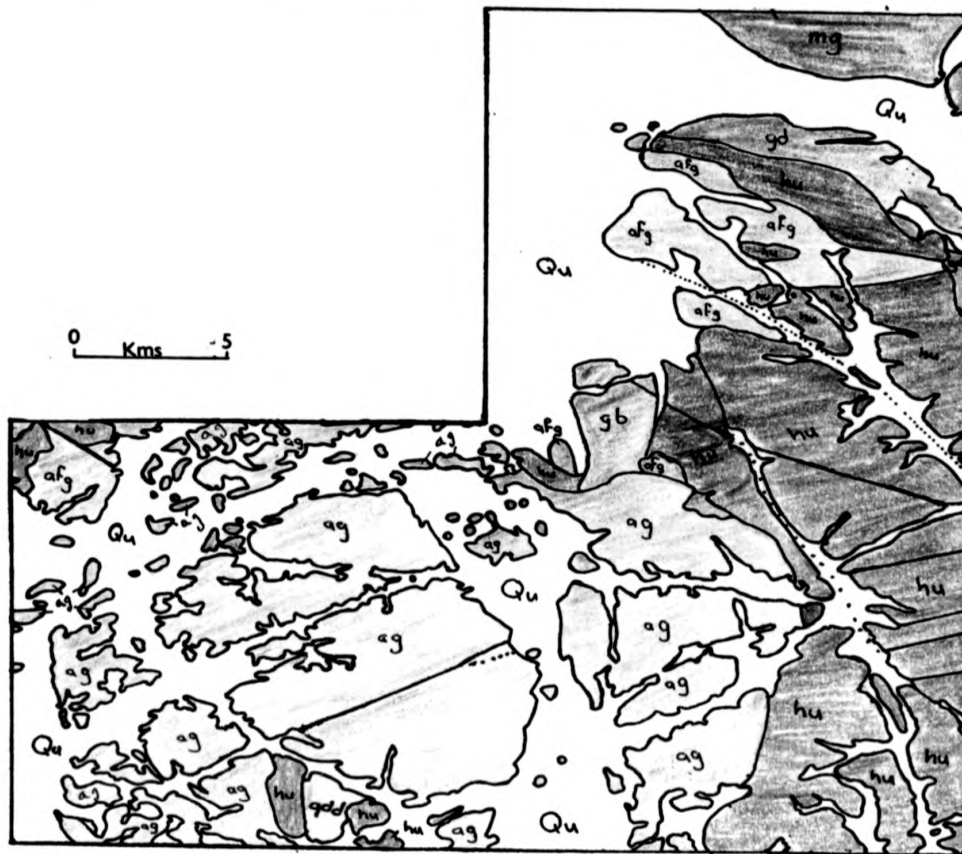
the orientation or trend and density measured on one scale (i.e. different satellite spatial resolution) are not necessarily the same as those mapped at some other scales (Gold 1980). For this reason it is interesting to compare the MSS and TM for lineament analysis because of their different resolution. Figure 4.1 shows a flow chart diagram for the steps followed to complete the lineament identification and analysis process in this study. These steps have fulfilled the first four aims of this chapter (Section 4.1).

#### **4.3 THE GEOLOGY OF THE TEST SITE (Jibal Rumman Area).**

The test site is located in the northeastern part of the study area (see the geologic map of the study area in Appendix 1 for location). It is well exposed except for a small amount of natural vegetation cover and some agricultural activity. There are different igneous rocks (Figure 4.2) in the chosen site and these cover around 675 Km<sup>2</sup>. The rocks of the Hadn Formation (hu) mapped in the 1:100,000 map as Al-Awashziah Formation (Leo, 1984) form steep sided hills and precipitous cliffs. The rock surface is weathered with rusty red brown to black colour (Plate 4.1). It is a volcanic rock composed of rhyolitic to rhyodacitic ash-flow tuff, lesser amounts of arkosic sandstone and conglomerate. The internal stratigraphy of the Hadn Formation is poorly understood (Quick and Doebrich,

**Figure 4.1**  
**Flow Chart showing the different steps followed to complete lineament identification and analysis. Double lined boxes for image processing carried out on Micro-Vax computer using certain algorithms before the processed data was transferred to R-CHIPS System.**





- Qu Undivided Quaternary deposits
- gb Gabbro
- ag Alkali granite
- afg Biotite Alkali - feldspar granite
- mg Kilab monzogranite
- gd Maa Complex - Granodiorite to tonalite
- qdd Juwayy Rashib Complex - Diorite
- Hadn Formation - Rhyolitic to rhyodactic ash flows
- Lithologic contact
- Fault (dotted where concealed)

**FIGURE 4.2**  
 Geologic map of the Jibal Rumman (test site) area compiled from Quick, 1983 ; Leo, 1984 and Quick and Doebrich, 1987



**PLATE 4.1**  
The Hadn Formation in the field.

1987). This rock unit covers a large area in this test site. A major source area for the Hadn Formation is a Caldera and part of it is present in the test site area (eastern part of the test site) (Figure 4.2), (Leo, 1984; Quick and Doebrich, 1987). The Maa Complex (gd) occupies a small area in the northeastern section of the test site and is medium to coarse grained and the composition grades from granodiorite to tonalite. In the field it forms small hills with a grey to green colour. The Juwayy Rashib Complex (qdd) is composed of quartz diorite to diorite and forms only small hills located in the south of the test site. Kilab monzogranite (mg) is present in the area as small low, weathered outcrops and is located only in the northern part.

There are two different types of granite, which belong to the Salma Complex (Quick and Doebrich, 1987), sometimes referred to as Salma granite, the first is biotite alkali-feldspar granite (afg) and the second is alkali granite (ag), (Section 1.7.3). The biotite alkali-feldspar granite occurs as relatively small intrusions while the alkali granite forms long large plutons in the south and southwest of the test site. This rock is readily distinguishable from the surrounding granite by its ragged topography (Plate 4.2). It occurs as steep sided mountains. The alkali granite intrudes the Hadn Formation.

There are only small eroded hills of gabbro located mainly in the central part of this test site. The Quaternary deposits



PLATE 4.2 The alkali granite in the field.

Qu) alluvium and colluvium occur primarily in valleys, channels. Figure 4.3 shows a structural sketch map for study area; the test site area is shown in the rectangle. Drury, (1987) has reported that where granite contains a high quartz content in arid lands, weathering is dominated by physical processes such as heating and cooling. Because of the different coefficients of thermal expansion of quartz and feldspar, the rocks rapidly crumble. In the test site, although this process has undoubtedly occurred in the alkali granite, the joints and other lineaments visible in Plate (4.2) may have resulted from deeper stated lances cooling of magma, tectonism, unloading.

The test site is covered by three 512 x 512 pixels, sub-scenes, thus for full resolution display, these images were displayed separately.

Part of this site has been chosen to examine and develop a new method for automatic lineament extraction (Chapter 6).

#### **4.4 COMPARISON BETWEEN THE TECHNIQUES AND THEIR RESULTS**

A comparison was made among the seven different edge enhancement techniques and the unstretched and linearly contrast stretched original TM band 5 (Black and White). (Table 4.1 and Plates 4.3-4.5). A total of 175 lineaments (clear and weak) from the TM data for the test site with a total approximate length of 373.5 KM were found . Figure 4.4 shows all these lineaments.

Only lineaments with a length of 1.5 KM and above are shown, and



Table (4.1) shows the total detected lineaments traced from each individual image. A total of 169 lineaments, which represents 97.6% of the total lineaments, were present in the ripping membrane result (Figure 4.5) while the rolling ball technique was the second in the number of the detected lineaments - a total of 119 lineaments - which is 68% of the total number of lineaments in the test site. (Figure 4.6).

Only the northeast-southwest high-pass directional filtered image among the other high-pass filtered images produces a considerable number of lineaments mainly because the sun azimuth angle was low enough to produce shadowing in that direction, (Figure 4.7) while the original TM band 5 and the high-pass non-directional filtered images were the poorest in detecting lineaments (Figure 4.11) and (Figure 4.12). This can be attributed to the difficulty in viewing the short lineament. Figures 4.5 - 4.12 show lineament maps for each technique for the test site.

Table 4.2 highlights the difference between the filtration techniques and the two new contextual techniques. One of the dangers with using directional filters is that it might produce artificial edges which look like regular geological features (Drury, 1987), and tend to produce confusing images. But in the case of using the ripping membrane and rolling ball techniques, the artificial edges tend not to be produced. This can best be explained with reference to Figures 4.13 - 4.14. The Laplace

TABLE 4.1  
 Showing the comparison between the different  
 individual image results regarding the lineament  
 type and number

IMAGE TECHNIQUE PRODUCTS	TOTAL NUMBER OF LINEAMENTS			% OVERALL TOTAL IN FINAL LINEAMENT MAP			PLATE NUMBER	FIGURE NUMBER (LINEAMENTS MAP)
	CLEAR	WEAK	TOTAL	CLEAR	WEAK	TOTAL		
Ripping Membrane	88	81	169	94.6%	99.0%	97.6%	4.4a	4.5
Rolling Ball	50	69	119	55.6%	84.0%	68.0%	4.4b	4.6
Northeast Direct. Filter	41	45	86	44.0%	54.0%	49.0%	4.5a	4.7
Northwest Direct. Filter	19	52	71	20.4%	63.4%	40.6%	4.5b	4.8
East Direct. Filter	37	30	67	39.8%	36.6%	38.3%	4.5c	4.9
North Direct. Filter	27	37	64	29.0%	45.0%	36.6%	4.5d	4.10
Non-directional. Filter	13	9	22	14.0%	11.0%	12.6%	4.5e	4.11
Row TM Data Band 5	22	6	28	23.7%	7.3%	16.0%	4.3	4.12
Total Lineaments from all the enhanced images in the final Lineament Map	93	82	175					4.4

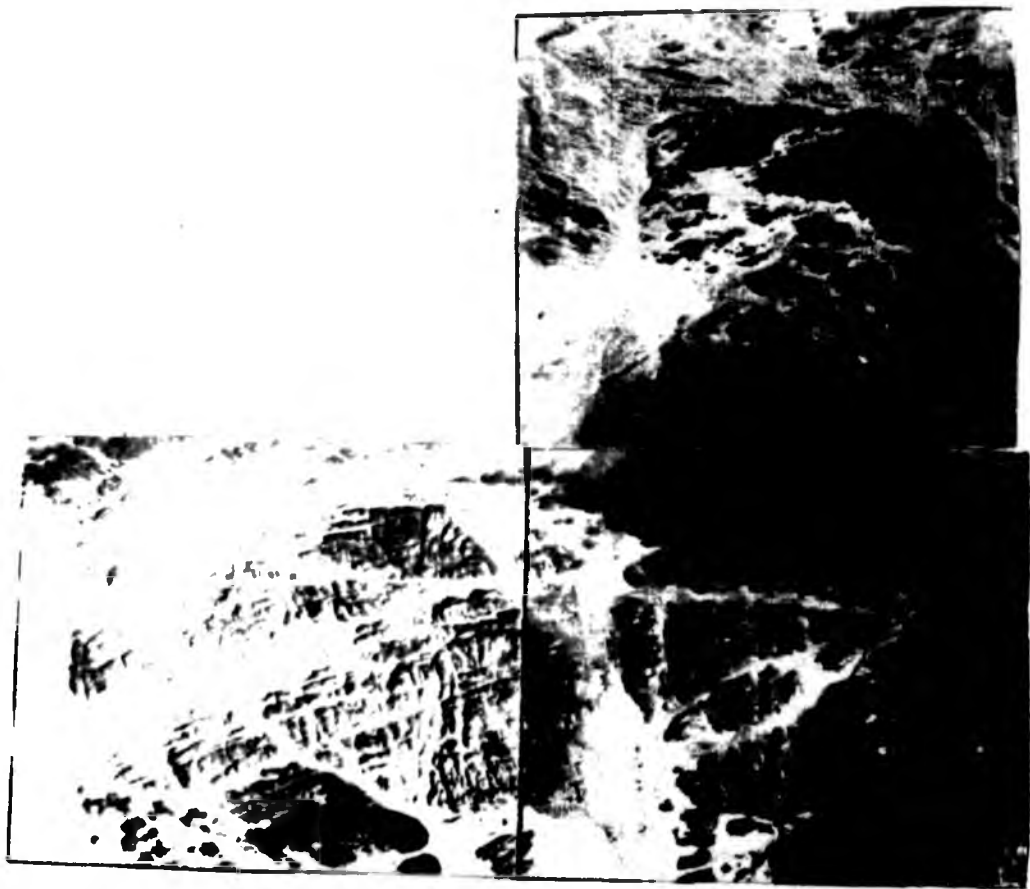
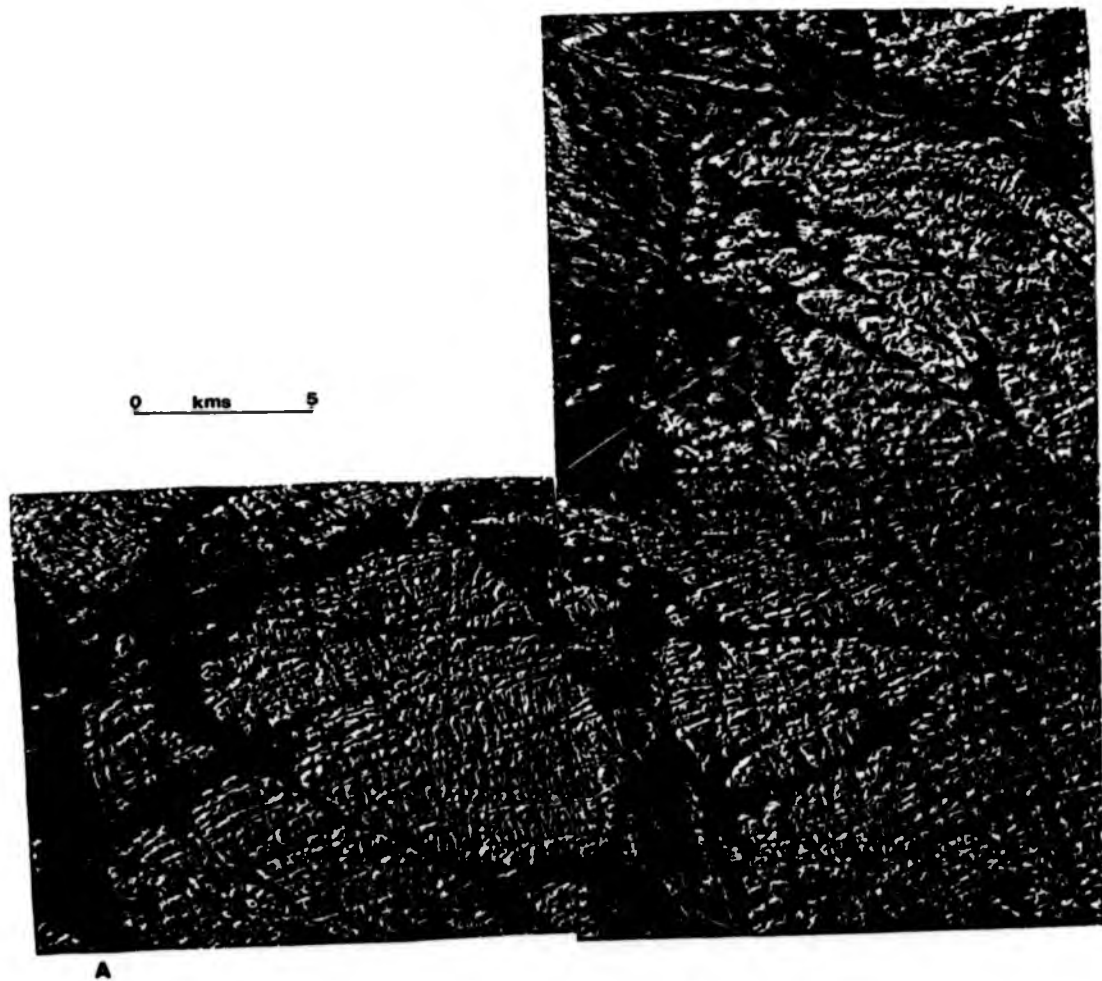
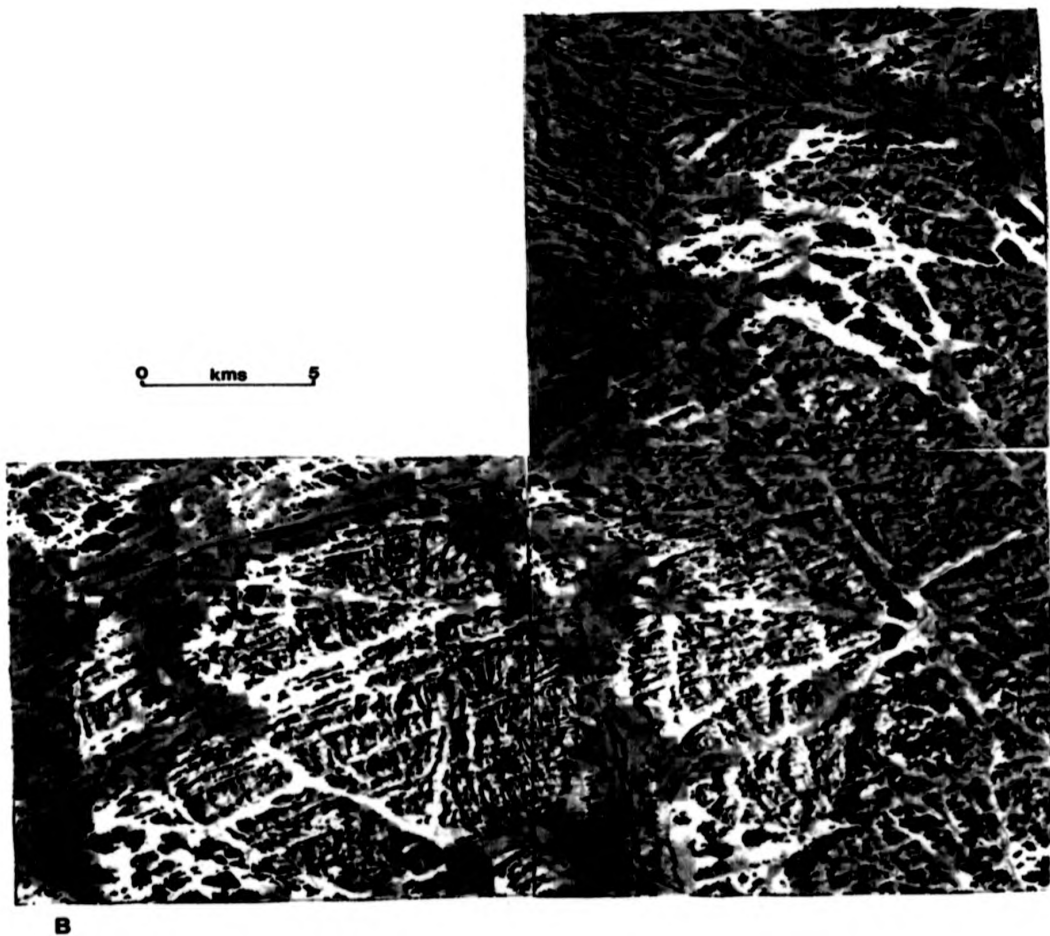


PLATE 4.3 Contrast stretched TM band 5 for the test site. (Jibal Rumman area).



**PLATE 4.4(a)**  
Edge enhanced image using the Ripping membrane technique  
for the test site area.

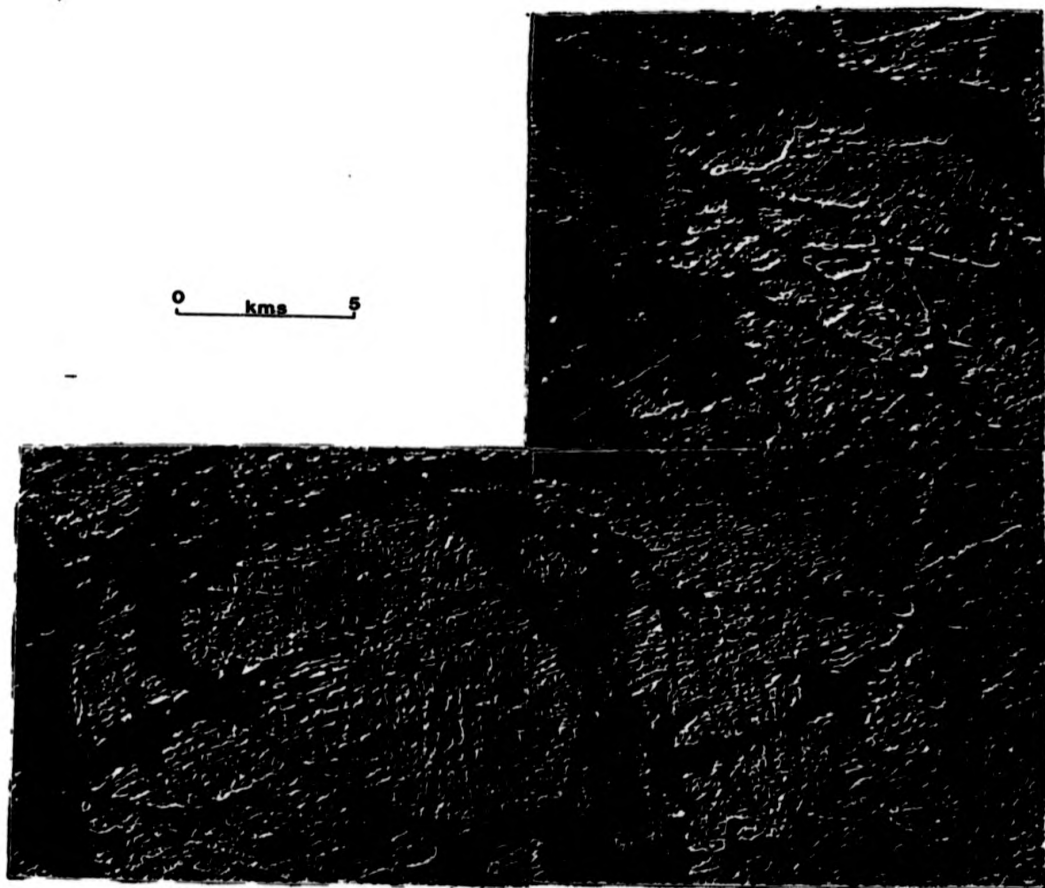


**PLATE 4.4 (b)**

Edge enhanced image using the Rolling ball technique for the test site area.

**PLATE 4.5**

- Edge enhancement techniques images for the test site:
- a) Northeastern directional high-pass filtered image;
  - b) Northwestern directional high-pass filtered image;
  - c) East directional high-pass filtered image;
  - d) North directional high-pass filtered image;
  - e) Non-directional (Laplace) high-pass filtered image.



A

**PLATE 4.5(a)**  
Northeastern directional high-pass filtered image.

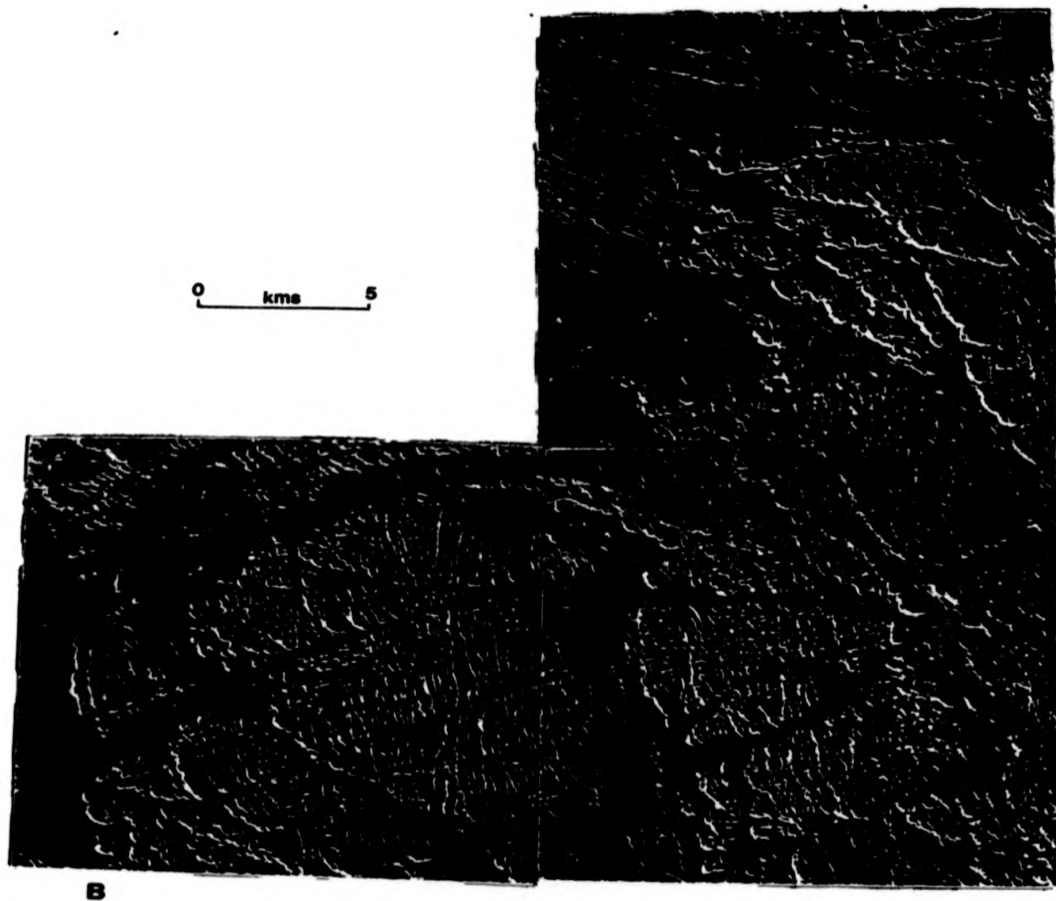


**PLATE 4.5 (b)**  
Northwestern directional high-pass filtered image.

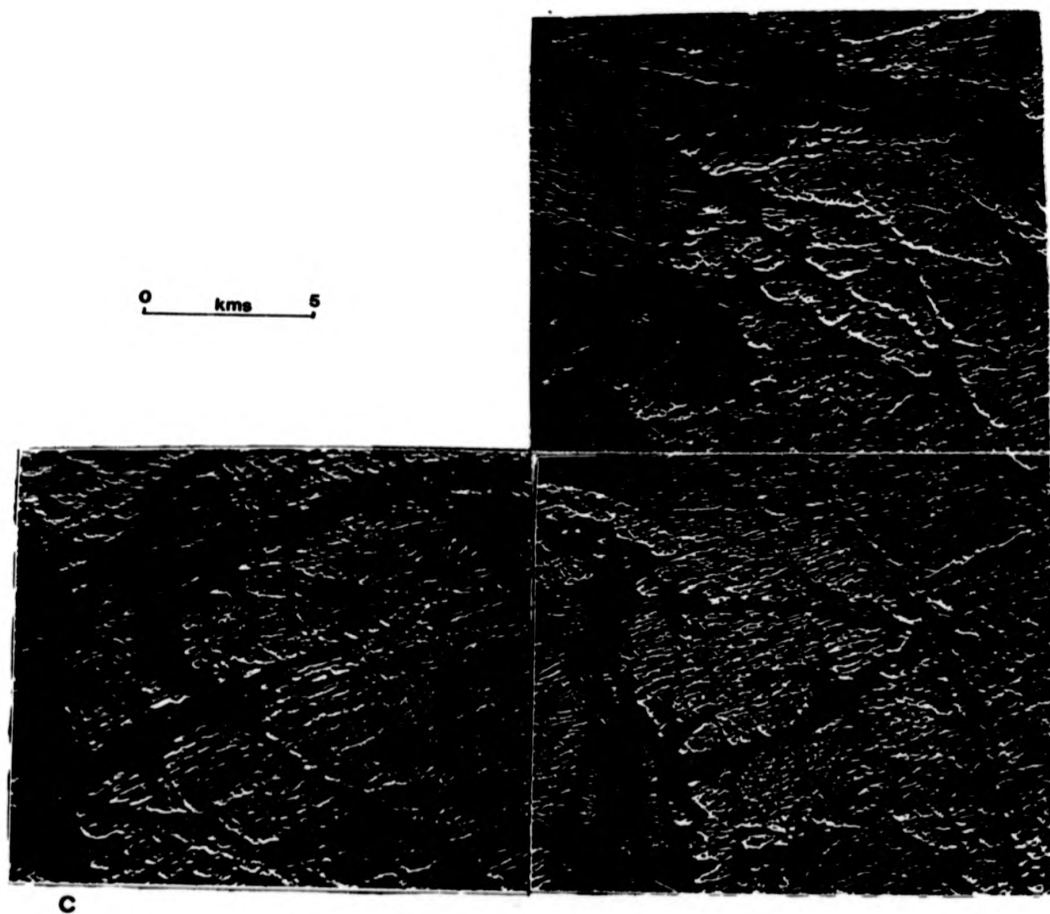


**PLATE 4.5 (c)**  
East directional high-pass filtered image.



**PLATE 4.5(d)**  
North directional high-pass filtered image.

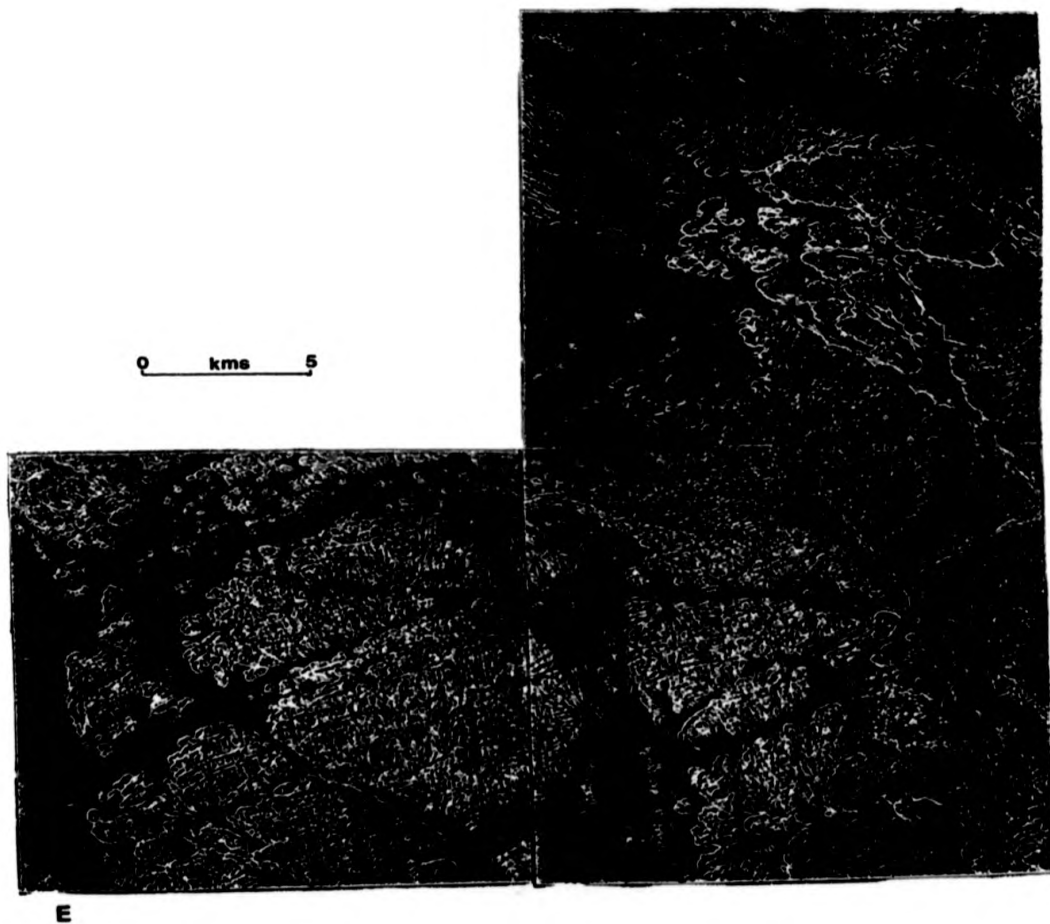


**PLATE 4.5(e)**  
Non-directional (Laplace) high-pass filtered image.

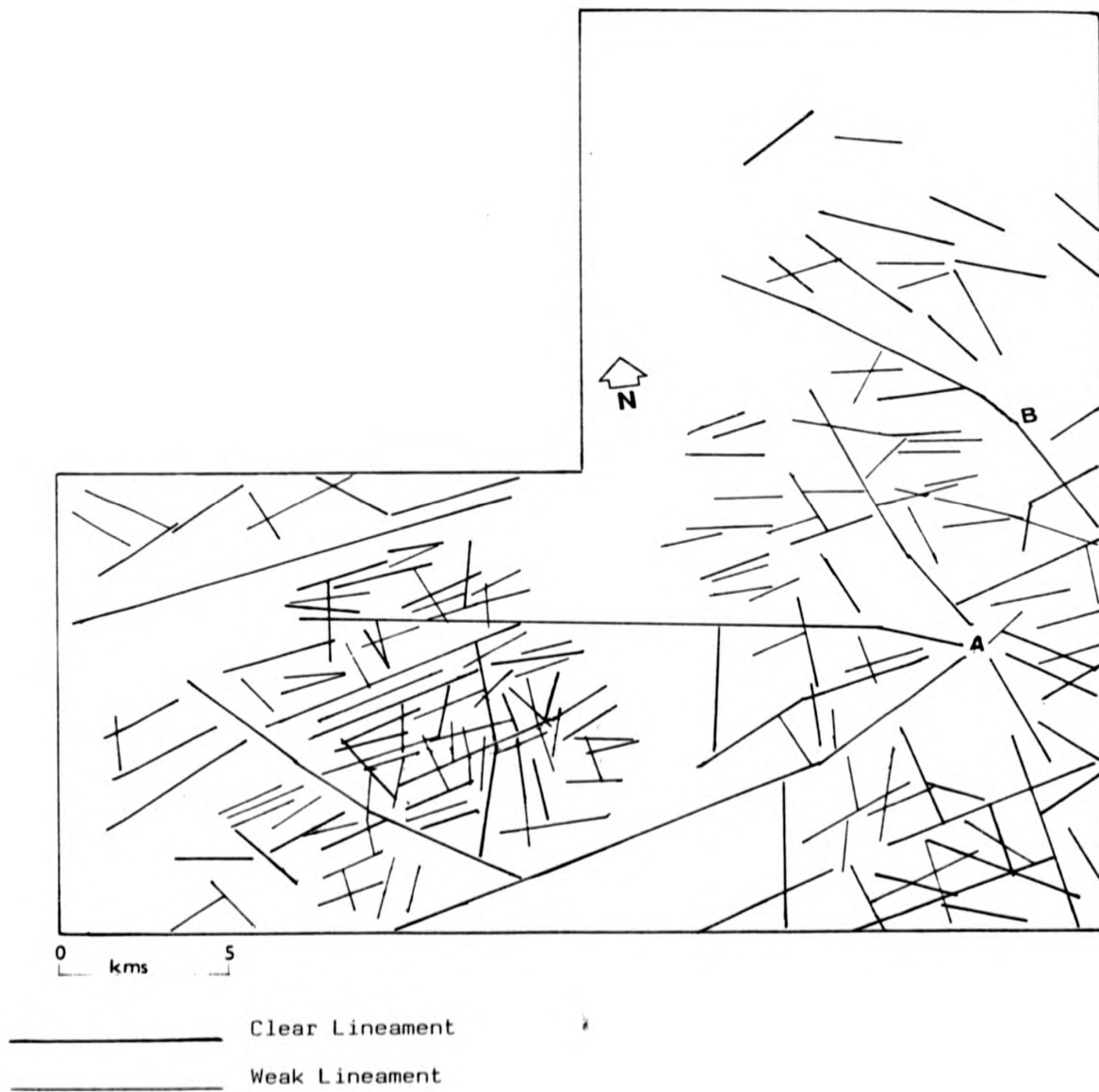
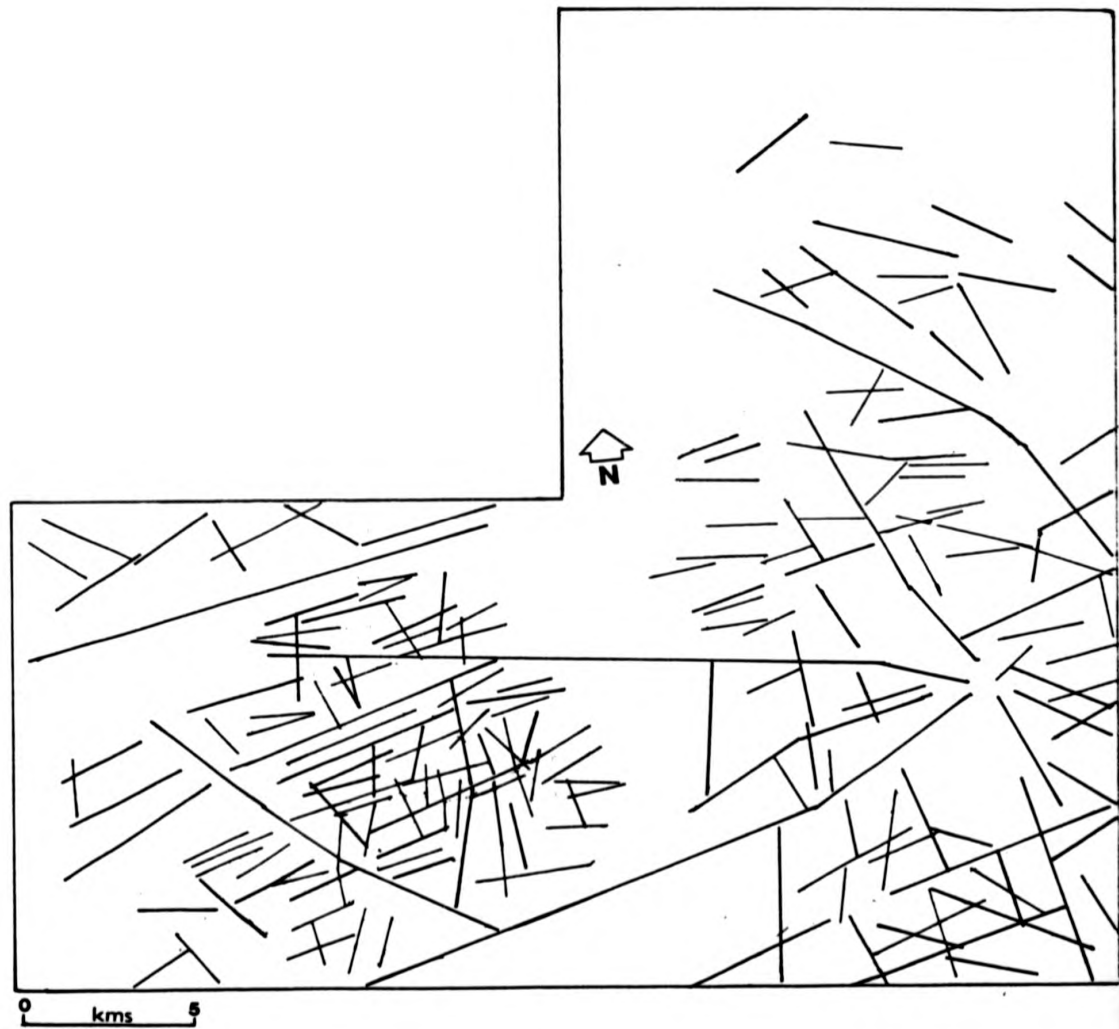
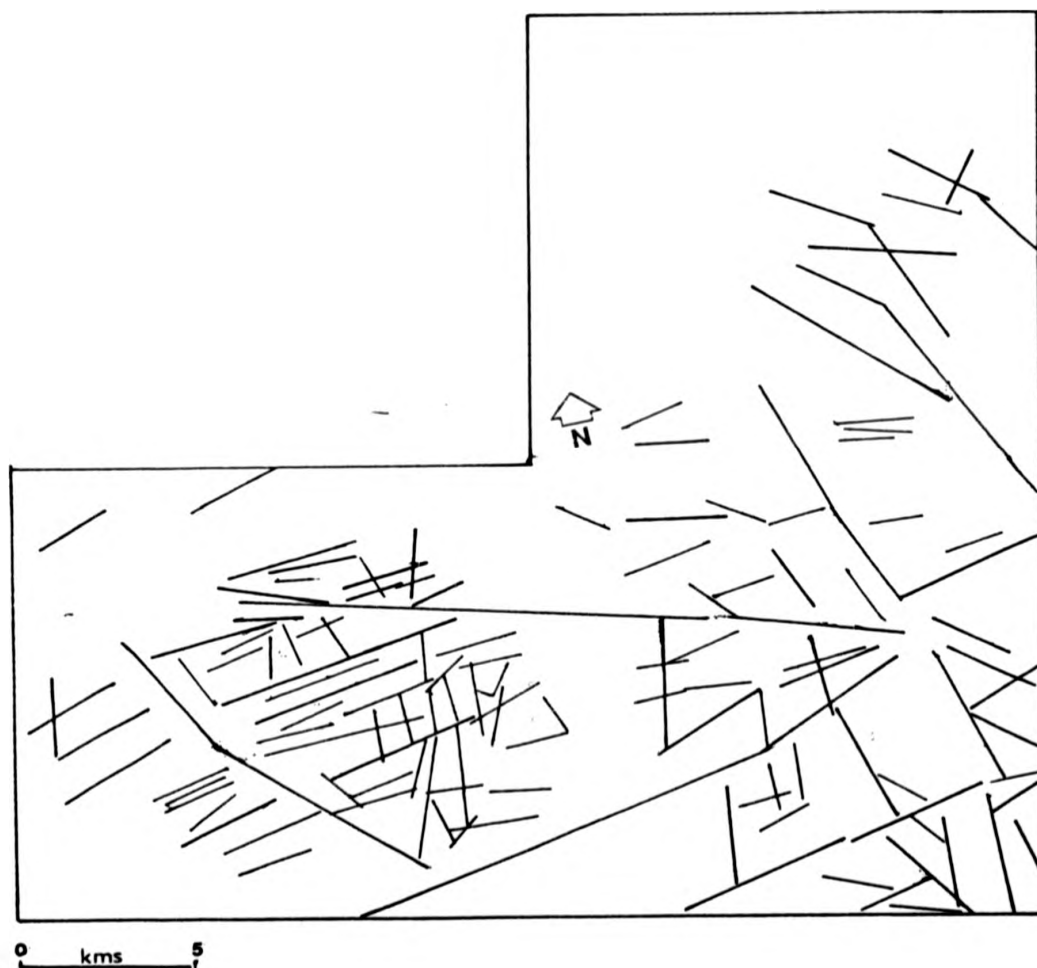


**FIGURE 4.4**  
Lineament maps for the test site area derived from the TM images.  
See Figure 4.2 - 4.3 for comparison with mapped fault of this  
area (all lineaments are greater than 1.5km).



————— Clear Lineament  
————— Weak Lineament

**FIGURE 4.5**  
Lineament map drawn from the ripping membrane technique resultant  
image for the test site.  
(TM Band 5).



————— Clear Lineament  
————— Weak Lineament

**FIGURE 4.6**  
Lineament map drawn from the rolling ball technique result image  
(TM band 5).

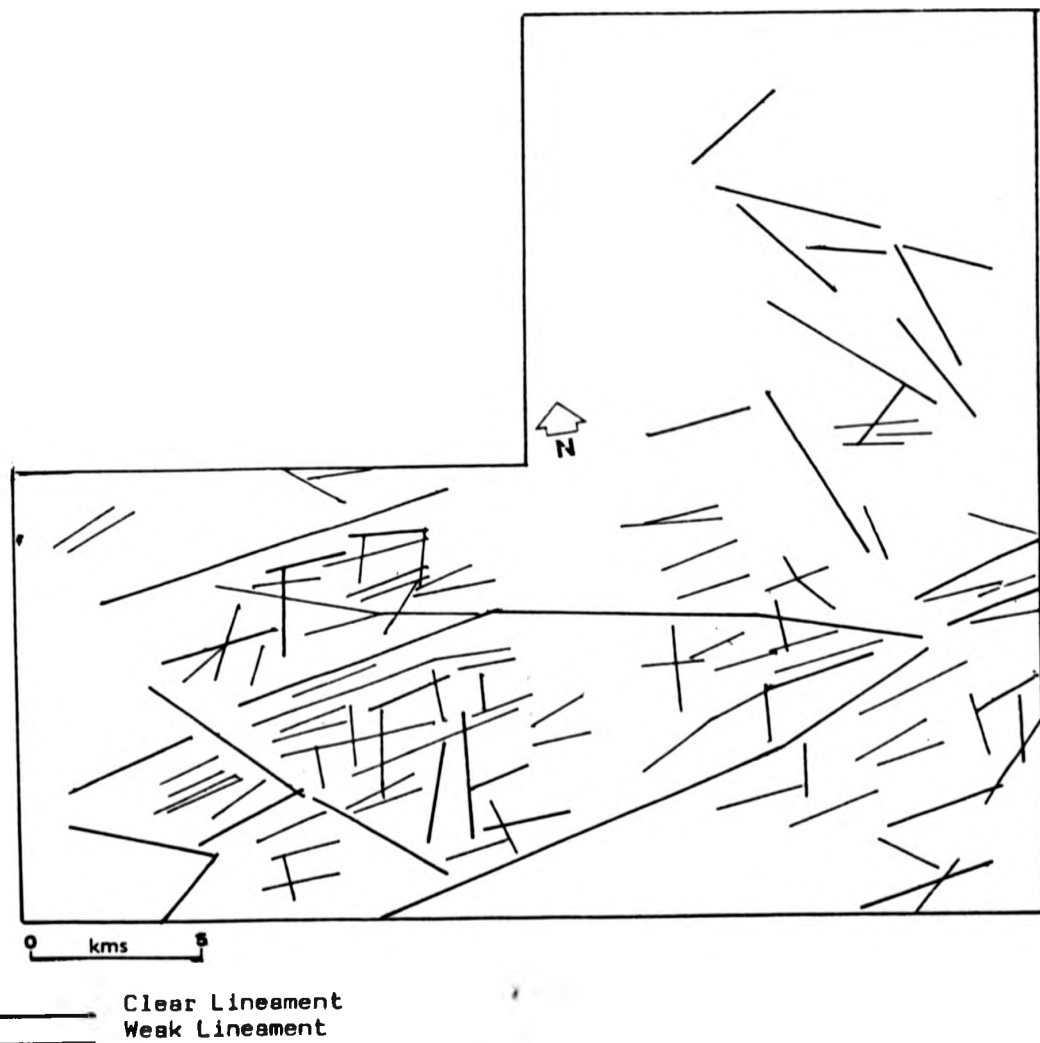


**FIGURE 4.7**  
Lineament map drawn from the northeast-southwest directional  
high-pass filtered TM band 5 image.

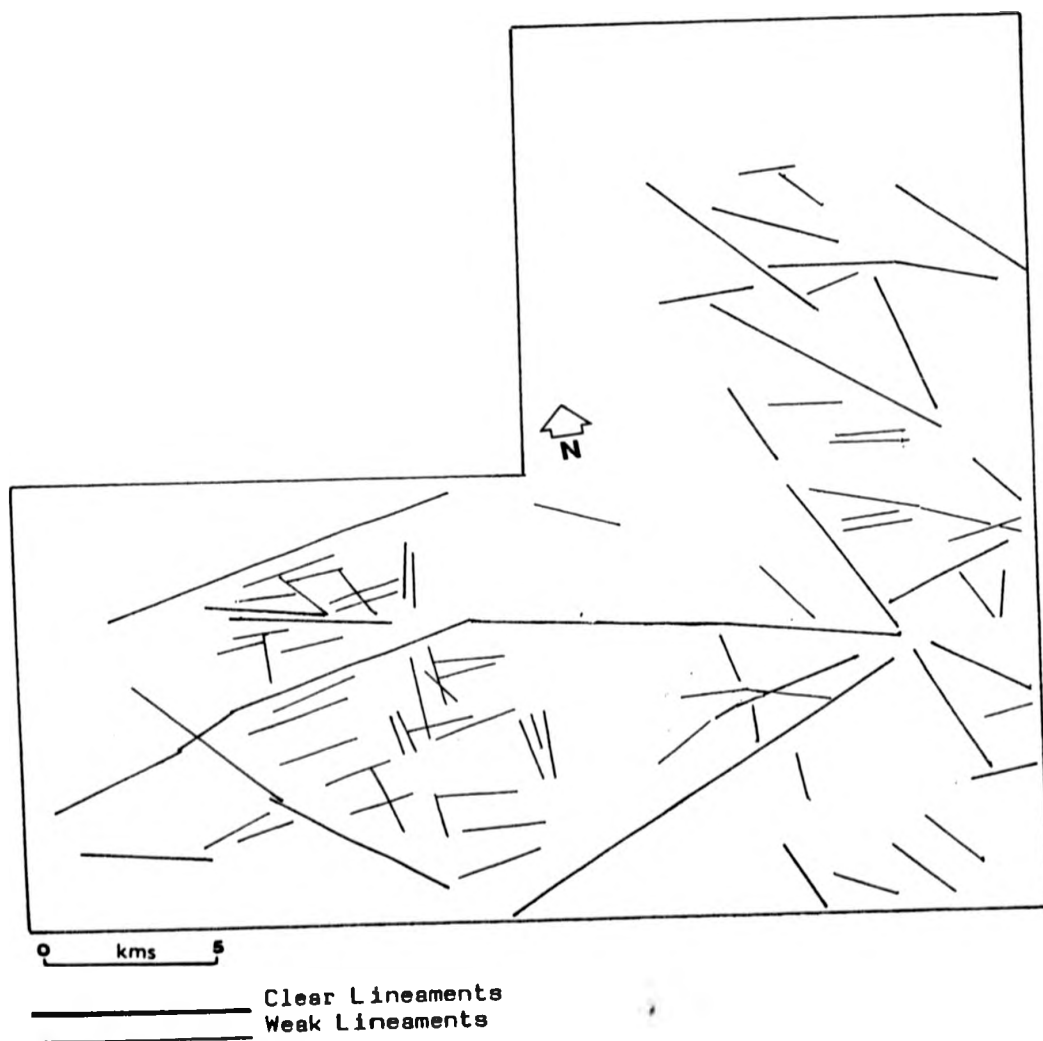
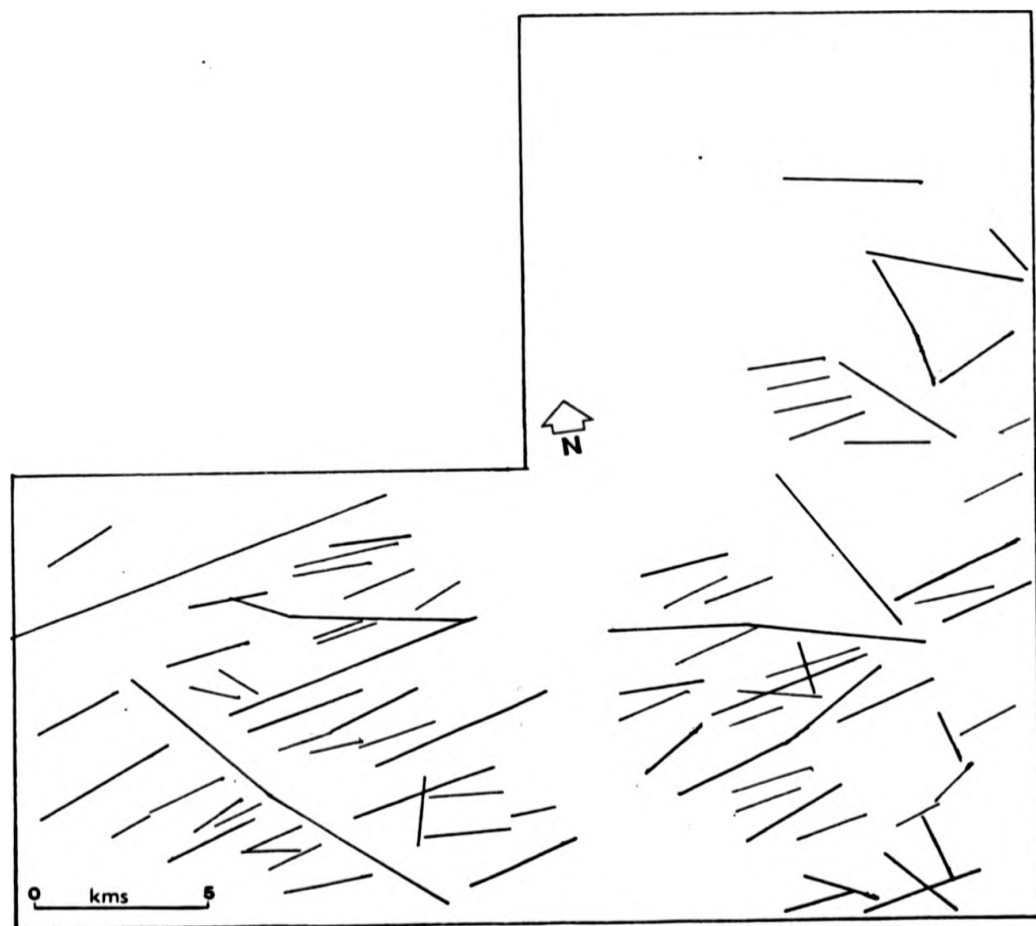
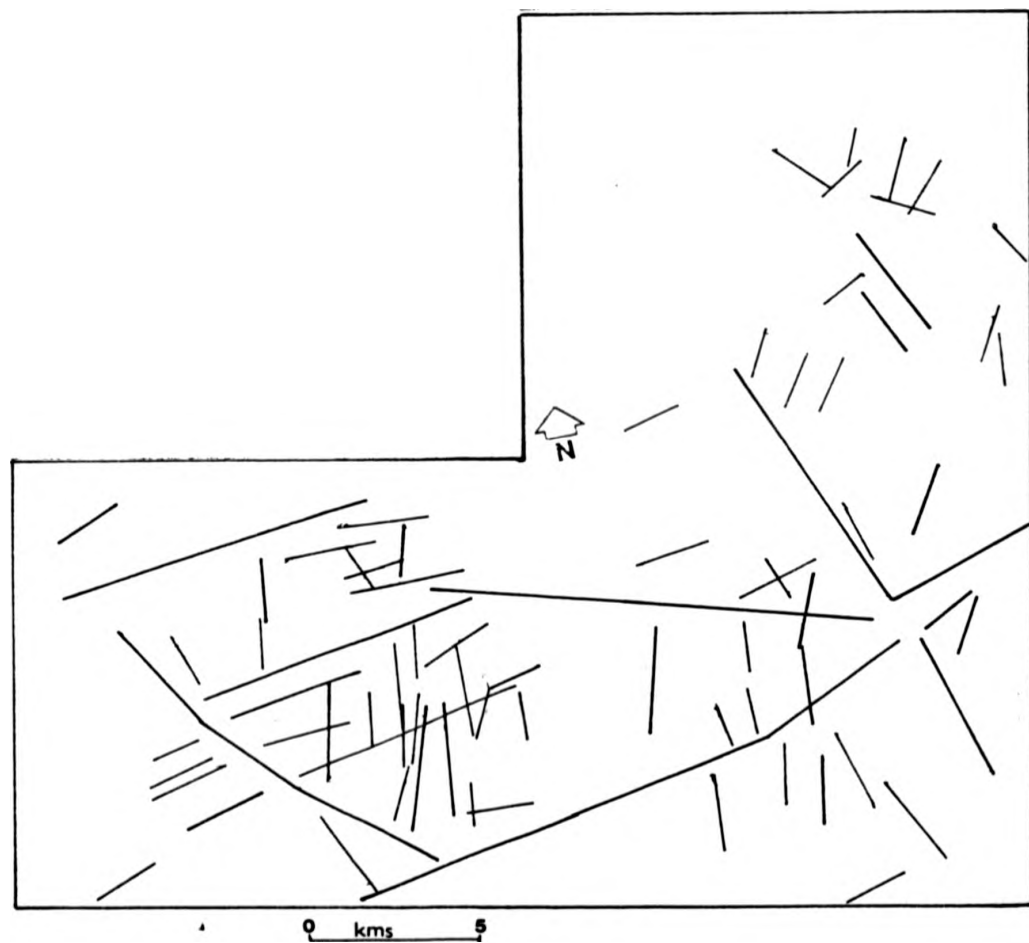


**FIGURE 4.8**  
Lineament map for lineament derived from northwest-southeast  
directional high-pass filtered TM band 5 image.



————— Clear Lineament  
————— Weak Lineament

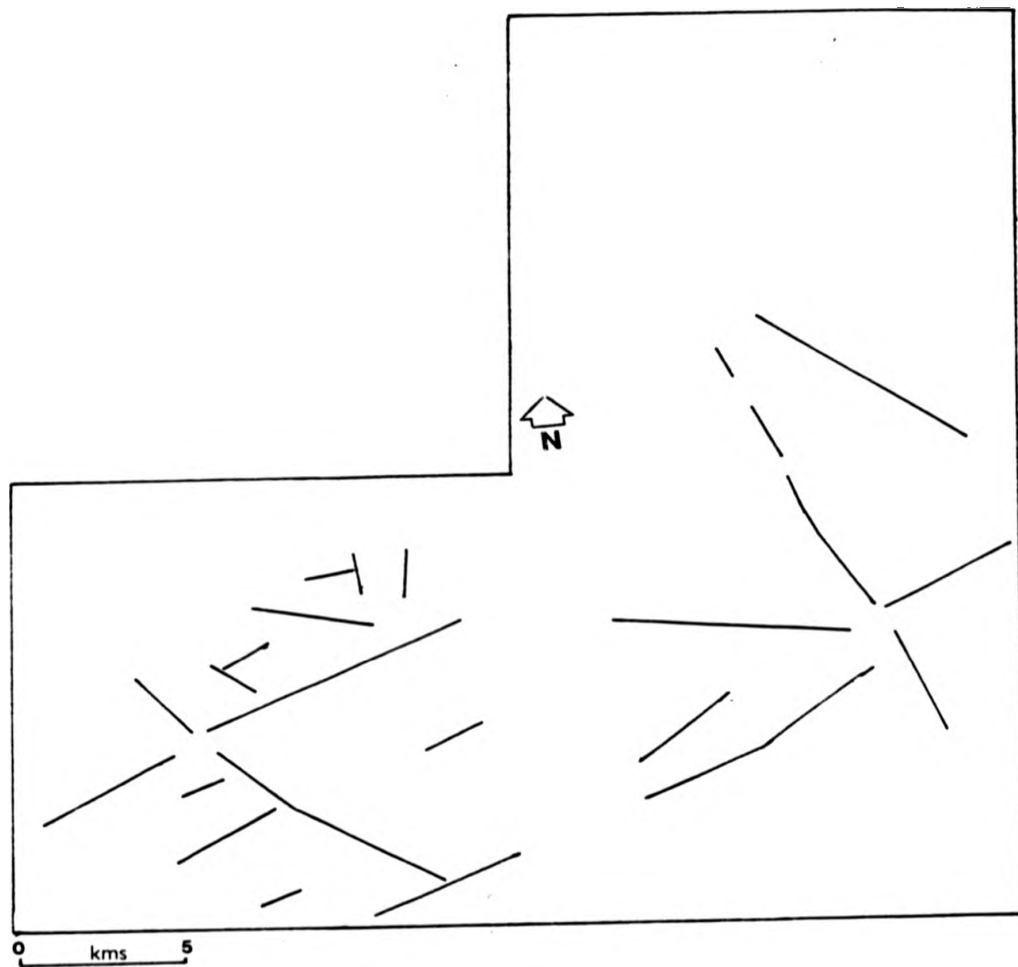
**FIGURE 4.9**  
Lineament map drawn from the east-west directional high-pass filtered  
TM band 5 image.



————— Clear Lineament  
————— Weak Lineament

**FIGURE 4.10**

Lineament map for lineament derived from north-south directional high-pass filtered TM band 5 image.



————— Clear Lineament  
- - - - - Weak Lineament

**FIGURE 4.11**  
Lineament map drawn from non-directional high-pass filtered  
TM band 5 image.

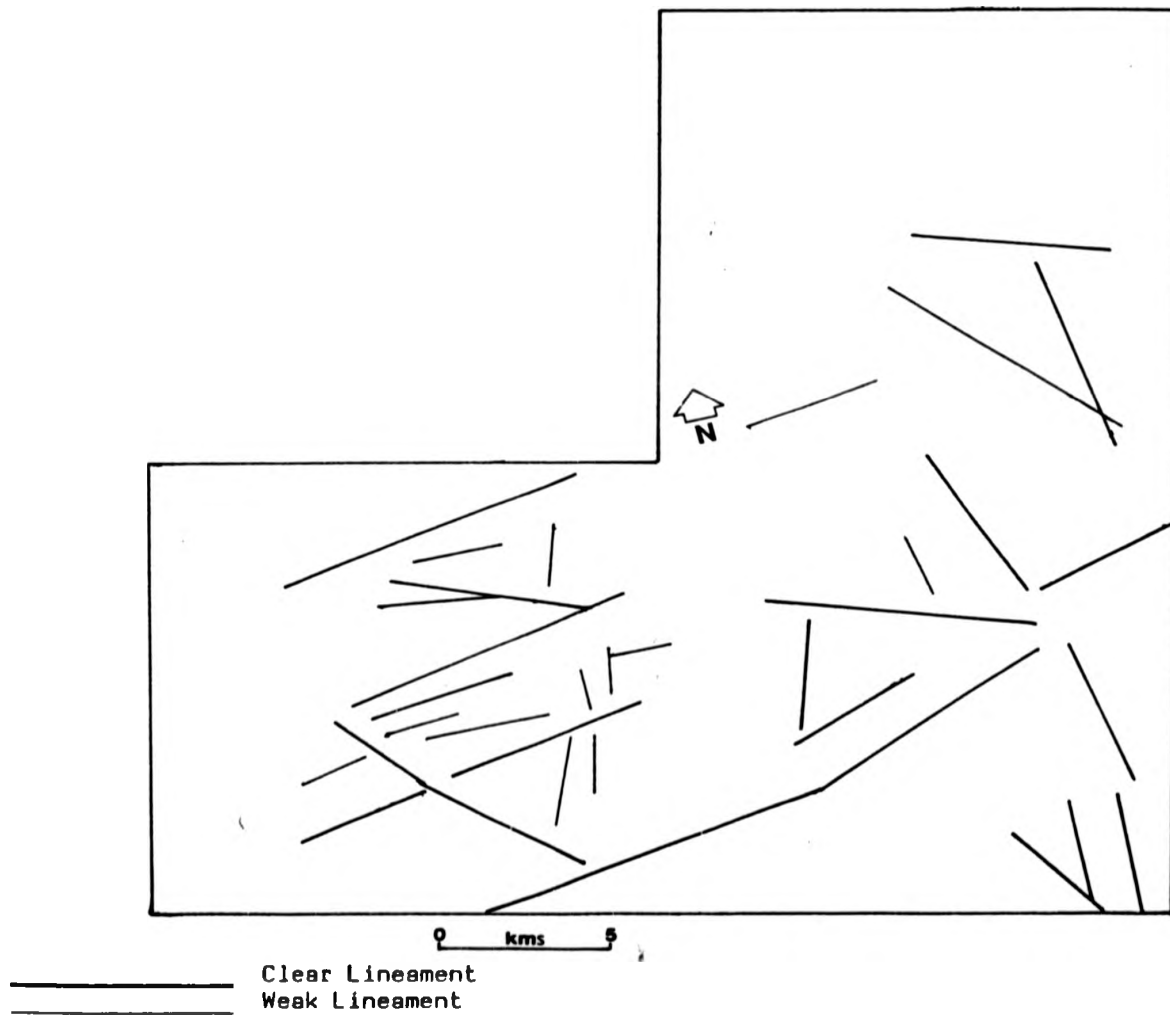


**FIGURE 4.12**  
Lineament map drawn from the TM band 5 image.

and rolling ball transformation are applied to the same image and it is obvious that the Laplace filter produces a very complex pattern that obscures the simple underlying edges, whereas the rolling ball produces a simple transformation.

For comparison purposes between the MSS and TM data, in terms of lineament mapping and analysis, the two contextual techniques were applied to the MSS band 4 (Plates 4.6 and 4.7) which cover the same test site, and only 79 lineaments were detected from the two contextual techniques but, again, the ripping membrane showed the highest number of lineaments (Figure 4.15).

These two techniques were also applied to SPOT-2 panchromatic (10x10 meter resolution). However, this study concentrates on regional lineament interpretation and analysis and the SPOT data was found to be unsuitable for the purposes of this study. The range factor must be increased when the spatial resolution is reduced in order that the spatial range on the ground remains the same.

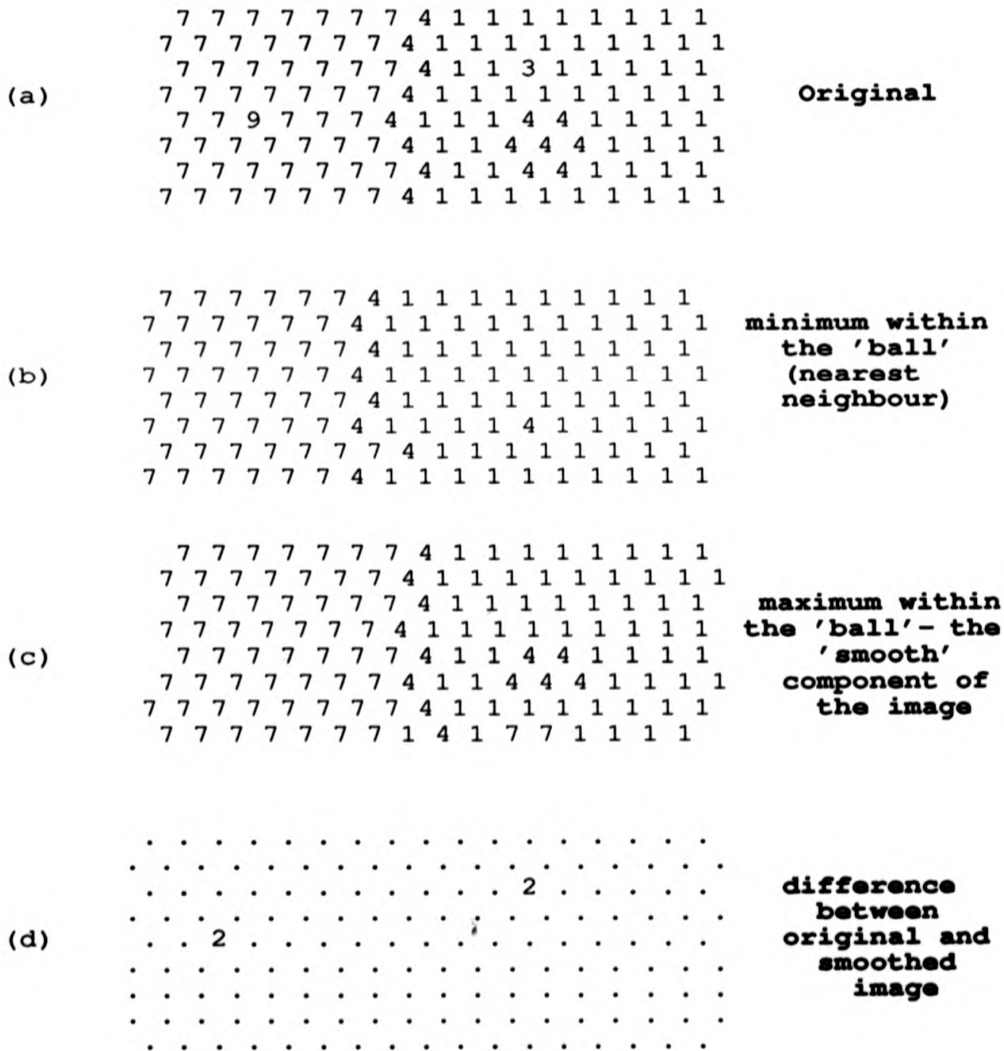
In the case of SPOT the computer time taken for the same ground range was far too long hence, the techniques could not be used with SPOT data. Further, the SPOT data was collected in the summer period which is not very useful in lineament identification and analysis.

TABLE 4.2

Showing a comparisons between the spatial filtration technique and the new contextual techniques

SPATIAL FILTRATION TECHNIQUE	NEW CONTEXTUAL TECHNIQUES (ROLLING BALL, RIPPING MEMBRANE)
1. To perform complete directional analysis, requires passes four principal compass directions.	1. One pass enough
2. Easy and fast to apply because it is available in all the image processing systems.	2. It needs computer time and space because of the sophisticated algorithm calculations
3. Needs one band only at a time.	3. Needs only one band at a time
4. Can be used to add back to the original images as edge enhancement.	4. Can not be added to the original image.
5. It has been used successfully for many years in lineament detection in arid and semi-arid lands.	5. First time to be applied to satellite data and for lineament detection.
6. It could be used on a colour composite.	6. The smooth component of the ripping membrane can be used as colour composite to show the boundaries of the different regions. (Sections 5.6 - 5.7)
7. The first pixel of the image cannot be enhanced when the filter operator passing.	7. All the pixels in all the images will be processed
8. Might produce artificial edges in the final result.	8. There are no artificial edges in the final result.

**Figure 4.13**  
**The Rolling Ball Edge Enhancement**  
**Technique Processing**



**Figure 4.14**  
**The Spatial Filtration Processing**

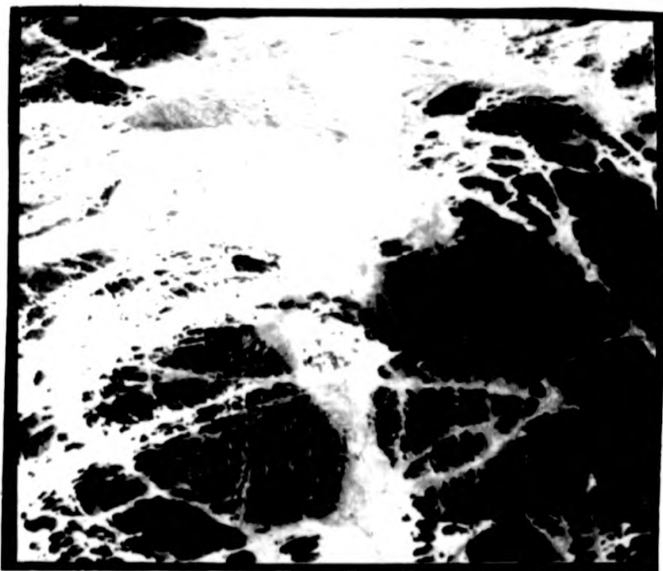
```

. . . . . 9 6-3 . . . . .
. . . . . 3-6-9 . .-2-2 . . .
. . . . . 9 6-3 .-2 2-2 . . .
. . . . . 3-6-9 . .-5-8-2 . . .
. .-2-2 . 9 6-3 .-6 9 9-6 . .
. .-2 9-2 3-6-9 .-3 9 .-9-9 . .
. .-2-2 . 9 6-3 .-6 9 9-6 . .
. . . . . 3-6-9 . .-3-6-3 . .

```

**Result of applying a Laplace transform to the same image as in Figure 4.13. The difference in this case is quite 'confusing' and complex compared to the difference that results from the rolling ball.**

In addition, it was noticed during the interpretation stage, that the contextual technique enhanced the texture of the rocky regions and thus, the drainage pattern. Appendix 2 shows a sample extract of 512 x 512 pixels to show how the contextual technique (ripping membrane) improve and enhance the appearance of the drainage pattern in part of the study area.



0 kms 10

**PLATE 4.6**  
Linearly contrast stretched MSS band 4 for the test site  
(Jibal Rumman) area.

(a)



0 km 10

(b)

**PLATE 4.7**

Edge enhanced images for MSS band 4 using the new contextual techniques for the test site (Jibal al Rumman) area,

(a) Rolling ball technique

(b) Ripping membrane.

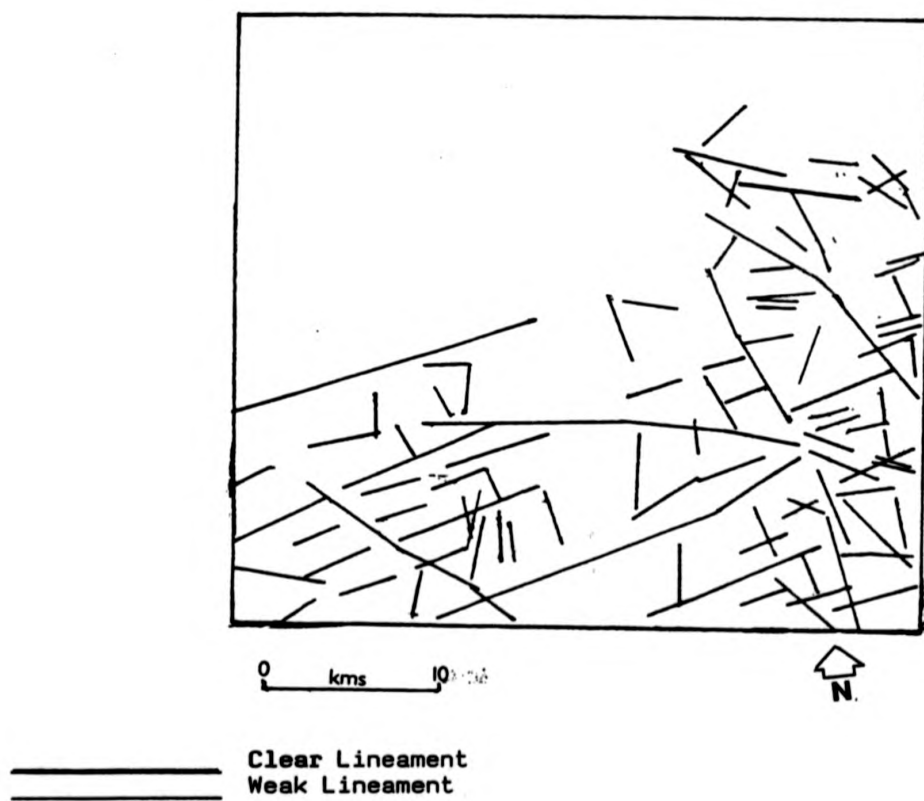


**FIGURE 4.15**  
Lineament map drawn from the MSS images for the test site.

#### 4.5 GENERAL LINEAMENT INTERPRETATION AND MAPPING

There were three reasons for choosing the test site area.

These were:-

1. The study area was located around two different faulting systems and therefore should have lineaments in different directions (the Najd Faulting system and the Saqf Faulting system). (Section 1.7.2).
2. The test site area had a rugged topography which should have provided a good test of the new techniques' ability for lineament detection.
3. The test site area had different rock types, of different origin and age. The lineament mapping, interpretation and lineament analysis might reveal the dominant direction in each individual rock type.

Both TM and MSS data were examined and both produced similar results, regarding the major clear lineament type interpretations, but TM was clearly superior. Figure 4.16 shows only the clear lineaments that have been observed and/or followed during the ground survey. The main reason for the survey was to verify that the proposed lineaments were not due to cultural influence.

During the field study, it was discovered that the agricultural activities water wells, natural trees, and palm trees were located in or around the major lineament lines, and at the lineament intersections. Thus the extraction of lineaments from imaging may be of some use in the search for water in the study area.

From the lineaments map (Figure 4.4) it can be seen that the lineaments, in general, can be divided into two groups, either parallel lineaments or intersecting lineaments. The recognition of these groups can help in the geological interpretation of the study area.

There are six long major lineaments running toward or from a small circular area at the central eastern quarter of the test site (labelled (A) in Figure 4.4). These lineaments cut the Hadn Formation and alkali granite. Also, there are four major lineaments running from or towards a small triangle feature at the north-eastern part of the test site (labelled (B) in Figure 4.4). The distance between the two features is short (around 8 Km).

Most of the NE-SW trending lineaments, either clear or weak, are located in or around the alkali granite rock in the west and central quarter of the test site area. In the Hadn Formation, the NE-SW trending lineaments are located only at the north-western boundaries, toward the alkali granite rock.

The alkali granite rock is cut by an extensive set of lineaments in many directions and it shows the highest lineament concentrations whereas gabbro shows the lowest number of lineaments. The mapped faults, which appear in Figure 4.2 and Figure 4.3 have been detected during the interpretation stage (Figure 4.4).

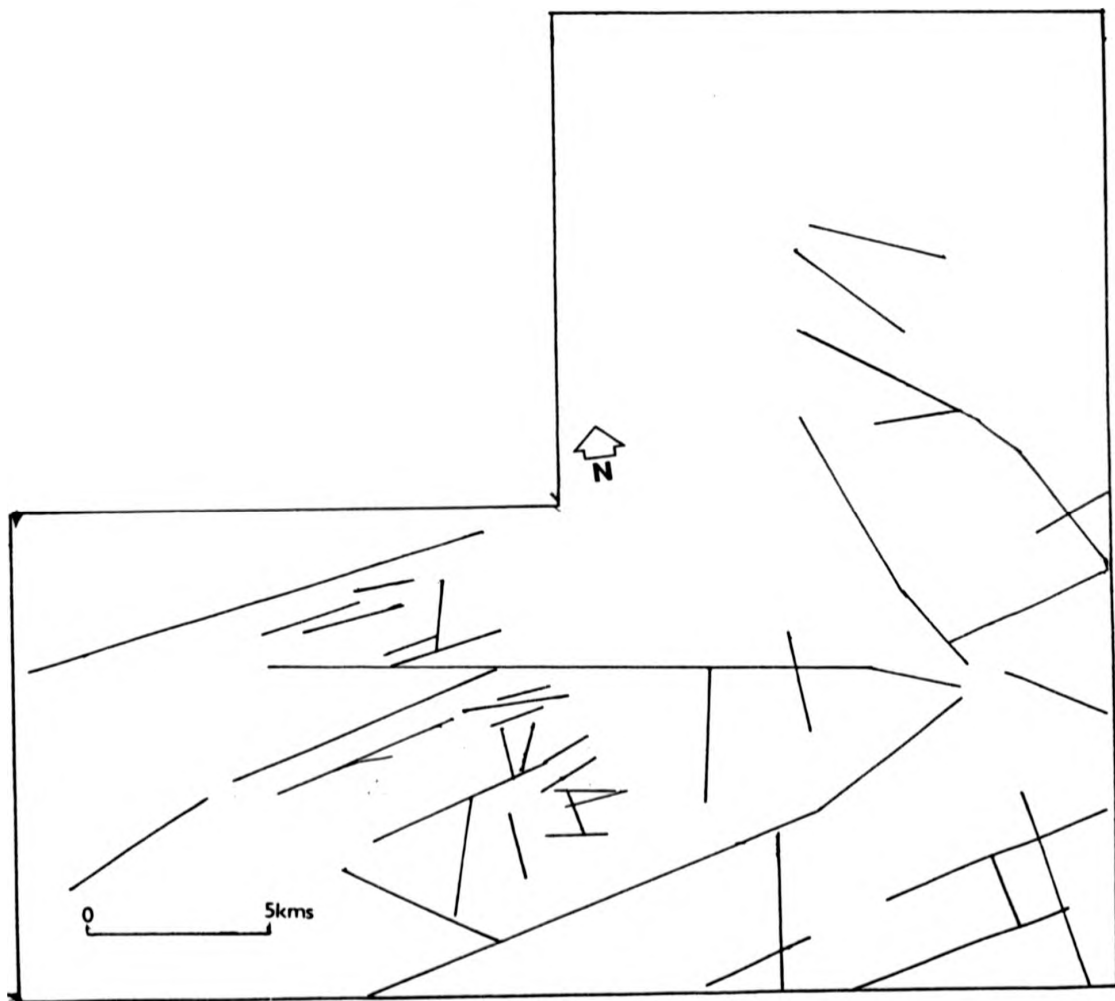


FIGURE 4.16  
Lineament were observed in the field

#### 4.6 LINEAMENTS ANALYSIS (ROSE DIAGRAMS)

The previous sections, (4.5 and 4.6) <sup>was</sup> concerned with the first stage of lineament analysis, which was the identification and mapping of the lineaments. This section discusses the analysis of the derived lineament map (Figure 4.4). In the analysis of lineaments, the location, direction and length are the primary attributes of the lineaments. The analysis of azimuthal frequency rose diagram depends on the fact that an area may have lineaments with a major trend. Thus, this type of diagram enables the distribution in direction of lineaments to be investigated.

Due to the method of interpretation described in the two previous sections, (4.5 and 4.6), visually distinct lineaments are shown as single continuous lines and the less distinct ones either clear or weak lineaments as a composite structure, composed of many short aligned portions or lines. It is therefore unreasonable to produce a rose diagram by cumulating the frequencies of lineaments within different azimuth ranges by number, as this might create an error or bias the distribution towards the less visually distinct structures (Johari, 1990).

Therefore in this analysis the total length of lineaments within a given range of  $5^\circ$  as well as the total number of lineaments within a given range of  $5^\circ$ , were plotted in a rose diagrams as was done by Maude (1987). This interval proved to be well proportioned to the scale of the investigation, and to the

spatial resolution of the TM and MSS. During the lineaments analysis stage, the rock types in the test site have been divided into two categories. One is the alkali granite as granite rock unit, and the second rock unit consists of all the other rock types. Table (4.3) shows, in detail, the total number and the general direction of lineaments that have been detected in the two major rock units in the test site. From this table, it can be seen that the alkali granite rock area had a total of 120 lineaments, and this is higher than the total number of lineaments traced in the volcanic rock and all other rocks in the test site. Separate rose diagrams for the two categories of lineaments weak and clear were plotted, as well as a combined diagram for each rock unit. Also, three rose diagrams were plotted for lineaments detected from over all the test site area. These diagrams were plotted in order to find out the dominant direction (trend) for each rock unit. The rose diagram of the frequency of the clear lineaments in the alkali granite rock unit (Figure 4.17a) shows major trends in  $N61^{\circ}-65^{\circ}E$  and  $N71^{\circ}-75^{\circ}E$ . This group of lineaments represent 42% of the total clear lineaments in this rock unit, while the weak lineaments rose diagram for the same rock unit, does not show any preferential trend of lineament but a general prevailing direction over a wide azimuthal range  $N61^{\circ}-80^{\circ}E$ . (Figure 4.17b). This represents 40% of the total number of weak lineaments in this rock unit.

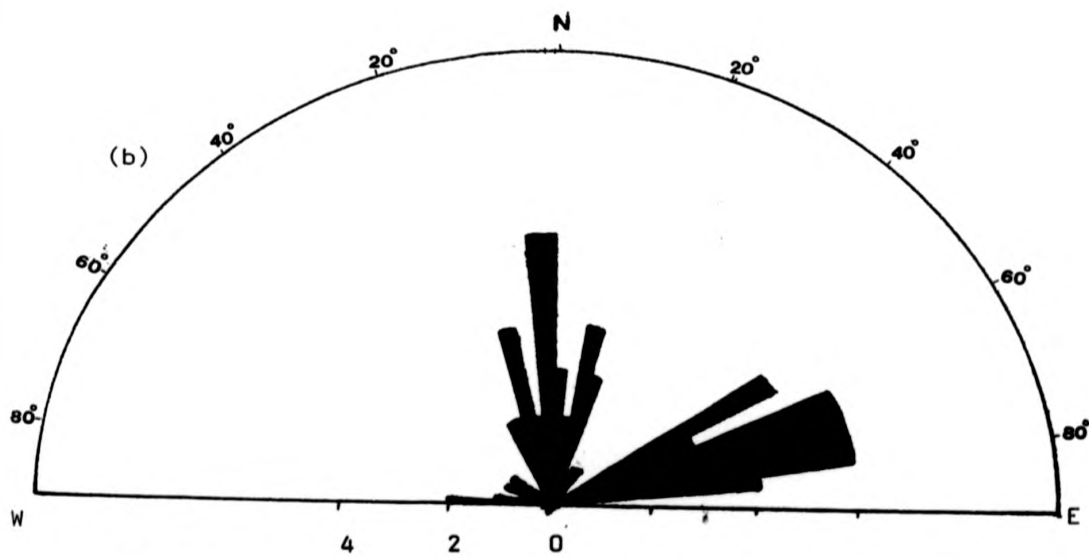
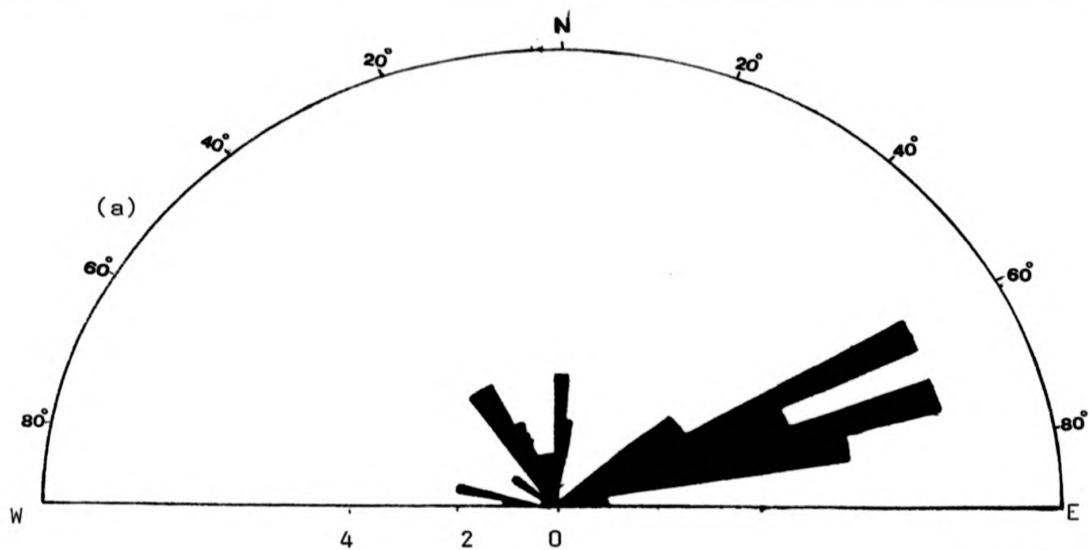


**FIGURE 4.17**  
Rose diagram of the azimuthal frequency distribution of lineaments  
in the first rock unit (alaski granite rock) area in Figure 4.4.  
(a) Clear lineaments; (b) Weak lineaments

TABLE 4.3

Shows in detail the total number and the lineaments detected in each rock unit

LINEAMENT TYPE	FIRST ROCK UNIT			TOTAL NO. OF CLEAR LINEAMENTS	SECOND ROCK UNIT			TOTAL OVERALL NOS.
	NORTH - EAST DIR	NORTH - WEST DIR	NORTH DIR		NORTH - EAST DIR	NORTH - WEST DIR	NORTH DIR	
Clear Lineaments	38	14	3	55	10	30	-	40
Weak Lineaments	44	21	-	65	10	5	-	15
				120				55

If these two rose diagrams are combined in one rose diagram (Figure 4.18) again, the highest concentration of lineaments show a wide azimuthal range  $N61^{\circ}-80^{\circ}E$  but there is a major trend in  $N71^{\circ}-75^{\circ}E$ . From all these rose diagrams it is clear that in the alkali granite rock unit area, the major lineament trend is in  $N71^{\circ}-75^{\circ}E$ .

The second rock unit showed a smaller number of lineaments compared to the granite rock unit area. The total number of lineaments was 55 which include 40 clear lineaments and 15 weak. (Table 4.3). The rose diagram of the frequency of the clear lineaments, in the second rock unit, Figure 4.19a shows two major trends in the directions  $N56^{\circ}-60^{\circ}W$  and  $N71^{\circ}-75^{\circ}W$ . Only a few weak lineaments were detected, and were not analysed separately. All the lineaments in this rock unit (clear and weak), are plotted together in one diagram (Figure 4.19b).

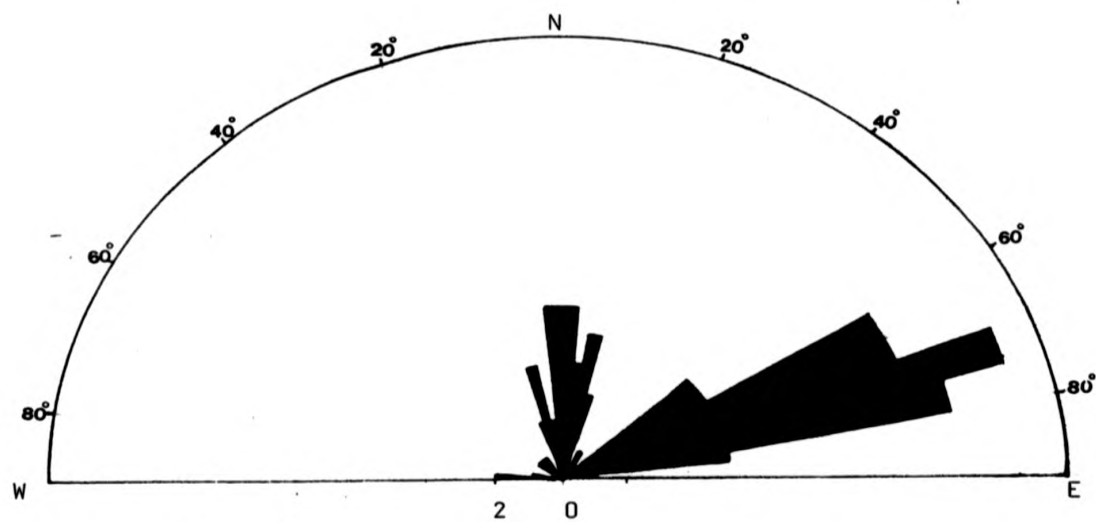


**FIGURE 4.18**  
Rose diagram of the azimuthal frequency distribution of all the lineaments in the first rock units (alkali granite rock) in Figure 4.4.

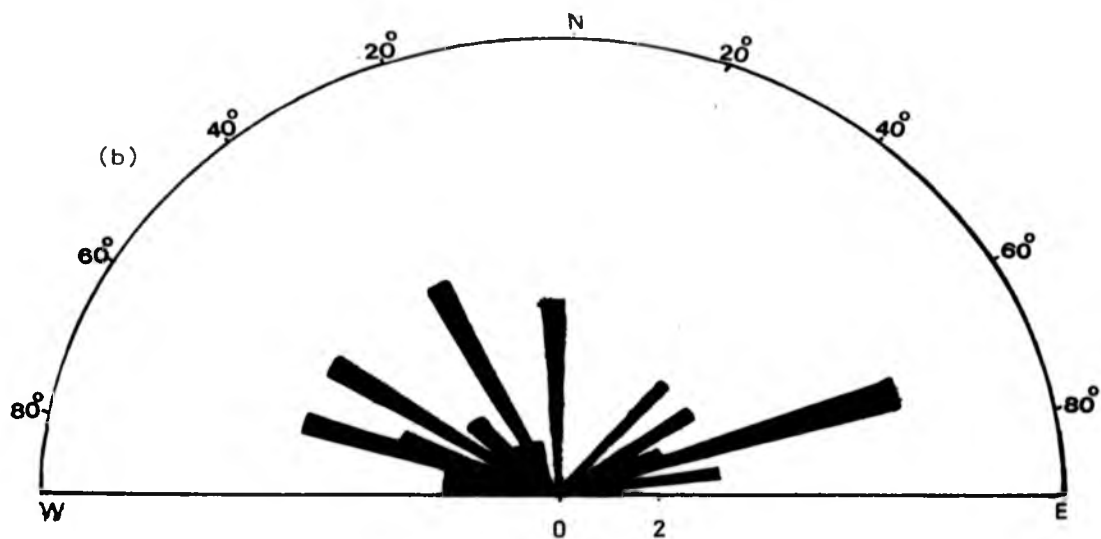
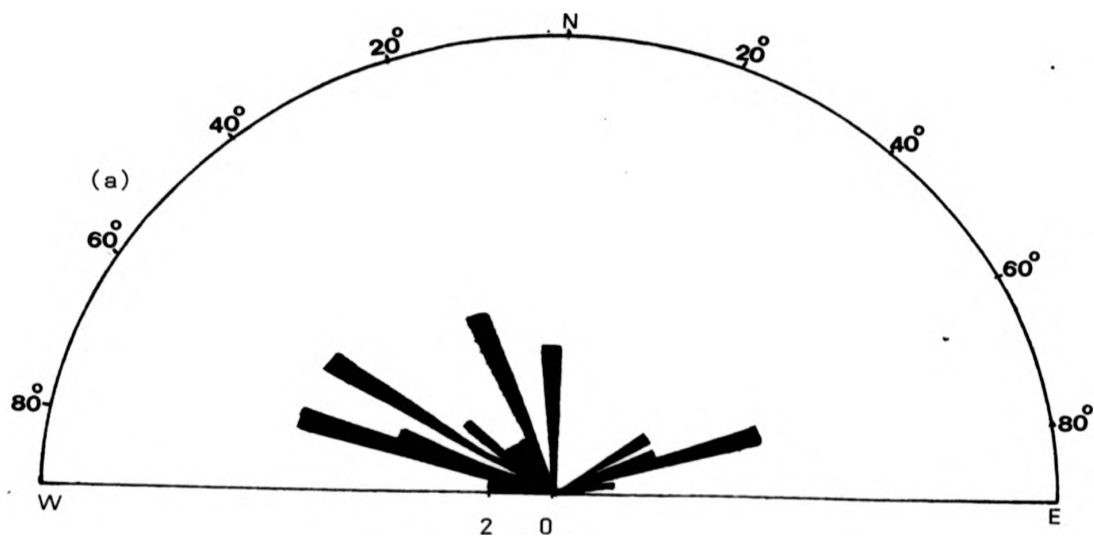


FIGURE 4.19

Rose diagram of the azimuthal frequency distribution of all the lineaments in the second rock unit in Figure 4.4.  
 (a) Clear lineaments only  
 (b) All lineaments.

Again, the major trend is in  $N71^{\circ}-75^{\circ}E$  and the second trend is  $N26^{\circ}-30^{\circ}W$ ,  $N56^{\circ}-60^{\circ}W$ ,  $N71^{\circ}-75^{\circ}W$ . The second major trends were located mostly in the Hadn Formation.

One rose diagram was plotted (Figure 4.20) showing the distribution of all the lineaments in (over)all the rock units. The major lineament trend is in  $N71^{\circ}-75^{\circ}E$ . The rose diagram for the distribution of total length (Figure 4.21) for each interval of the azimuthal angle shows that there is one major orientation in the  $N71^{\circ}-75^{\circ}E$  direction. This means that the analysis of the directional distribution of lineaments in terms of number or length in the test site does tend to be correlated.

In order to find out, if the same lineament directions obtained from the TM and MSS are the same or not, one rose diagram for the distribution of total number of lineaments detected from the MSS data (79 lineaments) (Figure 4.22) was plotted. It shows that the major trend in the test site is  $N71^{\circ}-75^{\circ}E$  direction and therefore agrees with the conclusions reached from the analysis using TM imagery.

#### 4.7 DISCUSSION

It is clear from Table 4.1 and the Plates (4.3 - 4.5) that the two new contextual techniques provided the best result for lineament detection, and that they are clearly an improvement over previously used techniques (i.e. spatial high-pass filters).

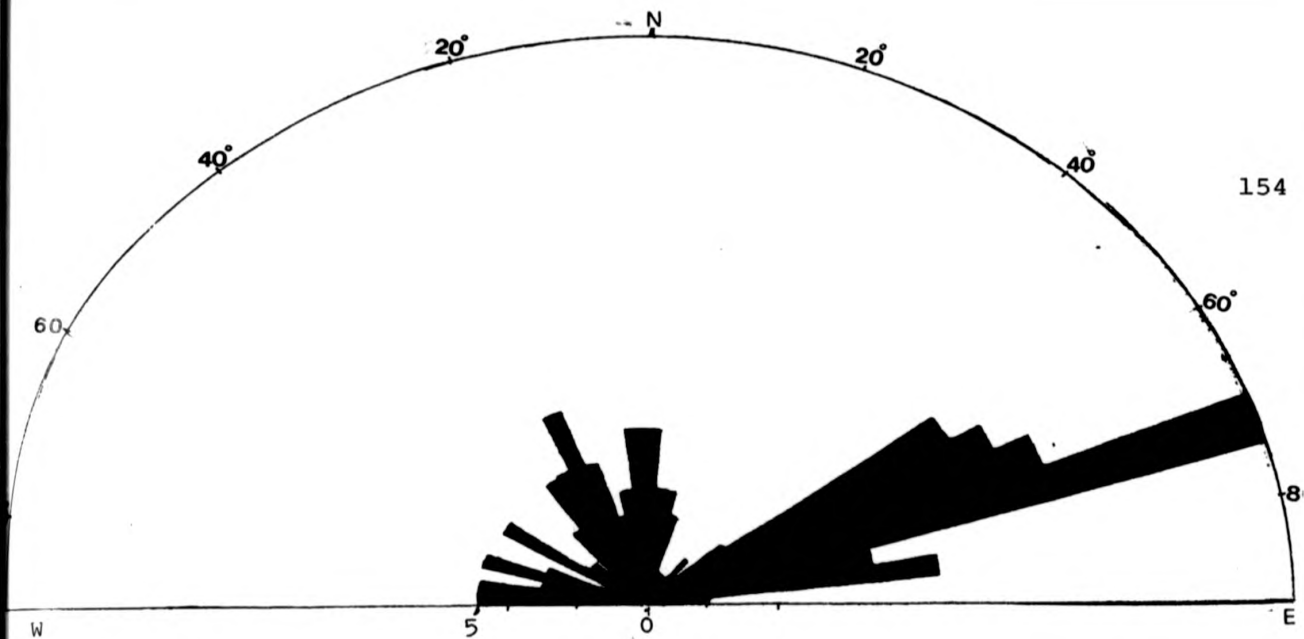


FIGURE 4.20

Rose diagram of the azimuthal frequency distribution of all the lineaments in the test site area (in Figure 4.4).

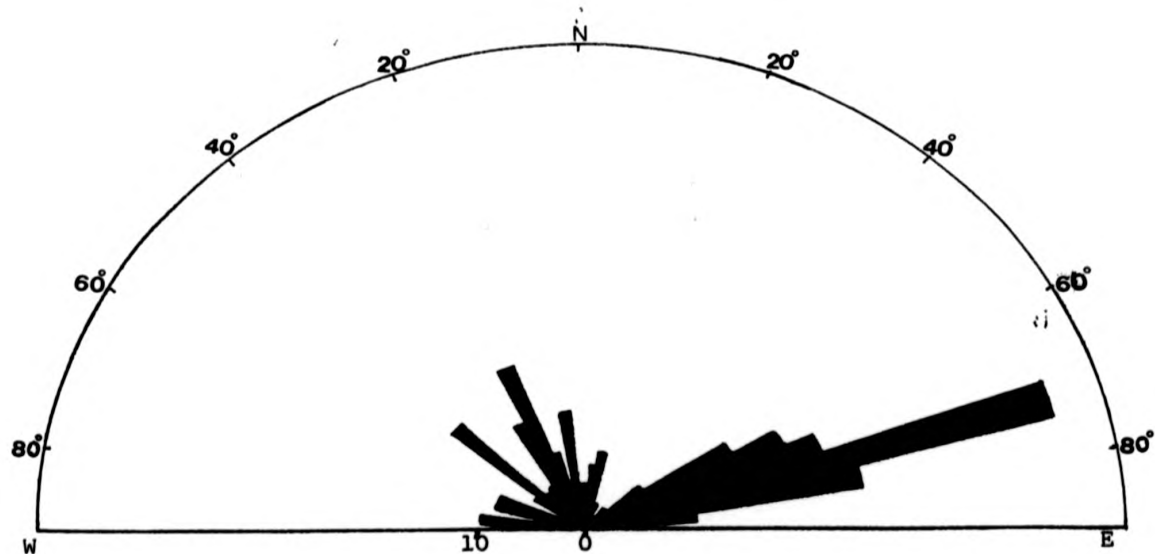
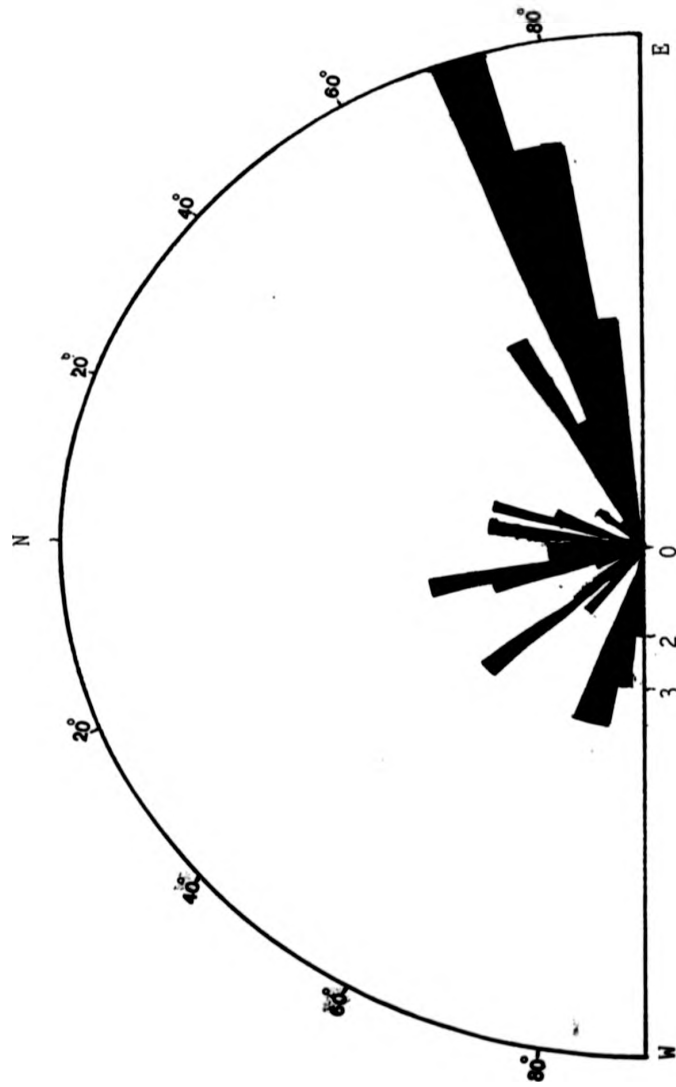


FIGURE 4.21

Rose diagram for distribution of total length for each interval of azimuthal angle for all the lineaments in the test site (in Figure 4.4).



**FIGURE 4.22**  
Rose diagram summarising the azimuthal frequency distribution of the  
lineament of the test site detected from the MSS data in Figure 4.15.

From the image interpretation and lineament analysis, there are three points to be noted:-

1. Most of the lineaments in the alkali granite rock unit are in the direction to NE-SW, ENE-WSW.
2. Most of the lineaments in the Hadn Formation (volcanic rock) and the other rock in the test site are directed towards NW-SE and WNW-ESE.
3. By observing all the rose diagrams for the test site, there is a major direction toward  $N71^{\circ}-75^{\circ}E$ .

It is clear from the interpretation map that the northeast directions of the lineaments are located in the western and central part of the test site but these die or are truncated by northwest trending faults in the eastern part on Hadn Formation. From the literature it is known that the test site is located very close to the Najd Faulting System zone, (Section 1.7.2), (a strike-slip and dip-slip movement).

The geological interpretation and analysis of lineament depends on the principle that systems of faults and joints (i.e. lineaments) which are formed during one geological age commonly have more or less parallel alignment lineament. Therefore, all the northwest lineaments in the test site are likely to belong to this Najd Fault System (Leo, 1984; Quick and Doebrich, 1987). The northeast trending lineaments in the study area are attributable to the Saqf Fault System (Quick and Doebrich, 1987).

The Saqf Fault System has been interpreted by Quick (1985) to be a conjugate system to the Najd Fault System and may have continued longer than the Najd Fault System.

#### 4.8 SUMMARY

1. The comparison of methods for extracting lineaments showed that the new contextual techniques, ripping membrane and rolling ball, provide an excellent tool for linear feature mapping and analysis. The others do not provide anywhere near as good 'data' upon which to base geological conclusion.

2. The result of this study implies that in lineament interpretation and analysis -

- a. The NE-SW and ENE-WSW lineament orientation is dominant in the alkali granite,
- b. The NW-WNW lineament is dominant in the Hadn Formation, Maa complex Juwayy Rashib Complex, Kilab monzogranite, gabbro and biotite alkali-feldspar granite.
- c. The major trends are easy to identify ( $N71^{\circ}-75^{\circ}E$ ) and the same answer can be obtained from the TM rose diagram for frequency of numbers and the total length, also from the corresponding MSS lineament rose diagram.
- d. There are many unmapped lineaments and new orientations

discovered during the interpretation and analysis. These are N56° - 65°E and east-west in the test site.

- e. Also, it was noted that the new contextual technique can be used to study the drainage system in the arid areas, but this is not within the scope of this study.

## **CHAPTER FIVE**

### **THE USE OF CONTEXTUAL TECHNIQUES IN IMAGE SEGMENTATION FOR GEOLOGICAL APPLICATIONS**

- 5.1 INTRODUCTION
- 5.2 COMPUTER VISION
- 5.3 DENSITY SLICING
- 5.4 DEFINITION OF IMAGE SEGMENTATION
- 5.5 REVIEW OF IMAGE SEGMENTATION METHOD
- 5.6 WATERSHED IMAGE SEGMENTATION METHOD
- 5.7 IMAGE SEGMENTATION BY LASERSCAN SYSTEM METHOD
- 5.8 DISCUSSION
- 5.9 SUMMARY

## 5.1 INTRODUCTION

Image segmentation is the process of dividing an image into meaningful regions. In general, there are two primary objectives that image segmentation may achieve -

1. Classification and interpretation may be improved by processing regions as separate units.
2. The segmented image may better meet the need of automatic processing (Estes *et al.*, 1983).

This Chapter contains an introduction and definition of computer vision and density slicing which were used during the image segmentation process. This is followed by a review of image segmentation methods. Two different methods of region based segmentation were applied to an image of an arid area (Study area). The purpose was to evaluate the accuracy with which the methods segmented the image compared with the known rock units.

The two methods consisted of three main steps: region growing, region labelling and finally, region editing.

## 5.2 COMPUTER VISION

Computer vision is the construction of explicit, meaningful descriptions of physical objects from images (Ballard and Brown, 1982). It includes many techniques which are useful by themselves, such as encoding and transmitting images, as statistical pattern classification, and image segmentation. Nevatia (1978) has defined the requirements of a computer vision system and they

fall into three qualitative and broad classes:-

1. The objects in the scene are completely known and their location and orientations are also known. The computer has to determine the exact location and orientation of the object.
2. The neighbourhood of the objects is small and known but the system has to determine or identify the objects and their location and orientation.
3. The number of objects is not known, and objects may occur in any physical shape and spatial relationship.

Four factors need to be considered in specifying the environment of any computer vision systems (Nevatia, 1978).

1. **Sensor Type** - each sensor usually has different detectors for different wavelengths, (i.e. spectral bands) for example TM data has wider wavelengths than MSS. (Section 2.2).
2. **Data Resolution** - high resolution data are necessary for describing small fine objects in the scene, for example the panchromatic mode of SPOT satellite images show more spatial details than the Landsat TM images (Sections 2.3 - 2.4).
3. **Type of Object** - the solid and smooth objects are easy to extract from images compared with heterogeneous and unsolid objects.
4. **Complexity of Scene** - some scenes are much more complex than others, for example, an image containing one object and background is less complex than an image containing

many objects.

It has to be noted that to devise computational algorithms (computer vision) whose performance is comparable to human visual system, is not an easy task. In this chapter, and subsequent chapter, the computer vision methodology is described and applied to the problem of generating useful information which may be used to identify rock boundaries, and detecting lineaments, using the different contextual (spatial) information and contextual techniques.

### 5.3 DENSITY SLICING

Density slicing or level slicing is a technique used to map the distribution of grey levels (digital numbers, DN) in an image into a binary image (or an image with a very restricted number of grey levels). This can be done in two steps:-

1. display and inspection of the image histogram to find out the ranges of grey levels for each individual surface category. Each grey level range is called a slice and the slices must fall within the range of 0 - 255 grey level (Mather, 1987).
2. These ranges (slices) can be highlighted on the screen by assigning a colour to each range.

The resulting image is a colour image which is simpler but shows less detail. The loss of detail is due to the conversion from a 256 level image to an image represented in terms of a few (2 or 3) grey levels, this means that the density slicing is also

a type of grey level modification.

This technique is effective for:-

1. An image containing homogeneous areas with few grey levels.
2. An image that is to be used only for quick visual interpretation.

If the image histogram (DN distribution and frequency) has many modes then each mode may be assumed to correspond to one category of object and troughs in the histogram can form boundaries for density slicing for image segmentation (Gupta 1991).

Density slicing techniques have been used in this study during the automatic segmentation methods, and the automatic line and lineament feature extraction (Chapter 6). This technique was available on R-CHIPS system (Section 2.5) and the Laserscan system (Section 5.7).

#### **5.4 DEFINITION OF IMAGE SEGMENTATION**

Image segmentation is the process of dividing or sub-dividing an image into a number of non-overlapping regions or segments, each of which is spatially connected and homogeneous, and differs from its neighbouring regions, by having different properties, such as intensity, texture, colour etc. Wilson and Spann, (1988) define it as "the splitting of an image into a set of disjointed regions, each of constant properties, separated by well defined boundaries". The region interior should be simple

and without many small holes (Haralik and Shapiro, 1985).

The segmentation of images into regions can be done in many ways, from pixel classification method using DN values and local feature values, to sophisticated split and merge techniques using statistical homogeneity tests. The simple case is to have only two regions, an object region, and a background region, or there may be many object regions on the background. In natural scenes for example, there may be many regions to segment like cloud, buildings, trees, streets and mountains. In this case, the different regions may be called classes. The image segmentation techniques assume that the objects have smooth homogeneous surfaces, that correspond to regions of constant or smoothly varying reflectance (DN), and that the DN value changes abruptly at the boundaries, or at the contact line. These are ideal conditions that are not always valid. There may be physical boundaries between similar surfaces that do not appear as image boundaries. Surface texture and noise also cause additional problems for image segmentation.

The image properties can be related to geological characteristics, e.g. the grey level to the albedo of rocks, and the image texture to the micro relief of ground objects. Therefore, image segmentation is a process which may enable the automatic mapping of lithological features (Gupta, 1991).

The aim of this study is to test and develop automatic segmentation methods that can segment satellite images of arid

lands, containing well exposed rock types, with the following characteristics:-

1. The test site (image extract) may contain one or more rock type, either large or small bodies (hill or mountain) or both of any shape, and alluvial deposits as the background, (i.e. the image may contain any number of objects with any size and shape).
2. The image may have high or low contrast, (i.e. different rock types).
3. Boundary lines, of any segmented region must be connected.

#### 5.5. REVIEW OF IMAGE SEGMENTATION METHODS

There is no universal method of segmenting an image containing many different types of objects into different regions. The choice of the segmentation method depends on the description that is required or the specific application. Most of the image segmentation methods have been used with black and white images, because they are easier to handle. The image segmentation methods have been divided into two general approaches - edge based methods and region based methods.

In edge based segmentation methods, the edge in this case is the boundary between two adjacent rock types (regions). The local discontinuities are detected first and then connected to form longer, hopefully complete boundaries. It is difficult to use this method to define regions (Mason et al., 1986) because small gaps would allow the merging of dissimilar regions, (e.g. the wide lineament within mountains).

In the region based method, areas of image with homogeneous properties are found first and then the boundaries are found. One major advantage of using region based method over edge based methods is that it always produces closed regions.

A recent example using a combination of both methods, region growing and edge detection is described in Pavlidis and Liow (1990). There are many commonly used region based segmentation methods, these are:-

#### **1. Thresholding -**

Thresholding is the simplest form of region based method. It is not designed to enhance contrast, but to isolate specific or distinct grey level regions, from their surroundings. According to Niblack (1986) thresholding image segmentation can be divided into two types:-

##### **(a) Fixed Threshold -**

This is a single based thresholding and the simplest one. In this method, it is assumed that the objects have pixel values (DN) generally different from the background. The output image is in a binary form, only zero's (0) (background) and one's (1) (objects).

The threshold selection is usually based on information contained in the grey level histogram (one dimensional histogram) of the image. It is possible to make different threshold selection one at a time, and review the results.

##### **(b) Multiple and Variable Thresholding**

Usually no single threshold can separate accurately the

objects from the background. In order to obtain a better result, alternative or additional processing must be done. One alternative is to use multiple threshold or thresholds that vary across an image. Both threshold methods are useful in segmenting scenes containing a homogenous object or objects against highly contrasting uniform backgrounds. A good explanation of threshold methods for image segmentation can be found in Rosenfeld and Kak, 1982; Schowengerdt, 1983; Nakegawa and Rosenfeld, 1979 and Yanowitz and Bruckstein, 1989.

### **2. Region Growing Method -**

In this method, the image is first divided into a large number of regions. These regions are small groups of pixels or single pixels which are nearly uniform. Then all the neighbouring regions are merged, provided that they are sufficiently similar. This method can be divided into three categories, (a) single linkage region growing, (b) hybrid linkage region growing and, (c) centroid linkage region growing. For more detail see (Haralick and Shapiro, 1985).

### **3. Split and Merge Method -**

In split and merge methods, both region splitting and region merging processes take place. Region merging involves finding small groups of pixels, with similar properties such as grey levels (DN's), then merging adjacent similar regions until no more adjacent regions can be merged according to the present criteria. Splitting regions involves starting with a large region, and then splitting it into many regions, and again the

process continues until no further splitting can occur, when all the regions satisfy the criteria of homogeneity. At that point, the regions are merged and so on, the two processes of splitting and merging alternating until no changes occur. At this point the image has been segmented into homogeneous regions. This method has been used to segment remote sensing images (MSS) by Cross and Mason, 1985, and Cross et al., 1988. Gerbrands and Backer (1988) have applied this method to segment side looking airborne radar (SLAR) images (Section 2.4).

Considerable effort has been spent in developing and examining different segmentation algorithms for many years. For example image segmentation using (1) contextual analysis or classification (e.g. Kittler and Föglein, 1983; Chassery and Garbay 1984; Elliman and Lancaster 1990); (2) image segmentation using spatial clustering algorithms or analysis (e.g. Narendra and Goldberg, 1980; Seddon and Hunt, 1985; Pappas and Jayant 1989; Terauchi et al., 1989; Krishnapuram and Munshi, 1991; and Celenk, 1991); (3) image segmentation by using the relaxation method (e.g. Mester and Franke, 1988 and Karssemeijer, 1990); (4) a product for interactive pyramid segmentation (e.g. Wharton, 1988); (5) using pyramid structures for image segmentation (e.g. Baraneti et al., 1990); (6) image segmentation using exact statistics (e.g. Kartikeyan and Sarkar, 1989); (7) image segmentation using contrast and homogeneity measures, (Pal and Pal, 1987).

There are however, only a few published works reported on the application of segmentation techniques to segment remote sensing

images. Oddy and Rye, (1983), for example, applied a method called a similarity rule image segmentation to segment satellite-born synthetic aperture (SAR) image (Section 2.4). Quegan and Wright, (1984) have applied an automatic segmentation method to segment agricultural scenes using satellite-born synthetic aperture radar (SAR). Rye and Wright, (1985) have developed a multi-frequency segmentation method to segment SAR images covering a number of agricultural fields and roads. Cross and Mason (1985) used a split and merge image segmentation method to segment a 10 M resolution areal MSS data. Gerbrands and Backer (1988) have applied the split and merge segmentation method to segment side looking airborne radar (SLAR) images to detect the boundaries of the agricultural field within the images.

From the literature, the following conclusions can be drawn:-

1. It is not possible to define one segmentation method that would work on all digital images. One image may exhibit several different segmentations depending on the application (O'Connor, 1988)
2. It is clear that the development of an independent automatic, unsupervised, segmentation method for remote sensing images is not an easy task.
3. Most of the published works used radar images but none have used TM images, and the applications were mainly on agricultural areas, which are smooth and homogeneous.

In this study a new automatic Watershed segmentation method (Section 5.6) was used to segment the images of arid areas (the

study area) containing igneous rocks and mixture of alluvial deposits (Section 1.7.3). An alternative method was used for the same purpose and this consisted of first smoothing the image using the 'ripping membrane' technique (as contextual technique) and then extracting the rock boundaries as polygons using Laserscan system programmes (e.g. VICTORISE DTICOMBINES...etc). In essence, the 'ripping membrane' first smoothed the image, and simplified it, to the point that simple density slicing and boundary finding techniques (applied by the Laserscan software packages) could operate.

#### **5.6 WATERSHED IMAGE SEGMENTATION METHOD**

Watershed segmentation is a region based segmentation method. It is a particle extraction program that divides up any digital image on the basis of connectivity, (Figure 1.8) into separate groups or particles. Serra (1982) explains the method by analogy with a rain over a mountainous region, the water streams down the slopes and reaches distinct sinks. The domain of attraction of each sink is called its watershed basin and defines a segment.

A program called IMMENSE (Watson pers.comm. 1991) whose function is to segment digital images by the watershed segmentation method was used. This program was part of a series of programs which were used for automatic watershed classification only (e.g. Watson 1987, 1992; Watson et al., 1992).

There were two stages of processing in this segmentation method, the first consists of defining regions; and the second

consists of defining the boundaries.

The image extracts are for arid areas with rocky regions well exposed. Each extract was 512 x 512 pixels (Section 1.7.3), and they are displayed in Plates 5.1 and 5.4. In these images, it was obvious that the pixel values DN are variable even for the same rock type, (e.g. alkali granite). To overcome this problem of heterogeneity preprocessing techniques were used to prepare the images for watershed segmentation program. The preprocessing techniques are:-

#### 1. Image Smoothing -

Image smoothing consists of transforming the DN values of a pixel so that nearby pixels from the same region have similar grey levels. Milgram and Rosenfeld (1981) point out a number of reasons for spatial image smoothing. First, smoothing can eliminate insignificant local changes of contrast, otherwise the output of edge or region detection operations, based on differencing, can have many tiny spurious edges, which tend to obscure the main edge or boundary. The second reason for making an image spatially more uniform or homogeneous, is that it increases the probability that points, which belong to the same region, will be treated identically.

In this study, two techniques of image smoothing were investigated, (a) the ripping membrane and (b) the median filters, both being contextual techniques. The first method, ripping membrane technique (RM) was applied to TM Bands 4, 5 and 7 independently using four ranges of smoothing parameters

(ranges) (10, 20, 40 and 60). (Section 3.4.1). The idea of the RM technique is to replace the DN value of a pixel by a value which is proportionately closer to the average DN value of its neighbourhood. If a difference of larger than a threshold value (related to the range) has been used, the DN value is left unaltered. The process is repeated until no pixel in the image changes value. As the RM ranges value gets larger, the resultant image will be smoother, and the fewer discontinuities will be left in the resulting image. (Section 3.4.1). The smoothed TM band 5 was found the best to be segmented compared with the other two bands. This is because rock boundaries clear.

The second method of image smoothing was the median filter (MF) which replaces the grey level of each pixel by the median of the grey levels for the neighbourhood of that pixel. At each point of an image, the median value of ( $S \times S$ ) neighbourhood is computed. The size of the window  $S$  depends on the amount of local noise variation. By increasing the window size a greater degree of smoothing is achieved. In this work, a median filter ( $5 \times 5$  and  $11 \times 11$  pixels) was used to smooth TM Band 5 only.

## **2. Box Classification -**

Box classification (or parallelepiped classification) is the second preprocessing technique and is a supervised classification. Each class has to be specified by defining the range of values (e.g. grey level) for each class in the training area. This range may be simply defined by the minimum and

maximum digital number (pixel value) in each band, and appears as a rectangular area in the two channel feature diagrams (Lillesand and Kiefer, 1987). An unknown pixel is classified according to the class spectral range within which it lies. The pixel will remain unclassified if it lies outside all class ranges.

The parallelepiped classifier (box classification) is very fast and efficient and is employed in several image analysis systems (Estes et al., 1983). For more detail about parallelepiped classification, (Mather, 1987, and Lillesand and Kiefer, 1987).

In this study, TM Bands 4, 5 and 7 have been smoothed by RM (range 40) independently. These bands were chosen for box classification processing because they are the most informative bands for rock boundaries. Each rock type in the training area was displayed in order to find out the appropriate minimum and maximum pixel values. It was clear that the granite showed a very variable range of pixel values in all the three bands. The resultant image was a single classified image.

Automatic watershed segmentation was applied using the IMMENSE program to segment seven preprocessed images independently which were four difference range smoothed (RM) images (10, 20, 40, and 60), two median filtered images, (5 x 5 and 11 x 11 pixels window) and one parallelepiped classified image.

All those segmented images were visually compared with the geological maps and false colour composite TM of bands 7, 5 and 4 in red, green and blue respectively. All the segmented images were unacceptable in general, but some rock bodies are segmented well but the rest were overlapping.

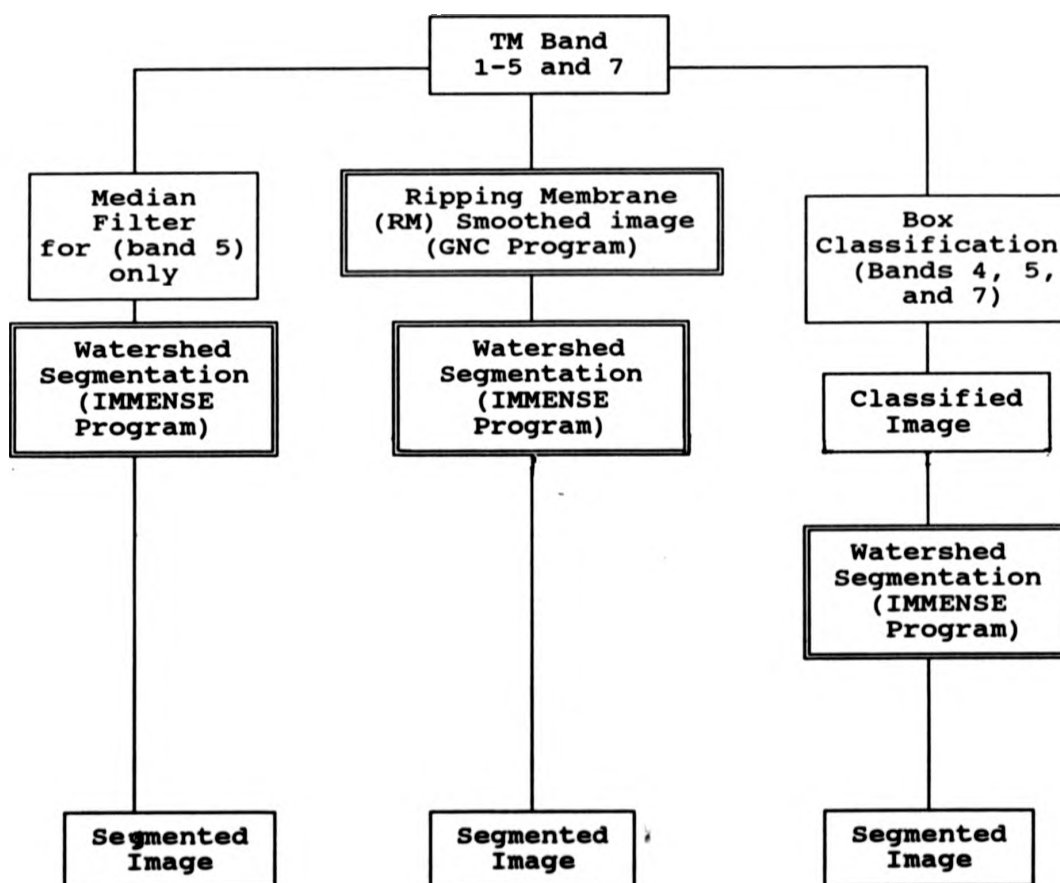
All the smoothed images were sub-sampled (Shrinking) because these images still contained isolated points (pixels) and small noise regions. The method consists of two processes: sub-sample and expand. The purpose of the first process is to shrink the objects in a uniform way so the small unwanted pixels might disappear entirely. The images were converted from 512 x 512 pixels in size to 256 x 256 pixels. Watershed segmentation program was applied to the seven sub-sampled images.

In the second process (expand) the segmented region was regrown to its original image size. The segmented region in the images were unacceptable. Therefore the automatic watershed image segmentation method failed to achieve the aim of producing a simple segmentation for arid area images.

Figure 5.1 shows a flow chart for the different steps followed for the automatic watershed segmentation method used in this study.

FIGURE 5.1

Flow Chart showing the different steps followed for Watershed Segmentation. Double-lined boxes for image processing carried out on Micro-Vax computer using certain algorithms before the processed image was transferred to R-CHIPS system.



### 5.7 IMAGE SEGMENTATION BY LASERSCAN SYSTEM METHOD

Laserscan Automated Map Production System (LAMPS) is mainly used for reproduction of maps by digital methods. LAMPS consists of modular software packages, which can be used individually or in any combination. These modules cover data input verification, quality control and restructuring and presentation.

LAMPS has the capability of common functions which are:-

1. Accepting data inputs in many formats (e.g. analog map and overlay information, digital image data.)
2. Storing and maintaining information with the necessary spatial relationship.
3. Manipulating data (search and retrieval, computations, etc.)
4. Presenting data output to a plotter.

LAMPS is connected to the Micro-Vax computer system. All the images can be displayed on (1024 x 1024 pixel) colour monitor. Only colour coded or grey level images can be displayed. Only a few software packages were used during this study (Appendix 3). The following steps were followed in order to get the best result of simple image segmentation (boundaries extraction), and rock region boundaries using LAMPS:

#### 1. Preprocessing -

In this step, TM Bands 4, 5 and 7 were chosen to be processed because they are most informative bands for rock boundaries. These three bands were smoothed independently by using the Ripping Membrane with high smoothing range

(40 - 60). (Section 3.4.1). This is dependent on the image to be processed.

**2. Image formatting -**

All the smoothed images were converted from digital image data format into digital terrain image coded format (DTI) (Grid cell coding). All the three TM Bands were converted independently using RAST512 program.

**3. Image combination and displaying -**

In this stage, all the three TM smoothed images were combined to produce a single image which had sharper edges using the DTICOMBINE PROGRAME.

The ROVER program in LAMPS software package was used to display the images. This program allows both raster based or vector (polygon) data to be displayed and manipulated. Both raster and vector data may be displayed singularly or in combination. Each image to be segmented was first displayed in full grey level range then each grey level range has a colour code as in density slicing method, (Section 5.3). Knowing the exact brightness range of the alluvial deposits (minimum-maximum), these were assigned to black until only the rock types remained on the image. The remaining data was automatically stretched and regrouped in new grey legend intervals. The resultant image was stored in the Micro-Vax computer disk and was subsequently segmented.

**4. Image segmentation, or boundary extraction -**

The boundaries were found using the VECTORISE program. (The method of finding the boundary is that used for

finding a contour line between low bright contour line and bright data). This program extracts the boundaries of areas in raster image (e.g. satellite image) and stores the boundary lines in a junction structured vector (polygon) IFF format, (Interval feature format). All the resulting boundaries for all the test sites were closed Polygons (regions). The final results were confirmed by displaying the results as an overaly on top of the original TM band 5 image and by comparing with the available geological map.

Most of the rock boundaries have been extracted with an acceptable accuracy. Only one very short line has been added to one of the image extracts. The segmentation obtained by this method was later compared with those traced by hand using magnifying lenses.

#### **5. Image Reformatting -**

The boundary images were converted to raster image format. The program I2-GRID program in LAMPS software package was used to convert and label the regions within the IFF vector file. Each region was labelled with a different grey level number. INVRAST program was then applied to convert the Laserscan grid data back to the normal image format.

#### **6. Small region elimination editing -**

There are small regions located within or around the rock bodies, especially the alkali granite rock, which had many 'holes' due to erosion or fracture cracks. Those regions, with a size of less than 200 - 300 pixels, were merged with their neighbours which were the closest in tone. This

was done by using REGIONGRO program.

Four different extracts (512 x 512 pixels) were chosen to test and develop this segmentation method. Two extracts are demonstrated in this chapter and two in Chapter (6). The results shown in this chapter are for illustration purposes.

**First Extract:**

The first extract contained alluvial deposits (background) and only one rock type (object), which is the Hadn Formation (volcanic rock) (hu). For more geological description see Section (1.7.3) and see Appendix (1) for the location of this extract in the study area. Figure 5.2 shows the geological map for the first extract. This map is visually (manually) traced from TM band 5. Plate 5.1 shows TM band 5 for this extract.

Plates 5.2 and 5.3 show all the results of the processing steps for the RM technique and image segmentation method. Plate (5.2a) shows a three colour composite image of TM bands 7, 5 and 4 in red, green and blue respectively which has been smoothed using the ripping membrane programme with a range of 40. Plate (5.2b) shows three histograms for the smoothed images, the first histogram for band 7, the second for band 5 and the third for band 4. These histograms show the distribution of DN's in these images. Plate (5.3) shows the image segmentation result; Plate (5.3a) shows the labelled segmented image before elimination

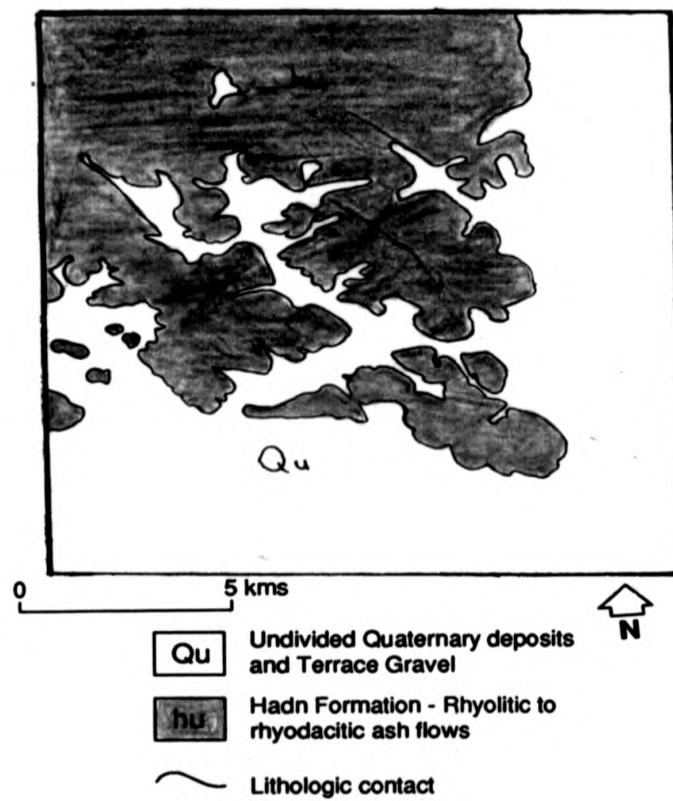


**FIGURE 5.2**  
Hand traced (segmentation) map based on TM data for the first extract

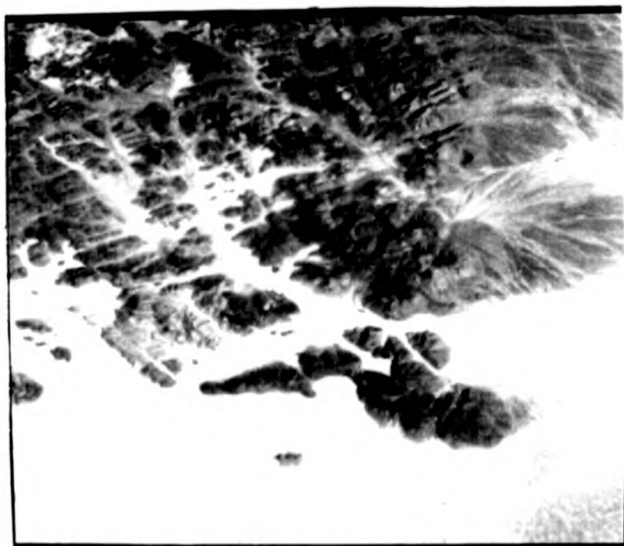


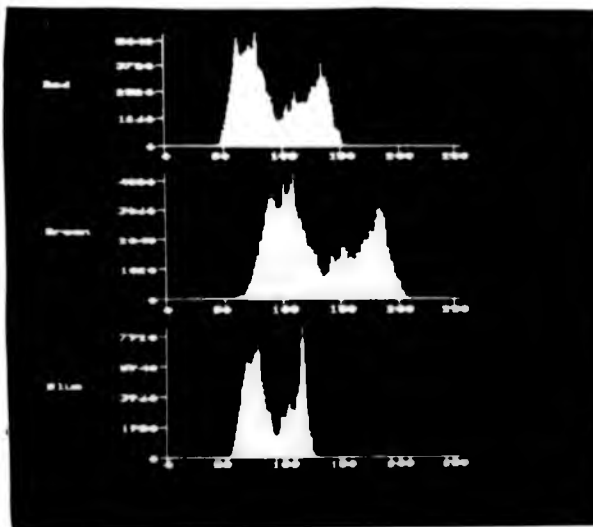
**PLATE 5.1**

Linearly contrast stretched TM band 5 for the first extract area.

(a)



(b)

**PLATE 5.2**

(a) Three colour composite image of TM bands 7,5 and 4 in red, green and blue respectively for the first extract. These images were smoothed using the ripping membrane technique.

(b) The histograms for the images in plate 5.2 (a).

(editing) of the small regions. No line edition has been done so far in this extract. All the small regions were eliminated in order to simplify the result (Plate 5.3b).

**Second Extract:**

The second extract has three different classes of rock types (objects), and alluvial deposits (background). The rock types are the alkali granite (ag), biotite alkali-feldspar granite (afg) and Hadn Formation (hu). (See Section 1.7.3 for more geologic description and Appendix 1 for the location of this extract in the study area).

Figure (5.3) shows the geologic map for the second extract. This map was visually (manually) traced from TM band 5.

Plate (5.4) shows a linearly contrast stretch TM band 5 for the second extract area.

Plates (5.5), and (5.6) show all the results of the image segmentation processing steps for the second extract.

Plate (5.5a) shows a three colour composite image of TM bands 7, 5 and 4, in red, green and blue respectively. These images were smoothed using the ripping membrane technique with a range of 40.

Plate (5.5b) shows the histograms of all these smoothed images, first band 7, second band 5, and third for band 4 respectively.

These histograms show the distribution of the DN's in these images.

(a)



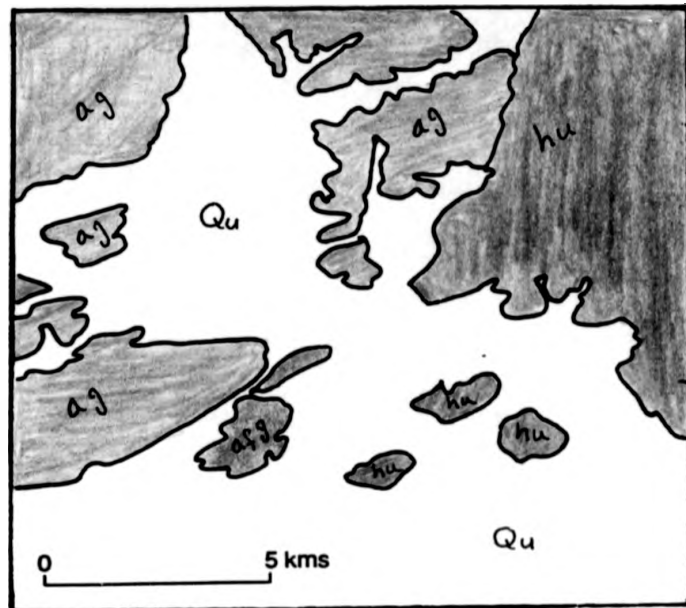
0 km 5

(b)

**PLATE 5.3**

The resultant image of ripping membrane/Laserscan image segmentation method for the first extract.

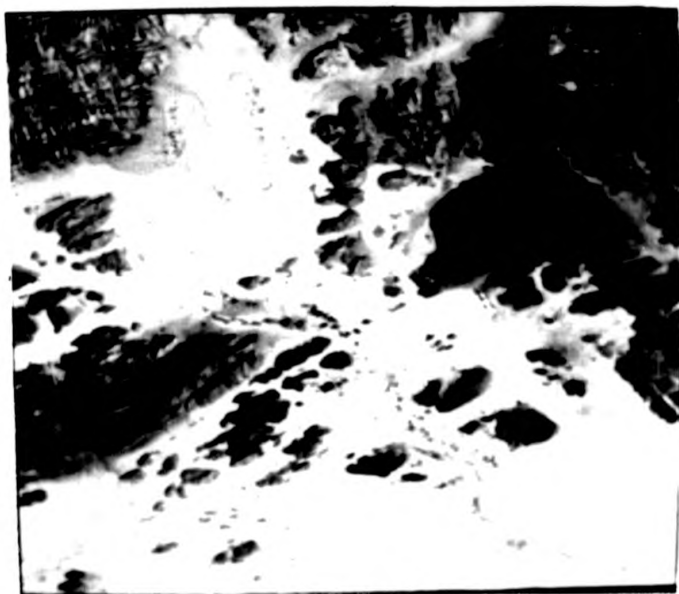
- (a) the labelled segmented image.
- (b) the labelled segmented image after the elimination of small regions.



- |     |   |   |
|-----|---|---|
| Qu  | Undivided Quaternary deposits                       | <br>N |
| hu  | Hadn Formation - Rhyolitic to rhyodacitic ash flows |   |
| ag  | Alkali granite                                      |   |
| afg | Biotite alkali - feldspar granite                   |   |

~ Lithologic contact

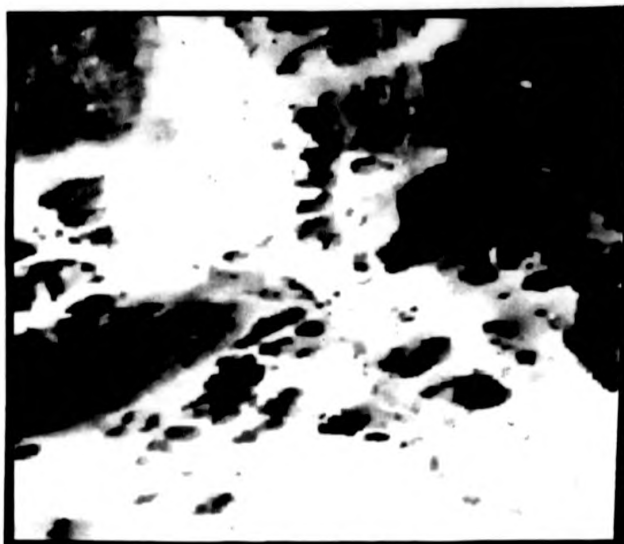
**FIGURE 5.3**  
Hand traced (segmentation) map based on TM data for the second extract



0 kms 5

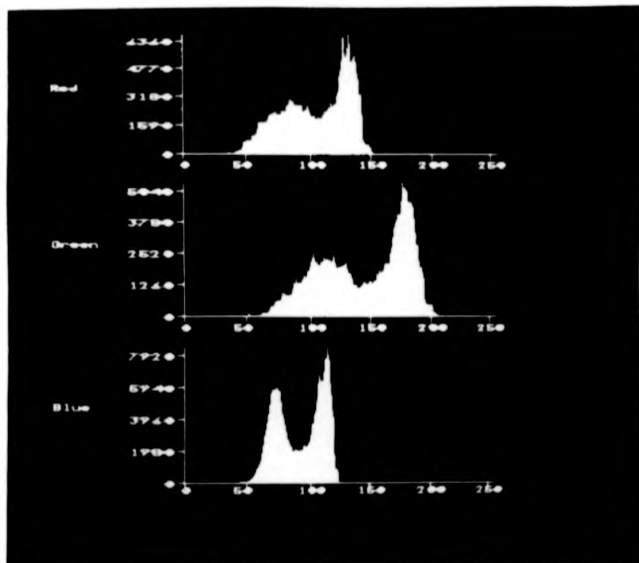
**PLATE 5.4**  
Linearly contrast stretched TM band 5 for the second extract area.

(a)



0 kms 5

(b)

**PLATE 5.5**

(a) Three false colour composites of TM bands 7, 5 and 4 in red, green and blue respectively for the second extract area. These images were smoothed using the ripping membrane technique.

(b) The histograms for the images in plate 5.5 (a).

Plate (5.6) shows the labelled segmentation results. Plate (5.6a) is the labelled segmented image before the small regions were eliminated.

Plate (5.6b) shows the labelled segmentation result after the elimination process.

### 5.8 DISCUSSION

Two different methods of image segmentation have been tested. First, the automatic watershed segmentation, was applied to segment eight different preprocessed images. All images were segmented incorrectly. The errors could be attributed to:-

1. The varnished surface (weathered surface) plays a role in obscuring the differences in the spectral reflectances, (Section 1.4), especially in the alkali granite areas.
2. The test site contains rugged mountains and hills (Plates 4.1-4.2) and this caused shadows in many parts of the image, (e.g. lineaments). Since the shadows caused abrupt changes in the DN values, these changes can be confirmed with the real boundaries and hence decrease the accuracy of automatic segmentation.

The alternative method was used a supervised editing method, that takes the results of a preprocessing smoothing algorithm, and interactively produces an acceptable segmentation. The ripping membrane (RM) was found very helpful in reducing the data complexity and enabling image segmentation. Then the Laserscan system was used for the image segmentation.

(a)



0 kms 5

(b)

**PLATE 5.6**

The resultant image of ripping membrane technique/Laserscan image segmentation method for the second extract area.

- (a) the labelled segmented image  
(b) the labelled segmented image after the elimination of small regions.

### 5.9 SUMMARY

This chapter discussed the definition of computer vision and image segmentation methods as well as their application in digital image processing and remote sensing images.

Image segmentation has not previously been demonstrated in any geological studies using remote sensing images. Two different image segmentation methods were used for the first time to segment two extracts of an arid area (study area) containing igneous rocks and a mix of alluvial deposits. These methods were (a) automatic watershed segmentation and (b) the ripping membrane/Laserscan system method. The first method failed to produce reasonable results for simple segmentation. The second method produced an acceptable result for the four extracts tested. The idea of this method was, first, to smooth the images using 'ripping membrane' technique and then extract the rock boundaries as polygons using the grey level (or contour) following algorithm.

## **CHAPTER SIX**

### **THE USE OF CONTEXTUAL TECHNIQUES IN AUTOMATIC LINE AND LINEAMENT FEATURE EXTRACTION AND ANALYSIS**

- 6.1 INTRODUCTION
- 6.2 AUTOMATIC LINE AND LINEAMENT FEATURE  
EXTRACTION AND ANALYSIS: A REVIEW
- 6.3 AUTOMATIC LINE AND LINEAMENT FEATURE  
EXTRACTION AND ANALYSIS: METHODOLOGY
- 6.4 AUTOMATIC LINE AND LINEAMENT FEATURE  
EXTRACTION AND ANALYSIS: APPLICATION
- 6.5 DISCUSSION
- 6.6 SUMMARY

## 6.1 INTRODUCTION

Automatic computer technique (computer vision) for lineament feature extraction from remotely sensed digital images is an additional tool available to the analyst because the automatic method may identify edges, where the human interpreter may not. The visual lineament detection and interpretation is widely used, by tracing and drawing a line on an image, using different sizes of pencils to indicate the position of a visually detected line (lineament) (Chapter 4). This method is dependent on the observer's (interpreter's) knowledge and experience. In other words, if any image is interpreted by the same observer on two different occasions, or by two different observers, it is possible to find discrepancies in the interpretation, whereas the automatic method will never vary in its results.

Podwysoki et al., (1975) and Huntington and Raiche, (1978) showed that there were differences between four different interpretations of the same image. Any lineament patterns obtained by different interpreters should be similar, and it is only by using computer algorithms can this sort of reliability be achieved.

Moore and Waltz (1983) have criticised visual lineament detection and interpretation because of the subjectivity associated with human interpreters, and they preferred using machine processing, while Wang and Howarth, (1990) have said that visual interpretation provided reliable results in many applica-

tions.

Thus, there is a real need for objective automatic lineament extraction techniques. The aim of this Chapter is to describe an attempt to develop and test an automatic lineament extraction method based on the contextual information, relationship, and techniques. The method was not expected to completely eliminate the need for manual checking for 'cultural' features and lineaments. The elimination of such 'mistakes' is very difficult and very time consuming, and it was thought that a less ambitious goal could be achieved, and would be of practical benefit.

Before any automatic extraction of linear feature, the author produced a detailed map of lineaments visually. These were taken to be the ground truth. Many of these were checked during a field excursion to the study area.

## **6.2 AUTOMATIC LINE AND LINEAMENT FEATURE EXTRACTION: A REVIEW**

In recent years, considerable effort has been directed towards the extraction of information from digital remotely sensed data by visual interpretation while the automatic computer extraction (computer vision) has attracted little attention.

Vanderburg, (1977) has tested three local detectors in order to extract linear features from images. The three detectors are the linear, the non-linear and the semi-linear algorithms. The semi-linear detector was found to be slightly superior to the linear detector, and it did not respond to edges. However it

responded to background noise and it produced thicker lines than the non-linear detector. The detectors were able to detect the basic structures of the linear features of a Landsat image.

Ehrich (1976) used directional averaging filters to obtain piece-wise linear approximations to linear features or segments of them. Different parameters of the algorithm were tested to make the filters selective, such that only straight edges or lines were detected.

Nevatia and Babu (1979) developed a technique for extracting man-made linear features from an image by a process of edge detection and line linking. In addition, they attempted to derive higher level descriptions from the extracted lines. The edge detection and line finding was done in four stages of processing. The first stage is edge detection and starts by convolving the image with masks (5 x 5 matrices in six directions) corresponding to ideal step edges. The second step is thresholding and thinning process; during this stage, the presence of an edge at a pixel is decided by comparing the edge data with some of the eight neighbouring pixels. The third step is linking; criteria for connecting two edge points were set, such that they had to be neighbours in the eight neighbour sense, and that they had to be edge directions differing by not more than a certain limiting value. The fourth step is linear approximation; at this step each boundary segment is approximated by a series of piecewise linear segments.

Gurney (1980) examined a line detection algorithm (using local operators) with different thresholds (single and multiple thresholds) to detect lines with less than one pixel in width, from MSS band 4. It is found that the results always contain a significant amount of noise. Post-processing techniques were used to reduce this noise.

Burdick and Speirer (1980) developed a method for linear feature detection. They used two different computer programs in two stages. The first stage is to determine if each image point is either darker or lighter than the two adjacent points. If the points are the same, the point is saved as a black dot, if not, the point is blanked out or turned white. In the second stage a moving window or slit was passed over the image at discrete 5° increments from 5° to 180°. If the data within the window is blacker than the data on each side of the window, then they are saved. The lighter data were ignored, they claimed that almost all lineaments determined by the programs are valid.

Moore and Waltz (1983) examined Landsat-3 MSS Band 7 (0.8 -1.1  $\mu\text{m}$ ) by first using a low pass filter to remove the high frequency component of the image. Second, they applied to each enhanced feature a series of directional filters that tended to be linearly oriented, in one of eight compass directions. This step produced a set of eight filtered images, each showing the linear feature in a specific direction. Smoothing procedures were applied to remove undesirable short-range variation and the

brightness values were revealed to produce a visually sharper image.

The Hough transformation has been used in the detection of geological features (e.g. linear features, aligned points and circular structures) by many authors (e.g. Cross and Wadge, 1988; Wadge and Cross, 1988, 1989; Wang and Howarth, 1990 and Taud and Parrot 1992). The Hough transformation is mainly designed to detect straight lines in a binary image and it was introduced by Duda and Hart (1972). The Hough transformation is able to generate rapidly a visual impression of the directions and densities of lineament patterns in an area, also, a quantitative measure for specific areas can be readily calculated (Wang and Howarth, 1990). Therefore such a procedure permits a rapid overview of a study area and aids the geologist in the analysis of structural characteristics of the area (Wang and Howarth, 1990). For more mathematical detail, see Duda and Hart, 1972; Ballard and Brown, 1982; and Wang and Howarth, 1990.

Cross and Wadge (1988) have used the Hough transform to detect the lineaments for areas of East African rift, from MSS data. The detection was achieved in three stages. In the first stage the image was smoothed using a Gaussian filter. In the second stage, a threshold was applied to the image. In the third stage a Hough transform was applied to detect lines in the image. They claim that the method they used succeeded in detecting the majority of mapped faults but the commission errors were very

high because the method cannot discriminate against non-geological alignments.

Wang and Howarth (1990) used a Hough transform as an automated lineament detection method and applied it to a Landsat TM image of the Canadian shield (Canada). Their method had four stages. In the first stage a 3 x 3 median filter was applied to smooth the image. In the second stage an "edge operator" is used to obtain the magnitude and direction of an edge for every pixel. This is based on determining the locations where maximum changes in digital values occur, and in what direction these changes are. This procedure can be applied to detect the edges as well as light or dark lines depending on the appearance of the lineaments in the image. In the third stage, the starting points for the edges were identified. Finally, edge following as a graph searching (EFGS) algorithm was used to trace all the edges on the image. For more detail about the EFGS algorithm, see Wang and Howarth, (1990).

These algorithms have a varying degree of success but clearly all of them depend to a large degree on generating an 'edge' from the original image. All proceed by some subtraction or differencing method, and this inevitably leads to a very noisy and error prone starting point for the rest of the algorithms. For this reason, new methods, which are based upon using more of the local contextual information to derive more reliable estimates of edges and lines, were developed in this study.

### 6.3 AUTOMATIC LINE AND LINEAMENT FEATURE EXTRACTION AND ANALYSIS: METHODOLOGY

Feature extraction in general can be done by two steps; separation of the important information (high frequency component of data) from the unwanted, unimportant information or noise. The second step is reduction of this information (data) in order to simplify the calculation or measurements, and to extract the object or feature. As remarked, there is a need to find an automatic technique or techniques of extracting lineaments. In this section, an automatic method for lineament extraction and the measurement of the azimuth angles will be discussed and developed. This method makes use of contextual (spatial) relationship between the pixels within any image. (Section 1.5).

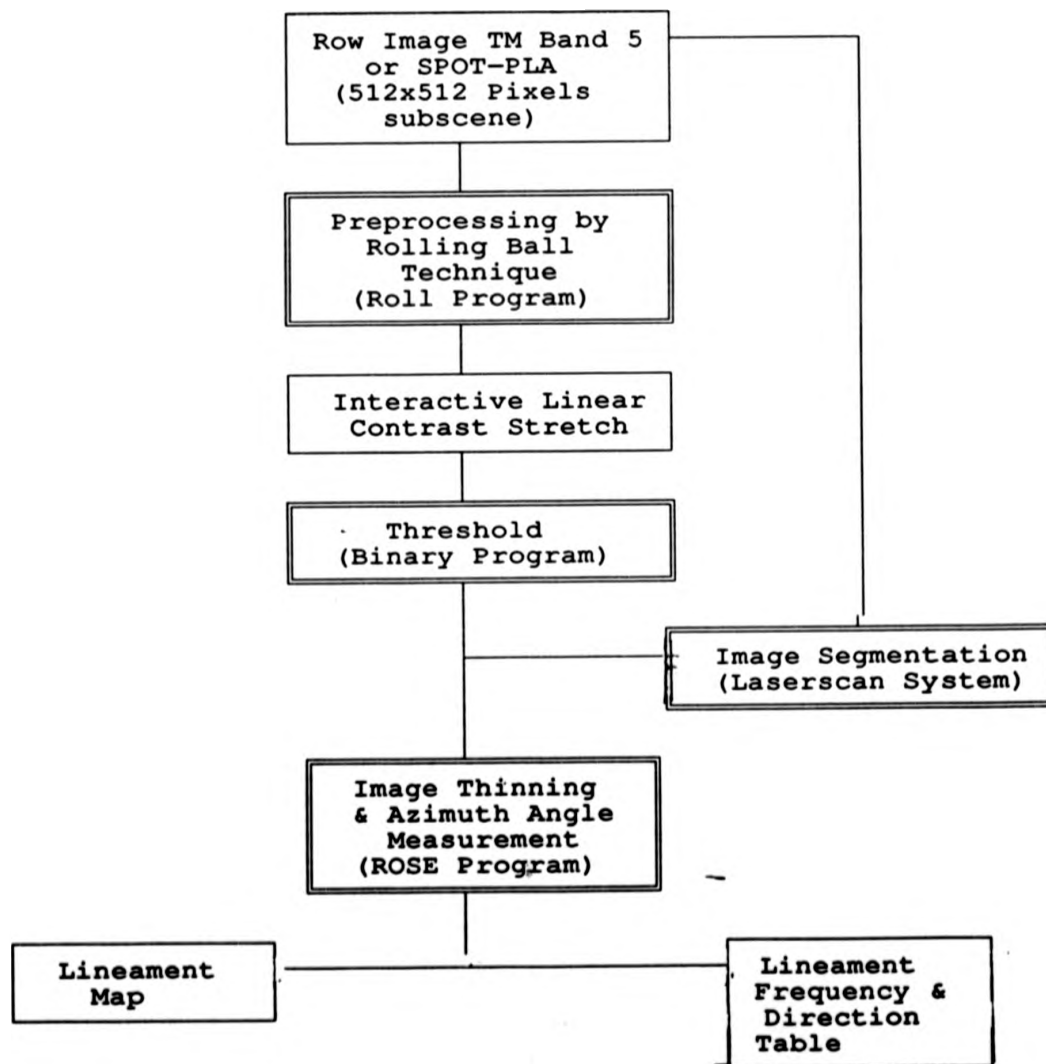
Two different satellite images with different spectral and spatial resolutions have been examined. (TM Band 5 and SPOT panchromatic mode (PLA)). The proposed scheme (method) has four stages. These are preprocessing, thresholding process, image segmentation, lineament extraction and their azimuth angle measurement, Figure 6.1 shows a flow chart for the proposed scheme (or method).

The method developed here contains different novel features. First, there was an attempt to create a relationship between image segmentation and linear feature extraction in order to find out the megatexture in each rock type automatically. Different lineament directions might be expected in each different rock type. Second, was the use of a rolling ball (contextual)

FIGURE 6.1

**FLOW CHART OF PROCESSING USED IN AUTOMATIC  
LINE AND LINEAMENT FEATURE EXTRACTION METHOD  
USING THE CONTEXTUAL TECHNIQUES**

Double line boxes for image processing carried out on computer using certain algorithm applied on MICRO-VAX before the processed data are transferred to R-CHIPS System.



technique, as an input image and preprocessing method to reveal the texture.

The four stages of the proposed method are:-

1. **Preprocessing** -

This refers to those transformations applied to the raw image data for the purpose of correcting, simplifying and regularising the imagery. The resulting images should be amenable to further processing, i.e. for subsequent algorithms. For the majority of row images it is important to apply a filter to the image to smooth it and remove most of the noise but in this work a contextual technique (rolling ball) with a high range (ball diameter) of 10 was used. (Section 3.4.2). There are three reasons for using this technique as a preprocessing method -

- a) Because 10x 10 pixels are used to define the 'context' a far more reliable estimate can be found for the local average, and hence a more reliable estimate can be found for the departure of a pixel from the expected average.
  
- b) The lineaments may have gaps due to poor contrast of the lineaments with its surroundings. The rolling ball technique as a contextual technique will emphasise any similar group of pixels in the neighbourhood, whether they are black against a white background, or the reverse.
  
- c) The technique produces a much more defined distribution of grey levels (histogram) that allow easy and unambiguous

selection of a threshold.

The reasons for not using the high pass filtered image (directional or non-directional) (Section 3.3) as input preprocessed images were because, firstly, they produced a random noise, which was unevenly distributed, and secondly, the directional filter show only the lineaments in the orientation selected.

The TM band 5 was chosen to find out the major trend of lineaments in the area, while SPOT-2 PLA image data was tested to see if the change in resolution had any effect. Three different extracts (512 x 512 pixels), two of TM data and one SPOT data were tested. This size of image was chosen because of computation time and storage requirement and displaying. Plates 6.1 and 6.5 show the two TM enhanced (preprocessed) images for the TM data. Plate 6.9 shows the SPOT panchromatic enhanced (pre-processed) image.

## **2. Threshold Processing -**

The rolling ball transformation produces two images. One is the smooth 'contextual' average, and the other contains the 'spikes' and 'dimples' that represent the departure from the local contextual average. The 'spikes' and 'dimples', bright and dark pixels, can be separated into two images, by a simple threshold (Section 5.5). Each of the resulting images should contain complimentary information about the lineaments. Since the absolute brightness is now irrelevant, in either the 'spikes' image or the

'dimples' image, a simple density slice can transform each to 1's and 0's. The ones represent the presence of a lineament and the 0 the background. Plate 6.2 and Plate 6.6 show the binary images resulting from the threshold process of the two TM extracts. Plate 6.10 shows the binary images for SPOT-2 PLA threshold images. By careful manipulation of the threshold images, it has been found that the straight lineaments can be made obvious in these images.

### **3. Image Segmentation -**

Two different image segmentation techniques were used to segment the images. These were the unsupervised (automatic) watershed image segmentation method (Section 5.6) and supervised image segmentation method using the ripping membrane and the Laserscan system (Section 5.7). The second method produced a better result than the first method.

All the detected regions were labelled with different numbers and the small regions, which were less than 200-300 pixels in total were eliminated. Thus it became possible to relate all extracted lineaments to their location. Thus, it became easy to find the dominant direction of lineament in each rock type or region automatically.

### **4. Lineament extraction -**

At this stage, the segmented image and the binary image were prepared for automatic lineament extraction on a

regional basis. A program called ROSE (Watson pers. comm. 1991) was tested and developed during the period of this study. This program had three different stages of processing. These were - feature detection (extraction), feature thinning, and azimuth angle measurement.

**(a) Feature detection (extraction)**

Each possible feature was found sequentially and labelled.

**(b) Feature Thinning -**

In turn each feature was removed without causing discontinuation of the extracted feature, until only the 'skeletal' pixels remained. This process was performed using the Golay L processing element. (For more detail see Serra, 1982).

Gurney (1980) used a postprocessing technique (utilising the contextual information) to interpolate missing segments of lines and to remove isolated noise, while in this study the contextual techniques were used before the extraction of the lineaments, and therefore, reduced the noise beforehand. At this stage of processing, all the elongated objects, i.e. lines of varying width were thinned down to one pixel in width.

**(c) Lineaments Azimuth Angle Measurement -**

For all the 'lines' from the thinning process, their azimuth angles were measured using standard regression methods, and the azimuth frequencies for each region were recorded. The program produced a table containing the regions' number (label), frequency of lineaments in 5°

intervals, starting from west up to a 180° angle in the east.

#### **6.4 AUTOMATIC LINE AND LINEAMENT FEATURE EXTRACTION AND ANALYSIS: APPLICATION**

In this section, the proposed automatic method, and the visually traced method for lineaments extraction are compared and discussed. The discussion for each processed image will be separate because these images have, either different rock types, or have different spectral and spatial resolutions (SPOT or TM).

Two extracts (512 x 512 pixels) of TM data from the test site (Jibal Rumman area) which have been examined for visual lineament detection in Chapter (4) were used in this chapter. The extracts were located in the left quadrant and middle quadrant respectively of the test site (see Appendix 1 for location of these two extracts). These are:-

##### **First Extract:**

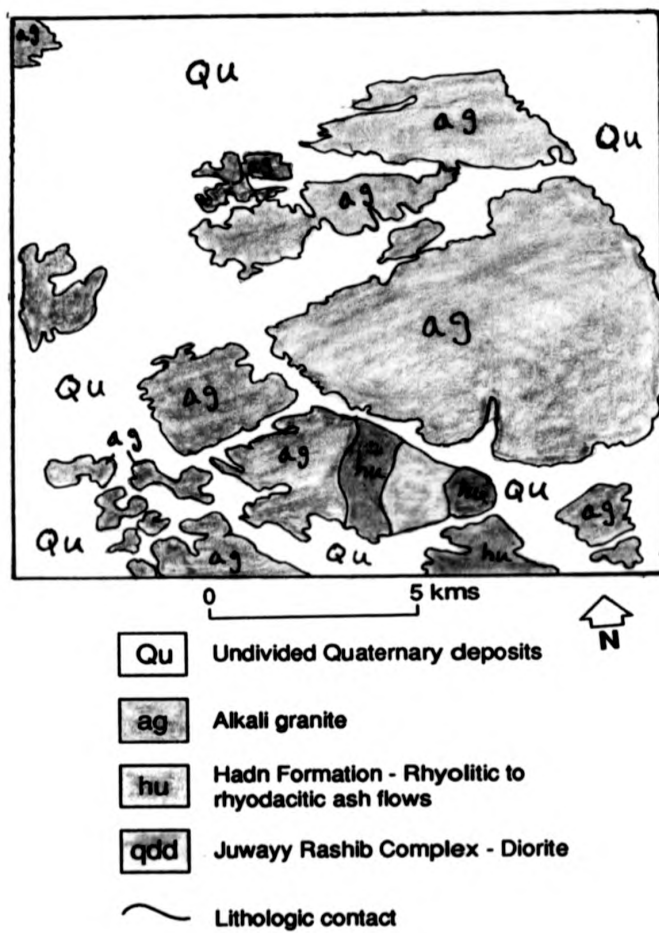
This area contained three rock types. The major rock type was alkali granite which covers two thirds of this extract area. The other two rock types were the Hadn Formation and Juwayy Rashib Complex (qdd) and they were located in the southern part of the alkali granite area. For more geological description see the geological map (Figure 6.2), (Sections 1.7.3 and 4.3).

Plate (6.1) to 6.4) show all the results of the different stages of the proposed automatic lineament extraction method for

the first extract.

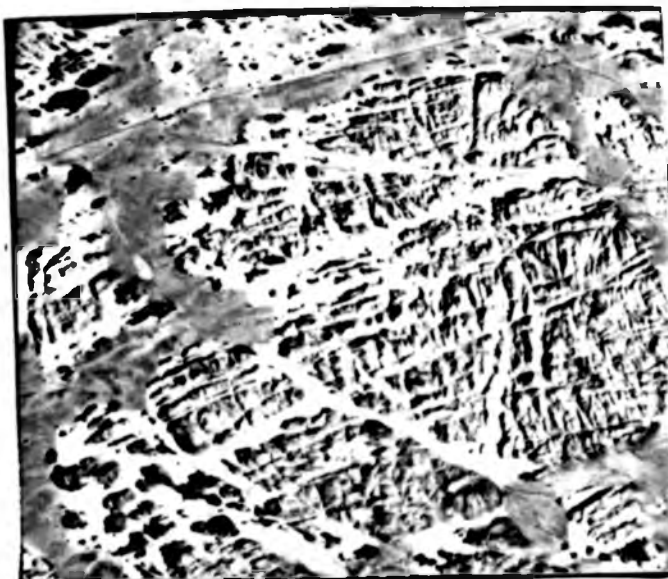
Plate (6.1a) is the resulting image of the rolling ball technique, using a high range of (10) for TM band 5. It can be seen that the shadowed areas are well defined and easily distinguished from the valleys or wadis. Plate (6.1b) shows the distribution of the DN's and their frequencies over the image. This histogram showed that the data can be divided into two parts (categories) from the middle of the histogram. The first part was between (1-128) DN's value which represents the dark pixels and the second part was between (134-247) DN's value which represents the light pixels in the image.

The above values were used to threshold the image in Plate 6.1a into two images, one containing the dark pixels (dimples) and the other containing the light DN's (spikes). It was found that the light DN's were best to use for further processing (Plate 6.2). The choice was made based upon the apparent greater number of major lineaments it revealed, especially within the rocky regions. These lineaments were too thick and needed a thinning process. Plate (6.3) shows the result of the ripping membrane/ Laserscan image segmentation method for the same extract. In this image, all the three rock types have been segmented into individual regions. The final result was compared with the available geologic map. This indicated that the alkali granite rocks had been segmented very well and needed no human intervention or line editing.



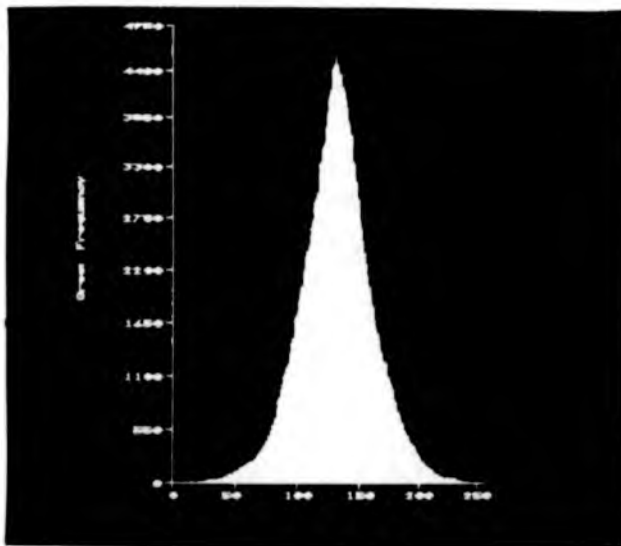
**FIGURE 6.2**  
Hand traced (segmentation) map based on TM data for the first extract

(a)



0 kms 5

(b)

**PLATE 6.1**

(a) Preprocessed image using the rolling ball technique for the first (TM) extract.

(b) Histogram to show the distribution of the DN's and their frequencies over the image in plate 6.1(a).

**PLATE 6.2**

Binary image for the first (TM) extract. This image is a result from a single threshold process for plate 6.1(a).

0      kms      5

**PLATE 6.3**

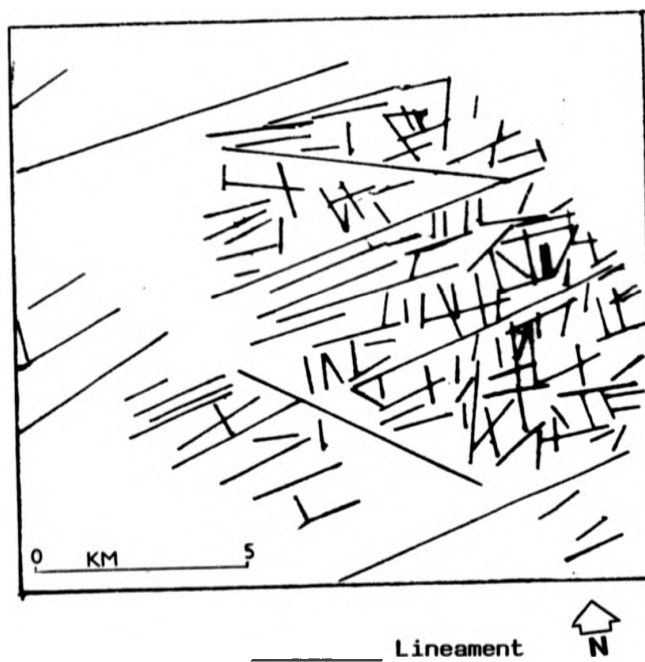
The resultant image of ripping membrane technique/Laserscan image segmentation method for the first (TM) extract. All the small labelled regions were eliminated.

Figure (6.2) shows the visually traced rock boundaries (segmentation) for the same area based on TM band 5 and compared with the geologic maps.

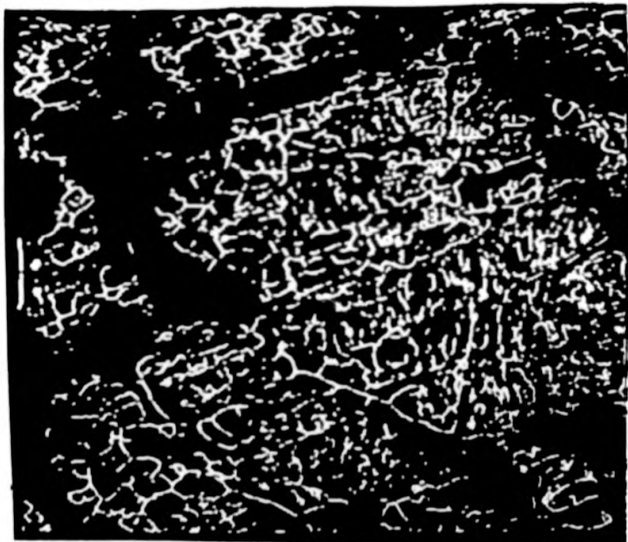
The ROSE program was then applied to the binary and the segmented images and a lineament map was produced (Plate 6.4) as well as a table showing the lineaments' azimuth angle and their frequencies for each region. Figure 6.3 shows the visually traced lineaments from the rolling ball enhanced image. Only the clear lineaments (Section 4.2) have been considered with no restriction to the length.

The final step in this study was to draw a diagram which shows the azimuth frequency to reveal the significant trend or density of lineaments for the regions. Rose diagrams were plotted for the alkali granite only because the Hadn Formation and the Juwayy Rashib Complex (diorite) in this extract were very small scattered hills, (small regions). Therefore these rocks do not have a reasonable number of lineaments for analysis. The automatic and visual methods were compared. All the rose diagrams have been plotted according to the vertical in the image and not to the true north, for convenience.

Figure (6.4a) shows the first rose diagram based on the visually traced lineaments from the alkali granite rock only (Figure 6.3). It is clear that the major trend is in the direction ( $150^{\circ}$ - $155^{\circ}$ ) in the image and this is equal to ( $N69^{\circ}$



**FIGURE 6.3**  
Lineament map identified from plate 6.1(a) by visually tracing method for the first (TM) extract.



0      kms      5

**PLATE 6.4**

Lineament map produced by the automatic method for the first (TM) extract.

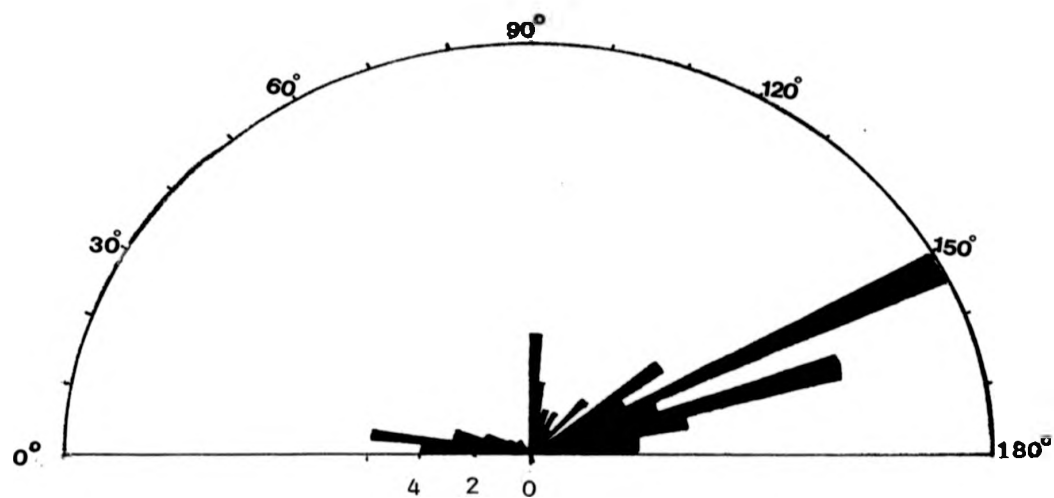
-74°E) with respect to the true north.

Figure (6.4b) shows the rose diagram for the automatically extracted lineaments for the alkali granite rock regions only (Plate 6.4). The major trends were the (0°-5°) and (90°-95°) also 135 in the image. By carefully observing the lineament using the zooming procedure on R-CHIPS, it was found that these directions represent only two adjacent pixel lineaments in length, which connected to one pixel in different direction (undirected lineaments) as in Figure 6.5. From the experience from Chapter 4, there are few lineaments oriented in these directions. (Figure 4.17). Both directions have been plotted but subsequently ignored in this work because they represent mostly the short and essentially ambiguous lineaments. When these directions are ignored, the major trend is (135°-140°) equal to (N54°-59°E) from the true north. The two rose diagrams have indicated that the major trend is in ENE-WSW but they differ in the exact angles of the direction and the difference was 15°.

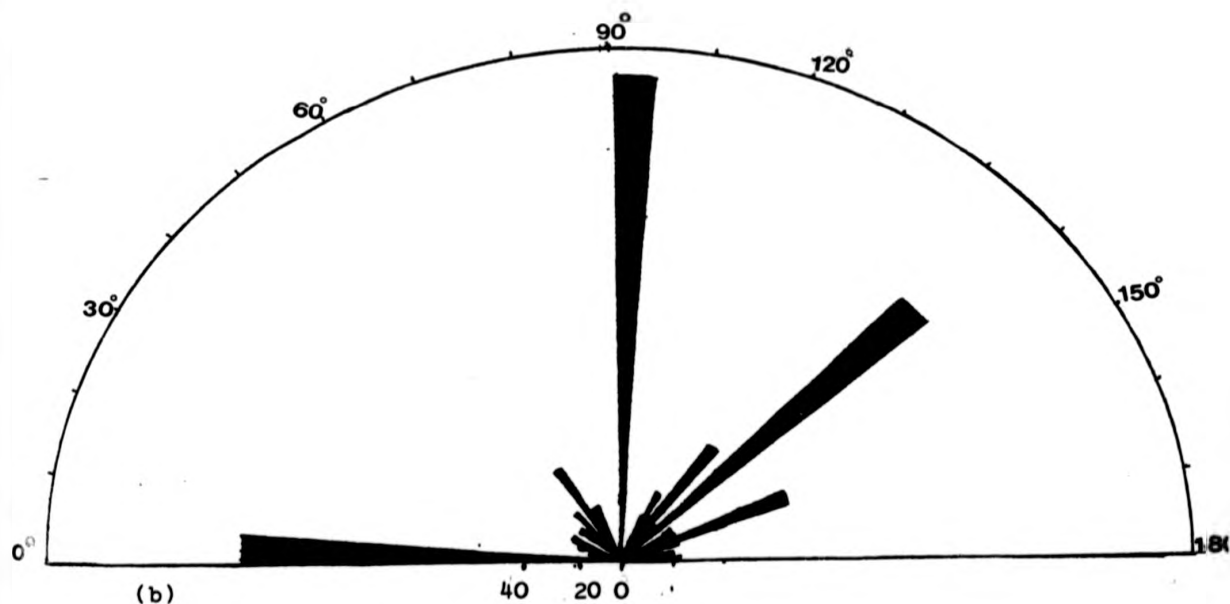
**Second Extract:**

This extract has four rock types which are alkali granite, biotite alkali-feldspar granite, Hadn Formation and gabbro. For more geologic description see Figure (6.6), Sections (1.7.3 and 4.3).

Plate (6.5) to Plate (6.8) shows all the results of the different stages of the automatic lineament extraction method for the second (TM) extract. All these images are lineally contrast



(a)



(b)

**FIGURE 6.4**

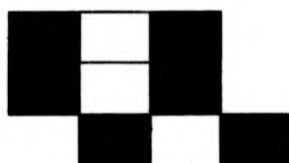
Rose diagram of the azimuthal frequency distribution of the lineaments in the first (TM) extract: (Plate 6.1a):

- (a) Lineament visually traced  
 (b) Lineament extracted by the automatic method

(These diagrams plot the number of lineaments but do not consider lineament length).

FIGURE 6.5

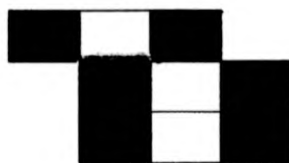
Two adjacent pixels lineament in length connected to one pixel only (very short lineament). The white pixels are the lineament and the black pixels are the background.  
 (From: Gurney, 1980)



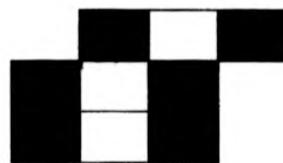
(a)



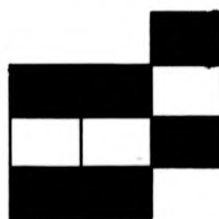
(b)



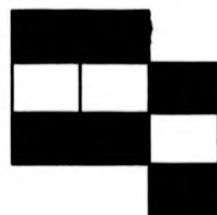
(c)



(d)



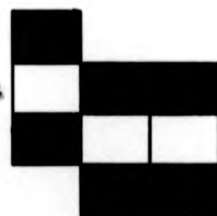
(e)



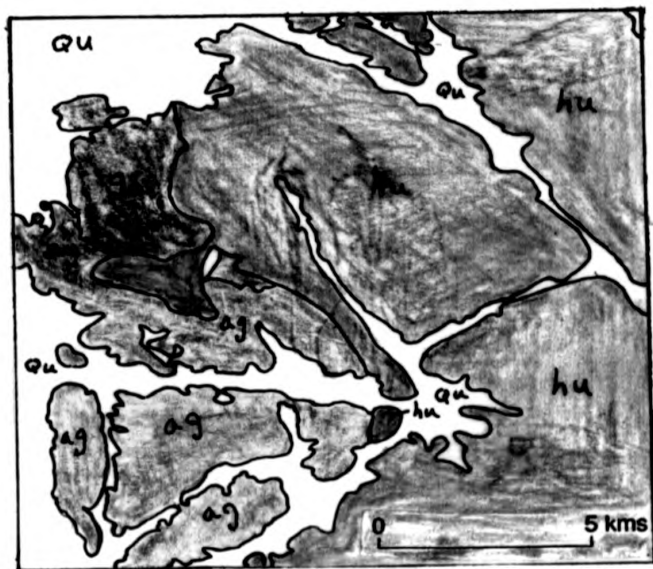
(f)



(g)



(h)



Qu Undivided Quaternary deposits

gb Gabbro

ag Alkali granite

atg Biotite alkali - feldspar granite

hu Hadn Formation - Rhyolitic to rhyodacitic ash flows

~ Lithologic contact

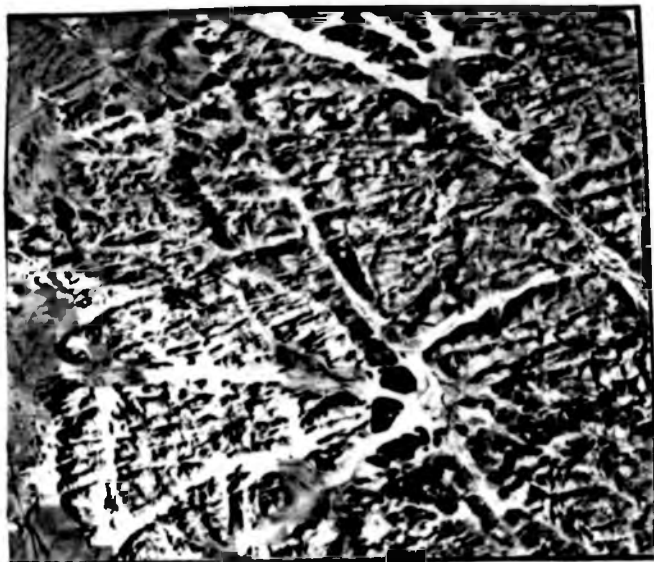
**FIGURE 6.6**  
Hand traced (segmentation) map based on TM data for the second extract

stretched. Plate (6.5a) is the resulting image after applying the rolling ball technique using a high range of (10) for TM band 5. By carefully observing this image, it has been found that the shadow areas are well defined and distinguished from valleys or wadis.

Plate (6.5b) shows the distribution of the DN's and their frequencies for the whole image (histogram). This histogram showed that the data could be divided into two parts (categories) from the middle of this histogram. The first part was between (8-128) DN values. This represented the dark pixels and the second part was between (131-244) DN values which represented the light pixels in the image. Both parts of the histogram have been examined as a limit (minimum-maximum) for a single threshold process. Two threshold images were produced for this image. The threshold image for the light DN's was the best to use for further processing (Plate 6.6). The choice was made, again because this image showed more major lineaments in the area, specially the lineaments within the rock regions. All these lineaments in this image were thick and needed thinning.

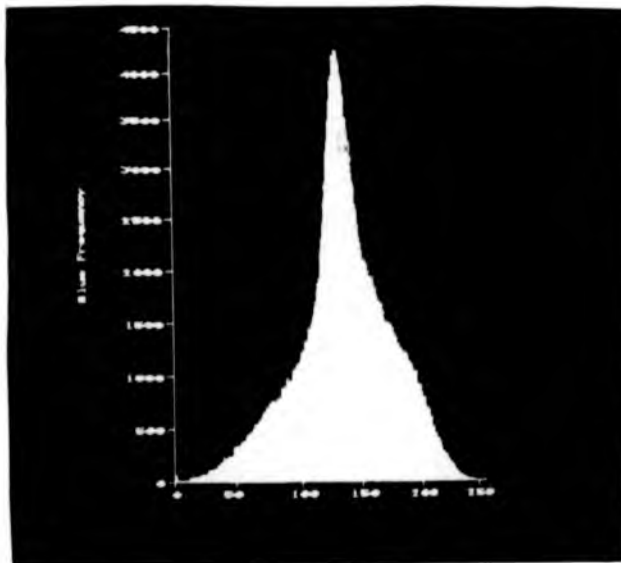
Plate 6.7 shows a segmented image for the second extract by using the ripping membrane/Laserscan segmentation method. This extract, which contains three classes of objects, the alkali granite, the Hadn Formation and gabbro, and the alluvial deposit as the background. All the boundaries have been detected, except the boundary between the gabbro, and the alkali granite.

(a)



0 kms 5

(b)

**PLATE 6.5**

(a) Preprocessed image using the rolling ball technique for the second (TM) extract.

(b) Histogram to show the distribution of the DN's and their frequencies over the image in plate 6.5(a).



**PLATE 6.6**  
Binary image for the second (TM) extract. This image is a result from a single threshold process for plate 6.5(a).



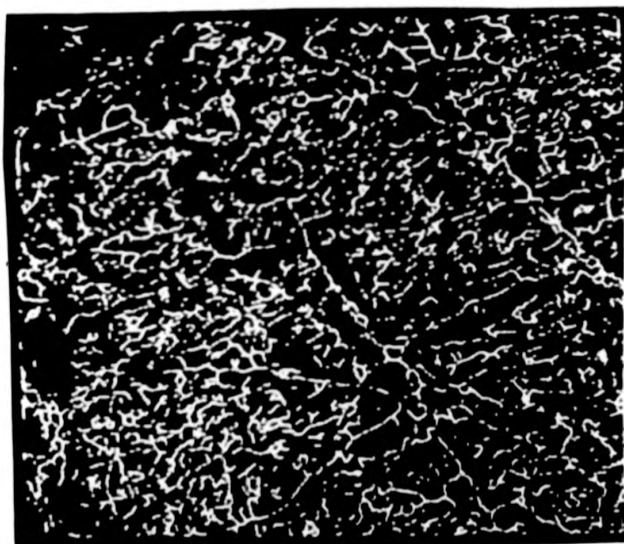
**PLATE 6.7**  
The resultant image of ripping membrane technique/Laserscan image segmentation method for the second (TM) extract. All the small labelled regions were eliminated.

This may be due to the spectral similarity between the gabbro and the alkali granite. The gabbro rock formed very small scattered eroded hills, and doesn't have a reasonable number of lineaments for analysis, therefore it was decided to accept its inclusion with the alkali granite as the same region. There has been no editing of boundaries except the elimination of the small regions (less than 200 pixels). Figure (6.6) shows the visually traced rock boundaries (hand segmentation) for the same area, based on TM false colour composites of bands 7, 5 and 4 in red, green and blue respectively, and the geologic maps.

The ROSE program has been applied to the thresholded (binary images) and the segmented images. Then a lineament map was produced (Plate 6.8) as well as a table showing the lineaments' azimuth angle and their frequencies for each region.

Figure (6.7) shows the visually traced lineaments from the same input images, only the clear lineaments (Section 4.2) have been traced with no restriction to the length.

Three rose diagrams have been plotted for this extract, one for the lineaments extracted from Hadn Formation region using the automatic method (Figure 6.8), in order to find out if the automatic method picks up only specific direction in this rock and compare this diagram with the alkali granite rose diagram (Figure 6.4b). The automatic method did not reveal any difference in the lineament azimuth angles between the alkali



0 kms 5

**PLATE 6.8**  
Lineament map produced by the automatic method for the second (TM) extract.

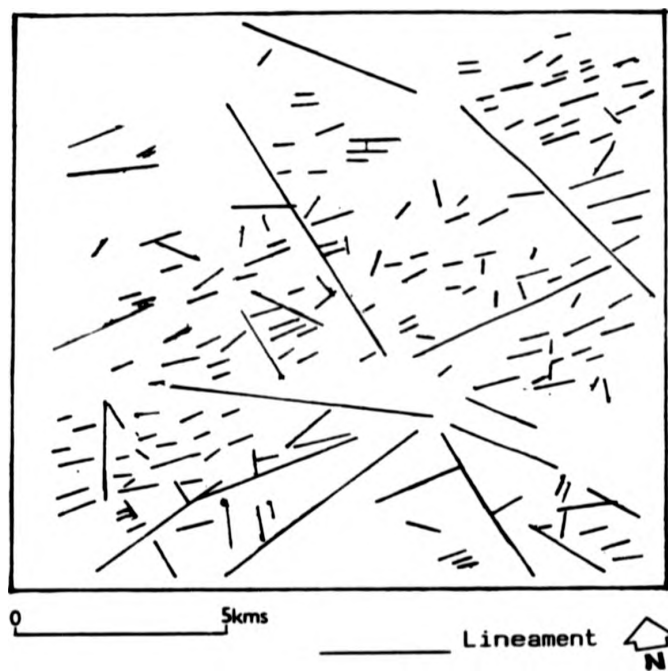


**FIGURE 6.7**  
Lineament map drawn from Plate 6.5a by visually tracing method for the second (TM) extract.

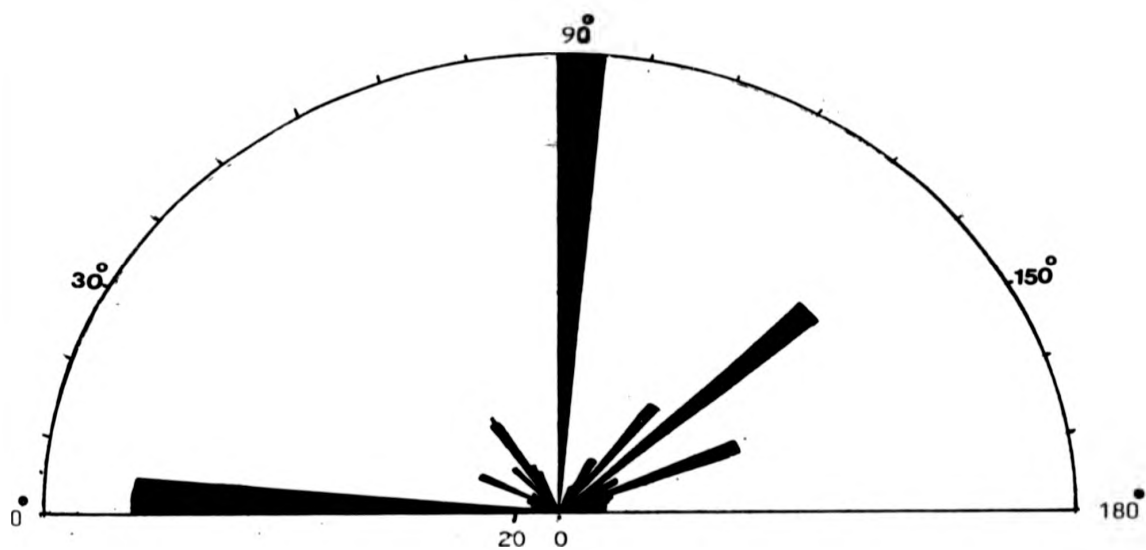


FIGURE 6.8 Rose diagram of Azimuthal frequency distribution of the lineaments (extracted by the automatic method) in the Hadn Formation within the second (TM) extract (Plate 6.5a).

granite and Hadn Formation and both rose diagrams showed the same major trends. Two rose diagrams have been plotted which combine all the rock types in the second TM extract; one for the automatic method lineaments and one for the visually traced lineaments (Figure 6.9).

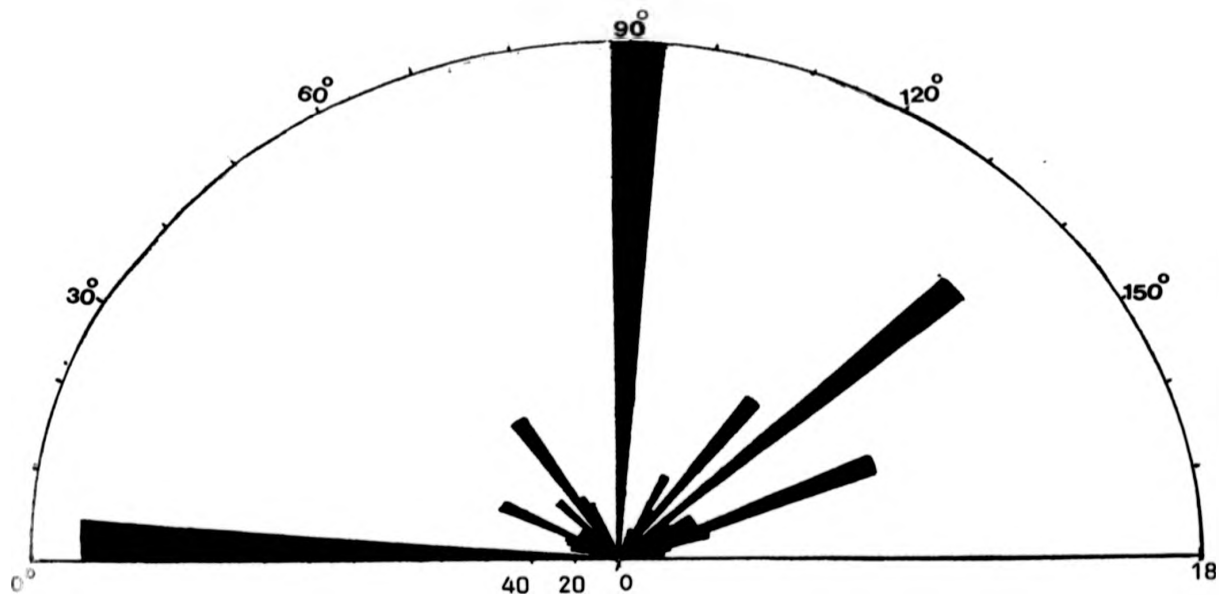
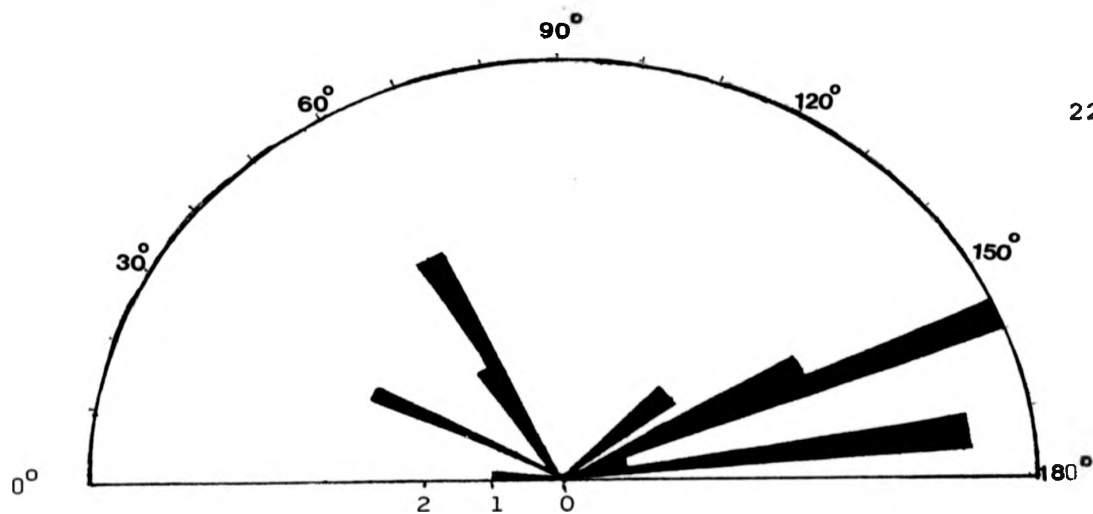
Figure (6.9a) shows the rose diagram for the for all visually detected lineaments from the second (TM) extract image, the major trend is in the direction ( $155^{\circ}$ - $160^{\circ}$ ) in the image which is equal to ( $N74^{\circ}$ - $79^{\circ}$ E) in respect of the true north.

Figure (6.9b) shows the rose diagram for the automatic extracted lineaments from the second extract image. By ignoring again both directions ( $0^{\circ}$ - $5^{\circ}$ ) and ( $90^{\circ}$ - $95^{\circ}$ ) from the lineament analysis the major trend is seen to be ( $135^{\circ}$ - $146^{\circ}$ ) in the image which is equal to ( $N54^{\circ}$ - $59^{\circ}$ E) in respect of the true north.

The second major trend is in the direction ( $155^{\circ}$ - $160^{\circ}$ ) which is equal to ( $N74^{\circ}$ - $79^{\circ}$ E) in respect to the true north and this was the major trend in the visually traced lineament (figure 6.9a) for this extract. Again the automatic method found out the overall major trend in this area which is ENE-WSW as the visually traced lineament but at a different angle.

**SPOT extract:**

This extract is located in part of the Hadn Formation (See Appendix 1 for location of this extract in the study area).



**FIGURE 6.9**  
 Rome diagram of azimuthal frequency distribution of the lineaments  
 in the second TM extract. (a) the lineament visually traced method,  
 (b) lineament extracted by the automatic method (from Plate 6.5a).

(Plate 6.9a) shows the result of applying the rolling ball technique to the SPOT panchromatic mode (PLA) (small range 5).

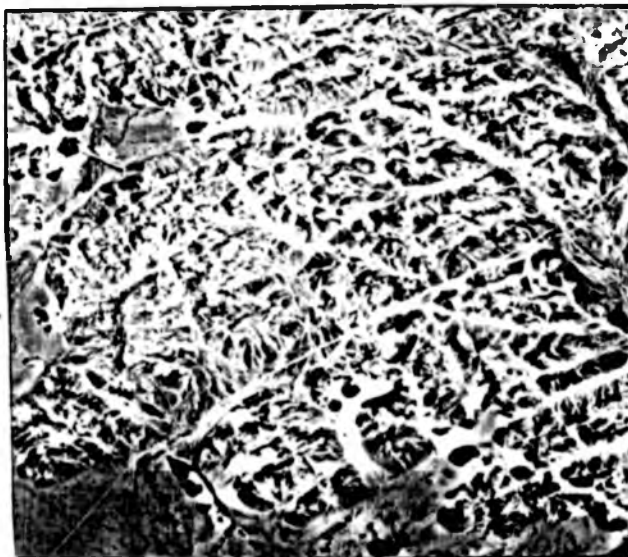
Plate (6.9b) shows the distribution of the DN's and their frequencies for the whole image histogram. This histogram showed that the data can be divided into two parts (categories) from the middle of this histogram, representing the black DN's pixels (62-128) and DN's of light pixels (131-177). Both parts have been used as a limit for the threshold process, thus two threshold images have been produced and used as input images for the ROSE program. The white pixel limit produced the best result. (Plate 6.10). The SPOT image has not been segmented because the corresponding multispectral imagery was not available. Figure (6.10) shows the visually traced lineament derived from the SPOT rolling ball enhanced image. Plate (6.11) shows the lineament extracted by the automatic method for the SPOT data extract.

**Conclusion:**

By observing the visually traced lineaments map from the same input image (rolling ball technique image) and the extracted automatic lineament map for the two TM extract images and one SPOT image. It was concluded that:-

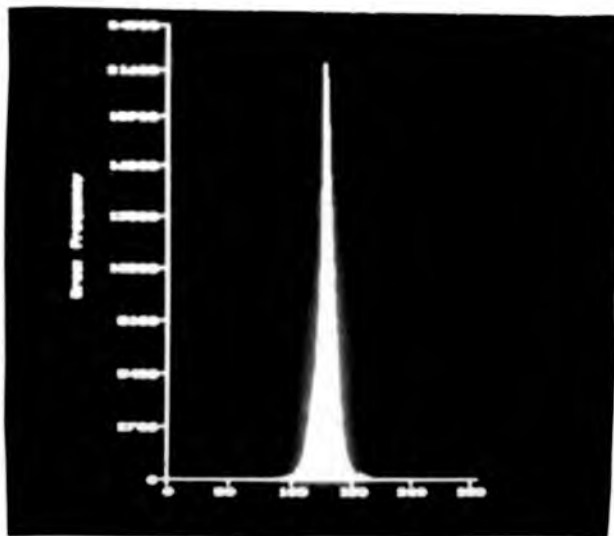
1. The automatic method has extracted most of the visually traced lineaments.
2. The automatic method produced more clearer lineaments in the binary image (threshold image), while the thinning process divided the lineaments into small segments (non-continuous lines). This is due to the lineament intersection. The pixels within the intersection were connected

(a)

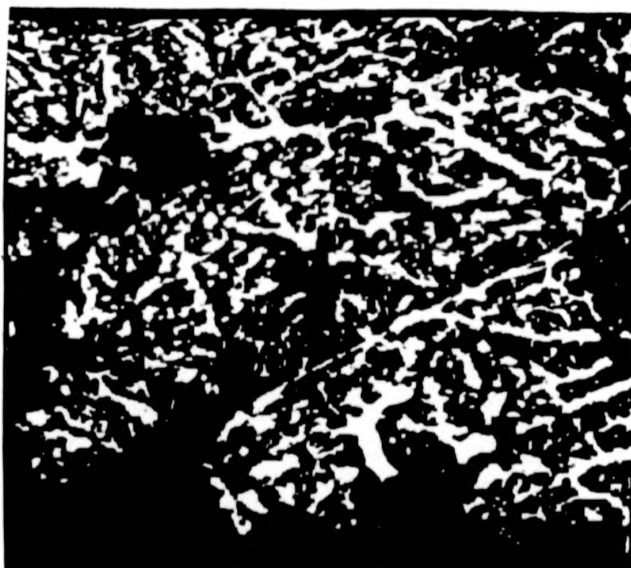


0 km 1

(b)

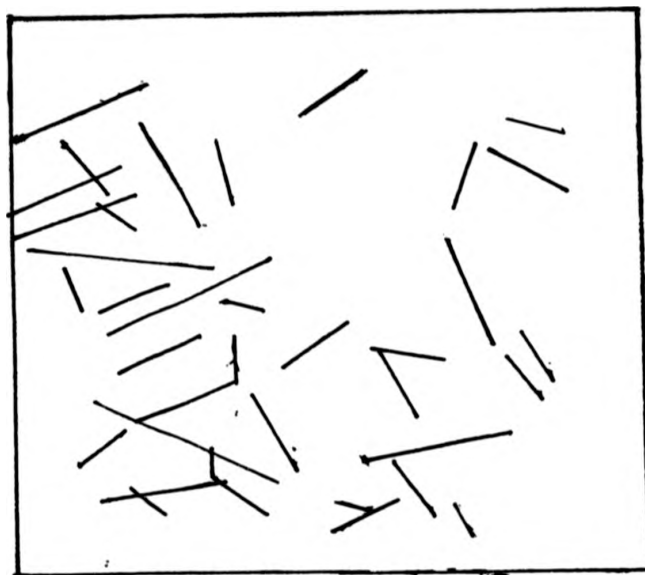
**PLATE 6.9**

- (a) Preprocessed image using the rolling ball technique for the SPOT extract.
- (b) Histogram to show the distribution of the DN's and their frequencies over the image in plate 6.9(a).



0 km 1

**PLATE 6.10**  
Binary image for the SPOT extract. This image is a result of single threshold process for plate 6.9(a).



0 km 1

**FIGURE 6.10**  
Visually traced lineaments map from SPOT extract (Plate 6.9a).

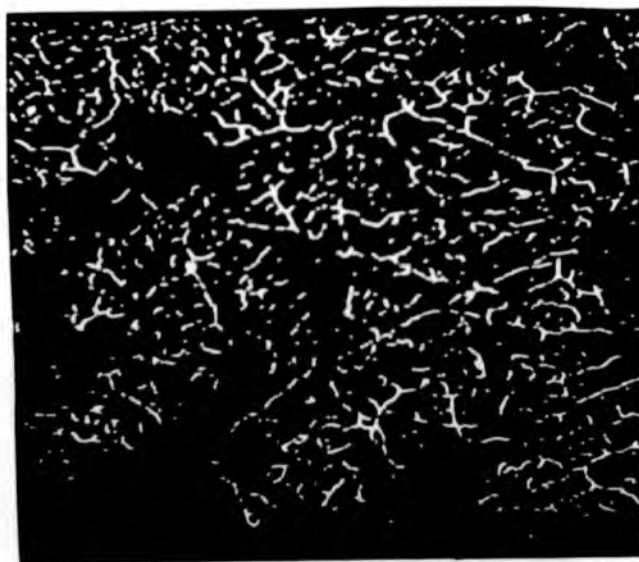


**PLATE 6.11**  
Lineament map produced by the automatic method from SPOT image.

to more than two oriented pixels and therefore are 'ambiguous'. This problem is well presented in the alkali granite rock because it has more than two lineament trends.

3. Between 75-85 percent of the thinned extracted lines or segments can be easily related to lineaments or edges in the input image or to the original image.
4. The SPOT image has produced clearer lineaments in the same area than the TM data. This means that the resolution plays a significant role in detecting or extracting the linear features. Because the SPOT data was collected in the summer season, a very small number is expected from this image. Thus, if the winter season data were available, even more clearer lineaments could be expected.

## 6.5 DISCUSSION

By examining the automatic contextual techniques for lineament extraction, it has been found that most of the mapped (Figure 4.2) and the visually traced lineaments were extracted.

There are some points that have been observed during the interpretation, and in the field. These are:-

1. The alkali granite (ag) has intruded the Hadn Formation (hu), so there are large, eroded spots of the Hadn Formation within the alkali granite areas. This was observed in the lineally contrast stretched colour composite images (TM band 7, 4 and 2 and 7, 5 and 4 in red, green and blue respectively) for the two extract areas and this is

very clear in the field (Plate 6.12). This may have created an error, but not a major error, during the thresholding and segmentation processing.

2. Both selected extract areas are cut by an extensive network of lineaments, and some of the drainage streams run through these lineaments, and are filled by very big boulders of different rocks. These were very noticeable at the intersections of the lineaments. This might cause an error during the threshold, but not a major one.
3. During the thinning process it was not an easy task for the computer to decide in which direction to thin the lines at the intersection point. This caused discontinuities in the extracted lines. Therefore, the major long lineaments were not extracted as continuous lines but as discontinuous lines, while the short lineaments can be seen clearly in the final lineament image.
4. The man made features, like roads, were not a major problem because they were very few and easily recognised and ignored.
5. This method provided interesting results although it is clear that the automatic method has many drawbacks and needs the active intervention of the analyst who can use his knowledge or experience.
6. It was not possible to find a dominant direction (as megatexture) of the lineaments in each individual rock type using the automatic method from the TM data, in such



**PLATE 6.12**  
Showing one of the Hadn Formation (hu) spot within the alkali  
granite (ag) area.

areas, but it might help in another area which has no more than one lineament trend in each individual rock type.

7. It is difficult to transfer all the visual interpretation by experienced observers into mathematical /machine language, so as to be suitable for machine processing. But, by comparing the final results of the automatic, visual methods and the geologic map, there are no big difference (15 - 25%) and the azimuth angle difference is  $10^{\circ} - 15^{\circ}$ .
8. This method has shown better results in using SPOT panchromatic mode (10 meter) compared with TM band 5 (30 meter). This means the resolution does play a role in such method, and therefore the SPOT multispectral scanner (MLA) mode might show better results.

#### 6.6 SUMMARY

A new automatic line and lineament features extraction method was examined in this chapter. This method contained several novel features. First, there was an attempt to create a relationship between image segmentation and the linear feature extraction, in order to find out the megatexture. Second, was the use of the rolling ball technique as a preprocessing technique. 75-85% of the extracted lineament can be easily related to lineament or edges in the original image.

**CHAPTER SEVEN**  
**THE USE OF SPECTRAL ENHANCEMENT TECHNIQUES IN**  
**ROCK DISCRIMINATION**

7.1 INTRODUCTION

7.2 BAND COMBINATION AND CONTRAST MANIPULATION

7.3 COLOUR RATIO COMPOSITE

7.4 PRINCIPAL COMPONENT ANALYSIS

7.5 BAND SELECTION OF LANDSAT TM DATA  
FOR ROCK DISCRIMINATION

7.6 IMAGE INTERPRETATION

7.7 DISCUSSION

7.8 SUMMARY

## 7.1 INTRODUCTION

Any single band of digital remote sensing data is a representation of how the electromagnetic radiation energy reflected by the surface is distributed in two spatial dimensions. In order to distinguish between different rock types, the information provided by spectral reflectance (Section 1.4) can be of importance. However, the electromagnetic response recorded over any rock is a function of several factors; these are the state weathering, composition of rock, moisture content, soil and vegetation (Gupta, 1991). Therefore, spectral enhancement followed by visual interpretation is generally preferred for rock discrimination studies. Several image processing techniques using spectral data (colour ratio composite, principal component and decorrelation stretch) usually used for rock discrimination purposes, are discussed. These techniques were applied to three selected test sites of the study area (TM data), and their products have been evaluated in terms of their photo-characteristics, grey level (tone) or colour enhancement, and whether the images could be interpreted and allowed the identification of lithological units. This was one of the aims of this study.

There are a few studies concerned with the use of satellite data for rock discrimination using TM or ATM data for the area of the Arabian Shield. These include Loughlin and Tawfiq, 1985; Bird et al., 1985; Al-sari, 1989; Davis and Berlin, 1989, and Qari, 1990. However, there is still a need to investigate the Arabian Shield using remote sensing techniques.

## 7.2 BAND COMBINATION AND CONTRAST MANIPULATION

In order to enhance imagery, two simple contrast manipulations are frequently used; (a) contrast stretching and, (b) histogram equalisation. These two techniques are used for rock discrimination purposes and are applied either on a single band or band combination to produce enhanced false colour composite image. Contrast stretching is designed to improve the contrast between features of interest in digital images, such as rock units. It is used to expand the data to fill the digital number (DN) range from 0 to 255 or black to white. The redistribution can be linear (uniform expansion) or non-linear (non-uniform expansion).

In the histogram equalisation, each histogram class (0 to 255) in the display image must contain approximately the same number of pixel values (DN) and the histogram of these displayed values will then be almost uniform or smooth in shape (Mather, 1987). If this is done, the DN in the image and the information content of the image will be increased and it may be easier to interpret the image.

Unfortunately, each image has its own uniqueness. Thus, a contrast enhancement which produces a good result for a given image may not necessarily be good for another image, and there is no universal acceptable method.

The contrast stretched band combinations (false colour composite) are heavily used in rock discrimination studies.

### 7.3 COLOUR RATIO COMPOSITE

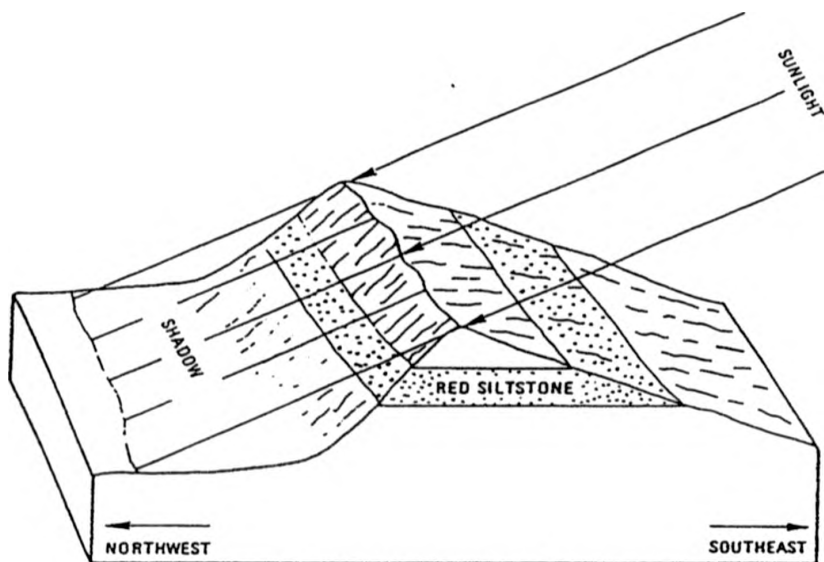
Ratioing is an extremely useful procedure for enhancing features within an image. A band ratio is the ratio of one band to another and is prepared by dividing the DN of a pixel in one band by that of the same pixel in another band (Drury 1987), according to the equation:-

$$DN_{new} = M \frac{(DN_1 \pm S_1)}{(DN_2 \pm S_2)} + N$$

Where  $DN_1$  and  $DN_2$  are the DN (digital number) values in first and second input images,  $S_1$  and  $S_2$  are the factors which take care of path radiance present in the two input images and M and N are scaling factors for the grey level (Gupta, 1991).

One advantage in using the band ratio technique is to improve the spectral or colour differences while removing first order brightness variations caused by topography (i.e. sunlight or shadowed stripes), (Figure 7.1). Therefore, materials in an image having the same spectral reflectance characteristics will appear as the same colour in a colour ratio composite (CRC), regardless of brightness differences in the original image caused by differing surface aspects and slopes.

The disadvantage of the ratio image is the suppression of differences in albedo; materials that have similar relative



ILLUMINATION	SILTSTONE REFLECTANCE		
	TM BAND 3	TM BAND 1	RATIO 3/1
Sunlight	94	42	2.24
Shadow	76	34	2.23

FIGURE 7.1 Suppression of illumination differences on a ratio image (From: Sabins, 1987)

reflectance, but different average albedo, may be indistinguishable in ratio images (Sabins 1987).

Band ratioing commonly enhances spatial radiance variations and generally is more informative than three colour composite (Crippen, 1988). Figure (7.2) shows spectral curves of two objects A and B;  $\lambda_1$  and  $\lambda_2$  being the two sensor spectral channels (bands). The objects A and B have overlapping spectral responses in both bands however, if the ratio of the two bands is taken, the spectral slopes would be given by  $A_1 - A_2$  and  $B_1 - B_2$  lines which make discrimination between the objects A and B possible. In the band ratio images, the white and black extremes of the grey level scale represent the greatest difference in reflectance between the input spectral bands. For example, the darkest DN's value are areas where denominator of the ratio is greater than the numerator and vice versa. If the numerator and denominator are the same, there is no difference between the two spectral bands (Sabins, 1987).

Unfortunately preprocessing for noise removal is necessary, because ratioing tends to enhance noise patterns. Ratio images can be cleaned up using a moving 3 x 3 median filter and this removes much of the speckle and residual striping (Drury, 1987). In addition, the atmospheric effects (Section 2.6.2) (haze component) must be removed or corrected before ratioing (Davis, et al., 1987; Drury, 1987; Davis and Berlin, 1989). If the atmospheric scattering component is present, ratioing does not remove it, because the unequal effects of atmospheric scattering

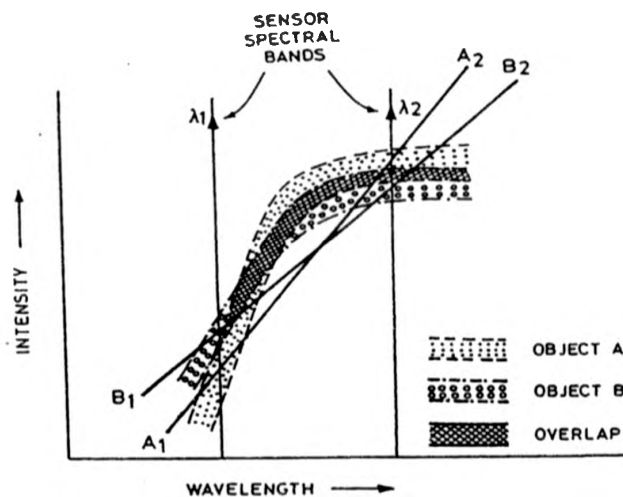


FIGURE 7.2 shows spectral curves of two objects (A) and (B)  $\lambda_1$  and  $\lambda_2$  are being the two sensor spectral channels. The objects A and B have overlapping spectral responses in both channels,  $\lambda_1$  and  $\lambda_2$ , and no single channel is able to give unique results. However, if the ratio of the two channels is taken, the spectral slopes would be given by  $A_1 - A_2$  and  $B_1 - B_2$  lines, which makes discrimination between the objects A and B possible. (From: Gupta 1991).

are not cancelled by the band division. Table 7.1 shows some of the important ratios commonly used in discrimination of surface types.

**TABLE NO. 7.1**  
**Showing the common ratios used in discrimination**  
**of surface types (From Drury and Hunt, 1989)**

NUMERATOR	DENOMINATOR	APPLICATION
7	5	Argillic versus non argillic
3	4	Rocks versus vegetation
5	1	Fe <sup>2+</sup> Fe <sup>3+</sup> free
5	4	Argillic versus Fe <sup>2+</sup>
4	7	Argillic versus Fe <sup>3+</sup>
4	2	Fe <sup>2+</sup> versus non Fe <sup>2+</sup>

The ability to distinguish between different surface materials can be significantly increased by selectively combining three black and white ratio image sets into a false colour ratio composite (band ratio combinations). The improvement in discrimination occurs for two primary reasons:-

1. When three different ratio images are combined, the total amount of information displayed must be greater than if just three bands are used.
2. The wide variety of colours created provide a wider range of visual discriminations (Blodget et al., 1978).

Colour ratio composites have been used frequently in rock

discrimination in arid and semi arid areas by many authors, (e.g. Loughlin and Tawfiq, 1985; Kruse ,1986; Kepper, et al., 1986; Sabins, 1987; Kaufmann, 1988, and Davis and Berlin, 1989). Ratioing has been used in mapping hydrothermal alteration by many authors (e.g. Magee et al., 1986).

#### **7.4 PRINCIPAL COMPONENT ANALYSIS**

Multispectral remote sensing sensors provide data in the form of several spectral images of the observed ground features. Each band represents the spatial distribution of the reflected light, of frequency lying in the corresponding spectral band. Rather high correlation can be expected between the different spectral images (adjacent bands) of the same object. The actual degree of correlation depends on the physical nature of the surface feature and the widths of the spectral bands. The presence of correlations between the bands implies that there is redundancy in the data, in other words, some information is being repeated. The principal component analysis, also called principal component transformation or Karhunen-Loeve transformation (PC) is a unique and powerful mathematical transformation, based on reducing the dimensionality of multispectral image data. It is based on, either the scene covariance or correlation matrix, and produces new variables, known as components or axes, that are linear combinations of the original bands, and where each component contains data uncorrelated with the other components (Canas and Barnett, 1985).

Normally we should expect that the first, second and third principal component (PC) images would contain more information than any three of the raw channels (bands) of data. The first principal component (axis) has the largest spread of data, usually around 90% of image variance (Rothery, 1987). The PC analysis increases the overall separability between spectral classes and reduces dimensionality and therefore is very useful in image classification (Gupta, 1991). A colour composite generated from the three leading PC's might be preferable, therefore to a conventionally generated colour image.

Principal components have been widely used in remote sensing image analysis especially for discriminating between rock types, (e.g. Blodget et al., 1984; Rothery, 1985; Drury, 1986; Greenbaum, 1987, and Davis and Berlin, 1989).

One disadvantage of using PC's is that the colours in the PC's images cannot be related simply to the surface spectral response. To some extent, this can be overcome by applying the decorrelation stretch, which is a modification of PC.

Gupta, (1991) has summarised the steps in the decorrelation stretch process as follows:- (1) a principal component analysis, (2) followed by a contrast equalisation by Gaussian stretch and, (3) a co-ordinate transformation that is the inverse of the principal component rotation.

Decorrelation stretch (DCS) is used in geological application. Rothery, (1987a, 1987b) has demonstrated this transformation in an arid area (Oman) using TM bands 7, 5 and 4 for rock discrimination. He found that the result improved the discrimination. In this study, these two techniques have been used in order to generate a PC's and DCS images to improve the discrimination between rock types in the selected test sites images of the study area.

#### 7.5 BAND SELECTION OF LANDSAT TM DATA FOR ROCK DISCRIMINATION

The Landsat MSS sensor is restricted to four bands in the region  $0.5 - 1.1\mu\text{m}$  and it has limited use for discrimination between rock types, (Podwysocki et al., 1983; Condit and Chavez, 1979; Blodget and Brown, 1983; Rothery, 1985; Belliss et al., 1985, and Berhe and Rothery, 1986).

The infrared channels recorded by the Landsat TM make this instrument (sensor) more suitable than the MSS because it has higher spectral and spatial resolutions. Figure (7.3) shows reflectance spectra for selected minerals and indicates the positions where significant absorption features may occur in relation to the spectral bands detected by MSS and TM systems.

It is clear from Table (2.1) and Figure (7.3) that the first four bands of TM coincide with the absorption of iron oxides. The most common strongest absorption band for  $\text{Fe}^{+2}$  is near TM band 4 ( $1.0\mu\text{m} - 1.1\mu\text{m}$ ) from electronic field transitions of  $\text{Fe}^{+2}$

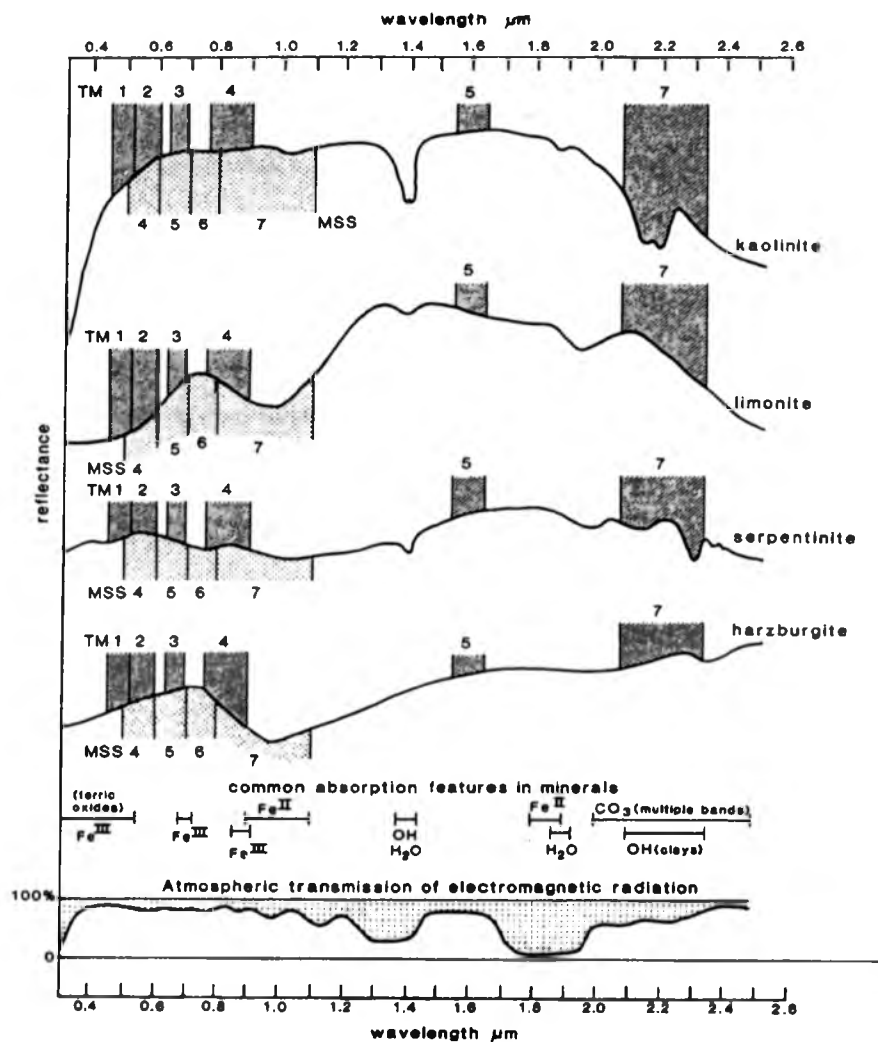


FIGURE 7.3

Reflectance spectra of rock and mineral samples related to Landsat MSS TM spectral bands, the wavelengths of common absorption features and atmospheric transmission. Spectral features due to ferrous iron generally become progressively weaker in mafic, intermediate and acidic rocks as ferro-magnesian content decreases. Thermal band is beyond the range of this diagram (From : Rothery, 1987).

(Hunt and Salisbury 1970).  $\text{Fe}^{+2}$  produces a strong absorption at about  $0.4\mu\text{m}$  (near TM band 1 wavelength) from intervalence charge transfer between  $\text{Fe}^{+2}$  and  $\text{O}^{-2}$ , and weaker absorptions about  $0.45\mu\text{m}$ ,  $0.49\mu\text{m}$  (both within TM band 1 wavelength),  $0.7\mu\text{m}$  (near TM band 3 wavelength), and  $0.87\mu\text{m}$  (within TM band 4 wavelength) from electronic transitions (Hunt and Salisbury, 1970 and Goetz, 1989). The TM band 5 ( $1.55 - 1.75\mu\text{m}$ ) and band 7 ( $2.08 - 2.35\mu\text{m}$ ) are very useful in rock discrimination because they discriminate between  $\text{OH}^-$  and  $\text{CO}_3^{2-}$  bearing minerals according to the rapidly decreasing reflectance between  $1.6 - 2.5\mu\text{m}$  (Goetz, 1989; Goetz et al., 1983). (See Section 1.4 for more detail).

A considerable effort has been directed towards using the TM and Airborne Thematic Mapper (ATM) in rock discrimination and mapping in arid or semi-arid areas, (e.g. Loughlin and Tawfiq, 1983; Hunt et al., 1986; Magee et al., 1986; Sultan et al., 1986a, 1986b; Kruse, 1986; Davis et al., 1987; Rothery, 1987; Tibaldi and Ferrar, 1988; Kaufmann, 1988; Crosta and Moore, 1989; Davis and Berlin, 1989; Greenbaum, 1987; Drury and Hunt, 1989; Al-Sari, 1989; Davis and Berlin, 1989; Chavez and Kwarteng, 1989; Qari, 1990; Loughlin, 1991, and Patel and Rampal, 1992).

In selecting the individual bands, and band combination for rock discrimination, the author was faced with the problem of deciding which bands contain the most geological information. However, from the literature, it has been found that the colour

composite TM band selection can be based on one or more of the following methods:-

1. Selection based on the interpreter/analyst's own knowledge about the study area, rock types, so he/she displays as much as possible of three band colour composite (FCC), and colour ratio composite (CRC).
2. Selection, by using the combination of TM bands used by previous authors to discriminate between similar rock types, or similar climate. This method cannot be guaranteed to give useful results for different areas with different geology (Crosta and Moore, 1989).
3. Band selection based on using statistical analysis of the six reflecting TM bands to determine which combination of three TM bands or three band ratios provide Optimum Information Content (OIF), (Sheffield, 1985).

The results of this method do not necessarily produce the best images for qualitative interpretation (Crosta and Moore, 1989, and Hunt et al., 1987).

In this study, the author decided to use all three methods for band selection as much as possible to produce the best colour image for rock discrimination. In using the first method it was found to be time consuming considering all the possible three-colour composites and colour ratio composite. It was found that most of the authors used TM bands 7 and 5 in different combinations. In this study the third method of band selection was used by applying a program called OIF which produces the same results

as the Sheffield, (1985) method.

#### 7.6 IMAGE INTERPRETATION

Three different test site areas were chosen to examine the capability of TM data and the image processing technique. Two of these sites are 512 x 512 pixels and one 1024 x 1024 pixels in size. The role of image processing is to reduce the dimensionality or size of the data set, to fit within the dynamic range of the display medium and display it, in such a way that the human eye can extract (from the colour information) the data for lithological discrimination: therefore, four image processing techniques were examined and these included contrast stretch for the three false colour composites, (FCC), colour ratio composite (CRC), principal component (PC) and decorrelation stretch (DCS).

Contrast enhanced single bands were examined prior to subjecting them to a number of band combinations and other processing techniques. From this, it became apparent that some bands provide more geological information than others. The longer wavelength bands, particularly band 5 and 7, individually or combined with other bands, produced images with better contrast between geological units. Table 7.2 shows all the false colour composites FCC's have been examined in this study. Most of the band combinations have been examined by many authors, in general, for rock discrimination in arid or semi-arid areas.

**TABLE NO 7.2**  
**Shows all the false colour composites (FCC) have**  
**been examined in this study**  
**(R = Red, G = Green, B = Blue)**

<b>R</b>	<b>G</b>	<b>B</b>	<b>THE PURPOSE OF DISCRIMINATION</b>	<b>USED BY</b>
7	5	2	Argillic and ferruginous alteration in arid area (Arabian Shield)	Loughlin and Tawfiq 1985, and Bird et al., 1985
7	4	2	Argillic and ferruginous alteration in arid area (Arabian Shield) Metigeneous and metasedimentry in semi-arid area (West Australia)	Loughlin and Tawfiq, 1985 Hunt et al., 1986
7	4	1	Volcanic and sedimentary rock arid area (Nevada desert) Altered basalt in complex igneous rock in arid area (Arabian Shield)	Davis et al., 1987 Davis and Berlin, 1989
7	5	4	General rock discrimination (Oman and West Australia)	Rothery, 1987b and Drury and Hunt, 1989
5	3	1	Metamorphic basement rocks in semi arid area (South East Spain)	Crosta and Moore, 1989
5	4	1	General rock discrimination, altered and unaltered basalt in arid area (Nevada Desert)	Sheffield, 1985, and Davis et al., 1987
4	7	1	General interpretation (Semi Arid area)	Lees et al., 1985
3	2	1	Field investigation for alteration zones in arid area (Arabian Shield) <sup>†</sup>	Loughlin and Twafiq, 1985
5	2	1	Used in this study	
5	4	2		
7	5	3		
7	3	1		

Table 7.3 shows the common single ratio image used in discrimination of surface type. Table 7.4 shows different colour ratio composites (CRC's) which were examined in this study. Some of these CRC's have been applied by many authors in arid and semi-arid areas, covered mainly by different igneous and/or metamorphic rocks. Some of these CRC images showed good discrimination between the rock types.

Table 7.5 shows different TM band combinations (Bands 1-5 and 7) from the Optimum Index Factor (OIF) for all the three test sites. Table 7.6 shows selected rock types from the three test sites and their brightness in specific ratios.

**TABLE NO 7.3**  
**Showing the common single ratios used in**  
**rock discrimination only and their purpose**

BAND RATIO	THE PURPOSE
3/1, 3/2, 7/1	Each of these ratios is effective; for enhancements relate to ferric and ferrous iron
7/4, 5/4, 4/5	There is a linear relation between Fe <sup>+2</sup> connection or iron-oxidation ratios and this ratio
5/7	The hydrothermal alteration may be distinguished using this ratio. The amount of clay alteration on the rock surface is directly related to the intensity of the 2.2 $\mu$ m absorption features in infrared bands.

**TABLE 7.4**  
Shows all the colour ratio composites (CRC)  
have been examined in this study  
R = Red, G = Green, B = Blue

CRC in RGB*	THE PURPOSE OF DISCRIMINATION	USED BY
4/2, 4/7, 5/7	Enhance hydroxylated sheet silicate and iron feature, in weathered rocks. In semi arid area (West Australia)	Drury and Hunt 1989
5/7, 3/1, 2/4	Alteration minerals mapping in arid area (Nevada Desert)	Kruse 1986
5/7, 3/1, 2/4	Distinguish hydrothermal alteration zone in arid area (Arabian Shield)	Loughlin and Tawfiq, 1985
5/7, 4/3, 7/4	Mineral exploration in arid area (Jourdan)	Kaufmann, 1988
5/7, 4/2, 7/3	Discrimination between the mafic rocks in arid area (Nevada Desert)	Kepper et al., 1986
3/1, 5/7, 3/5	Distinguish altered rocks and unaltered rocks in arid area (Nevada Desert)	Sabins, 1987
5/1, 5/7, (5/4x3/4)	Distinguish igneous and metamorphic rocks in arid area (East Egypt in Nubiun Shield)	Sultan et al., 1987
7/5, 5/4, 4/2	Distinguish altered basalt within complex igneous rock in arid area (Arabian Shield)	Davis and Berlin, 1989
3/4, 4/5, 5/7	Distinguish igneous rocks and sedimentary rocks in semi arid area (India)	Patel and Rampal, 1992
7/1, 5/4, 4/1 7/5, 5/4, 7/1 3/1, 4/2, 5/7 5/1, 4/2, 3/1	Used in this study	

**TABLE 7.5**  
**Showing different TM band combinations (Bands 1 - 5 and 7)**  
**from the Optimum Index Factor (OIF) for all three**  
**selected test sites images**

BAND COMBINATION			RANKING
First Test Site	Second Test Site	Third Test Site	
5 - 3 - 1	7 - 5 - 1	7 - 5 - 2	1
7 - 5 - 1	7 - 5 - 3	5 - 3 - 2	2
5 - 4 - 1	5 - 3 - 1	5 - 4 - 2	3
7 - 5 - 3	5 - 4 - 1	5 - 2 - 1	4
5 - 2 - 1	7 - 5 - 4	7 - 3 - 2	5
7 - 3 - 1	5 - 4 - 3	7 - 4 - 2	6
5 - 4 - 3	7 - 5 - 2	4 - 3 - 2	7
7 - 5 - 4	7 - 3 - 1	7 - 2 - 1	8
4 - 3 - 1	5 - 3 - 2	3 - 2 - 1	9
5 - 3 - 2	7 - 4 - 1	4 - 2 - 1	10
7 - 4 - 1	5 - 2 - 1	7 - 5 - 3	11
7 - 5 - 2	5 - 4 - 2	7 - 5 - 4	12
3 - 2 - 1	7 - 4 - 3	5 - 4 - 3	13
5 - 4 - 2	4 - 3 - 1	7 - 5 - 1	14
7 - 2 - 1	7 - 3 - 2	5 - 3 - 1	15
7 - 4 - 3	7 - 2 - 1	7 - 4 - 3	16
4 - 2 - 1	7 - 4 - 2	5 - 4 - 1	17
7 - 3 - 2	4 - 3 - 2	7 - 3 - 1	18
4 - 3 - 2	3 - 2 - 1	7 - 4 - 1	19
7 - 4 - 2	4 - 2 - 1	4 - 3 - 1	20

**TABLE 7.6**  
**Showing selected rock types from the study area and**  
**the brightness in specific band ratios.**  
**(For more description for the rock types,**  
**see Section 1.7.3**  
**D = Dark L = Light M = Moderate**

ROCK TYPE	3/1	3/4	3/5	4/2	4/5	4/7	5/1	5/4	5/7	7/5	7/3
Afna Formation (ha) (Basaltic-andesitic)	D	L	L	D	M	L	D	D	L	M	D
Afna Formation (ha) (Genesis)	D	L	D	D	D	D	M	L	L	D	L
Sedimentary and volcanic member (asv)	D	L	M	M	M	M	M	M	M	L	M
Biotite alkali feld- spar granite (afg)	D	L	L	L	L	L	D	D	L	L	M
Hadn Formation (hu)	M	M	M	M	M	M	M	M	D	L	D
Alkali Granite (ag)	L	L	L	M	L	L	D	D	L	D	M
Kilab monzogranite (mg)	M	M	M	M	M	M	L	M	M	M	M
Banana Formation (bg)	D	L	M	D	D	D	D	L	D	M	M
Granophyre (gph)	M	M	D	M	D	D	M	L	D	L	L
Maa Complex (gd)	M	M	D	M	M	D	L	L	L	M	L
Juwayy Rashib Complex (qdd)	D	M	M	D	M	L	D	L	L	D	L
Cenozoic Basalt (Qtb)	D	L	D	D	D	D	D	L	D	L	L
Jibalah Group (js)	M	M	L	M	L	L	D	D	M	M	D
Sufran Formation (sv)	M	M	L	M	D	D	D	L	D	M	L

**First Test Site: (Wadi ad Duwadimi Area)**

This test site is a 512 x 512 pixels from the southwestern part of the study area. (See the study area map for location in Appendix 1). It contains a variety of volcanic, metavolcanic rocks and granite rocks (Figure 7.4). These include Afna Formation (ha), limestone and marble member (lm), sedimentary and volcanic member (asv), granite (biotite alkali-feldspar granite) (afg) and Cenozoic (olivine) basalt (Qtb). For more detail see Section 1.7.3. All the band selection methods discussed in Section 7.3 were used to select the best band combinations for this site. It was found that none of the individual bands show very clear discrimination between all the rock types in this test site, however bands 1, 3, 5 and 7, relatively, did show more tonal /spectral variations. These four bands were then displayed in different combinations (Table 7.2). Application of OIF program to these TM bands resulted in 20 combinations summarised in Table 7.5, from which it can be seen that band 5 is present in all the first five rankings. The top rank OIF combination were bands 5, 3 and 1 displayed in red, green and blue respectively, but it produced a poor image for interpretation.

The best three TM band ratio images were integrated into one image (ratio colour composite, CRC). This was based on the brightness of rock types in each single ratio image listed in Table 7.6.

All the CRC's in table (7.4), PC's (six bands or three bands

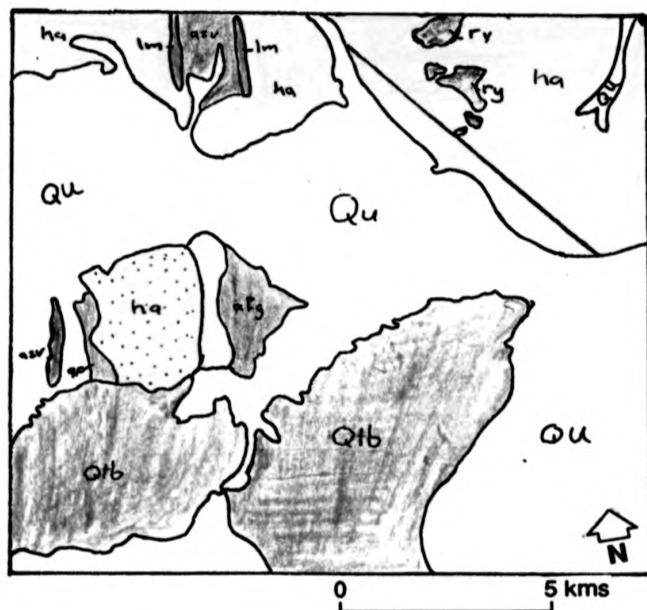
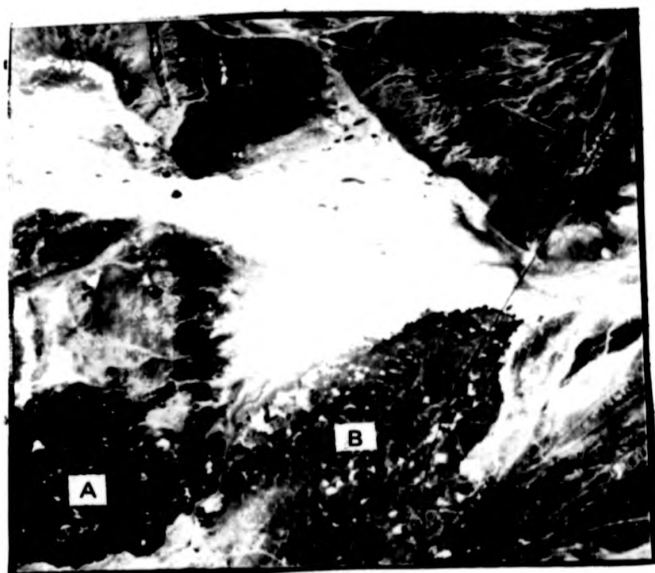


**FIGURE 7.4**

Geologic map for the first test site (Wadi ad Duwadimi area) compiled from O'Neill and Ferris, 1985 and Quick and Doebrich, 1987

4, 5 and 7) and DCS of band 4, 5 and 7 have been examined in order to produce the most colour contrasted images. Unfortunately none of these techniques provided any acceptable images for rock discrimination and interpretation that were any better than FCC of bands 7, 5 and 3 in red, green and blue respectively. (Plate 7.1). Therefore the interpretation for this site was based on Plate 7.1. In this plate, the Cenozoic (olivine) basalt (lava flows) in the southern quarter of this site is very dark blue to blue colour in the image. It is clear that there is some difference in colour brightness between Lava (A) and Lava (B). According to (O'Neill and Ferris, 1985, and Quick Doebrich, 1986), both lavas are composed of dense to vascular olivine basalt with the same age from Harrat Khybar Lava flow. But, during the interpretation and in the field, the author found that these lavas may be different in age and source, for the following reasons:-

1. The colour was different for both fresh surface and weathered surface; lava (A) is brownish in colour and lava (B) is black. Plate 7.2 shows these lavas in the field.
2. The geomorphologic shape: Lava (A) was more condensed still 3 to 4 meters high, while lava (B) was low (1 meter high).
3. Lava (A) was composed of very big boulders while lava (B) was composed of small rounded fragments.
4. As suggested by Fielding (1985), the reflectance variability between dark volcanic rocks (basalt and basaltic

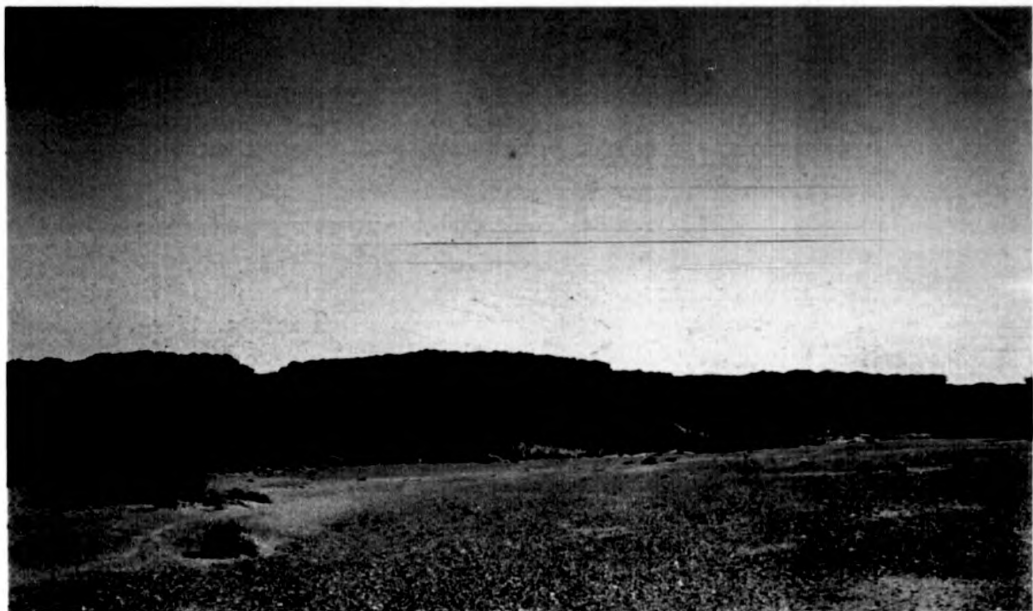


0 kms 5

**PLATE 7.1**

False colour composite of TM bands 7, 5 and 3 in red, green and blue respectively, covering the first test site area (Wadi ad Duwadimi).

(a)



(b)

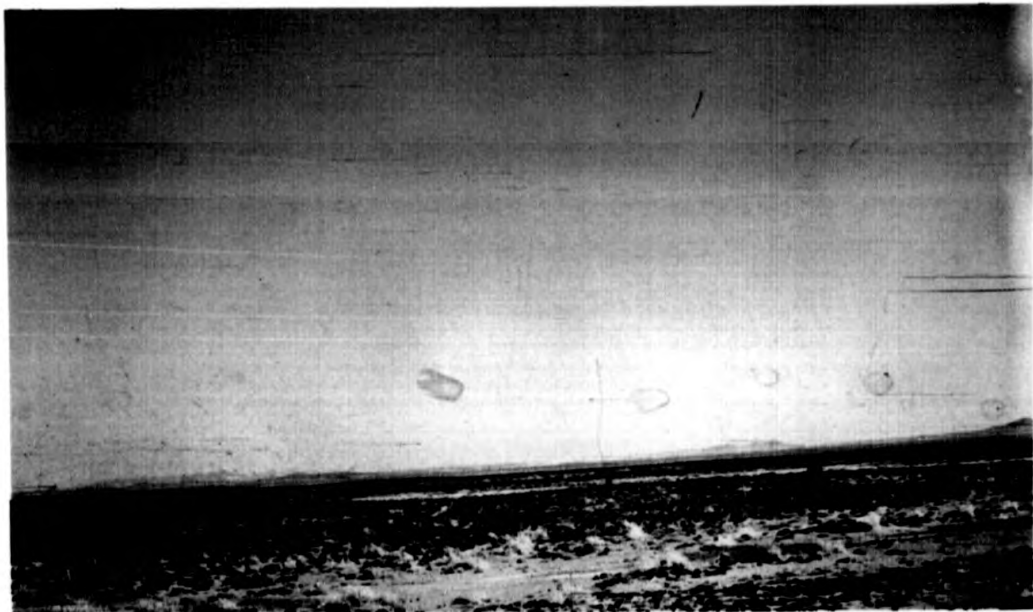


**PLATE 7.2**

The two Cenozoic basalt lavas in ground based views:

(a) lava (A)

(b) lava (B).

andesite) is largely an overall change in albedo, with older units tending to have higher albedo (and consequently higher radiance and the younger units lower radiance). Therefore the relative ages of basalt flows can be distinguished by the spectra and different patterns or texture of the flows (Fielding, 1985 and McBride et al., 1986).

The Afna formation (ha) in this area contains two different rock types; the first, a basalt to andesite rock located in the upper left quarter and central upper part of this site and was a very dark blue. The second rock type was similar, but it had been subjected to medium grade metamorphism, which produced a gneissic feature and more metamorphic hornblende. This was light green to yellowish-green in the images. The second rock has been classified by O'Neill and Ferris (1985) as separate gneiss and migmatite rock in the 1:100,000 map but later Quick and Doebirch (1987) have merged it with Afna Formation in the 1:250,000 map.

Both produced different colours in the FCC. Afna Formation has two members (Section 1.7.2) (Table 1.3). First, the interbedded sedimentary and volcanic rocks member (asv) (brown to dark brown in the image), which was easy to distinguish. The second member, a limestone and marble member (lm), which was white to light blue in the image, and was located in the upper central quarter of the image as a very thin elongated shape. The only rock which was not volcanic in origin was the biotite alkali-feldspar granite (afg) (rose colour in the image). This rock forms highly eroded small hills.

In such areas it has been found that certain obvious limitations occur in using the TM data for discrimination between geologic units mapped on the basis of location or age but are similar in rock composition (eg. basalt lava flow (Lava A) and basalt andesite to rock (ha). It was not easy to distinguish the rhyolite (ry) (very dark blue in the northeast quarter of the image) and the andesite.

**Second Test Site: (Wadi Al Qahad area)**

This test site is a 1024 x 1024 pixels from the southern part of the study area. See the study area map for location in Appendix 1. For detailed lithological interpretation, the image was subdivided into four 512 x 512 subscenes for displays on R-CHIPS at full resolution. It contains twelve different rock types (Figure 7.5). These are metamorphosed basaltic to andesitic volcanic rocks, sedimentary and silicic volcanic rocks, mix of volcanic and sedimentary rock, diorite to quartz diorite, granodiorite, monzogranite, granophyric intrusions, rhyolite, conglomerates, gabbro, olivine basalt, limestone and marble member.

All the proposed methods for TM band selection mentioned in Section 7.5 have been used to select the best band combinations for rock discriminations for this site. It has been found that none of the individual bands showed clear discrimination between all the rock types, however bands 3, 4 and 5 relatively showed more tonal/spectral variations, therefore, these bands have been



**Qp** Playa Lake deposit

**Qal**  
**Qu** Aluvium and undivided  
quaternary deposits

**Qrb** Olivine basalt

**Js** Jibalah Group -  
Conglomerate

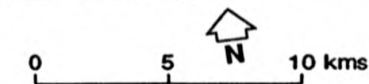
**Z** Zarghat Formation - Mixed  
volcanic & sedimentary rocks

**ha** Afna Formation -  
basaltic to andesitic rocks

**sv** Sufran Formation -  
Silicic volcanic rocks

**bg** Banana Formation -  
Metamorphosed basaltic to  
andesitic volcanic rocks

**gb** Gabbro



**ry** Intrusive rhyolite plugs

**gph** Granophyre

**mg** Kilab monzogranite

**gd** Maa Complex - Granodiorite  
to tonalite

**qdd** Juwayy Raship Complex -  
Diorite to quartz diorite

~ Lithologic contact

--- Fault

— Dikes

— Strike and Dip of Beds

**FIGURE 7.5**

Geologic map for the second test site (Wadi Al Qahad) area (From Quick and Doebrich, 1987)

examined in different combinations as well as the combinations previously used by other authors in Table (7.3).

The application of OIF program to TM bands (excluding the thermal band) resulted in 20 combinations summarised in Table (7.5). In this table, TM bands 3 and 5 are presented in most of the first seven rankings. The top rank of OIF combination of bands 7, 5 and 1, displayed in red, green, blue respectively (linearly contrast stretched) produced a poor FCC images for interpretation. There are two FCC's images, which do discriminate between all the rock types in this area (an eroded area), these are bands 7, 4 and 2 or bands 5, 3 and 1, in red, green and blue respectively but in general, the second combination was the slightly better. The lithological information contained in the three TM band ratio images for the test site have been integrated into one colour ratio composite CRC. This was based on the brightness of rock types in each single ratio image in Table (7.6) as well as the CRC previously used by other authors. (Table 7.4).

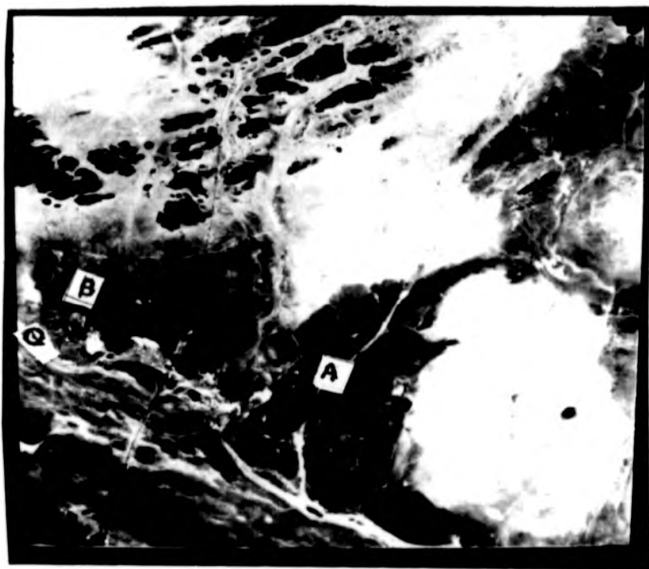
All the CRC, PC's (on six band or three bands 4, 5 and 7) and DCS bands 4, 5 and 7 have been evaluated in order to produce more colourful enhanced images. Unfortunately, none of these techniques provided acceptable images for rock discrimination and interpretation that was better than FCC bands 7, 4 and 2 or 5, 3 and 1, in red, green and blue respectively.

The image interpretation was based on the FCC of bands 5, 3 and 1 in red, green and blue respectively Plate (7.3) because it was the best image. In this plate, three different rock units showed the same a colour (which was blue to light maroon). These rock units are Banana Formation (bg) metamorphised basaltic to andesitic volcanic rock, (labelled by A), the Surfan Formation (Sv), partly metamorphosed silicic volcanic rock, (labelled by B) and the Maa Complex (gd), granodiorite to tonalite, located in the northern quarter of the test site area.

The colour of Zarghat Formation (zu), which composed of a mixture of volcanic and sedimentary rocks, (labelled by Q) is similar to that of the Jibalah Group (js), which is composed of conglomerate, marble and sandstone, and appears blue in the FCC. These rocks are located in the southwest quarter of this site.

The Kilab monzogranite (mg) was distinguishable from the other rock by its very light pink colour, but in the central quarter of the site, where it is in contact, with the Maa Complex (grandiorite), it was not possible to distinguish the boundaries between the two rocks. Juwayy Rashib Complex (diorite to quartz diorite) (qdd) and gabbro (gb) both located in the northeastern corner of the site are coloured a dark blue colour in FCC.

The granophyre (gph) intrusions are scattered throughout this site and they can be distinguished from all the other rock types



0 kms 5

**PLATE 7.3**

False colour composite of TM bands 5, 3 and 1 in red, green and blue respectively for the second test site (wadi Al Qahad) area. A: Banana Formation, B: Sufran Formation, Q: Zargaht Formation.

by their light brown colour in FCC. The biggest unit of this rock was located in the northwestern quarter of the site.

There was only one isolated plug of Cenozoic (olivine) basalt (Qtb) located in the southern quarter of this site and this appeared reddish in colour in the image. This site has a very wide valley, located in the southern quarter, called Wadi Al Qahad Graben (northwest trending). This Graben is caused by the Najd faults system (NFS) (Section 1.7.2) which runs through this area (O'Neill and Ferris, 1985, and Quick and Doebrich, 1987).

In such an area, it was found that limitations occur in using the TM data for discrimination between all the rocks units, especially between the weathered volcanic rock surfaces. The visible infrared wavelengths penetrates only 50 $\mu$ m below a rock's surface (desert varnish), (Buckingham and Sommer 1983), and the weathered surface may be the same in chemical composition irrespective of the underlying chemical composition. Thus it is such cases that textural information may help in discriminating between rock types (Chapter 8).

#### **Third Test Site: (Jabal Muwaysil area)**

This test site is a 512 x 512 pixels from northeastern part of the study area. See the study area map for this location in Appendix 1. This contains four different rock types (Figure 7.6) - diorite and quartz diorite (qdd), Hadn Formation (hu), biotite alkali feldspar granite (afg) and alkali granite (ag). For more

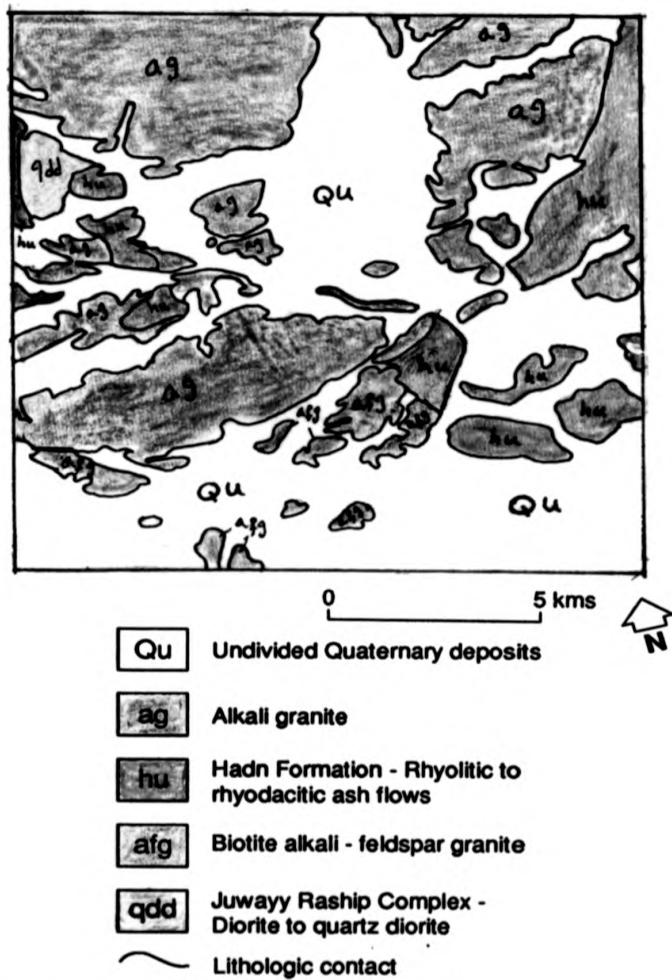


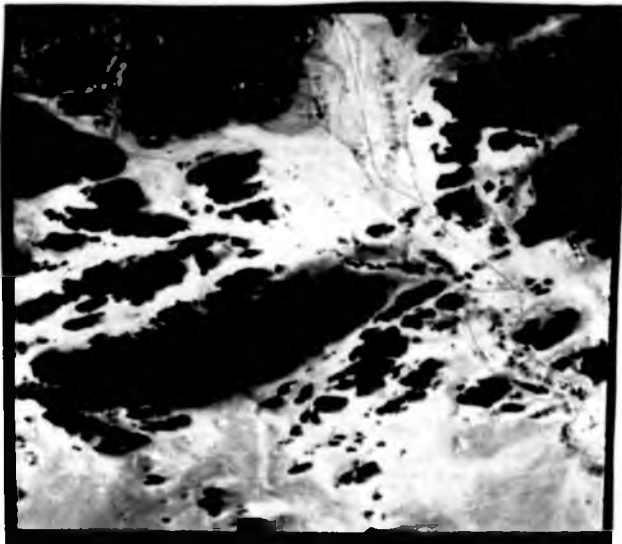
**FIGURE 7.6**  
 Geologic map for the third test site (Jabal Muwaysil) area - compiled from Leo, 1984 and Quick and Doebrich, 1987

geologic description, see Section 1.7.3.

The alkali granite and Hadn Formation are distributed in the area of the test site. The diorite was located in the northwestern quarter of the site. (Figure 7.6).

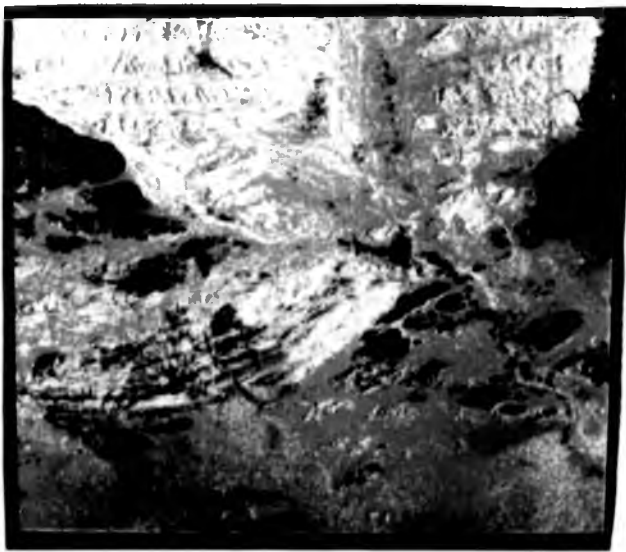
All the proposed band selection methods (Section 7.5) were used to select the best band combinations for this site. It was found that none of the individual bands showed clear discrimination between all the rock types, however, bands 5 and 7 showed the most tonal (spectral) variations. Application of OIF program to these TM bands (excluding the thermal band) resulted in 20 combinations, summarised in Table (7.5). In this table, TM band 7 and 5 are present in most of the first six rankings. The top rank OIF combination with bands 7, 5 and 2, lineally contrast stretched, displayed in red, green and blue respectively and produced an acceptable FCC images for interpretation but the best was FCC of bands 7, 4 and 1 in red, green and blue respectively. (Plate 7.4a). CRC's, PC's (six bands excluding the thermal band) and DCS bands 4, 5 and 7, have been applied to the same data in order to produce colourful and enhanced images. Only one CRC image enabled more discrimination in this site (7/5, 5/4, and 4/1 or 4/2) (Plate 7.4b) in red, green and blue respectively. This combination was used by Davis and Berlin, (1989), to discriminate between the altered basalt and complex igneous rock. The other techniques did not produce any better images.

(a)



0 kms 5

(b)

**PLATE 7.4**

Digitally enhanced TM images for the third test site (Jabal Muwaysil) area.

- (a) False colour composite of bands 7, 4 and 2 in red green and blue respectively.  
(b) Colour ratio composite of 7/5 , 5/4 and 4/2 in red green and blue respectively.

In Plate (7.4a,b) the alkali granite (ag) (brick red in FCC image and yellowish in CRC image) was recognisable in both images. But in the southwestern quarter of this site, the colours are mixed (pinkish and yellowish). In the field it was found that these pinkish areas belonged to the Hadn Formation (hu). (Plate 6.12). This can be explained, that the granite intrudes the Hadn Formation. The Hadn Formation, composed of rhyolitic to rhyolitic ash flow tuff appears red. In the eastern quarter of this site, the biotite alkali-feldspar granite (afg) appears light red. The Juwayy Rashib Complex (qdd) which is composed of diorite to quartz diorite, located in the north-western quarter of this site, appears dark blue in FCC and greenish in CRC images.

The sediment in the wadis consists primarily of mechanically weathered rock fragments, that have been transported a short distance. The vegetation shows a green colour in the FCC and blue in the CRC.

#### 7.7 DISCUSSION

The spectral image enhancement techniques (contrast manipulation) for the false colour composite (FCC), colour ratio composite (CRC), principal component (PC) and decorrelation stretched (DCS), are far from perfect and none can be considered superior to the others in discrimination between all the rock types in the selected test sites. The reason for the limitation can be attributed to one or more of the following reasons:-

1. Some rock types or group of rocks have been classified on the basis of age or location, although their composition is similar (eg. Zarghat Formation and Jibalah Group in the study area).
2. Discrimination between different rock types is reduced by the presence of a common desert varnish (Section 1.4).
3. The data cannot discriminate between two rock types that differ in the percentage of certain minerals (Crystals size). Hunt and Salisbury, (1970) have found that most of the minerals, which are usually used to classify the silicic rocks, do not produce distinct absorption features in visible, and near infrared wavelengths, and hence the reflectance can remain invariant despite gross chemical and physical differences.

In this work it was found that the band combination of 7, 4 and 2, 7, 5 and 3, and 5, 3 and 1 in red, green and blue respectively, provide, in general, better results than the principal component either six band or three band only, colour ratio composite or decorrelation stretched (three band) images. In one test site the colour ratio composite of 7/5, 5/4 and 4/1 in red, green and blue respectively provided a good discrimination. Thus it can be concluded that colour composites alone may not discriminate between the different rocks. Therefore, if further information can be found in the image data, it may be of use in supplementing the spectral information, derived from processing each pixel in rotation. Texture and, in general,

contextual information, that is the spatial pattern around every pixel, may provide that source of 'extra' information.

#### **7.8 SUMMARY**

False colour composite, colour ratio composite, principal component and decorrelation stretch were discussed in this chapter. The application of these techniques for three selected test sites (two 512 x 512 pixels and one 1024 x 1024 pixels) provided adequate means of distinguishing between some rock types, but failed to provide an acceptable discrimination between others. The selected test site areas were Wadi Ad Duwadimi, Wadi Al Qahad and Jabal Muwaysil.

**CHAPTER EIGHT**  
**THE USE OF TEXTURE ANALYSIS IN**  
**ROCK DISCRIMINATION AND**  
**IMAGE CLASSIFICATION**

8.1 INTRODUCTION

8.2 TEXTURE ANALYSIS

8.2.1 FOURIER TRANSFORM

8.2.2 FIRST ORDER TEXTURE MEASURES

8.2.3 SECOND ORDER TEXTURE MEASURES

8.3 SPATIAL GREY-LEVEL DEPENDENCY MATRIX

8.4 THE USE OF TEXTURE ANALYSIS IN GEOLOGICAL  
STUDIES

8.5 RESULT AND DISCUSSION

8.6 SUMMARY

### 8.1 INTRODUCTION

Texture is one of the characteristics used in the recognition of objects, or regions of interest, in an image, whether the image is an air photograph or a satellite image (Haralick et al., 1973). It has long been recognised as an important spatial element in the interpretation of satellite imagery (Harris, 1980).

Image texture can be defined as patterns of spatial relationships among grey levels of neighbouring pixels (Brunner and Veck, 1985). Blom and Daily, (1982), defined image texture as the spatial variation of image tone, while Haralick et al., (1973) define the textural features which contain information about the spatial distribution of tonal variation within the image (band).

Therefore, getting a 'good' definition of texture is almost as difficult as measuring it (Haralick, 1979, Dutra and Mascarenhas, 1984, Mather, 1987).

In general Photo-Interpretation of texture means the apparent pattern of a given area and it is ordinarily described by the terms smooth, fine, rough, coarse, lineated or irregular. In general, the concept of texture is poorly defined and it is not clear how the human eye perceives texture, nor how a machine (computer) should be designed to do so.

Image texture usually varies from place to place within an image and it is this variation which enables the user to use

texture as an indicator of image features.

The textural properties (smoothness, granulation, randomness, fineness, coarseness) of an image carries useful information for discrimination purposes and it is important to develop measures for texture (Haralick et al., 1973). In fact, the recognition of texture from the texture features is similar to the recognition of colour from colour composites, so that the texture can be defined by the relations existing between the reflectance of two neighbouring pixels.

The use of texture in image analysis generally involves the creation of new layer or supplementary information (image properties) from the raw spectral data, without the requirement of other additional data sets. This is important in image processing and image interpretation. Such textural information is sometimes the only way to characterise an image. A good understanding or interpretation of a natural image (i.e. remote sensing image) includes the description of both spectral and textural aspects of the image (Wang and He, 1990).

The first aim of this chapter is to demonstrate how to extract textural features from an image, and to discuss the usefulness of these features for discriminating between the different rock types in an arid area, where the spectral TM bands failed to discriminate (Section 7.6 and Section 7.7). The second aim is to use the addition of the textural features for image classifica-

tion using maximum likelihood.

## 8.2 TEXTURE ANALYSIS

Methods of texture analysis have been divided into two broad class approaches (Haralick, 1979; Harris, 1980). First is the structural approach to textural analysis method, where texture is considered in terms of the organisation or repetition, and relationships among its sub-structures. This method proved to be useful in regular or man made textures at high resolution where the simple texels are present (ie. cloth, tiling, etc). (Harris, 1980). This method has not been used widely for natural remote sensing images because of the complexity of the natural textures. The second textural analysis is the statistical method, sometimes termed spatial image processing (Harris, 1980), which generates parameters to characterise stochastic properties of the spatial distribution of grey levels in an image (Haralick, 1986). This method has been widely used in the study of natural remote sensing image texture. From the literature there are three main approaches usually used for statistical textural analysis (measures). These are first order texture measures, second order texture measures and Fourier transform measures. Comparison of these texture measures in an empirical test by Weszka et al., (1976) showed that the second order texture measures produce better results than first order texture measures and the first and second order texture measures performed better than Fourier transform measure.

### 8.2.1 Fourier Transform

The Fourier transform is a method of separating an image into its various spatial frequency components through the application of a mathematical operation. Because the Fourier transform measure is concerned with the spatial frequency, it has been used in texture analysis of images and can be performed optically and digitally. This method can give good results with textural features of a strongly periodic nature (Excell et al., 1989).

Many authors have used the Fourier transform in texture analysis for remote sensing images (Conner and Harlow, 1980; Blom and Daily, 1982; and Excell et al., 1989).

### 8.2.2 First order texture measures:

Simple statistical measures of the density variation in image sub-arrays have proved useful measures of image texture (Harris, 1980). In general, the framework used to analyse the spatial variation in an image is to divide it up into small areas (windows). The window size is usually between 3 x 3 to 11 x 11 pixels. The first order texture measure operates on the pixels in each window directly (Harris, 1987). The properties are calculated within a small convolution filter or kernel, for example, Laplacian filter (Section 3.3). The first order measure have been used by many authors (eg. Trendal, 1972; HSU, 1977; Conner and Harlow, 1980; Blom and Daily, 1982; Shih and Schoweng-erdt, 1983; and Crosta and Moore, 1989).

### 8.2.3 Second Order Texture Measures

According to Oldfield (1988) the second order measures of texture include:

1. **Autocorrelation** - The autocorrelation function enables the distance apart of similar tonal variations to be specified (Haralick, 1986).
2. **Neighbouring Grey Level Dependency Matrix (NGLDM)** - The neighbouring grey level dependency matrix (NGLDM) measures the number of neighbouring pixels with the same grey levels as the pixel being examined (Oldfield, 1988). (For more detail see Sun and Wee, 1983; Oldfield, 1988).
3. **Grey Level Run Length Matrix (GLRLM)** - The grey level run can be defined as a set of consecutive co-linear pixels having the same grey level value (Oldfield, 1988). The length of the run is the number of pixels in the run. This method is based on computing the number of grey level runs of various lengths. (For more detail see Galloway, 1975; Connors and Harlow, 1980).
4. **Spatial Grey Level Dependency Matrix (SGLDM)** - The major proponent of this class of statistical texture analysis is Haralick (Haralick, 1979; Haralick et al., 1973; Haralick and Shanmugan, 1974). The SGLDM method (co-occurrence method) computes an intermediate matrix of measures from the digital image data and then defines features as functions on this intermediate matrix (Haralick et al., 1973; Ballard and Brown, 1982).

Connors and Harlow, (1980), have made some theoretical comparisons of texture algorithms (SGLDM, NGLDM, GLRLM) measures. The results obtained indicate that the SGLDM is the most powerful algorithm. The most common textural measures used in the analysis and interpretation of remotely sensed data are the features derived from SGLDM method (Haralick et al., 1973; Shih and Schowengerdt, 1983). It has been shown that this kind of second order measure is a valid measure of the spatial distribution of grey levels within an image. It is for these reasons that this study concentrated on the use of SGLDM methods.

### 8.3 SPATIAL GREY LEVEL DEPENDENCY MATRIX (SGLDM)

In this method, coarse textures are those for which distribution changes only slightly with distance and fine texture are those for which the distribution changes rapidly with distance. It depends not only on the spatial relationships of grey levels but also on regional brightness background variation within the image. In other words, the SGLDM measures the probability of occurrence of two grey level values separated by a given distance in a given direction.

Table 8.1 shows a simple image window 4 x 4 pixels in which texture is to be calculated. The value of each pixel is in the range of 0 - 3 (grey level) for simplicity. The number of adjacent pixels with grey levels 'i' and 'j' is counted and placed in element (i, j) of the co-occurrence matrix P. Four definitions of adjacency can be used: (0°), (90°), (45°), (135°) (Figure 8.1) which are horizontal, vertical, diagonal (bottom to

**TABLE 8.1**  
**Example data and derived grey-tone spatial dependency**  
**matrices:**  
**(a) test dataset; (b)-(e) grey-tone spatial matrices for**  
**angles of 0°, 45°, 90° and 135° respectively.**  
**(From: Mather, 1987)**

0	0	0	2	1
0	1	1	2	2
0	1	2	2	3
1	1	2	3	3

(a)

	0°			
	0	1	2	3
0	4	2	1	0
1	2	4	3	0
2	1	3	2	2
3	0	0	2	2

(b)

	45°			
	0	1	2	3
0	2	1	0	0
1	1	4	3	0
2	0	3	6	0
3	0	0	0	2

(c)

	90°			
	0	1	2	3
0	4	3	0	0
1	3	4	2	0
2	0	2	6	2
3	0	0	2	2

(d)

	135°			
	0	1	2	3
0	0	4	2	0
1	4	0	3	0
2	1	3	0	0
3	0	0	3	0

(e)

left top right) and diagonal (top left to bottom right). There are four P matrices results (P0, P90, P45 and P135) respectively.

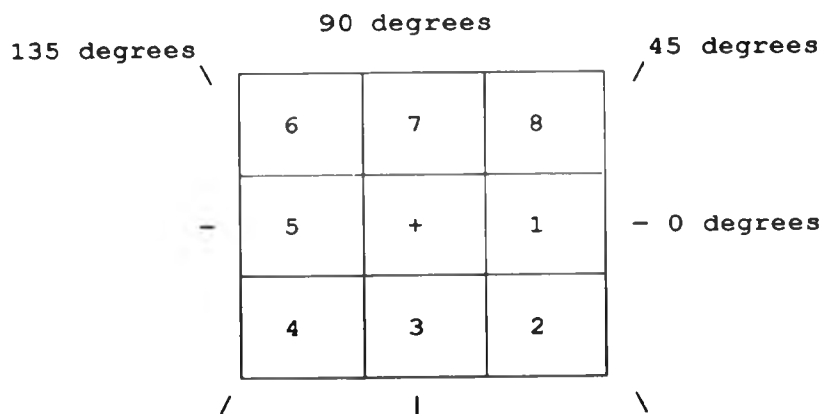
The element P0 (0,0) is the number of times a pixel with pixel value 0 is horizontally adjacent to a pixel which has a pixel value 0, counting from left to right as well as right to left.

The element P0 (1,0) is the number of pixels with value 1 that are adjacent or followed by pixels with value 0, but P0 (0,1) is the number of pixels with the value 0 that are followed by pixels with value 1 and looking in both the left - right and right - left directions. All the four co-occurrence matrices in this example are illustrated in Mather, (1987).

A set of texture features is defined from the SGLDM(co-occurrence matrix) measures by Haralick et al., (1973) which are (1) angular second moment, (2) contrast, (3) correlation, (4) variance, (5) inverse difference moment, (6) sum average, (7) sum variance, (8) sum entropy, (9,10) information measures of correlation, (11) maximal correlation coefficient, (12) entropy, (13) difference variance, and, (14) difference entropy. The SGLDM's may be calculated for different pixel displacement and orientation.

These texture features are calculated in the spatial domain, and the statistical nature is based on the assumption that the texture information in an image is contained in the overall or

**FIGURE 8.1**  
 Resolution cells 1 and 5 are 0° (horizontal)  
 nearest neighbours to resolution cell\*; resolution  
 cells 2 and 6 are 135° nearest neighbours;  
 resolution cells 3 and 7 are 90° nearest neighbours;  
 and resolution cells 4 and 8 are 45° nearest neighbours  
 to \*, (Note this information is purely spatial, and has  
 nothing to do with grey-tone values).  
 (From: Haralick et al., 1973).



'average' spatial relationship which the grey level in the images have to one another (Haralick et al., 1973).

Some of these measures relate to specific textural characteristics of the image such as homogeneity (angular second moment ASM), contrast (Contrast) and the presence of organised structure within the image (correlation measure). Other measures characterise the complexity and nature of grey level transitions which occur in the image (Haralick et al., 1973).

According to Weszka et al., 1976; Brunner and Veck, 1985; Franklin and Peddle, 1987, 1989; Roan and Aggarwal, 1987; Oldfield and Elgy, 1987; Oldfield, 1988; Peddle and Franklin, 1991, only four measures of the fourteen are useful. These are angular second moment (ASM)—a measure of homogeneity; contrast, amount of local variation in an image, entropy which inversely relates to ASM, and inverse difference moment. Therefore, in this study these four measures will be examined. A full list of all the different measurement equations and the mathematical detail is given in Haralick et al., 1973; Haralick, 1986.

Although it has been found that these features contain information about the textural characteristics of the image, it is hard to identify which specific textural characteristic is represented by each of these features (Haralick et al., 1973).

Texture analysis of remote sensing data (satellite and radar images) have been used in many applications including ecological studies (e.g. Saxon, 1984), forest and agricultural mapping (e.g. Gordon and Philipson, 1986; Pultz and Brown, 1987; Skidmore, 1989) geological and geomorphological studies (e.g. Blom and Daily, 1982; Saraph and Inamdar, 1982; Hsu, 1986; Shih and Schowengerdt, 1983; Brunner and Veck, 1985; Oldfield and Elgy, 1987; Oldfield, 1988; Franklin and Peddle, 1989; Wang and He, 1991), soil mapping (e.g. Agbu and Nizeyimana, 1991).

#### 8.4 THE USE OF TEXTURE ANALYSIS IN GEOLOGICAL STUDIES

In lithological discrimination in arid or semi-arid areas, the weathered surface can reduce the spectral difference between rock types, and hence texture has to be relied on as an indicator of difference (Brunner and Veck, 1985). For example, rocks that are similar in mineral composition may have different weathering surfaces, and therefore have quite different spectral reflectances. Also, rocks that are dissimilar in mineral composition may have similar weathering surfaces, therefore they will have the same spectral reflectance. These rocks are impossible to separate by spectral signature alone but could, in some cases, be separated by image textural attributes (Shih and Schowengerdt, 1983). Therefore, to differentiate between geological surfaces, the remote sensor interpreter should combine both spectral and textural information (Brunner and Veck, 1985).

The usefulness of image texture (texture features) for geological remote sensing has been demonstrated first by Haralick et al., 1973, and Weszka et al., 1976. Weszka et al., 1976 was able to distinguish between three rock types from 180 Landsat MSS image samples with good accuracy, based on textural measures and they have found that first and second order statistics measures gave better results than Fourier transforms, but Connors and Harlow, 1980; Oldfield, 1988, found the second order measure (SGLDM) better than the first order measures.

Saraph and Inamdar, 1982, used the textural features which

have been obtained by the textural analysis (angular second moment, contrast, correlation, variance, entropy) to discriminate and to classify the geological units in part of India (semi-arid area). The aim was to identify the physical features in mineralised zones using MSS data. They found that the classification obtained has given clarity to interpretation but they did not calculate the accuracy of this classification.

Blom and Daily, (1982), used the variances of square windows 61 x 61, 31 x 31, and 15 x 15 pixels as measures of texture in an analysis of rock type discrimination using seasat SAR image.

Shih and Schowengerdt, (1983), have used a texture algorithm (a first order measure) which measures the local edge amplitude and density of Landsat MSS data of semi-arid area (Arizona). The derived textural features are added to the original four MSS bands and the combined bands are then classified. They found that the classification accuracy improved compared to the classification using only the spectral bands.

Oldfield and Elgy (1987) and Oldfield (1988) have examined the first and second order SGLDM measures using Landsat MSS, TM and radar for geological mapping. The results for the TM show that, in most cases, the addition of texture measures does significantly increase the classification accuracy. The highest increase in classification accuracy being due to the second order measure (SGLDM). The study area was a semi-arid area (Argentina and

Chile).

Wang and He (1990) examined a new statistical texture analysis method where the local texture information for a given pixel and its neighbourhood is represented by corresponding texture units and the global texture of an image is characterised by its texture spectrum. They attempt to use this method in order to discriminate between the lithological units in airborne SAR image. They claimed the results were promising.

It is clear from the examples cited that the SGLDM measure is probably superior to all other methods and it is useful to classify the spectral textural data to help geological mapping in semi-arid areas.

### **8.5 RESULT AND DISCUSSION**

From the literature it is clear that in understanding and description of natural imagery, texture analysis is one of the more important analyses used in image interpretation and classification of the digital image for geological study purposes. In Chapter Seven, the results show that it is difficult to discriminate between some rock types in two test sites. Therefore it was decided to examine the usefulness of texture analysis in rock discrimination and image classification.

Four different remote sensing data sets were available for use. These were Landsat MSS, and TM, SPOT panchromatic (PLA) and

shuttle imaging radar (SIR-B) (Section 2.4). Shuttle Imaging Radar-B has been recorded from the Challenger Shuttle in October (1984) over Saudi Arabia. Table 2.4 shows the SIR-B system characteristics.

The SIR-B data was provided as hard copy in black and white print, covering only a small part of the study area (Appendix 4).

This data was digitised using a high resolutions digitisation camera connected to the Micro-Vax computer system. The digitised radar image was produced in different resolution using the zoom lenses in the camera. Unfortunately all the digitised radar images were not good enough to use in any sort of image analysis, because of the strong noise from the original image and from the digitisation process. Different smooth techniques were applied to reduce the noise. The resultant images contained little information and were not analysed further. The digital radar data is certain to be of use in providing textural information.

Shih and Schowengerdt, 1983, Oldfield, 1988; and Oldfield and Elgy, 1987, have found that using MSS data in textural analysis for arid or semi-arid areas (texture discrimination or image classification) did not provide any geological information better than the TM or radar. This was because of the poor spatial resolution and the spectral bands. Therefore, the only image data which can be used for texture feature extraction measures in this study were the TM or SPOT (PLA). Since two different

resolutions satellite of data were used for the same area, differences in the texture feature would be expected. This is because the observation of texture depends on two factors; one is the scale of the variation (texture scale), the second is the scale of observation (spatial resolution of the image), (Mather, 1987). Therefore, the TM data was used in this analysis because it provided more discrimination and less time of processing.

Haralick et al., 1973, described 14 texture features defined from the SGLDM measures, only seven of these measures have been applied during the course of this study. These were angular second moment (ASM), contrast, entropy, inverse difference moment, sum entropy, difference entropy, difference variance. The selection of these measures to be applied in this study was based on literature. A program called TEX written in Fortran (Watson pers. comm 1991/1992) produced 28 texture images. In applying the SGLDM measures, many texture features could be generated from each band (TM band 7 or 5), using different factors; (1) different window size, (2) orientations, and (3) grey level ranges (Haralick et al., 1973). In this study these factors were (1) a 3 x 3 pixel (nearest neighbour) or 5 x 5 pixels (2) all four directions (0°, 90°, 45°, 135°) (3) 256 x 256 grey level,. During the application of the SGLDM measures to the two test site images:-

1. The 3 x 3 pixels window size was the best to use because of the texture feature appearance and the computer time.
2. There were no noticeable differences between the texture

features which have been extracted in the four directions. This may be because the texture features were not oriented in the images.

3. Some of the extracted texture feature images showed texture discrimination between some rock types. These are entropy, inverse difference moments and angular second moment.

A spectral - textural false colour composite, linearly contrast stretched, was produced for both test sites for image classification purposes. Unfortunately neither showed any improvement in colour enhancement than the spectral images. Shih and Schowendgerdt, (1983) recommended using the application of textural features to TM bands in conjunction with the spectral ratio images (Section 7.3) to improve geologic mapping in arid areas. This method was examined in this study by using image addition (arithmetic operation section 3.5) of the textural feature image to the original TM bands (Bands 1-5 and 7), and produced a colour ratio composite (CRC) but none of the CRC's produced any acceptable image rock discrimination.

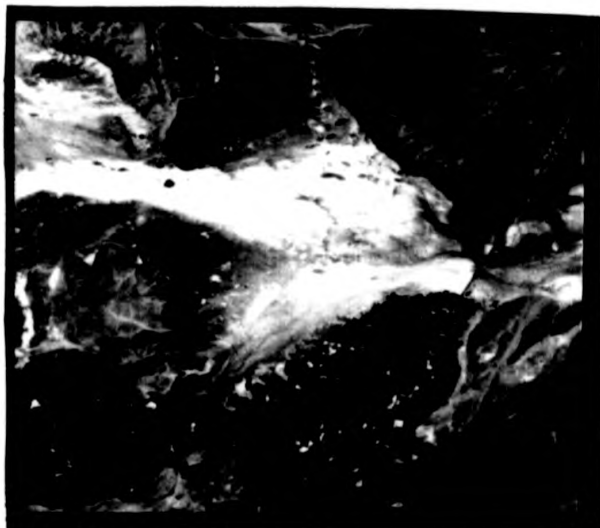
Two test sites, which are Wadi ad Duwadimi, and Wadi al Qahad, (the first and second test sites in Chapter 7) were chosen to apply the texture measures. (See Sections 1.7.3 and 7.6 for the geological description for each site).

**First Test Site: (Wadi ad Duwadimi area)**

In the first site, seven texture measures were applied to TM band 5 (Plate 8.1) and their results were visually compared with the spectral FCC (Bands 7, 5 and 3 in red, green and blue respectively) (Plate 7.1) and with the geologic map. It has been found that only two texture measures produce a recognisable image in terms of rock boundaries and texture appearance. These measures were (a) the entropy measure (Plate 8.2a) or measure of roughness and (b) inverse difference moment (IDM), (Plate 8.2b).

In both images the only important noticeable features were; first, most of the rock boundaries are well defined, second the two lava flows (olivine basalt) showed different texture properties. Lava (A) black in (Plate 8.2a) and white in (Plate 8.2b) is different from Lava (B) white in (Plate 8.2a) and (Figure 8.2b). In an entropy image, the white colour indicated for roughness and/or heterogeneity in texture.

During the field trip, it was found that Lava (A) is very thick (around 4 - 5 metres) and it contains very big boulders or pillow lavas and there was no sand invasion. This means that this lava has a smooth texture (Plate 7.2a). Lava (B) in nature is lower than lava (A) and some parts of it were covered by sand (Plate 7.2b). This means this lava will have a rough (coarse) texture in an image.



0 kms 5

**PLATE 8.1**

Linearly contrast stretched of TM band 5 image for the first test site (wadi ad Duwadimi) area.

(a)



0 kms 5

(b)

**PLATE 8.2**

The result image of applying the SGLDM measure for the first test site (Wadi ad Duwadimi) area.

(a) Entropy measure

(b) Inverse difference moment.

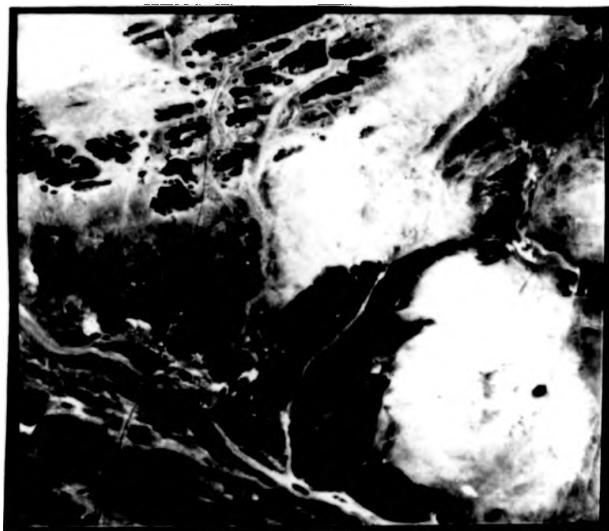
These images of texture features were added back to the spectral TM bands 1-5 and 7 to produce different false colour composites (Table 7.2), and to produce different colour ratio composites (Table 7.4). All the images produced from these FCC's and CRC's were not acceptable for image interpretation.

**Second Test Site: (Wadi al Qahad area)**

The seven texture measures were applied to TM band 5 (Plate 8.3a). By visual comparison between all the seven texture measure images, for the second test site (Section 7.6), it was found that only three texture measures provided a recognisable image. These are the angular second moment (ASM)—a measure of homogeneity and coarseness; the sum entropy (SE) and the inverse difference moment (IDM). In these three texture feature images, when linearly contrast stretched, it was easy to recognise the rock boundaries. The sum entropy produced the best image (Plate 8.3b) compared to the others. In this image some of the rock types showed a distinct texture. For example, the Kilab monzogranite (mg) showed a smooth texture compared to the Maa complex which showed a moderately coarse texture and appeared lineated. It was not possible to discriminate between these rocks in using the spectral data or to find rock boundaries. The Jibalah Group and Banana Formation showed a lineated texture feature compared with other rocks in this site.

All the three texture feature images have been added back to the spectral TM band 1-5 and 7, in order to produce different false FCC's (Table 7.2) and different CRC's (Table 7.4). All

(a)



0 kms 5

(b)

**PLATE 8.3**

- (a) Linearly contrast stretched TM band 5 for the second test site (wadi Al Qahad) area.
- (b) result image from applying the sum entropy of the SGLDM for the second test site (wadi Al Qahad) area.

the colour images produced from the FCC's and CRC's were not acceptable for image interpretation.

The texture analysis, using the spatial grey level dependence matrix SGLDM did not produce any useful texture features which can discriminate between all the rock types in each test site, even when the window size was changed in size and orientation. It did however, show some acceptable texture discrimination between some rock types.

Although multispectral analysis has received the greatest attention as a method of classification, it makes no use of spatial information present in the image. The inclusion of such information should improve classification accuracy (Rees, 1990). The image classification of multispectral remote sensing data has found limited use in geological-lithological mapping has proved unsuccessful result (Siegela and Abrams, 1976; Abrams, 1980; Boldget and Brown, 1982; Guha and Mallick, 1985; Drury, 1987; Gupta, 1991). All these studies have used only spectral information, and therefore the author decided to apply image classification to a combination of textural and spectral data.

To this end, unsupervised maximum likelihood classification was applied, using a program called MAXILIK on the Micro-Vax system, to the following data:-

1. The addition to bands 7, 5 and 3 images of either entropy, or inverse difference moment measures, for the

first test site.

2. The addition to TM bands 5, 3 and 1 of images of the sum entropy measure, for the second test site.

All the classification results were very poor in terms of the classes separability, and the matter was not pursued further. The failure may be due to a lack of proper definition of texture information, or to strong correlation between the spectral and spatial information.

#### 8.6 SUMMARY

This chapter contains a brief introduction to the use of textural analysis methods in geological studies, (i.e. rock discrimination and image classification for lithological mapping). All the commonly used methods of statistical texture analysis has been discussed in this chapter. The spatial grey-level dependency matrix (SGLDM) was applied to two different test sites in the study area.

Haralick et al, (1973), described 14 texture features defined from the SGLDM, only seven of these measures have been applied during the course of this study. The aim was to improve both the rock discrimination and the image classification using the unsupervised maximum likelihood classification.

The sum entropy, entropy and inverse difference moment measures produce a very limited capacity to discriminate between all the rock types. The resultant images of these measures were

added to the spectral bands for image classification purposes.  
The classified images were very poor.

added to the spectral bands for image classification purposes.  
The classified images were very poor.

**CHAPTER NINE**  
**CONCLUSION AND FUTURE WORK**

**9.1 CONCLUSION**

**9.2 FUTURE WORK**

### 9.1 CONCLUSION:

Remote Sensing Satellite Systems provide very useful data about the earth's surface. In general, two different satellite systems have been used in geologic applications. These are Landsat and SPOT satellites. The Landsat-5 satellite carries two instruments, the Multispectral scanner (MSS) and Thematic Mapper (TM). The greater spatial resolution of the TM coupled with a greater radiometric sensitivity allows smaller geologic features to be recognised and discriminated. The SPOT satellite can operate in two different image modes with different spectral and spatial resolutions. These are the Multispectral Mode (MLA) and the Panchromatic Mode (PLA).

The aim of this study was to investigate the use of these satellites (Landsat MSS and TM and SPOT PLA) together with radar (shuttle imaging radar (SIR-B)) to test the capabilities of digital image processing techniques for geologic studies. However, in an arid area, the TM data was chosen for use in all the investigations in this study for two reasons; first, the spatial resolution (30 x 30m) proved to be good enough for detailed interpretation; second, the spectral resolution of the six different bands (0.45 to 2.35  $\mu\text{m}$ ) proved to be useful in discriminating the lithological differences. The SPOT and radar were only available towards the end of the study and were only available for a small part of the study area.

Digital remotely sensed images usually contain three types of information, spectral, spatial and temporal. The first two were

used in this study. The spatial information has been interpreted in this study as context and texture. The second aim of this study is to examine the problem of extracting spatial information of use to geologists, from satellite images.

In general, digital image processing can be divided into three major areas of computer operation; which are preprocessing, enhancement and classification. Most remote sensing data are preprocessed to correct the data for errors (geometric or radiometric). Only three preprocessing techniques were used during the course of this study. These were de-stripping, atmospheric correction, and image-to-image registration. The de-stripping technique was needed only for the MSS data, and the method used, successfully removed the stripes. Two different methods of atmospheric correction were tested, to correct the TM bands 1-4, and the improved dark-object subtraction method for atmospheric scattering correction was found to give the best results.

Image-to-image registration enables the digital pixel values from different satellite bands to be compared and combined in many ways. In this study the TM image was taken as a reference. It was not possible to produce an acceptable registration of the MSS to the TM image. The reason for this failure was the lack of ground control points.

Image enhancement techniques are used to improve the detecta-

bility of objects or patterns in digital images. Several enhancement techniques were examined during the course of this study. These were contrast stretch, arithmetic operations, band ratios, principal component analysis, decorrelation stretch, density slicing, spatial filtration (Laplace, median filter) as well as several new contextual techniques which included the rolling ball technique, ripping membrane technique, and the automatic watershed image segmentation method. Two different image classifications were used in this study. These are:- the box (parallelepiped) and maximum likelihood classification.

There are two general objectives in the use of remote sensing data for geological investigation. These are the Lineament investigation and Lithological discrimination and mapping. In this study both objectives have been investigated. The study area was part of the Arabian Shield and was chosen to test the previously known and the new image processing techniques for lineament detection and rock discrimination.

Lineaments are important features for geologists. They can help in the understanding of the geological structure of an area, and can help in identifying potential areas of mineralisation.

The results of the two new contextual techniques, rolling ball and ripping membrane, and also of the spatial filtration techniques (e.g. Laplace) were evaluated and compared with respect to their capacity to detect, and make easily visible, the

lineaments of a variety of images.

The MSS band 4 and TM band 5 were found the best for lineament detection in terms of contrast, and definition of geological features. This study revealed structural lineaments, mostly mapped for the first time, which can be related to regional tectonics. It was found that the new contextual techniques provide excellent tools for visual detection, interpretation, and analysis of lineaments. A total of 97.6% of all the detected lineaments were present in the ripping membrane processed images while the rolling ball processed images were the second best (68%). Spatial filtration (directional and non-directional) produced very poor detection rates compared with the new techniques. All the mapped faults in the test site (Jibal Rummàn) area were detected during the interpretation.

Rose diagrams were drawn to find the main orientation of lineaments in each rock type within the selected test site area.

It was found that the major trend was in (N71°-75°E) from both the TM and MSS images. The study area was affected by a major and a minor faulting system. The major system is the Najd Fault System and the minor is the Saqf fault system. The second system is a conjugate system to the major system. The NW-SE lineaments may be related to the Najd Fault System and the NE-SW direction lineaments may be related to Saqf fault system.

The ripping membrane technique was found to be useful in

detecting and tracing the pattern of drainage systems in an arid area, but this was not within the scope of this study and was not pursued.

'Computer vision' is the enterprise of integrating a wide range of automatic processes, and representations on a computer, to mimic human perception (Ballard and Brown, 1982). There are four factors which need to be considered in specifying the environment of any computer vision systems; sensor type, spatial resolution, type of object and complexity of scene. Computer vision is never completely separated from the human supervision and often subsequent manual interpretations of the images and data are necessary. In this study the computer vision concept was used to perform image segmentation and automatic lineament feature extraction methods and analysis from the TM and SPOT data, using the contextual information and techniques. The choice of segmentation method depends on the description that is required or on the specific application. In general, image segmentation methods have been divided into two categories - edge based methods and region based methods. There are several commonly used region based segmentation methods, and these include thresholding methods, region growing methods and split and merge methods. Image segmentation has not been demonstrated in geological application because of the complexity of most images. This can be attributed to the heterogeneity of rocks.

Two different image segmentation methods were developed and

examined in this study. These methods were the automatic watershed segmentation and interactive image segmentation method, using ripping membrane/Laserscan system programmes (e.g. VICTORIES DTICOMBINE... etc.). Both methods required the preprocessing of the images by the ripping membrane technique. The second method produced an acceptable image segmentation. This method involved several stages of processing; first, preprocessing; second, image formatting and combination; third, rock boundaries extraction (segmentation), and fourth, 'clean up'.

The use of visual lineament detection methods have been criticised because of the subjectivity associated with human interpreters. Therefore there is a real need for an objective automatic lineament extraction technique. This study represents an attempt to test and develop a method of automatic line and lineament feature extraction. Further, there is a need to develop a method of examining the distribution of lineaments within each rock unit in an area. This implies that the images must be segmented first, and then the lineament distribution found within each segment. The method developed to achieve this end had four stages of processing. These were preprocessing, thresholding, image segmentation and lineament extraction and their azimuth measurements. The novelty in this method lies in:-

- creating a direct relationship between image segmentation methods and the automatic lineament feature extraction, in order to find out the megatexture in each rock type

- (region) automatically,
- using the contextual (spatial) relationship between pixels at all the different stages of lineament extraction.

A careful comparison was made between the automatic method and the visual method of tracing in terms of lineament maps and it was found as follows:-

- (a) Most of the visually traced lineaments were also extracted by the automatic method.
- (b) Between 75 - 85% of the thinned extracted lines or segments can be easily related to lineament or edges in the input image.
- (c) There was a difference equal to  $10^{\circ}$ - $15^{\circ}$  degrees between the major trends.
- (d) The minor lineament trends were detected.

Three selected test sites were chosen to examine the spectral image enhancement techniques. The test sites were: (a) Wadi Ad Duwadimi area, (b) Wadi al Qahad area, and (c) Jabal Muwaysil area. The spectral image enhancement techniques, e.g. contrast manipulation for false colour composites, colour ratio composites, principal component and decorrelation stretching. It was demonstrated that limitations occur in discrimination between some the rock types. The reason for this limitation could be attributed to one or more of the following:-

1. Some rocks have been classified into different units or formations on the basis of age or origin despite having the same rock composition.
2. The lithological data can not be discriminated if they have the same 'desert varnish' composition.
3. The lithologies cannot be discriminated if the differences are in terms of the grain or crystal size.

Texture, as spatial information, is one of the important characteristics used in recognition of the objects or regions of interest in an aerial photograph or satellite image. Textural features are very important in photo-geological interpretation and sometimes the texture differences are the only ones present in an image.

There are two broad approaches to texture analysis; these are structural analysis and statistical analysis. The structural analysis is concerned with the relationship between regions within an image and is not relevant to this study. The statistical analysis is widely used to analyse remote sensing images, and from the literature, it was found that there are three main approaches; the first order texture measure, second order texture measure, and Fourier transform. A comparison of these texture measures has been made by many authors and the consensus of opinion indicates that the spatial grey level dependency matrix (SGLDM) (the grey tone co-occurrence matrix) which is one of the second order textures is the most useful in practice for

the extraction of textural information (features) from digital images.

Haralick et al., (1973) described 14 texture features defined from the SGLDM. Only seven of these measures have been applied during the course of this study. These were the angular second moment, contrast, entropy, inverse difference moment, sum entropy, difference entropy, and difference variance. The selection of these measures was based on the results obtained from previous work reported in the literature.

Attempts were made to apply the SGLDM measures to the SIR-B data but it was not possible because of noise in the data. Therefore only TM data were used. The results from the SGLDM method were not good in terms of textural discrimination between every rock type. There were, however a few acceptable texture discriminations between some rock types, and the boundaries between all the rock types were, in general, well defined. The maximum likelihood classification was applied to the combination of the spectral and textural features images in order to improve the classification. This proved to be abortive.

## **9.2 FUTURE WORK**

1. The new contextual techniques, (ripping membrane and rolling ball) need more testing in different areas with different environments (i.e. polar, temperal, tropical, as well as arid) to discover the capability of these

techniques for enhancing the lineaments or edges.

2. The ripping membrane technique as a contextual smoothing technique could be used in image classification studies. It can be applied in two different ways: (a) as preprocessing before an image classification. This leads to acceptable image segmentation or, (b) as a means of simplifying data by reducing its local variability, whilst preserving its regional differences.
3. The SPOT satellite has the capability to produce a stereoscopic image which is a very useful tool for structural geology. This characteristic has not been demonstrated in any part of the Arabian Shield for lineament study. The author recommends applying the rolling ball technique to SPOT data which will enhance the structural feature and this will appear clearly in the stereoscopic images.
4. In this study it was found that the subtraction of the smooth ripping membrane image from the original data enhances the drainage system features as well as the lineaments. For this reason this method should be examined in studying the drainage system.
5. Radar (SAR) shadows are a very good aid in the interpretation of topographic relief, relative to the rock

resistance (general geology) and geologic structure. Parts of Saudi Arabia have been covered by the Shuttle Imaging Radar (SIR-A and B) but only one study, so far, has used the SIR-B image for studying one lineament (Berlin et al., 1987). Clearly, this type of imagery could be exploited more fully as and when it becomes available.

- (a) Radar data could be used together with other satellite or airborne image data for texture analysis in order to discriminate or to map the rock types.
- (b) Radar image interpretation can be used to pick up lineaments which may not be shown in the spectral images. For this reason the radar data is another important source to be used for structural studies in the Arabian Shield.

7. There are six long major lineaments running toward or from a small circular feature area. Also, there are four major lineaments running from or towards a small triangle feature area. Both features are located within Jibal Rumman area and both need more ground geological investigation.

8. According to (a) the interpretation of the spectrally enhanced images and the textural features image and (b) the field inspection for the two lavas located in the Wadi Al Duwadimi area, may be have different age and

source. Therefore, a geochemical analysis is needed for these lavas.

## REFERENCES

- AACH, T., FRANKE, U., and MESTER, R., (1989),** Top-Down Image Segmentation using Object Detection and Contour Relaxation, In: *Proceedings of IEEE*, 1981, 2673-2189.
- ABRAMS, M.J., (1980),** Lithologic Mapping. In: (B.S.Siegal and A.R. Gillespie, Eds.) *Remote Sensing in Geology*, (New York: Wiley) - 381-418.
- ABRAMS, M., KAHLE, A., and GILLESPIE, A., (1983),** Geologic Utility of Landsat-4 TM Data. In: *Proceedings of the Landsat-4 Science Characterisation Early Application Symposium. ELT NASA 2355.4: 127-130.*
- ABRAMS, M.J., ASHLEY, R.P., ROWAN, L.C., GOTEZ, A.F.H., and KHALE, A.B., (1977),** Mapping of Hydrothermally Alteration in the Cuprite Mining District; Nevada; Using Aircraft Scanner Images for the Spectral Region 0.46 to 2.36  $\mu\text{m}$ . *Geology* 5: 713-718.
- AGAR, R.A., (1987),** The Najd Fault System Revisited: A Two-way Strike - Slip orogen in the Saudi Arabian Shield. *Journal of Structural Geology*, 9: 40-48.
- AGBU, P.A., and NIZEYIMANA, E., (1991),** Comparisons between Spectral Mapping Units Derived from SPOT Image Texture and Field Soil Map Units. *Photogrammetric Engineering and Remote Sensing*, 57: 397-405.
- AL-KHATIEB, S.O., and NORMAN, J.W., (1982),** A Possibility Extensive Crustal Failure System of Economic Interest. *Journal of Petroleum Geology* 4: 319-324.
- AL-HINAI, K.G., (1988),** Quarternary Eolian Sand Mapping in Saudi Arabia Using Remotely Sensed Imagery. Unpublished Ph.D. Thesis, University of London.
- ALNOSO, F.G., and SORIA, S.L., (1991),** Using Contextual Information to Improve Land Use Classification of Satellite Images in Central Spain. *International Journal of Remote Sensing*, 12: 2227-2235.
- ALONSO, M.F., and TAHON, A., (1991),** Lithological Discrimination and Structural Trends in W-Rwanda (Africa) on Images of Airborne Radiometric and Aeromagnetic Surveys, Co-registered to a Landsat TM Scene. *Photogrammetric Engineering and Remote Sensing*, 57: 115-1162.

- AL-SARI, A.M., (1989),** A Geological Investigation of Multi-spectral Remote Sensing Data for Mahd Adh Dhuhab and Jabal Said Districts, Western Saudi Arabia. Unpublished Ph.D. Thesis, University of Durham.
- AL-SIYARI, S.S., and ZÖTEL, J.G., Eds (1987),** Quaternary Period in Saudi Arabia: New York:Wien), 300p.
- AL-WASH, M.A., ZAIDI, S.M., and TERHALLE, U., (1986),** Description of Arid Geomorphic Features Using Landsat TM Data and Ground Truth Information. (Wadi Fatima Kingdom of Saudi Arabia), *Catena*, 13: 277-293.
- AMOS, B.J., and GREENBAUM, D., (1989),** Alteration Detection Using TM Imagery: The Effect of Supergene Weathering in an Arid Climate. *International Journal of Remote Sensing*, 10: 515-527.
- AVERY, T.E., and BERLIN, G.L., (1985),** Interpretation of Aerial Photographs, (4th Edition), (Mineapolis: Burgess Publishing Co.).
- BALLARD, D.H., and BROWN, C.M., (1982),** Computer Vision. (New Jersey: Prentice-Hall, Inc).
- BARANETI, B.S., CASINI, A., LOTTI, F., FAVORI, L., and ROBERTO, V., (1990),** Variable Pyramid Structures for Image Segmentation. *Computer Vision Graphics and Image Processing*, 49: 346-356.
- BARRETT, E.C., and CURTIS, L.F., (1982),** Introduction to Environmental Remote Sensing (2nd Edition), (London: Chapman and Hall), 352p.
- BELLISS, S.E., FOWLER, A.D.W., and McDONNELL, M.J., (1985),** Linear Features in Wairarapa: Quantitive Study Using Landsat Imagery. *New Zealand Journal of Geology and Geophysics*, 28: 859-867.
- BERLIN, G.L., SHEIKHO, K.M., AL NASER, A., (1987),** SIR-B View of Jabal Hadn Lineament and its Ground Water Implications. In: *Proceedings 21st International Symposium on Remote Sensing of Environment*, An Arbor, Michigan, 1987, 709-719.
- BERLIN, G.L., TRABZOUNI, M.A., AL NASER, A.H., SHEIKHO, K.M., and LARSON, R.W., (1986),** SIR-B Subsurface Imaging of a Sand-Buried Landscape: Al Labbah Plateau, Saudi Arabia. *IEEE Transaction on Geoscience and Remote Sensing*, GE-2, 4: 595-601.
- BERHE, S.M., and ROTHERY, D.S., (1986),** Interactive Processing of Satellite Images for Structural and Lithological Mapping in Northeast Africa. *Geological Magazine*, 123: 393-403.

- BESAG, J., (1986)** On the Statistical Analysis of Dirty Pictures. *Journal of Royal Statistics Society, B48*, 259-302.
- BILLINGS, M.P., (1972)**, Structural Geology (3rd Edition), (New Jersey: Prentice-Hall), 606p.
- BIRD, A.C., GARRARD, G.R., ILES, A.R., and LOUGHLIN, W.P., (1985)**, An investigation of spectral signature from mineralised rock outcrop, as defined by airborne TM data of the Saudi Arabian shield. In: *Proceedings of the 3rd International Colloquium on Spectral Signatures of Objects in Remote Sensing, Les Arcs, France, 1985*, 415-417.
- BLACK, S.M., (1987)**, Interactive Digital Image Processing as an Aid in the Mapping of Brittle Structures Using Satellite Sensor Image Data. In: *Proceedings of Annual Conference of Remote Sensing Society, Advances in Digital Image Processing, Nottingham, 1987*, 343-344.
- BLACKSTONE, D.L., (1975)**, Mapping of Linear Structural Elements from Remote Sensing Imagery. *Contribution Geology*, 14: 1-6.
- BLAKE, A., and ZISSERMAN, A., (1983)**, Visual Reconstruction (London: The MIT Press), 225p.
- BLODGET, H.W., GUNTHER, F.J. and PODWYSOCKI, M.H., (1978)**, Discrimination of Rock Classes and Alteration Products in Southwestern Saudi Arabia with Computer Enhanced Landsat Data: NASA Technical Paper 1327.
- BLODGET, H.W., and BROWN, G.F., (1982)**, Geologic Mapping by Use of Computer-Enhanced Imagery in Western Saudi Arabia. U.S. Geological Survey Professional Paper, 1153, 10p.
- BLODGET, H.W., ANDRE, C.G., MARCELL, R., and MINOR, T.B., (1984)**, Multispectral, Thermal Infrared Satellite Data for Geologic Applications. In: *Proceedings of International Symposium on Remote Sensing of Environment, 3rd Thematic Conference, Remote Sensing for Exploration Geology, Colorado, 1984*, 917-928.
- BLODGET, H.W., GUNTHER, F.J., and PODOWYSOCKI, M.H., (1978)**, Discrimination of Rock Classes and Alteration Products in South Western Saudi Arabia with Computer Enhanced Landsat Data: U.S. National Aeronautics and Space Administration Technical Paper, 1237, 34p.
- BLOM, R.G., ABRAMS, M.J., and ADAMS, H.G., (1980)**, Spectral Reflectance and Discriminations of Plutonic Rocks in the 0.54 to 2.45 Micrometer Region. *Journal of Geophysical Research*, 85: 2638-2648.
- BLOM, R.G., and DAILY, M., (1982)**, Radar Image Processing for

Rock Type Discrimination. *IEEE Transactions on Geoscience and Remote Sensing*, GE-20, 343-351.

- BODECHTEL, J., and FREI, M., (1992)**, Geoscientific Achievements. *International Journal of Remote Sensing*, 13: 1305-1318.
- BRAUN, O.P., (1982)**, A Structural Synthesis of Brazil, Based on the Study of Major Lineaments Derived from Remote Sensing Imagery Interpretation. *Photogrammetria*, 37: 77-108.
- BROWN, G.F., SCHMIDT, D.L., and HUFFMAN, A.C., (1989)**, Geology of the Arabian Peninsula: Shield Area of Western Saudi Arabia. *U.S. Geological Survey Professional Paper*, 560-A: 188p.
- BRUNNER, J.S., and VECK, N.J., (1985)**, Image Texture Encoding for Geological Mapping. In: *Proceeding of International Conference Remote Sensing Society and CERMA*, on Advance Technology for Monitoring and Processing Global Environmental Data. London, 1985: 331-339.
- BUCKINGHAM, W., and SOMMER, S., (1983)**, Mineralogical Characterisation of Rock Surfaces Formed by Hydrothermal Alteration and Weathering - Application to Remote Sensing. *Economic Geology*, 78: 664-674.
- BURDICK, R.G., and SPEIRER, R.A., (1980)**, Development of a Method to Detect Geologic Faults and other Linear Features from Landsat Images. *U.S. Department of Interior Bureau of Mines*, 8413, 74p.
- BURNS, K.L., and SHEPHERD and BERMAN, M., (1976)**, Reproducibility of Geological Lineaments and other Discrete Features Interpreted from Imagery: Measurement by a Coefficient of Association. *Remote Sensing of Environment*, 5: 267-301.
- BURNS, K.L., and BROWN, G.H., (1978)**, The Human Perception of Geological Lineaments and Other Discrete Features in Remote Sensing Imagery: Signal Strengths, Noise Levels and Quality. *Remote Sensing of Environment*, 7: 163-176.
- CAMP, V.E., (1984)**, Island Arcs and their Role in the Evolution of the Western Arabian Shield. *Geological Society of America Bulletin*, 95: 913-921.
- CANAS, A.C., and BARNETT, M.E., (1985)**, The Generation and Interpretation of False-Colour Composite Principal Component Images. *International Journal of Remote Sensing*, 6: 867-881.

- CARDAMONE, P., CASNEDI, R., CASSINS, G., CASSINIS, R., MARCOLONGO, B., and TONELLI, A., (1976),** Study of Regional Linears in Central Sicily by Satellite Imagery. *Tectonophysics*, 33: 81-96.
- CASTLEMAN, K.R., (1979),** Digital Image Processing. (New Jersey : Hall International Inc.) 429p.
- CELENK, M., (1991),** Colour Image Segmentation by Clustering, In: *IEEE Proceedings - Computers and Digital Techniques*, 1991, 138: 368-376.
- CHASSERY, J.M., and GARBAY, C., (1984),** An Interactive Segmentation Method based on Contextual Colour and Shape Criterion. In: *Proceedings of 7th International Conference on pattern Recognition*, 1984, 642-644.
- CHAVEZ, P.S., (1988),** An Improved Dark-Object Subtraction Technique for Atmosphere Scattering Correction of Multispectral Data. *Remote Sensing of Environment*, 24: 459-479.
- , **P.S., (1992),** Comparison of Spatial Variability. In *Visible and Near-Infrared Spectral Images. Photogrammetric Engineering and Remote Sensing*, 58: 957-964.
- CHAVEZ, P.S., and BEUER, B., (1982),** An Automatic Optimum Kernel-Size Selection Technique for Edge Enhancement. *Remote Sensing of Environment*, 12: 23-38.
- CHAVEZ, P.S., BERLIN, G.L., and SOWERS, L.B., (1982),** Statistical Method for Selecting Landsat MSS Ratios. *Journal of Applied Photographic Engineering*, 8: 23-30.
- CHAVEZ, P.S., and KWARTENG, A.Y., (1989),** Extracting Spectral Contrast in Landsat Thematic Mapper Image Data Using Selective Principal Component Analysis. *Photogrammetric Engineering and Remote Sensing*, 55: 339-348.
- CHOO, A.P., MAEDER, A.J., and PHAM, B., (1990),** Image Segmentation for Complex Scenes. *Image and Vision Computing*, 8: 155-163.
- COCHRANE, G.R., and TIANFENG, W., (1983),** Interpretation of Structural Characteristics of the Taupo Volcanic Zone New Zealand from Landsat Imagery. *International Journal of Remote Sensing*, 41: 111-128.
- COLLWELL, R.M. (Ed.), (1982),** Manual of Remote Sensing. (Falls Church: American Society of Photogrammetry), 2440p.
- COMPANY PROFILE, (1990),** Laserscan System Data Capture in the 90's, *Mapping Awareness*, 4: 45-47.

- CONDIT, C.D., and CHAVEZ, P.S., (1979), Basic Concepts of Computerised Digital Image Processing for Geologists. *U.S. Geological Survey Bulletin* 1462, 16p.
- CONNERS, R.W., and HARLOW, C.S., (1980), Theoretical Comparison of Texture Algorithms. *IEEE Transaction on Pattern Analysis and Machine Intelligence PAMI-2*: 205-223.
- CRACKNELL, A., and HAYES, L. (1991), *Introduction to Remote Sensing*. (London: Taylor and Francis), 293p.
- CRIPPEN, R.E., (1987), The Regression Intersection Method of Adjusting Image Data for Band Ratioing. *International Journal of Remote Sensing*, 8: 137-155.
- , (1988), The Dangers of Under-Estimating the Importance of Data Adjustments in Band Ratioing. *International Journal of Remote Sensing*, 9: 767-776.
- CROSS, A.M., (1988), Detection of Circular Geological Features Using the Hough Transform. *International Journal of Remote Sensing*, 9: 1519-1528.
- CROSS, A., and MASON, D.C. (1985), Segmentation of Remotely-Sensed Images by a Split-and-Merge Process. In: *Proceedings of International Conference of Remote Sensing Society on Advanced Technology for Monitoring and Processing Global Environmental Data*. London, 1985, 177-185.
- CROSS, A., MASON, D.C., and DURY, S.J., (1988), Segmentation of Remotely-Sensed Images by a Split-and-Merge Process. *International Journal of Remote Sensing*, 9: 1329-1345.
- CROSS, A., and WADGE, G., (1988), Geological Lineaments Detection Using the Hough Transform. In: *Proceedings of IGARSS'88 Symposium, Moving Toward 21st Century*, Edinburgh, 1988, 1779-1782.
- CROSTA, A.P., and MOORE, J.M., (1989), Geological Mapping Using Landsat Thematic Mapper Imagery in Almeria Province, South-East Spain. *International Journal Remote of Sensing*, 10: 505-514.
- CSILLAG, F., (1982), Significance of Tectonics in Linear Feature Detection and Interpretation on Satellite Images. *Remote Sensing of Environment*, 12: 235-245.
- CURRAN, P.L., (1985), *Principles of Remote Sensing, Scientific and Technical*, (London : Longman), 282p.
- CZAKO, T., (1981), Structural Analysis of Western Hungary. *Advance Space Research* 1: 237-247.

- DAVIS, P., and BERLIN, G.L., (1989),** Rock Discrimination in the Complex Geologic Environment of Jabal Salma, Saudi Arabia, using Landsat Thematic Mapper Data. *Photogrammetric Engineering and Remote Sensing*, 55: 1147-1160.
- DAVIS, P., and GROLIER, M.J., (1984),** Discrimination of Granitoids and Mineralised Granitoids in the Midyan Region, North-Western Arabian Shield, Saudi Arabia by Landsat MSS Data Analysis. In: *Proceedings of International Symposium on Remote Sensing of Environment, 3rd Thematic Conference, Remote Sensing for Exploration Geology, Colorado, 1984:* 361-373
- DAVIS, P., BERLIN, G.L. and CHAVEZ, P.S., (1987),** Discrimination of Altered Basaltic Rocks in the South Western United States by Analysis of Landsat Thematic Mapper Data. *Photogrammetric Engineering and Remote Sensing*, 53: 45-55.
- DIKKERS, A.J., (1977),** Sketch of a Possible Lineament Pattern in Northwest Europe. *Geologie en Mijnbouw*, 556: 275-285 GM.
- DIXON, T.H. and GOLOMBEK, M.P., (1988),** Late Precambrian Crustal Accretion Rates in North East Africa and Arabia. *Geology*, 16: 991-994.
- DOZIER, J., and FREW, J. (1981),** Atmospheric Corrections to Satellite Radiometric Data Over Rugged Terrain. *Remote Sensing of Environment*, 11: 191-205.
- DUDA, R.O., and HART, P.E., (1972),** Use of the Hough Transformation to Detect Lines and Curves in Pictures. *Graphic and Image Processing*, 15: 11-15.
- DUNCAN, I.J., RIVARD, B., ARVIDSON, R.E., and SULTAN, M., (1990),** Structural Interpretation and Tectonic Evolution of a Part of The Najd Shear Zone (Saudi Arabia) Using Landsat Thematic Mapper Data. *Tectonophysics*, 178: 309-335.
- DUTRA, L.V., and MASCARENHAS, D.A., (1984),** Some Experiments with Spatial Features Extraction Methods in Multispectral Classification. *International Journal of Remote Sensing*, 5: 303-313.
- DRURY, S.A., (1985),** Applications of Digital Image Enhancement in Region Tectonic Mapping of South India. In: *Proceedings 18th International Symposium: Remote Sensing Environment, Paris, 1985, 1895-1904.*
- **(1986),** Geological Structures on Landsat TM Images of Southern Britain. In: *Proceedings ISPRS/Remote Sensing Society Symposium, Mapping from Modern Imagery, Edinburgh, 1986, 710-718.*

- (1987), *Image Interpretation in Geology*, (London: Allen & Unwin), 243p.
- DRURY, S.A. and HUNT, G.S., (1989)**, Geological Uses of Remotely Sensed Reflected and Emitted Data of Lateritised Archaean Terrain in Western Australia. *International Journal of Remote Sensing*, 10: 475-497.
- EHRICH, R.W., (1976)**, Detection of Global lines and Edges in Heavily Textured Images. In: *Proceedings of the Second International Conference on Basement Tectonics*. Newark, Delaware, 1976, 508-513.
- EKREN, E.B., (1984)**, Geology of the Precambrian Rocks of the Ha'il Quadrangle, Sheet 27E, Kingdom of Saudi Arabia, Open-File Report. *USGS-of-04-15*, Jiddah, Saudi Arabia: Deputy Ministry of Mineral Resources.
- EKREN, E.B., VALSET, D., and BERTHIOUX, A., (1987)**, Explanatory Notes to the Geologic Map of the Ha'il Quadrangle, Sheet 27E, Kingdom of Saudi Arabia. *Geoscience Map GM-115C*. Kingdom of Saudi Arabia: Deputy Ministry of Mineral Resources.
- ELACHI, C., (1987)**, *Introduction to the Physics and Techniques of Remote Sensing*. (New York: John Wiley and Sons), 413p.
- ELLIMAN, D.G., and LANCASTER, I.T., (1990)**, A Review of Segmentation and Contextual Analysis Techniques for Text Recognition, *Pattern Recognition*, 23: 337-346.
- EL SHAELY, H., (1987)**. Discrimination of Geological Features Using Digital and Photographic Enhancements of Landsat Multispectral Scanner Data. *Journal of African Earth Sciences*, 6: 119-126.
- ENGEL, A.E., DIXON, T.H., and STERN, R.J., (1980)**, Late Precambrian Evolution of Afro-Arabian Crust from Ocean Arc to Craton. *Geological Society of America Bulletin*, 91: 699-706.
- ENGEL, J.L., and WEINSTEIN, O., (1982)**, The Thematic Mapper, In: An Overview. *International Geoscience and Remote Sensing Symposium, Munich, 1982 (Digest: New York Institute of Electrical and Electronics Engineering)*, 1: 1.1-1.7.
- ESTES, J.E., HAJIC, E.J., and ATINNEY, C.R., (1983)**, Fundamentals of image analysis of visible and Thermal Infrared data. In: R.N. Colwell (Ed), *Manual of Remote Sensing (2nd Edition)*, (Falls Church: American Society of Photogrametry), 1053-1054.

- EXCELL, P.S., CAMPBELL, DODD, A., NEWBY, S., and STEVENS, R., (1989),** Classification of Quasi-Periodic Textures in Thematic Mapper Scenes Using Fourier Transforms. In: *Proceedings of 15th Annual Conference of the Remote Sensing Society, Bristol, 1989, 123-128.*
- FIELDING, E.J., (1985),** Lithologic Discrimination of Volcanic and Sedimentary Rocks by Spectral Examination of Landsat TM Data from the Puma, Central Andes Mountains. In: *Proceedings of Fourth Thematic Conference: Remote Sensing for Exploration Geology, California, 1985, 619-630.*
- FORST, R.T., (1977),** Tectonic Patterns in the Danish Region - as Deduced from a Comparative Analysis of Magnetic, Landsat, Bathymetric and Gravity Lineaments, *Geologie en Mijnbouw*, 56: 351-362.
- FRANKLIN, S.E., (1989a),** Ancillary Data Input Satellite Remote Sensing of Complex Phenomena. *Computers and Geosciences*, 15: 799-808.
- **(1989b),** Spectral Texture for Improved Class Discrimination in Complex Terrain. *International Journal of Remote Sensing*, 18: 1437-1443.
- **(1990),** Classification of SPOT HRV Imagery and Texture Features. *International Journal of Remote Sensing*, 11: 551-556.
- FRANKLIN, S.E., and PEDDLE, (1987),** Texture Analysis of Digital Image Data Using Spatial Co-Occurrence. *Computers and Geosciences*, 13: 293-311.
- **(1989),** Spectral Texture for Improved Class Discrimination Complex Terrain. *International Journal of Remote Sensing*, 10: 1437-1443.
- FRANKLIN, S.E. and WILSON, B.A., (1991),** Spatial and Spectral Classification of Remote Sensing Imagery. *Computers and Geosciences*, 17: 1551-1172.
- FRANKLIN, S.E., PEDDLE, D.R., and MOULTON, J.E., (1989),** Spectral /Gemorphometric Discrimination and Mapping of Terrain: A Study in Grosmorne National Park. *Canadian Journal of Remote Sensing*, 15: 28-42.
- GALLOWAY, M.M., (1975),** Texture Analysis Using Grey Level Run Lengths. *Computer, Graphic Image Process*, 4: 172-179.
- GASS, I.G., (1977),** The Evolution of The Pan African Crystalline Basement in N.E. Africa and Arabia. *The Geological Society of London*, 134: 129-138.

- , (1981), Pan African (Upper Proterozoic) Plate Tectonics of the Arabian-Nubian Shield. In: A. Krömer (Ed.) *Precambrian Plate Tectonics*, (Amsterdam: Elsevier Scientific Publishing Co.), 387-405.
- GERBRANDS, J.J., and BACKER, E., (1988), Split and Merge Segmentation of SLAR-Imagery: Segmentation Consistency. In: *Proceedings of IGARSS'88 Symposium Moving Toward the 21st Century*, Edinburgh, 1988: 284-286.
- GILMOUR, T., (1987), Image Smoothing as an Aid to Classification. In: *Proceedings Annual Conference of Remote Sensing Society, Advances in Digital Image Processing*, Nottingham, 1987, 55-64.
- GOETZ, A.F.H., (1989), Spectral Remote Sensing in Geology. In: (G.Asrar, Ed). *Theory and Applications of Optical Remote Sensing*. (New York: John Wiley & Sons), 491-525.
- GOETZ, A.F.H., and ROWAN, L.C., (1981), Geological remote Sensing, *Science*, 211: 781-791.
- GOETZ, A.F.H., ROCK, B.N., and ROWAN, L.C., (1983), Remote Sensing for Exploration: An Overview. *Economic Geology*. 78: 573-590.
- GOLD, D.P., (1980), Structural Geology. In: B.S. Seigal, and A.R. Gillespie, (Eds), *Remote Sensing in Geology*, (New York: Wiley), 419-484.
- GONZALEZ, R.C., and WINTZ, P., (1987), *Digital Image Processing*, (2nd Edition). New York: Addison Wesley.
- GORDON, D.K., PHILIPSON, W.R., (1986), A Texture Enhancement Procedure for Separating Orchard From Forest in Thematic Mapper Data. *International Journal of Remote Sensing*, 8: 301-304.
- GREENBAUM, D., (1987), Lithological Discrimination in Central Snowdonia Using Airborne Multi-Spectral Scanner Imagery. *International Journal of Remote Sensing*, 8: 799-816.
- GUHA, P.K., and MALLICK, S.B., (1985), Digital MSS and Spectral Reflectance Data in Lithological Discrimination. *ITC Journal*, 1: 42-46.
- GUO, L.J., (1991), Balance Contrast Enhancement Techniques and its Application in Image Colour Composition. *International Journal of Remote Sensing*, 12: 2133-2151.
- GUPTA, R.P. (1991), *Remote Sensing Geology*. (New York, Springer-Verlag), 356p.

- GURNEY, C.M., (1980),** Threshold Selection for Line Detection Algorithms. *IEEE Transaction Geoscience Remote Sensing*, 18: 204-211.
- GURNEY, C.M., and TOWNSHEND, J.R., (1983),** The Use of Contextual Information in the Classification of Remotely Sensed Data. *Photogrammetric: Engineering and Remote Sensing*, 49: 55-64.
- HALBOUTY, M.T., (1976),** Application of Landsat Imagery to Petroleum and Mineral Exploration. *American Association Petroleum Geologists Bulletin*, 60: 745-793.
- HANSON, A.R., and RISEMAN, E.M. (1978),** (Eds.) *Computer Vision, Systems*, (New York: Academic Press).
- HARALICK, R.M. (1979),** Statistical and Structural Approaches to Texture. In: *Proceedings of the IEEE*, 67: 786-804.
- , (1980), Edge and Region Analysis of Digital Image Data. *Computer Graphics and Image Processing*, 12: 50-73.
- , (1986), Statistical Image Texture Analysis, In: (T.Y. Young and K.S. Fu, Eds.), *Handbook of Pattern Recognition and Image Processing*, New York: Academic Press, 247-280.
- HARALICK, R.M., and LEE, J.S. (1990),** Context Dependent Edge Detection and Evaluation. *Pattern Recognition*, 23: 1-19.
- HARALICK, R.M., and SHANMUGAM, K.S. (1974),** Combined Spectral and Spatial Processing of ERTS Imagery Data. *Remote Sensing of Environment*, 3: 3-13.
- HARALICK, R.M. and SHAPIRO, L.G., (1985),** Image Segmentation Techniques, *Computer Graphics and Image Processing*, 29: 100-132.
- HARALICK, R.M., SHANMUGAM, K., and DINSTEN, I., (1973),** Textural Features for Image Classification. *IEEE Transactions on Systems, Man and Cybernetics*, 3: 610-621.
- HARRIS, R., (1980),** Spectral and Spatial Image Processing for Remote Sensing. *International Journal of Remote Sensing*, 1: 361-375.
- , (1985), Contextual Classification Post-Processing of Landsat Data Using a Probabilistic Relaxation Model. *International Journal of Remote Sensing*, 6: 847-866.
- , (1987), *Satellite Remote Sensing: An Introduction* (London: Routledge and Kegan Paul), 220p.

- HARTL, P.H. (1976)**, Digital Picture Processing. In: (E.Schanda, Ed.), *Remote Sensing for Environmental Sciences*, 304-367.
- HAWKINS, J.K. (1970)**, Texture Properties for Pattern Recognition. In: B.S. Lipkin and A. Rosenfield, (Eds.) *Picture Processing and Psychopictorics* 347-361.
- HJORT, N.L., and MOHN, E. (1984)**, A Comparison of Some Contextual Methods in remote Sensing Classification. In: *Proceedings of The 18th International Symposium on Remote Sensing of Environment*, Paris, 1984, 1693-1703.
- HJORT, N., MOHN, E., and STORVIK, (1986)**, A simulation Study of Some Contextual Classification Methods for Remotely Sensed Data. In: *Proceedings of IGARSS86 Symposium*, Zurich, 1986, ESA SP254: 541-545.
- HOBBS, W.H. (1904)**, Lineaments of the Atlantic Border Region. *Geological Society American Bulletin*, 15: 483-506.
- HOBBS, B.E., MEANS, W.D., and WILLIAMS, P.F. (1976)**, *An Outline of Structural Geology*. (New York: John Wiley & Sons), 571p.
- HORD, R.M., (1982)**, *Digital Image Processing of Remotely Sensed Data*. (New York: Academic Press), 256p.
- (1986)**, *Remote Sensing: Method and Application*. New York: John Wiley and Sons), 362p.
- HSU, S. (1977)**, Texture Tone Feature Extraction and Analysis, Rome Air Development Center Airforce Base Systems Command, Rome, (New York: RADC-TR): 77-279.
- (1978)**, Texture Tone Analysis for Automated Land Use Mapping. *Photogrammetric Engineering and Remote Sensing*, 44: 1393-1404.
- (1980)**, Texture Perception and the RADC/HSU Texture Feature Extractor. *Photogrammetric Engineering and Remote Sensing*, 46: 1051-1058.
- (1986)**, Rock Type Discrimination with AI-Based Texture Analysis Algorithms. In: *Proceedings of Annual Meeting of ASPRS/AGSM*, (Washington), 1986, 169-178.
- HUNT, G.A., (1977)**, Spectral Signatures in Particular Minerals in the Visible and Near-infrared. *Geophysics*, Vol. 42, 501-513.
- (1979)**, Near-Infrared (1.3-2.4 $\mu$ m) Spectra of Alteration Minerals: Potential for use in Remote Sensing. *Geophysics*, 44: 1974-1986.

- , (1980), Electromagnetic Radiation: The Communication Link in Remote Sensing. In: B.S. Siegal, A.R. Gillespie (Eds). *Remote Sensing in Geology*, (New York: John Wiley & Sons), 5-45.
- HUNT, G.A., DRURY, S.A., and ROTHERY, D. (1986)**, Technique for Choosing the Optimum Thematic Mapper Channel Combinations for Lithological Mapping in Semi-arid Terrains. In: *Proceedings of ASPRS/Remote Sensing Society Symposium, Mapping for Modern Imagery*, Edinburgh, 1986, 637-647.
- HUNT, G.R., and ASHLEY, R.P., (1979)**, Spectra of Altered Rocks in the Visible and Infrared. *Economic Geology*, 74:1613-1629.
- HUNT, G.R. and SALISBURY, J.W., (1970)**, Visible and Near-Infrared Spectra of Minerals and rocks: I Silicate Minerals. *Modern Geology*, 1: 283-300
- , (1971), Visible and Near-Infrared Spectra of Minerals and Rocks:II Carbonates. *Modern Geology*, 2:23-30.
- , (1976a), Visible and Near Infrared Spectra of Minerals and Rocks: XI. Sedimentary Rocks. *Modern Geology*, 5: 211-217.
- , (1976b), Visible and Near Infrared Spectra of Minerals and Rocks: XII. Metamorphic Rocks. *Modern Geology*, 5: 219-228.
- HUNT, G.R. SALISBURY, J.W., and LENHOFF, C.J., (1971)**, Visible and Near-Infrared Spectra of Minerals and Rocks: III Oxides and Hydroxides. *Modern Geology*, 2: 195-205.
- (1974), Visible and Infrared Spectra of Minerals and Rocks: IX Basic and Ultrabasic Igneous Rocks. *Modern Geology*, 5: 15-22.
- HUNTINGTON, J.F. and RAICHE, A.P., (1978)**, A Multi-Attribute Method for Comparing Geological Lineament Interpretations. *Remote Sensing of Environment*, 7: 145-161.
- IRANPANAH, A., (1989)**, Thematic Mapping of Basement-Related Cross-Strike Structural Discontinuities and their Relationship to Potential Oil-Bearing Structures. *Photogrammetric Engineering and Remote Sensing*, 46: 225-229.
- IRANPANAH, A., and ESFANDIARI, B., (1980)**, Interpretation of Structural Lineaments Using Landsat-1 Images. *Photogrammetric Engineering and Remote Sensing*, 46:225-229.
- IRONS, J.R. and PETERSEN, G.W., (1981)**, Texture Transforms of Remote Sensing Data. *Remote Sensing of Environment*, 11: 359-370.

- ISIORHO, S.A., (1984),** Radar Geology in the Shelleng-Numam area in Nigeria. An Evaluation. *International Journal of Remote Sensing*, 5: 519-531.
- JENSEN, J.R., (1986),** *Introductory Digital Image Processing. A Remote Sensing Perspective.* (New Jersey: Elgewood Cliffs), 379p.
- JOHARI, A.M., (1990),** Digital Processing of Satellite Images for Geological Applications with Examples from North-East Scotland and North-West Malaysia. Unpublished Ph.D. Thesis, University of Stirling.
- JOHNSTONE, J.E., MILLER, R.L. and ENGLUND, K.J. (1975),** Applications of Remote Sensing to Structural Interpretations in the Southern Appalacian. *Journal Research, U.S. Geological Survey*, 3: 285-293.
- JOHNSON, M.R., and FROST, R.T., (1977),** Fault and Lineament Patterns in the Southern Highlands of Scotland, *Geologie en Mijbouw* 56: 287-294
- JONES, A.R., (1984),** Applicability of Digital Satellite Imagery for Gemorphological Mapping in Arid Region. In: *Proceedings od Annual 10th Anniversary International Conference of the Remote Sensing Society, Satellite Remote Sensing Review and Preview, Reading, 1984*, 351-359.
- KAHLE, A.B., and ROWAN, L.C. (1980),** Evaluation of Multi-Spectral Middle Infrared Aircraft Images for Lithologic Mapping in the East Tintic Mountains, Utah. *Geology*, 8: 234-239.
- KARSSEMEIJER, N. (1990),** A Relaxation Method for Image Segmentation Using a Spatially Dependent Stochastic Model. *Pattern Recognition Letters*, 11: 13-23.
- KARTIKEYAN, B., and SARKAR, A., (1989),** A Unified Approach for Image Segmentation Using Exact Statistics. *Computer Vision, Graphics and Image Processing*, 48: 217-229.
- KAUFMANN, H., (1988),** Mineral Exploration Along the Agaba-Levant Structure by use of TM Data Concept, Processing and Results. *International Journal of Remote Sensing*, 9: 1639-1658.
- KAUFMANN, H., and PFEIFER, B., (1988),** Image Optimisation Versus Classification - An Application Oriented Comparison of Different Methods by Use of Thematic Mapper Data. *Photogrammetria (PRS)*, 42: 311-324.

- KEPPER, J.C., LUGASKI, T.P., and MacDONALD, J.S. (1986),** Discrimination of Lithologic Units, Alteration Patterns and Major Structural Blocks in Tonopah, Nevada Area Using Thematic Mapper Data. In: *Proceedings 5th Thematic Conference: Remote Sensing for Exploration Geology*, Reno, Nevada, 1986, 97-101.
- KIM, S.K., (1979),** Analysis of Lineaments Extracted from Landsat Images of the Korean Peninsula. *Journal of Earth Science*, Nugoya University : 26/27: 49-74.
- KITTLER, J., and FÖGLEIN, J., (1983),** A General Contextual Classification Method for Image Segmentation. In: *Proceedings of 3rd Conference on Image Analysis*, Copenhagen, 1983, 90-95.
- , (1984), Contextual Classification of Multispectral Pixel Data. *Image and Vision Computing*, 2:13-29.
- KRISHNAPURAM, R., and MUNSHI, A., (1991),** Cluster-Based Segmentation of Range Images using Differential-Geometric Features. *Optical Engineering*, 30: 1468-1478.
- KRUSE, F.A., (1986),** Digital Mapping of Alteration Zones in a Hydrothermal System Using Landsat Thematic Mapper Data: An Example from the Northern Grapevine Mountains, Nevada, California. In: *Proceedings of 5th Thematic Conference: Remote Sensing for Exploration Geology*, Reno, Nevada, 1986, 393.
- LAKE, S.D., MUNDAY, T.J. and DEWEY, J.F., (1984),** Lineament Mapping and analysis in the Wessex Basin of Southern England: A Comparison between MSS and TM Data. In: *Proceedings of Annual Conference of Remote Sensing Society, Satellite Remote Sensing Review and Preview*, Reading, 1984, 361-374.
- LAPORTE, J.M., (1983),** Texture Analysis on SPOT Simulations, *Proceedings of 17th International Symposium on Remote Sensing of Environment*. 1243-1252.
- LEES, R.D., LETTIS, W.R., and BERNSTEIN, R. (1985),** Evaluation of Landsat Thematic Mapper for Geologic Applications. In: *Proceedings of the IEEE*, 73: 1108-1117.
- LEO, G.W., (1984),** Reconnaissance Geology of Al Awshaziyah Quadrangle, Sheet 26/41B, Kingdom of Saudi Arabia: Saudi Arabian Deputy Ministry for Mineral Resources Open File Report USGS-OF-04-33, 29p.

- LEO, G.W., (1986)**, Geochemical Reconnaissance of Late Proterozoic Volcanic and Mafic Plutonic Rocks of Al Awshaziyah Quadrangle and Related Rocks in the Qufar Quadrangle, Northern Arabian Shield. *U.S. Geological Survey Bulletin*, 1680, 16p.
- LEWIS, A., (1978)**, Geoscience Application of Imaging Radar Systems: *Remote Sensing of the Electromagnetic Spectrum*, 3: 152p.
- LILLESAND, T.M. and KIEFER, R.W., (1987)**, *Remote Sensing and Image Interpretation* (2nd Edition). (New York: John Wiley and Sons). 721p.
- LO, C.P. (1987)**, *Applied Remote Sensing*. (New York: Longman Scientific and Technical), 393p.
- LOUGHLIN, W.P., (1991)**, Principal Component Analysis for Alteration Mapping, *Photogrammetric Engineering and Remote Sensing*, 57: 1163-1169.
- LOUGHLIN, W.P., and TAWFIQ, M.S., (1985)**, Discrimination of Rock Types and Alteration Zones from Airborne MSS Data: The Samran-Shayban and Mahd Adh-Dhab Areas of Saudi-Arabia. In: *Proceedings, International Symposium on Remote Sensing of Environment, 4th Thematic Conference, Remote Sensing for Exploration Geology*, California, 1985, 207-225.
- LYON, R.J.P., (1965)**, Analysis of Rocks by Spectral Infrared Emission (8-25) 241  $\mu\text{m}$ . *Economic Geology*. 60: 715-736.
- McBRIDE, J.H. FIELDING, G.J., and ISACKS, B.L., (1986)**, Discrimination and Supervised Classification of Volcanic Flows of the Puna-Altiplano Central Mountains Using Landsat TM Data. In: *Proceedings of Fifth Thematic Conference: Remote Sensing for Exploration Geology*, Reno, Nevada, 1986, 693-699.
- MACDONALD, H.C., (1976)**, Operation and Characteristics of Imaging Radar Systems. In: (A.J. Lewis (Ed.), *Geoscience Applications of Imaging Radar Systems*, 3: 23-45.
- MAGEE, R.W., MOORE, J.M., and BRUNNER, J., (1986)**, Thematic Mapper Data Applied to Mapping Hydrothermal Alteration in Southwest New Mexico. In: *Proceeding, 5th Thematic Conference: Remote Sensing for Exploration Geology*, Reno, Nevada, 1986, 373-380.
- MALAN, O.G., ERASMUS, P.F., and FOURIE, C., (1989)**, Spectral Contextual Classifications of SPOT and Landsat TM Data for Analysis of the Johannesburg Urban Area. *Advance Space Research*, 9: (1)121-(1)124.

- MARINO, C.M. and TIBALDI, A., (1988),** Computer Processing of Satellite Data for Geological Structural Zoning of a Collisional Boundary, Significance and Field Cracks: The Example of Tunisia. *Geocarto International*, 1: 13-28.
- MARRS, R.W., and RAINES, G.L., (1984),** Tectonic Framework of Powder Basin, Wyoming and Montana, Interpreted from Landsat Imagery. *American Association of Petroleum Geologists Bulletin*, 68: 1718-1731.
- MASON, D.C., CARR, D.G., CROSS, A., HOGG, D. and TAILOR, A., (1986),** Knowledge-Based Segmentation of Remotely Sensed Images. In: *Proceedings of the International Symposium, Remote Sensing Society, Mapping from Modern Imagery*, Edinburgh: 501-510.
- MASON, D.C., CARR, D.G., CROSS, A., HOGG, D.C., LAWRENCE, D.H., PETROU, M., and TAILOR, A., (1987),** Progress Toward a Knowledge-Based Segmentation System for Remotely Sensed Images. In: *Proceedings of 13th Annual Conference of the Remote Sensing Society, Advance in Digital Processing* Nottingham, 1987, 99-111.
- MATHER, P.M., (1987),** *Computer Processing of Remotely Sensed Images, An Introduction*, (New York: John Wiley and Sons), 352p.
- MAUDE, R., (1987),** Lineaments in Enhanced Landsat Images from a Portion of West Wales. *Geological Journal*, 22: 107-118.
- MESTER, R., and FRANKE, (1988),** Statistical Model Based Image Segmentation Using Growing, Contour Relaxation and Classification. *Visual Communication and Image Processing: SPIE* 1001: 616-625.
- MILGRAM, D.L. and ROSENFELD, A., (1981),** Object Detection in Infrared Images. In: L.Bolc and Z.Kupla (Eds). *Digital Image Processing Systems*, (New York: Springer-Verlag), 228-235.
- MOLNAR, A., and TAPPORNIER, P., (1975),** Cenozoic Tectonics of Asia: Effects of a Continental Collision. *Science*, 89: 419-426.
- MOORE, G.K. and WALTZ, F.A., (1983),** Objective Procedures for Lineament Enhancement and Extraction. *Photogrammetric Engineering and Remote Sensing*, 49: 641-647.
- MOORE, J.D., and HINKLE, F., (1977),** High-Yield Wells and Springs along Lineaments Interpreted from Landsat Imagery in Madison County, Alabama, U.S.A. In: J.S. Jolson and F.L. Doyle (Eds.) *Karst Hydrogeology*, , 447-486.

- MOORE, J.M., (1976),** A Major Lineament in the Arabian Shield and its Relationship to Mineralisation. *Mineral Deposita*, 11: 323-328.
- , (1979), Tectonics of the Najd Transcurrent Fault System, Saudi Arabia. *Journal Geological Society of London*, 136: 5441-454.
- MUERLE, J.L., (1970),** Some Thoughts on Texture Discrimination by Computer. In: B.S. Lipkin and A. Rosenfield (Eds). *Picture Processing and Psychopictorics*. (New York: Academic Press), 371-379.
- NAKAGAWA, Y., and ROSENFELD, T., (1979),** Some Experiments on Variable Thresholding, *Pattern Recognition*, 11: 191-204.
- NARENDA, P.M., and GOLDBERG, M., (1980),** Image Segmentation with Directed Trees. *IEEE Transaction PAM* 1-2: 185-191.
- NEVATIA, R., (1978),** Characterisation and Requirements of Computer Vision Systems. In: A. Hanson and E. M. Riseman, (Eds) *Computer Vision Systems*. (New York: Academic Press), 81-85.
- , (1986), Image Segmentation. In: T.Y. Young and K.S. Fu, (Eds.) *Handbook of Pattern Recognition and Image Processing*. (New York: Academic Press), 215-231.
- NEVATIA, R., and BABU, K.R., (1979),** Linear Feature Extraction and Description. In: *Proceedings of 6th IJCAI, Tokyo*, 2: 639-641.
- , (1980), Linear Feature Extraction and Description, *Computer Graphics Image Processing*, 13 : 257-267.
- NIBLACK, W., (1986),** *An Introduction to Digital Image Processing*. (Prentice-Hall International). 200p.
- O'CONNOR, K.L., (1988),** Image Segmentation Through Optimal Tessellation. Unpublished Ph.D. Thesis, Imperial College, London.
- ODDY, C.J., and RYE, A.J., (1983),** Segmentation of SAR Images Using a Local Similarity Rule. *Pattern Recognition Letters*, 1: 443-449.
- OFFIELD, T.W., ABBOTT, E.A., GILLESPIE, A.R., and LOGUERCIO, S.O., (1977),** Structure Mapping on Enhanced Landsat Images of Southern Brazil: Tectonic Control of Mineralisation and Speculation on Metallogeny. *Geophysics*, 42: 482-500.

- O'LEARY, D.W., FRIEDMAN, J.D., and PHON, H.A., (1976),** Lineament Linear Lineation. Some Proposed New Standards for Old Terms. *Geological Society of America Bulletin*, 87: 1463-1469.
- OLDFIELD, R.B., (1988),** Lithological Mapping of Northwest Argentine with Remote Sensing Data Using Tonal, Textural and Contextual Features. Unpublished Ph.D. Thesis, Aston University.
- OLDFIELD, R.B. and ELGY, J., (1987),** Geological Mapping from Remotely Sensed Data Using Tonal, Textural and Contextual Features. In: *Proceeding Annual Conference of Remote Sensing Society, Advances in Digital Image Processing*, Nottingham, 1987, 533-536.
- O'NEILL, J.M., and FERRIS, D.C., (1985),** Reconnaissance Geology of Ar Rawdh Quadrangle, Sheet 26/40D, Kingdom of Saudi Arabian Deputy Ministry for Mineral Resources Open File Report, *USGS-OF-05-3*, 24p.
- PAL, S.K., PAL, N.R., (1987),** Segmentation using Contrast and Homogeneity Measures. *Pattern Recognition Letters*, 5: 293-304.
- PAPPAS, T.N., (1992),** An Adaptive clustering Algorithm for Image Segmentation. *IEEE Transactions on Signal Processing*, 40: 901-914.
- PAPPAS, T.N., JAYANT, N.S., (1989),** An Adaptive Clustering Algorithm for Image Segmentation. In: *IEEE Proceedings*, 1989, 1667-1670.
- PARSON, A.J., and YEARLEY, R.J., (1986),** An Analysis of Geologic Lineaments Seen on Landsat MSS Imagery. *International Journal Remote Sensing*, 7: 1778-1782.
- PATEL, N., and RAMPAL, K.K., (1992),** Discrimination of Rock Types Using Landsat Thematic Mapper Data. *Advance Space Research*, 12: (7), 35-38.
- PAVLIDIDS, T., and LIOW, Y.T., (1990),** Integration Region Growing and Edge Detection. *IEEE Proceedings*, 1990, 72: 795-812.
- PEDDLE, D.R., and FRANKLIN, S.E., (1991),** Image Texture Processing and Data Integration for Surface Pattern Discrimination. *Photogrammetric Engineering and Remote Sensing*, 57: 413-420.

- PETERSOV, A.V., (1992),** Remote Sensing in Geology. In: *Proceedings of the 18th Annual Conference of the Remote Sensing Society. Remote Sensing From Research to Operation.* Dundee, 1992, 129-146.
- PODWYSOCKI, M.H., MOIK, J.G., and SHOUP, W.C., (1975),** Quantification of Geologic Lineament by Manual and Machine Processing Techniques. *NASA Earth Resources Survey Symposium, Houston, Texas.* NASA TM-X-58168, 885-905.
- PODWYSOCKI, M.H., SALISBURY, J.W., BENDER, L.V., JONES, O.D., and MIMMS, D.L., (1983),** Analysis of Landsat-4 TM Data for Lithologic and Image Mapping Purposes. In: *Proceeding, NASA Conference Publication 2326:* 35-39.
- POHN, H.A., (1990),** Lineament Analysis of the Glens Falls 1°x 2° Quadrangle, New York, Vermont and New Hampshire. *US Geology Survey Bulletin 1886:* E1-E6.
- PONTUAL, A., (1987),** The Effect of Weathering Minerals on the Spectral Response of Rocks in Landsat TM Imagery. In: *Proceedings of Annual Conference of Remote Sensing Society Advances in Digital Image Processing.* Nottingham, 1987, 549-558.
- PULTZ, T.J., and BROWN, R.J., (1987),** SAR Image Classification of Agricultural Targets using First and Second Order Statistics. *Canadian Journal of Remote Sensing,* 93: 85-91.
- QARI, M.Y., (1990),** Geological Analysis of Parts of the Southern Arabian Shield Based on Landsat TM Imagery. Unpublished Ph.D. Thesis, University College London.
- QUEGAN, S., and WRIGHT, A., (1984),** Automatic Segmentation Techniques for Satellite-Borne Synthetic Aperture Radar (SAR) Images. In: *Proceedings of the 10th Anniversary International Conference of the Remote Sensing Society, Satellite Remote Sensing review and Preview.* Remote Sensing Society, Reading, 161-167.
- QUICK, J.E., (1983),** Reconnaissance Geology of the Ghazzalah Quadrangle Sheet 26/41A Kingdom of Saudi Arabia, Open File Report 83-331 (Jiddah, Saudi Arabia: Deputy Ministry for Mineral Resources).
- , (1984), Reconnaissance Geology of Zarghat Quadrangle, Sheet 26/40b, Kingdom of Saudi Arabia: Saudi Arabian Deputy Ministry for Mineral Resources Open-File Report USGS-OF-04-28, 37p.

- , (1985), Reconnaissance Geology of the As Sulaymi Quadrangle, Sheet 26/41c, Kingdom of Saudi Arabia: Deputy Ministry for Mineral Resources, Open-File Report USGS-OF-05-18, 50p.
- QUICK, J.E., and DOEBRICH, J.L., (1987), Geology of the Wadi, AS Shu'bah Quadrangle, Sheet 26E, Kingdom of Saudi Arabia, Open-File Report USGS-OF-04-11: Deputy Ministry for Mineral Resources, Jiddah, Saudi Arabia.
- RAKSHIT, A.M. and S.W. AMINATHAN, V.L., (1985), Application of Digitally Processed and Enhanced Landsat Imagery for Geological Mapping and Mineral Targeting in the Sighbum Precambrian Mineralised Belt, Bihar-Orissa. *International Journal of Remote Sensing*, 6: 457-471.
- RAMBERG, I.G., GARBRIELSEN, R.H., LARSEN, B.T., and SOLLI, A., (1977), Analysis of Fracture Patterns in Southern Norway. *Geologie en Mijbouw*, 56: 295-310.
- REDDY R.K., (1991), Digital Analysis of Lineaments - A Test Study on South India. *Computer and Geosciences*, 17:549-559.
- REES, W.G., (1990), Physical Principals of Remote Sensing (New York: Cambridge University Press), 247p.
- REEVES, R.G., (1975), Terrain and Minerals: Assessment and Evaluation. In R.G. Reeves (Ed). (1st Edition) Manual of Remote Sensing, (Falls Church, Virginia: American Society of Pphotogrammetry), 1107-1351.
- RICHARDS, J.A., (1986), *Remote Sensing Digital Image Analysis: An Introduction*. (Berlin: Springer-Verlag).
- RICHASON, B.F., (ED.), (1983), *Introduction to Remote Sensing of the Environment*, (2nd Edition). Iowa: Kindall/Hunt, Iowa, 582p.
- ROAN, S.J., and AGGARNAL, J.K., (1987), Multiple Resolution Imagery and Texture Analysis. *Pattern Recognition*, 20:17-31.
- ROBINSON, J.E., and CARROLL, S., (1977), Software for Geologic Processing of Landsat Imagery. *Computer and Geosciences*, 3: 459-464.
- ROSENFELD, A., (1969), *Picture Processing by Computer* (New York: Academic Press), 196p.
- , (1984), Image Analysis, In: M.P. Ekstrom, (Ed). *Processing Techniques*, (New York: Academic Press), 257-287.

- ROSENFELD, A., and KAKI, A.C., (1976),** *Digital Picture Processing*, (First Edition): (New York: Academic Press) 349p.
- , **and KAKI, A.C., (1982),** *Digital Picture Processing*. (Second Edition) : (Orlando, Florida : Academic Press), 2: 349p.
- ROTHERY, D.A., (1982),** Supervised Maximum Likelihood Classification and Post-Classification Filtering Using MSS Imagery for Lithological Mapping in the Oman Ophiolite. In: *Proceedings of International Symposium on Remote Sensing of Environment, 2nd Thematic Conference: Remote Sensing for Exploration Geology*, Forth Worth, 1982, 417-426.
- , **(1985),** Interactive Processing of Satellite Images for Geological Interpretation: A Case Study, *Geological Magazine*, 122: 57-63.
- , **(1987a),** Decorrelation Stretching and Related Techniques as an Aid to Image Interpretation in Geology. In: *Proceedings of Annual Conference of Remote Sensing Society*, Nottingham, 1987, 194-203.
- , **(1987b),** Improved Discrimination of Rock Units Using Landsat Thematic Mapper Imagery of the Oman Ophiolite. *Journal Geological Society*, London, 144: 587-597.
- ROTHERY, D.A., and DRURY, S.A. (1984),** The Neotectonics of the Tibetan Plateau. *Tectonics*, 3: 19-26.
- ROTHERY, D.A., HUNTER W.M., DRURY, S.A., and HUNT G.A., (1986),** Large Scale Geological Mapping Using Airborne Thematic Mapper Imagery in Western Australia. In: *Proceedings of Annual Meetings of Remote Sensing Society: Mapping From Modern Imagery*, Edinburgh, 1986, 359-368.
- ROMAN, L.C., WETLAUFER, P., GOETZ, A.F., BILLINGSLEY, F. and STEWART, J. (1974),** Discrimination of Rock Types and Detection of Hydrothermally-altered Areas in South-Central Nevada by the use of Computer-enhanced ERTS images, US Geological Survey, Professional Paper No.883, Washington, DC.
- ROMAN, R.L. (1975),** Application of Satellites to Geological Exploration. *American Scientist*, 63: 393-403.
- RYE, A.J., and WRIGHT, A., (1985),** Segmentation: The Extraction of Spatial Information from radar Images. In: *Proceeding of the (International Conference of Remote Sensing Society. Advance Technology for Monitoring and Processing Global Environmental Data*, 1985, 305 -317.

- SABINS, F.F., (1987),** *Remote Sensing - Principals and Interpretation* (2nd Edition, (New York: Freeman and Company), 445p.
- SALISBURY, J.W., and HUNT, G.R. (1974),** Remote Sensing of Rock Type in the Visible and Near-Infrared. In: *Proceedings of 9th International Symposium on Remote Sensing of the Environment: Ann Arbor, Michigan, Environmental Research Institute of Michigan, VIII: 1953-1958.*
- SANTISEBAN, A., and MUNOZ. L., (1978),** Principal Components of Multispectral Image: Application to a Geological Problem. IBM. Research Development, 22: 444-454.
- SARAPH, P.R., INAMDAR, A.B, (1982),** Use of Textural Discrimination Techniques in Landsat Digital Analysis for Physical Feature Identification in Mineralised Zones. In: *Proceedings of International Symposium Remote Sensing of Environment, 2nd Thematic Conference, (Fort Worth), 1982, 977-985.*
- SAXON, E.C., (1984),** Multitemporal Texture Transformed Landsat for Mapping Ecological Gradients. In: *Proceedings of the Third Australian Remote Sensing Conference. Brisbane, Australia, 1984, 255-259.*
- SCHOWENGERDT, R.A., (1983),** *Techniques for Image Processing and Classification in Remote Sensing.* (New York: Academic Press), 249p.
- SEDDON, A.M., and HUNT, G.E., (1985),** Segmentation of Clouds Using Cluster Analysis, *International Journal of Remote Sensing* 6: 717-731.
- SERRA, J., (1982),** *Image Analysis and Mathematical Morphology,* (London: Academic Press). 610 pp.
- SESÖREN, A., (1976),** Lineament Analysis from ERTS (Landsat) Images of the Netherlands. *Geologie en Mijnbouw, 55:612-67.*
- SHEFFIELD, C., (1985),** Selecting Band Combinations from Multispectral Data. *Photogrammetric Engineering and Remote Sensing, 51: 681-687.*
- SHIH, E., and SCHOWENGERDT, (1983),** Classification of Arid Surfaces Using Landsat Spectral and Textual Features. *Photogrammetric Engineering and Remote Sensing, 49: 337-347.*
- SHORT, N.M. (1982),** Landsat Tutorial Workbook, NASA Reference Publication 1078 (Washington: NASA Scientific and Technical Information Branch), 553p.
- SHORT, N.M., and LOWMAN, P.D., (1973),** Earth Observation from

Space: Outlook for the Geological Sciences. NASA TM X-70519, 119p.

**SIEGAL, B.S., and ABRAMS, M.J., (1976),** Geologic Mapping Using Landsat Data. *Photogrammetric Engineering and Remote Sensing*, 42: 325-337.

**SIEGAL, B.S., and GILLESPIE, A.R., (1980),** *Remote Sensing in Geology* (New York: Wiley).

**SIEGAL, H.J., SWAIN, P.H., and SMITH, B.W., (1980),** Parallel Processing Implementations of a Contextual Classification for Multispectral Remote Sensing Data. In: *Proceedings of 1980 Machine Processing of Remotely Sensed Data Symposium*, Purdue, 1980, 19-29.

**SLATER, P., (1989),** *Remote Sensing Optics and Optical Systems* (Reading Mass: Addison-Wesley).

**SKIDMORE, A.K. (1989),** Unsupervised Training Area Selection in Forests Using a Non-parametric Distance Measure and Spatial Information. *International Journal of Remote Sensing*, 10: 133-146.

**SMITH, W.L. (ED.), (1977),** Remote Sensing Application for Mineral Resources. In: W.L. Smith (Ed.), *Remote Sensing Application for Mineral Exploration*, (Stroudsburg: Dowden, Hutchinson and Ross), 300p.

**SPETZ, D.M., TARAMIN, J., and HSU, L.C. (1989),** Differentiating Volcanic Rock Assemblages Using Landsat Thematic Mapper Data. Influence of Petrochemistry and Desert. *Advance Space Research*, 9: 193-198.

**STEFOULI, M., (1983),** The Remote Sensing of Geologic Feature and its Application to the Structure of Crete. Unpublished Ph.D. Thesis, University of Bristol.

**STEFOULI, M., and OSMASTON, H.A., (1984),** The Remote Sensing of Geological Linear Features using Landsat: Matching Analytical Approaches to Practical Applications. In: *Proceedings Remote Sensing Society Annual Conference, Satellite Remote Sensing Review*, Reading, 1984, 227-236.

**STENBERG, S.R., (1983),** Biomedical Image Processing Computer, *IEEE Computer Society*, 16: 22-34.

**STOESER, D.B. and CAMP, V.E., (1985),** Pan-African Microplate Accretion of the Arabian Shield. *Geological Society of America Bulletin*, 96: 817-826.

**SULTAN, M., ARVIDSON, R.E., and STURCHIO, N.C. (1986a),** Digital Mapping of Ophiolite Melange Zones from Landsat Thematic

Mapper (TM) Data in Arid areas Meatiq dom, Egypt. *Geologic Society of America Bulletin*, 18: 766.

-----, (1986b), Mapping of Serpintimites in the Eastern Desert of Egypt by using Landsat Thematic Mapper Data. *Geology*, 14: 995-999.

**SULTAN, M., ARVIDSON, R.E., STURCHIO, N.C., and GUINNESS, E.S., (1987)**, Lithologic Mapping in Arid Regions with Landsat Thematic Mapper Data: Meatiq dom, Egypt. *Geologic Society of America, Bulletin*, 99: 748-762.

**SULTAN, M., ARVIDSON, M., DUNCAN, I.J., STERN, R.J. and ELKALIOUBY, B., (1988)**, Extension of the Najd Shear System from Saudi Arabia to the Central Eastern Desert of Egypt Based in Integrated Field and Landsat Observations. *Tectonics*, 7: 1291-1306.

**SUN, C., and WEE, W.G., (1983)**, Neighbouring Grey Level Dependence Matrix for Texture Classification; *Computer Vision Graphic and Image Processing*, 23: 341-352.

**SWAIN, P.H., SIEGEL, H., and SMITH, B.W., (1979)**, A Method for Classifying Multispectral Remote Sensing Data Using Context. In: *Proceedings of 1979 Machine Processing of Remotely Sensed Data Symposium, Prudue, 1979*. New York. IEEE, 1: 343-353.

**SWAIN, P.H., VARDEMAN, S.B. and TILTON, J.C., (1981)**, Contextual Classification of Multispectral Image Data. *Pattern Recognition*, 13: 429-441.

**TAMURA, H., MORI, S., and YAMAWAKI, (1978)**, Textural Features Corresponding to Visual Perception. *IEEE Transactions on Systems, Man and Cybernetics, SMC*, 8: 460-472.

**TAUD, H., and PARROT, J.F., (1992)**, Detection of Circular Structures on Satellite Images. *International Journal of Remote Sensing*, 13: 319-335.

**TERAUCHI, M., NAJAMACHI, M. ITO, K., and TSUJI, T., (1989)**, Image Segmentation by Local Feature Based Clustering for Understanding Natural Scene. In: *Proceedings of International Workshop Industrial Applications of Machine Intelligence and Vision (MIV-89) Tokyo, 1989*, 124-127.

**TIBALDI, A., and FERRAR, M., (1988)**, Potential of Landsat TM Image for Crystalline Rock Type Discrimination, Gregory Rift, Kenya. *Geocarto International*, 3: 3-12.

**TIWARI, O.N., and JHINGRAN, V., (1991)**, A Comparative Study of Lineament Analysis Techniques for Base Metal Exploration. *Asian-Pacific Remote Sensing Journal*, 3: 39-48.

- TOGLIATTI, G., LECHI, G., and MORIONDO, A. (1988),** Tests of Topographic Mapping with Thematic Mapper Images. *International Journal of Remote Sensing*, 9: 1681-1686.
- TOWNSEND, T.W., (1987),** A Comparison of Landsat MSS and TM Imagery for Interpretation of Geologic Structure. *Photogrammetric Engineering and Remote Sensing*, 53: 1245-1249.
- TOWNSHEND, J.R.G., (Ed)., (1981),** *Terrain Analysis and Remote Sensing.* (London: George Allen and Unwin), 232p.
- TRENDAL, E.E., (1972),** Automatic Terrain Mapping by Texture Recognition. In: *Proceedings of the 8th International Symposium of Remote Sensing.* New York, 1972, 771-776.
- TUNSTALL, K.W., (1975),** Recognising Patterns: Are There Processes That Precede Feature Analysis. *Pattern Recognition*, 7: 95-106.
- VANDERBRUG, G.J., (1977),** Experiments in Interactive Enhancement of Linear Features. *Computer Graphic and Image Processing*, 6: 25-42.
- VILJOEN, R.P., VILOJEN, M.J., GROOTENBOER, J., and LONGSHAW, T.G., (1975),** ERTS-1. Imagery: An Appraisal of Applications in Geology and Mineral Exploration. *Minerals Science Engineering*, 7: 132-168.
- VINCENT, R.K., and SCOTT, G.W., (1978),** Ground Water Exploration in North Western Tamil Naidu, India, with Landsat Data. In: *Proceedings of the 12th International Symposium Remote Sensing of Environment*, 3, 1978: 1053-1060.
- WEDGE, G., and CROSS, A., (1988),** Quantitative Methods for Detecting Aligned Points: An Application to the Volcanic Vents of the Michoucan-Guamajuato Volcanic Field, Mexico. *Geology*, 16, 815-818.
- , (1989), Identification and Analysis of the Alignments of Point-Like Features in Remotely Sensed Imagery: Volcanic Cones in the Pinacate Volcanic Field, Mexico: *International Journal of Remote Sensing*, 10:455-474.
- WANG, J. and HOWARTH, P.J. (1990),** Use of the Hough Transform in Automated Lineament Detection. *IEEE Transaction on Geoscience and Remote Sensing*, 28: 561-565.
- , (1990), A New Statistical Approach for Texture Analysis. *Photogrammetric Engineering and Remote Sensing*, 56: 61-66.

- WANG, J., and HE, D.C., (1991),** Recognition of Lithological Units in Airborne SAR Images Using New Texture Features. In: *Proceedings of International Geoscience and Remote Sensing Symposium - IGARSS'91.* (ESPOO, Finland, 1991), 1701-1705.
- WANG, X., and HAN, Y., (1989),** Determining Soil Cover Percentage by Image Segmentation, In: *Proceedings of IEEE,* 1989, 153-157.
- WATSON, A.I., (1984),** The Physical Basis of Remote Sensing. In: *Proceedings of University of Dundee summer School 'Remote Sensing Applications in Civil Engineering'.* Dundee: 1984, (ESA SP-216), 9-13.
- , (1987), A New Method of Classification for Landsat Data Using the 'Watershed' Algorithm. *Pattern Recognition Letters,* 6: 15-19.
- , (1990), Application of Pattern Recognition to Geological and Soil Thin Section. In: *Proceedings of University of Dundee Summer School,* 1990, 1-8.
- , (1992), Comparison of Classification Methods. In: *Proceedings of the 18th Annual Conference of the Remote Sensing Society, Remote Sensing from Research to Operation,* Dundee, 1992, 539-543.
- WATSON, J.A., VAUGHAN, R.A., and POWELL, M. (1992),** Classification Using the Watershed Method. *International Journal of Remote Sensing,* 13: 1881-1890.
- WESZKA, J.S., DYER, C.R., and ROSENFELD, A., (1976),** A Comparative Study of Texture Measure for Terrain Classification. *IEEE Transaction Systems. Man and Cybernetics* 10: 269-285.
- WHARTON, S.W., (1988),** PIPS: A Procedure for Interactive Pyramid Segmentation. In: *Proceedings of IGARSS '88 Symposium. Moving towards the 21st Computer,* Edinburgh, 1988, 197-200.
- WILLIAMS, P.L., and SIMONS, F.W., (1985),** Reconnaissance Geology of the Al Baayith Quadrangle, Sheet 26/41D, Kingdom of Saudi Arabia: Deputy Ministry for Mineral Resources Open-File Report, USGS-OF-05-18, 50p.
- WILLIAMS, R.S., Jr. (1983),** Geological Applications. In: R.N. Collwell (Ed). *In Manual of Remote Sensing, 2nd Edition,* (Falls Church: American Society of Photogrammetry), 2: 1667-1951.

- WILSON, R. and SPANN, M. (1988)**, Image Segmentation and Uncertainty, (Letchworth: Research Studies Press Ltd.) 146p.
- WISE, D.U., (1982)**, Linesmanship and The Practice of Linear Geo-Art. *Geological Society of America Bulletin*, 93: 886-888.
- WOODCOCK, C.E., and RYHERD, S.L., (1989)**, Generation of Texture Images Using Adaptive Windows. In: *Proceedings Convention-ASPRS Technical Paper*, 2: 11-22.
- YANOWITZ, S.D., and BRUCKSTEIN, A.M. (1989)**, A New Method for Image Segmentation. *Computer Vision Graphics and Image Processing*, 46: 82-95.
- ZILIOLI, E., and ANTONINETTIE, M., (1987)**, Geostructural Evaluation of Southern Alps: Lineaments Trends Detected on Landsat Images. *Remote Sensing of Environment*, 23: 479,492.

**APPENDIX 1**

**The geological map covering the study area. The test sites and extracts examined in this study are shown in the superimposed rectangles.**

Jibal Rummàn area (test site).

The two extracts examined for image segmentation (Chapter 5).

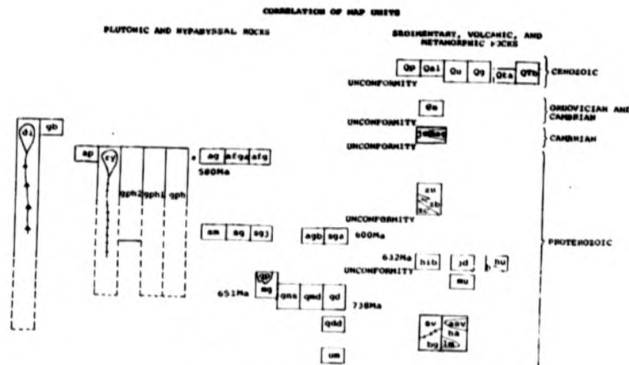
The two extracts examined for automatic line and lineament extraction method (Chapter 6).

The Wadi ad Duwadimi area (test site).

The Wadi Al Qahad area (test site).

The Jibal Muiwaysil area (test site).

SPOT extract used in Chapter 6.



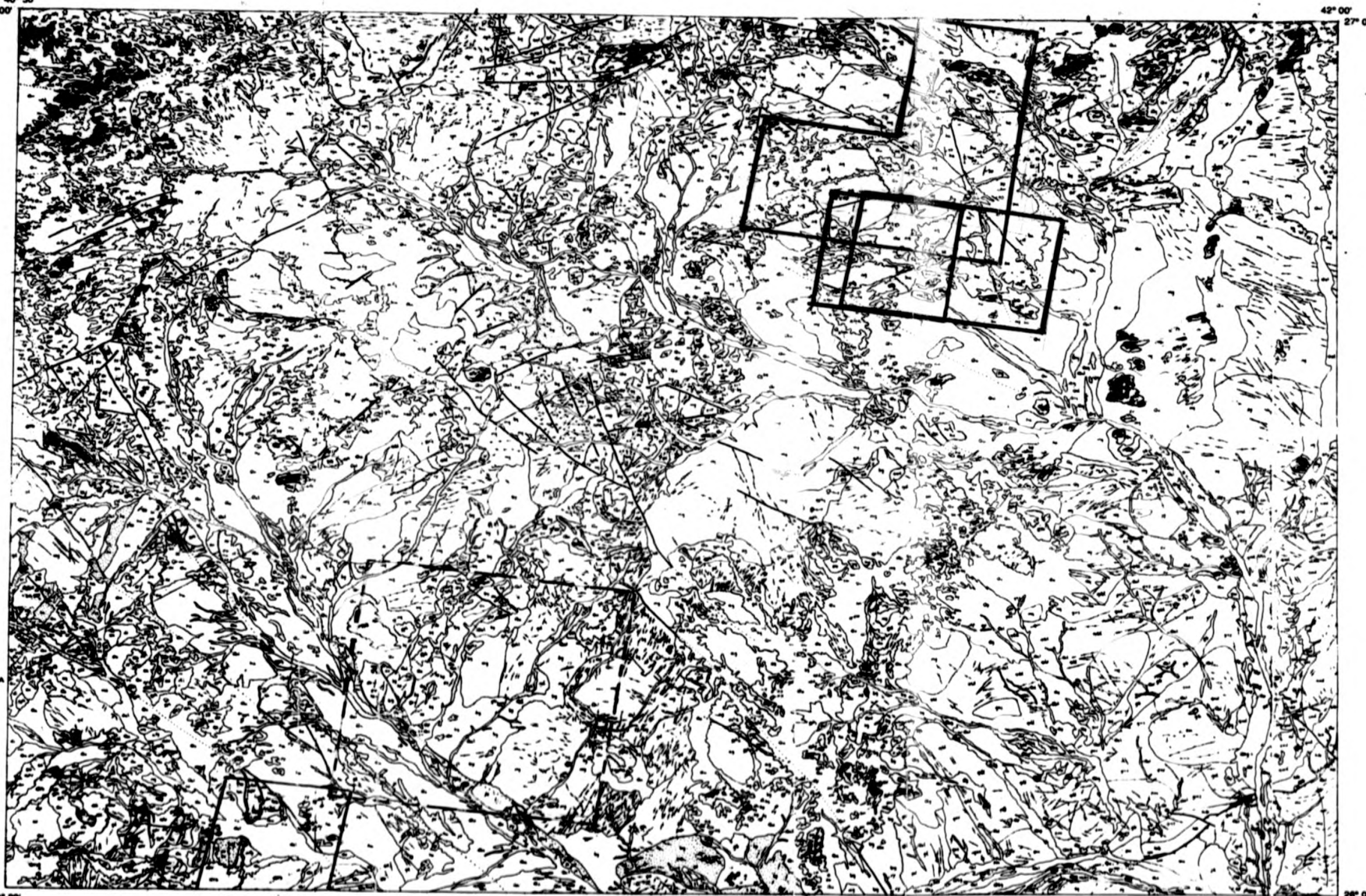
DESCRIPTION OF MAP UNITS

- |  |   |
|--|---|
| <b>CENOZOIC SEDIMENTS AND VOLCANIC ROCKS</b> | <b>LATE PRECAMBRIAN TO EARLY PALAEZOIC INTRUSIVE ROCKS</b>  |
| Qp PLAYA LAKE DEPOSITS                       | d1 DIABASE Dikes AND Lenses   |
| Qa1 ALLOVIUM                                 | q1 QABBIO   |
| Qa2 UNDIVIDED QUATERNARY DEPOSITS            |   |
| Qa3  |   |
| Qa4  |   |
| Qa5 TERRACE GRAVELL                          | ap APLITE   |
| Qa6  | if INTERTRIVE INVOLUTE Dikes AND FLOCS  |
| Qa7  | g1 GRANITE--inclut = two-feldspar granophyre (g11), alkali-feldspar granophyre (g12), and undivided granophyre (g1) |
| Qa8  | g2 SALIN CHARITE LUMP CO--alkali granitic (g2)  |
| Qa9  | g3 Alkalifeldspar granophyre (g31), and undivided granophyre (g3)   |
| Qa10   | g4 BOUTON ALKALI feldspar granite (g4)  |
| Qa11   | g5 TULGAR COMPLEX   |
| Qa12   | g6 AG SAFRA STERNOGRAM 11   |
| Qa13   | g7 JUBAYFAN STERNOGRAM 11   |
| Qa14   | g8 ADH SHU'BAH COMPLEX--Ba'gham granite (g8); Granite, undivided (g8a)  |
| Qa15   | g9 SHIMAYAN SUITE--saturated pegmatite (g9); R100; Romboid mica (g9)  |
| Qa16   | g10 RA'AYIN COMPLEX   |
| Qa17   | g11 FARIHAN QUARTZ Mica Gneissite   |
| Qa18   | g12 RA'A COMPLEX  |
| Qa19   | g13 JUMAYYI HADIB COMPLEX   |
| Qa20   | g14 PERIDOTITE AND Gabbroic ROCKS   |
| Qa21   |   |
| Qa22   |   |
| Qa23   |   |
| Qa24   |   |
| Qa25   |   |
| Qa26   |   |
| Qa27   |   |
| Qa28   |   |
| Qa29   |   |
| Qa30   |   |
| Qa31   |   |
| Qa32   |   |
| Qa33   |   |
| Qa34   |   |
| Qa35   |   |
| Qa36   |   |
| Qa37   |   |
| Qa38   |   |
| Qa39   |   |
| Qa40   |   |
| Qa41   |   |
| Qa42   |   |
| Qa43   |   |
| Qa44   |   |
| Qa45   |   |
| Qa46   |   |
| Qa47   |   |
| Qa48   |   |
| Qa49   |   |
| Qa50   |   |
| Qa51   |   |
| Qa52   |   |
| Qa53   |   |
| Qa54   |   |
| Qa55   |   |
| Qa56   |   |
| Qa57   |   |
| Qa58   |   |
| Qa59   |   |
| Qa60   |   |
| Qa61   |   |
| Qa62   |   |
| Qa63   |   |
| Qa64   |   |
| Qa65   |   |
| Qa66   |   |
| Qa67   |   |
| Qa68   |   |
| Qa69   |   |
| Qa70   |   |
| Qa71   |   |
| Qa72   |   |
| Qa73   |   |
| Qa74   |   |
| Qa75   |   |
| Qa76   |   |
| Qa77   |   |
| Qa78   |   |
| Qa79   |   |
| Qa80   |   |
| Qa81   |   |
| Qa82   |   |
| Qa83   |   |
| Qa84   |   |
| Qa85   |   |
| Qa86   |   |
| Qa87   |   |
| Qa88   |   |
| Qa89   |   |
| Qa90   |   |
| Qa91   |   |
| Qa92   |   |
| Qa93   |   |
| Qa94   |   |
| Qa95   |   |
| Qa96   |   |
| Qa97   |   |
| Qa98   |   |
| Qa99   |   |
| Qa100  |   |

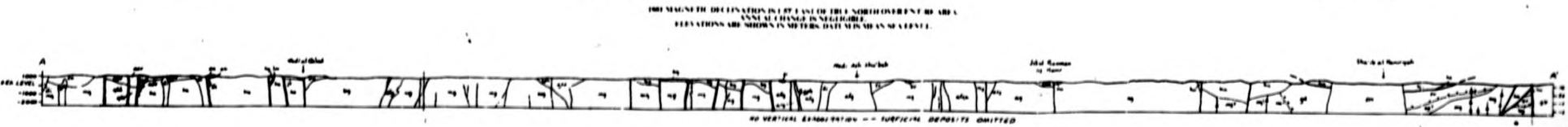
- SYMBOLS**
- CONTACT -- Dotted where concealed
  - FAULT -- Showing dip; dotted where concealed; arrows show direction of strike-slip
  - THRUST FAULT -- Showing dip; bars on upper plate; dotted where concealed
  - FOLDING -- Showing trace of axial plane
  - TRACE OF BENDING
  - STRIKE AND DIP OF BEDS -- Inclined, showing inclination
  - STRIKE AND DIP OF CONGLOMERATE -- Inclined, showing inclination
  - STRIKE AND DIP OF JOINTS -- Inclined, showing inclination
  - Vertical
  - STRIKE AND DIP OF FOLIATION -- Inclined, showing inclination
  - Vertical
  - LOCATION OF GEOCHEMISTRY SAMPLE, SHOWING AND ARBITRARY NUMBER

**LEGEND**

UNDIVIDED AND UNEXPOSED ROCKS



Presented by the United States Geological Survey for the Kingdom of Saudi Arabia. The map is based on data from the Saudi Geological Survey, Riyadh, Saudi Arabia, and the United States Geological Survey, Reston, Virginia, USA. The map is compiled by James E. Quick and Jeff L. Doebrich, 1984.

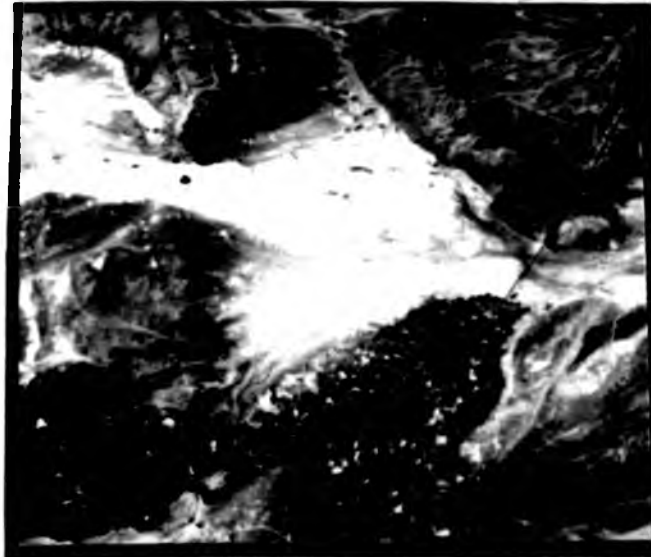


**GEOLOGIC MAP OF THE WADI ASH SHU'BAH QUADRANGLE, SHEET 26E, KINGDOM OF SAUDI ARABIA**  
 Compiled by James E. Quick and Jeff L. Doebrich  
 1984

## APPENDIX 2

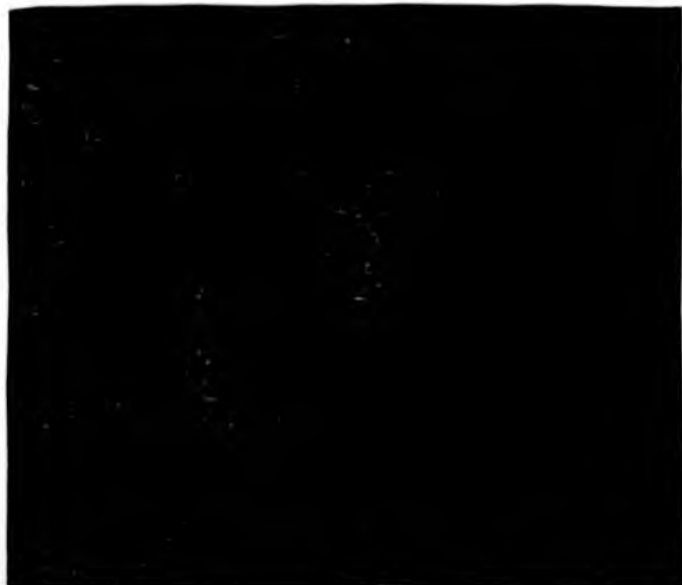
Shows a sample extract of 512 x 512 pixels to show how the new contextual technique (ripping membrane) can improve and enhance the appearance of the drainage pattern in part of the study area (Wadi ad Duwadimi area). (See Appendix 1 for location). (a) Contrast stretched TM band 5 image  
(b) The final result of the ripping membrane

(a)



0 kms 5

(b)



## APPENDIX 3

Showing the selected Laserscan Software Packages  
(and their commands) used for image segmentation.  
(In Chapter 5).

## 1. IMAGE AND ADDITION:

```
$DTICOMBINE  
DTICOMBINE> ENABLE DIAGNOSTICS  
DTICOMBINE> FILEA (First Image File Name)  
DTICOMBINE> FILEB (Second Image File Name)  
DTICOMBINE> FILEC (Third Image File Name)  
DTICOMBINE> (The Output Image Name)  
DTICOMBINE> WORD = A + B + C  
DTICOMBINE> GO  
DTICOMBINE> QUIT
```

## 2. IMAGE DISPLAY:

```
$ROVER  
ROVER> FILEIN (Image File Name)  
ROVER> PLANE 6 (Monochrome) or 7 (Colour Coded)  
ROVER> FRT VER  
ROVER> DISPLAY  
ROVER> RANGE ___ ___ (Digital Number Interval)  
ROVER> DISPLAY ___  
ROVER> EXIT
```

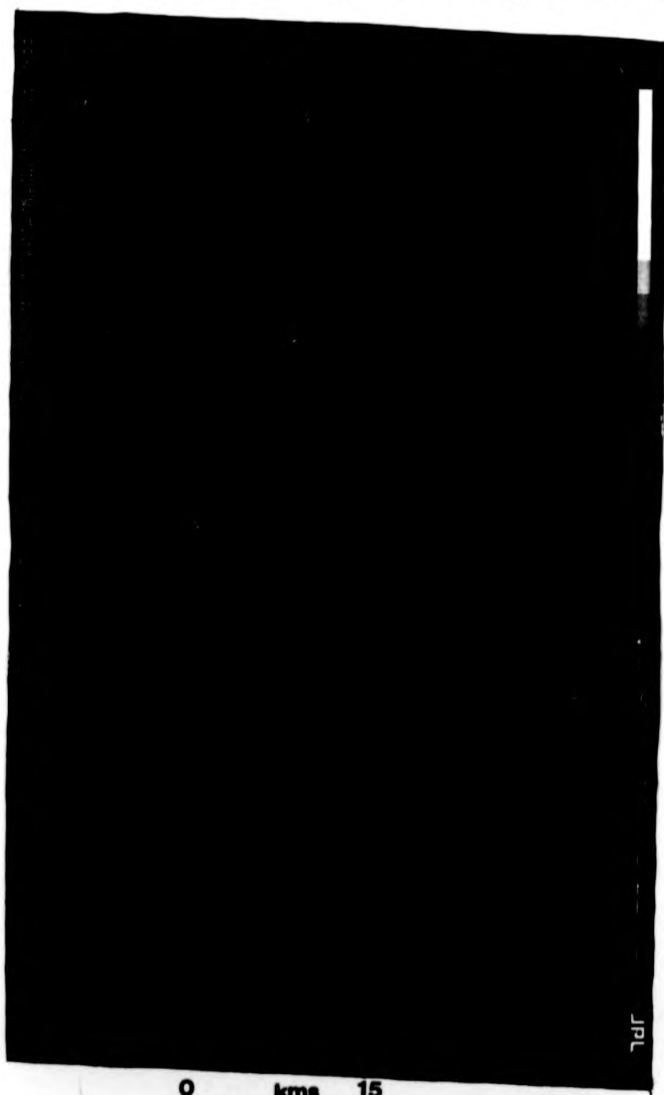
## 3. CREATING VECTOR FILE:

```
$VECTORISE  
VECTORISE> FILEIN (Input File Name)  
VECTORISE> RANGE ___ ___ (Digital Number Interval)  
VECTORISE> IFF ___ (New File Name)  
VECTORISE> SET BORDER FC  
VECTORISE> GO  
VECTORISE> EXIT
```

## APPENDIX 4

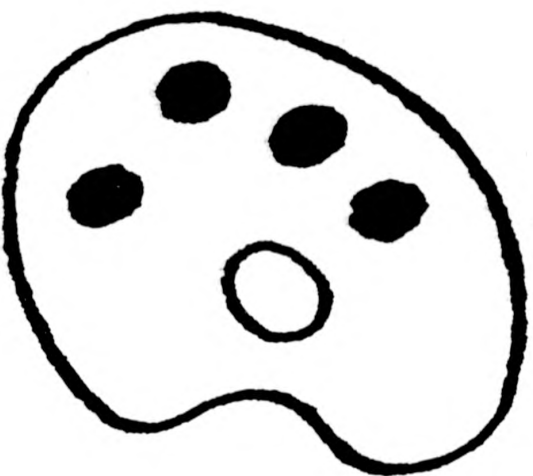
The Shuttle Imaging Radar (SIR-B) scene  
covering part of the study area.

Centre Lat: 25° 39.3'N  
Centre Long: 40° 19.5'E  
Scene: D11  
Pixel size: 12.5m  
centre incident angle: 50.0



0 kms 15

# NUMEROUS ORIGINALS IN COLOUR



VARIABLE PRINT

QUALITY

